

**UNIVERSIDAD COMPLUTENSE DE MADRID**  
**FACULTAD DE CIENCIAS QUÍMICAS**  
Departamento de Química Física



**TESIS DOCTORAL**

**Preparación de co-cristales farmacéuticos, aductos y  
composites usando CO<sub>2</sub> supercrítico como antidisolvente**

**Preparation of pharmaceutical co-crystals, adducts and  
composites using supercritical CO<sub>2</sub> as an antisolvent**

MEMORIA PARA OPTAR AL GRADO DE DOCTOR

PRESENTADA POR

**Isaac Alfonso Cuadra Mendoza**

Directoras

**Concepción Pando García-Pumarino**  
**Albertina Cabañas Poveda**

Madrid  
Ed. electrónica 2019

**UNIVERSIDAD COMPLUTENSE DE MADRID**

**FACULTAD DE CIENCIAS QUÍMICAS**

Departamento de Química Física



TESIS DOCTORAL

**Preparación de co-cristales farmacéuticos, aductos y  
composites usando CO<sub>2</sub> supercrítico como antidisolvente**

MEMORIA PARA OPTAR AL GRADO DE DOCTOR  
PRESENTADA POR

**Isaac Alfonso Cuadra Mendoza**

Directores

Concepción Pando García-Pumarino  
Albertina Cabañas Poveda  
Madrid, 2019



**UNIVERSITY COMPLUTENSE OF MADRID**

**SCHOOL OF CHEMICAL SCIENCES**

Physical Chemistry Department



**Preparation of pharmaceutical co-crystals, adducts and  
composites using supercritical CO<sub>2</sub> as an antisolvent**

THESIS SUBMITTED FOR THE DOCTORAL DEGREE

PRESENTED BY

**Isaac Alfonso Cuadra Mendoza**

**Supervisors**

**Concepción Pando García-Pumarino  
Albertina Cabañas Poveda**

**Madrid, 2019**





UNIVERSIDAD  
COMPLUTENSE  
MADRID

**DECLARACIÓN DE AUTORÍA Y ORIGINALIDAD DE LA TESIS  
PRESENTADA PARA LA OBTENCIÓN DEL TÍTULO DE DOCTOR**

D./Dña. Isaac Alfonso Cuadra Mendoza  
con número de DNI/NIE/Pasaporte 07251877T, estudiante en el Programa  
de Doctorado Química Avanzada,  
de la Facultad de Ciencias Químicas de la Universidad Complutense de  
Madrid, como autor/a de la tesis presentada para la obtención del título de Doctor y  
titulada:

Preparación de co-cristales farmacéuticos, aductos y composites usando CO2 supercrítico como antidisolvente

y dirigida por: Concepción Pando García-Pumarino

Albertina Cabañas Poveda

**DECLARO QUE:**

La tesis es una obra original que no infringe los derechos de propiedad intelectual ni los derechos de propiedad industrial u otros, de acuerdo con el ordenamiento jurídico vigente, en particular, la Ley de Propiedad Intelectual (R.D. legislativo 1/1996, de 12 de abril, por el que se aprueba el texto refundido de la Ley de Propiedad Intelectual, modificado por la Ley 2/2019, de 1 de marzo, regularizando, aclarando y armonizando las disposiciones legales vigentes sobre la materia), en particular, las disposiciones referidas al derecho de cita.

Del mismo modo, asumo frente a la Universidad cualquier responsabilidad que pudiera derivarse de la autoría o falta de originalidad del contenido de la tesis presentada de conformidad con el ordenamiento jurídico vigente.

En Madrid, a \_\_\_\_ de \_\_\_\_\_ de 20\_\_

Fdo.: \_\_\_\_\_

Esta DECLARACIÓN DE AUTORÍA Y ORIGINALIDAD debe ser insertada en  
la primera página de la tesis presentada para la obtención del título de Doctor.





UNIVERSIDAD COMPLUTENSE  
MADRID

**Concepción Pando García-Pumarino**, Catedrática y **Albertina Cabañas Poveda**, Profesora Titular del Departamento de Química Física de la Facultad de Ciencias Químicas de la Universidad de Complutense

**CERTIFICAN:** que el trabajo presentado como Tesis Doctoral en esta memoria titulada: “Preparación de co-cristales farmacéuticos, aductos y composites usando CO<sub>2</sub> supercrítico como antidisolvente” por Isaac Alfonso Cuadra Mendoza, para optar al grado de doctor dentro del programa de doctorado en Química Avanzada (“Advanced Chemistry”) ha sido realizado en el Departamento de Química Física, bajo la dirección de dichas personas, autorizando la presentación de la misma para su defensa y calificación por el tribunal correspondiente.

Y para que así conste, expiden el presente certificado en Madrid a 29 de abril de 2019.

**Fdo: Concepción Pando  
García-Pumarino**

**Fdo: Albertina Cabañas Poveda**





## Doctoral thesis as a compendium of publications aiming to obtain the European Doctor mention

This dissertation aims to obtain the European Doctorate mention. With this purpose, two research stays of three months each were conducted in the KIT (Karlsruher Institut für Technologie) and the TUHH (Technische Universität Hamburg-Harburg), under the supervision of Prof. Michael Türk and Prof. Irina Smirnova respectively.

Moreover, this thesis is presented as a compendium of four previously published scientific articles. The complete references of the articles that constitute the body of the thesis are the following:

1. Cuadra, I. A.; Cabañas, A.; Cheda, J. A. R.; Martinez-Casado, F. J.; Pando, C., *Pharmaceutical co-crystals of the anti-inflammatory drug diflunisal and nicotinamide obtained using supercritical CO<sub>2</sub> as an antisolvent*. Journal of CO<sub>2</sub> Utilization **2016**, 13, 29-37
2. Cuadra, I. A.; Cabañas, A.; Cheda, J. A. R.; Pando, C., *Polymorphism in the co-crystallization of the anticonvulsant drug carbamazepine and saccharin using supercritical CO<sub>2</sub> as an anti-solvent*. Journal of Supercritical Fluids **2018**, 136, 60-69.
3. Cuadra, I. A.; Zahran, F.; Martin, D.; Cabañas, A.; Pando, C., *Preparation of 5-fluorouracil microparticles and 5-fluorouracil/poly(L-lactide) composites by a supercritical CO<sub>2</sub> antisolvent process*. Journal of Supercritical Fluids **2019**, 143, 64-71.
4. Cuadra, I. A.; Martinez-Casado, F. J.; Cheda, J. A. R.; Redondo, M. I.; Pando, C.; Cabañas, A., *Production and Characterization of a New Copper(II) Propanoate-Isonicotinamide Adduct Obtained via Slow Evaporation and using Supercritical CO<sub>2</sub> as an Antisolvent*. Crystal Growth & Design **2019**, 19, 620-629.



*In loving memory of my parents*



## ***Acknowledgment***

First and foremost, I would like to express my gratitude to Prof. Concepción Pando and Prof. Albertina Cabañas for proposing the theme of the thesis, the working plan, and for their valuable discussions, knowledge, interest, coaching and patience. Without them this work would have not been possible.

Secondly, I would like to thank Prof. Michael Türk and Prof. Irina Smirnova for their warm welcome and for allowing me to perform research in their facilities. Part of this research is enclosed in this thesis and the other part opens the path of further work.

I would also like to show my gratitude to Prof. José A.R. Cheda for his valuable advice and allowing me to use the thermal analysis equipment, to Prof. M. I. Redondo for her valuable advice and allowing me to use the FTIR equipment, to Dr. Francisco J. Martínez-Casado for his valuable advice and to Prof. M.D Veiga-Ochoa for allowing me to use the dissolution test apparatus.

Additionally, I thank for their support in particle analysis the National center of electron microscopy, and the UCM research centers of X-ray diffraction and elemental microanalysis.

I would especially like to thank my family and friends for their support, encouragement and patience.

Finally, I gratefully acknowledge the financial support of the Ministry of Economy and Competitiveness through the research project CTQ2013-41781-P as well as the predoctoral grant (BES-2014-067777) and mobility fellowships (EEBB-I-17-12090 and EEBB-I-18-12765).



## TABLE OF CONTENTS

List of tables.....	xvii
List of figures.....	xix
List of abbreviations.....	xxvii
Summary.....	xxix
Resumen.....	xxxv
<b>1 INTRODUCTION .....</b>	<b>1</b>
1.1 Supercritical fluids.....	1
1.2 Phase diagrams of multicomponent systems involving supercritical fluids .....	4
1.2.1 Binary mixtures .....	5
1.2.2 Ternary mixtures .....	8
1.3 Supercritical fluid technology in the pharmaceutical industry .....	10
1.3.1 Micronization techniques using CO <sub>2</sub> as solvent .....	11
1.3.2 Micronization techniques using CO <sub>2</sub> as cosolvent or solute.....	14
1.3.3 Micronization techniques using CO <sub>2</sub> as nebulization agent.....	17
1.3.4 Supercritical fluid extraction of emulsions (SFEE) .....	17
1.3.5 Micronization techniques using CO <sub>2</sub> as antisolvent .....	18
1.3.6 Supercritical antisolvent (SAS).....	19
1.4 Pharmaceutical co-crystals .....	26
1.5 Co-crystal phase diagrams .....	30
1.5.1 Binary phase diagrams.....	30
1.5.2 Ternary phase diagrams .....	32
1.6 Polymorphs and co-crystal polymorphs .....	34
1.7 Preparation of co-crystals using SAS.....	35
1.8 Preparation of co-crystals using CSS.....	39
1.9 Metallic organic frameworks (MOFs) as pharmaceuticals and their preparation using supercritical CO <sub>2</sub> .....	40



1.10	Pharmaceutical composite microparticles and their preparation using supercritical CO <sub>2</sub> .....	41
	References.....	43
<b>2</b>	<b>OBJECTIVES .....</b>	<b>51</b>
	References.....	54
<b>3</b>	<b>METHODOLOGY .....</b>	<b>55</b>
3.1	Supercritical antisolvent precipitation .....	55
3.2	High-pressure variable volume view cell .....	61
3.3	Co-crystallization with supercritical solvent .....	64
3.4	Particle characterization.....	67
3.4.1	Dissolution profiles.....	67
3.4.2	Powder X-ray diffraction (PXRD).....	68
3.4.3	Elemental microanalysis.....	68
3.4.4	Scanning Electron Microscopy (SEM) and energy-dispersive detection X-ray (EDX).....	68
3.4.5	Infrared Spectroscopy (IR).....	69
3.4.6	Thermogravimetric Analysis (TGA).....	69
3.4.7	Differential scanning calorimetry (DSC).....	70
	References.....	72
<b>4</b>	<b>COMPREHENSIVE DISCUSSION OF RESULTS .....</b>	<b>73</b>
4.1	Preparation and characterization of 5-Fu-polymer composites using the SAS technique. Controlled drug delivery through supercritical CO <sub>2</sub> processing. ....	73
4.2	Preparation of pharmaceutical co-crystals via SAS. Evaluation of the influence of SAS parameters in the co-crystal production.....	76
4.3	Influence of SAS operating parameters in co-crystal polymorphism.....	80
4.4	Limiting parameters in the successful preparation of co-crystals using supercritical CO <sub>2</sub> . ....	87
4.5	Preparation of metal organic frameworks (MOFs) via SAS. Evaluation of the SAS technique. ....	90

References.....	95
<b>5 CO-CRYSTALLIZATION OF 5-FLUOROURACIL USING SAS AND CSS</b> .....	<b>97</b>
5.1 Introduction.....	97
5.2 Experimental procedure.....	104
5.2.1 Materials .....	104
5.2.2 Design of SAS experiments.....	105
5.2.3 Equipment validation and design of CSS experiments .....	106
5.3 5-Fu-urea co-crystal.....	109
5.3.1 SAS co-crystallization.....	109
5.3.2 CSS co-crystallization .....	117
5.4 5-Fu-thiourea co-crystal.....	121
5.4.1 SAS co-crystallization.....	121
5.4.2 CSS co-crystallization .....	127
5.5 5-Fu-acridine co-crystal .....	131
5.5.1 SAS co-crystallization.....	131
5.5.2 CSS co-crystallization .....	137
5.6 5-Fu-4HBA co-crystal .....	141
5.6.1 SAS co-crystallization.....	141
5.6.2 CSS co-crystallization .....	149
5.7 5-Fu-PZA co-crystal.....	151
5.7.1 SAS co-crystallization.....	151
5.7.2 CSS co-crystallization .....	152
5.8 5-Fu-SAC co-crystal .....	159
5.8.1 SAS co-crystallization.....	159
5.8.2 CSS co-crystallization .....	163
5.9 Conclusions.....	165
References.....	167

<b>6 PUBLICATIONS.....</b>	<b>173</b>
6.1 Preparation of 5-fluorouracil microparticles and 5-fluorouracil/ <i>poly(l-lactide)</i> composites by a supercritical CO <sub>2</sub> antisolvent process.....	173
6.2 Pharmaceutical co-crystals of the anti-inflammatory drug diflunisal and nicotinamide obtained using supercritical CO <sub>2</sub> as an antisolvent .....	181
6.3 Polymorphism in the co-crystallization of the anticonvulsant drug carbamazepine and saccharin using supercritical CO <sub>2</sub> as an anti-solvent .....	191
6.4 Production and characterization of a new copper(II) propanoate- isonicotinamide adduct obtained via slow evaporation and using supercritical CO <sub>2</sub> as an antisolvent .....	201
<b>7 CONCLUSIONS AND FURTHER WORK.....</b>	<b>211</b>
References.....	215
<b>8 CURRICULUM VITAE.....</b>	<b>217</b>

## List of tables

<b>Table 1.1</b> Comparison of properties in the gas, supercritical and liquid state.....	2
<b>Table 1.2</b> Critical properties of the most commonly used SCFs.....	3
<b>Table 3.1</b> Equipment employed in the SAS laboratory plant.....	60
<b>Table 3.2</b> Equipment employed in the high pressure view cell.....	63
<b>Table 3.3</b> Equipment employed in the CSS laboratory plant at the ITTK.....	65
<b>Table 4.1</b> Temperature and pressure conditions for 5-Fu and PLLA composite preparation using SAS and drug loading.....	74
<b>Table 4.2</b> Values for factors used in the SAS co-crystallization and the factorial design of experiments used. solution flow rate (1 mL/min), CO <sub>2</sub> flow rate (20 g/min), nozzle diameter (100 µm) were kept constant.....	76
<b>Table 4.3</b> Summary of conditions and results for the 1:1 CBZ-SAC co-crystallization by SAS using several solvents at 313 K and 10.0 MPa.....	81
<b>Table 4.4</b> Summary of conditions and results for the 1:1 CBZ-SAC co-crystallization using methanol as a solvent. CO <sub>2</sub> density for runs 1, 5, 6 and 7 was 0.63, 0.78, 0.6 and 0.6 (mg/mL), respectively.....	85
<b>Table 4.5</b> Summary of conditions and results of the SAS 5-Fu co-crystallization experiments with several cofomers.....	87
<b>Table 4.6</b> Operating conditions used in the preparation of MOFs using SAS.....	90
<b>Table 5.1</b> Data of the compounds used in the co-crystalization experiments.....	104
<b>Table 5.2</b> Summary of conditions and results in the SAS experiments (solvent used methanol, concentration of 5-Fu 5 mg/mL, pressure 10.0 MPa and temperature 313 K). .....	105
<b>Table 5.3</b> Summary of conditions and results in the CSS experiments (pressure 20.0 MPa, temperature 323 K, stirring rate 300 rpm and co-crystallization time of 20 h) .....	109
<b>Table 5.4</b> Infrared peaks (cm <sup>-1</sup> ) of commercial 5-Fu and their assignments: $\nu$ stretching; $\delta$ bending; $\gamma$ torsion; $\omega$ wagging; $tw$ twisting; $\rho$ rocking.....	114
<b>Table 5.5</b> Infrared peaks (cm <sup>-1</sup> ) of commercial urea and their assignments: $\nu$ stretching; $\delta$ bending; $\gamma$ torsion; $\omega$ wagging; $tw$ twisting; $\rho$ rocking.....	115
<b>Table 5.6</b> Infrared peaks (cm <sup>-1</sup> ) of commercial thiourea and their assignments: $\nu$ stretching; $\delta$ bending; $\gamma$ torsion; $\omega$ wagging; $tw$ twisting; $\rho$ rocking.....	125
<b>Table 5.7</b> Infrared peaks (cm <sup>-1</sup> ) of commercial acridine and their assignments : $\nu$ stretching; $\delta$ bending; $\gamma$ torsion; $\omega$ wagging; $tw$ twisting; $\rho$ rocking.....	135

**Table 5.8** Infrared peaks (cm<sup>-1</sup>) of commercial PZA and their assignments:  $\nu$  stretching;  
 $\delta$  bending;  $\gamma$  torsion;  $\omega$  wagging;  $tw$  twisting;  $\rho$  rocking. .... 157

**Table 5.9** Infrared peaks (cm<sup>-1</sup>) of commercial SAC and their assignments:  $\nu$  stretching;  
 $\delta$  bending;  $\gamma$  torsion;  $\omega$  wagging;  $tw$  twisting;  $\rho$  rocking. .... 162

## List of figures

<b>Fig. 1.1</b> Schematic phase diagram for a pure substance. ....	1
<b>Fig. 1.2</b> Relationship between reduced pressure ( $P_R$ ) and reduced density ( $\rho_R$ ) at different reduced temperatures ( $T_R$ ) for CO <sub>2</sub> . ....	2
<b>Fig. 1.3</b> P-x and T-x diagram for a binary mixture with complete miscibility under the critical point.....	5
<b>Fig. 1.4</b> Three dimensional representation of a P-T-x diagram for a two component mixture in which both components are miscible. ....	6
<b>Fig. 1.5</b> Six types of phase behaviour according to the Van Konynenburg and Scott classification in binary fluid systems. Points C <sub>1</sub> and C <sub>2</sub> correspond to the critical points of the pure components. Liquid (L); vapour (V); upper critical end point (UCEP); lower critical end point (LCEP). ....	8
<b>Fig. 1.6</b> VLE phase diagram at 348.4 K of CO <sub>2</sub> -ethanol and at 348.15 K of CO <sub>2</sub> -DMSO, and of CO <sub>2</sub> -[DMSO/ethanol] for DMSO/ethanol molar ratios: 3/7; 5/5 and 7/3.....	9
<b>Fig. 1.7</b> Schematic diagram of the rapid expansion of supercritical solutions (RESS) process. P and T represent pressure and temperature respectively at: s (solubilisation tank), 0 (pre-expansion), and f (precipitation chamber). ....	12
<b>Fig. 1.8</b> Schematic diagram of the particles from gas saturated solutions (PGSS) process. ....	14
<b>Fig. 1.9</b> Schematic diagram of gas antisolvent (GAS) process. ....	18
<b>Fig. 1.10</b> Schematic diagram of the supercritical antisolvent process (SAS). ....	20
<b>Fig. 1.11</b> Effect of operating temperature and pressure on droplet behaviour. Figure adapted from Werling and Debendetti. The CO <sub>2</sub> -toluene critical locus and the conditions for which densities of toluene and CO <sub>2</sub> are coincident are identified. ....	21
<b>Fig. 1.12</b> Jet break-up time (blue) and time for dynamic surface tension vanishing (red) as function of pressure and initial concentration in the yttrium acetate-DMSO system. Figure adapted from Marra et al. ....	24
<b>Fig. 1.13</b> Schematic representation of the possible solid states of an API. Figure adapted from Vioglio et al. ....	27
<b>Fig. 1.14</b> Frequent intramolecular synthons. ....	28
<b>Fig. 1.15</b> Binary phase diagram of a congruent melting system at constant pressure. ....	31
<b>Fig. 1.16</b> Binary phase diagram of an incongruent melting system at constant pressure. ....	32

<b>Fig. 1.17</b> Ternary phase diagram of a congruent saturating system at constant temperature and pressure.....	33
<b>Fig. 1.18</b> Ternary phase diagram of an incongruent saturating system at constant temperature and pressure.....	33
<b>Fig. 1.19</b> Evolution of naproxen-nicotinamide (NIC) solubility ratio with CO <sub>2</sub> molar fraction in (acetone-CO <sub>2</sub> ) mixtures at 10 MPa and — 298.15 K; — 310.65 K. Figure adapted from Ryelli et al. ....	37
<b>Fig. 1.20</b> Schematic description of the co-crystallization with supercritical solvent (CSS) setup used by Padrela et al.....	39
<b>Fig. 3.1</b> SAS apparatus. ....	55
<b>Fig. 3.2</b> Schematic diagram of the SAS equipment.....	56
<b>Fig. 3.3</b> Diagram of the precipitation chamber provided by Thar-SCF. Dimensions in inches. ....	57
<b>Fig. 3.4</b> Image of the high-pressure view cell and schematic diagram of the set up in our laboratory.....	61
<b>Fig. 3.5</b> Schematic representation of the CSS laboratory plant.....	64
<b>Fig. 3.6</b> PTFE carbon pan (a), stirring ball and metal grid (b) used in the co-crystallization experiments. ....	66
<b>Fig. 3.7</b> Representation of DSC curves in the binary phase diagram of a congruent melting system.....	71
<b>Fig. 4.1</b> SEM images of the 5-Fu composites and of pure 5-Fu and PLLA processed by SAS at 323 K and 18.0 MPa using as a solvent a 1:1 v/v % DMSO + DCM mixture. ..	75
<b>Fig. 4.2</b> Dissolution profiles of pure 5-Fu (●) and the 5-Fu-PLLA composite (■) obtained by SAS precipitation at 323 K and 18.0 MPa. ....	75
<b>Fig. 4.3</b> SEM images of the co-crystals obtained in experiments 1-3, 5, 7 and 9; commercial NIC (a) and DIF (b) and SAS processed NIC (c) and DIF (d). ....	77
<b>Fig. 4.4</b> View cell with the DIF-NIC solution at the concentration used in experiment 1 and a CO <sub>2</sub> molar fraction equal to 0.98 at 313 K and 10.0 MPa. ....	78
<b>Fig. 4.5</b> PXRD pattern of the DIF-NIC co-crystal obtained by SAS in experiment 1. ....	79
<b>Fig. 4.6</b> Dissolution profiles of the untreated diflunisal (●), and the DIF-NIC co-crystal obtained by SAS in experiment 1 (◆).....	80
<b>Fig. 4.7</b> PXRD patterns of CBZ-SAC co-crystals polymorphs I and II simulated from crystallographic information file. Experimental PXRD patterns of untreated CBZ , SAC and co-crystals of CBZ-SAC obtained in runs 1, 2, 3, 5, 6 and 7.....	82
<b>Fig. 4.8</b> SEM images of CBZ-SAC co-crystals obtained in runs 1,2,3,5,6 and 7. ....	83
<b>Fig. 4.9</b> SEM images of comercial CBZ and SAC, and SAS processed CBZ and SAC using conditions of run 1.....	84

<b>Fig. 4.10</b> PXRD pattern of the Cu(C <sub>3</sub> ) <sub>2</sub> -INA MOF obtained via: a) SAS experiment 1; b) slow evaporation; c) calculation from the Rietveld refinement at room temperature. ...	91
<b>Fig. 4.11</b> SEM images of: a) Cu(C <sub>3</sub> ) <sub>2</sub> prepared at our laboratory; b) commercial INA; c) Cu(C <sub>3</sub> ) <sub>2</sub> -INA formed by slow evaporation; d) Cu(C <sub>3</sub> ) <sub>2</sub> processed by SAS; e) INA processed by SAS; f) MOF formed by SAS.....	92
<b>Fig. 4.12</b> Thermal analysis data: a) TGA and DSC (5 K/min) of the adduct obtained by slow evaporation; b) TGA and DSC (5 K/min) of the adduct obtained by SAS in experiment 1; c) TGA (10 K/min) and mass spectroscopy results for 44 m/z (red), 77 m/z (green) and 104 m/z (blue) of the adduct obtained by slow evaporation; d) TGA (10 K/min) and mass spectroscopy results for 44 m/z (red), 77 m/z (green) and 104 m/z (blue) of the adduct obtained by SAS in experiment 1.....	93
<b>Fig. 5.1</b> Molecular structures displaying the H-bond connections of: a) 5-Fu polymorph I and b) 5-Fu polymorph II. Nitrogen (purple), oxygen (red), fluorine (green), carbon (grey) and hydrogen (white). .....	97
<b>Fig. 5.2</b> Molecular structure displaying the H-bond connections of the cofomers: a) urea polymorph I, b) orthorhombic thiourea, c) ACR polymorph III, d) ACR polymorph II, e) PZA polymorph α, f) 4HBA polymorph I and g) SAC. Nitrogen (purple), oxygen (red), sulphur (yellow), carbon (grey) and hydrogen (white). .....	102
<b>Fig. 5.3</b> Molecular structure displaying the H-bond connections of the co-crystals: a) 5-Fu-urea, b) 5-Fu-thiourea, c) 5-Fu-4HBA polymorph I, d) 5-Fu-4HBA polymorph II, e) 5-Fu-ACR. Nitrogen (purple), oxygen (red), fluorine (green) sulphur (yellow), carbon (grey) and hydrogen (white).....	103
<b>Fig. 5.4</b> PXRD patterns of: CSS co-crystallization powder of CBZ and SAC after 3 hours (top), commercial SAC (middle) and commercial CBZ (bottom).....	106
<b>Fig. 5.5</b> PXRD patterns of: CSS co-crystallization powder of CBZ and SAC after 20 hours (top), and CBZ-SAC co-crystal polymorph I calculated from CIF (bottom). .....	107
<b>Fig. 5.6</b> PXRD patterns of: SAS processed 5-Fu (top), 5-Fu polymorph I calculated from CIF (middle) and commercial 5-Fu (bottom). .....	110
<b>Fig. 5.7</b> PXRD patterns of: SAS processed urea (top), urea polymorph I calculated from CIF (middle), and commercial urea (bottom). .....	110
<b>Fig. 5.8</b> PXRD patterns of the 5-Fu-urea co-crystal obtained through: SAS (top), and calculated from CIF (bottom). .....	111
<b>Fig. 5.9</b> DSC thermograms of: SAS processed 5-Fu-urea (top), commercial urea (middle), and commercial 5-Fu (bottom). Heating rate 5 K/min. ....	112
<b>Fig. 5.10</b> TGA and DSC thermograms of SAS processed 5-Fu-urea. Heating rate 5 K/min. ....	113



<b>Fig. 5.11</b> DSC thermograms of 5-Fu-urea physical mixtures with molar ratios: 2:1 (top), 1:1 (middle), and 1:2 (bottom). Heating rate 5 K/min.....	113
<b>Fig. 5.12</b> FTIR spectrum of 5-Fu. ....	114
<b>Fig. 5.13</b> FTIR spectrum of urea.....	115
<b>Fig. 5.14</b> FTIR spectrum of SAS processed 5-Fu-urea.....	116
<b>Fig. 5.15</b> SEM images of commercial and SAS processed 5-Fu and urea.....	116
<b>Fig. 5.16</b> SEM images of SAS processed 5-Fu-urea. ....	117
<b>Fig. 5.17</b> PXRD patterns from top to bottom of: 5-Fu-urea CSS powder obtained using methanol, 5-Fu-urea CSS powder obtained without methanol, urea polymorph I calculated from CIF, and 5-Fu polymorph I calculated from CIF. ....	117
<b>Fig. 5.18</b> PXRD patterns of the 5-Fu-urea co-crystal obtained through: CSS with methanol (top), SAS (middle), and calculated from CIF (bottom).....	118
<b>Fig. 5.19</b> DSC thermogram of CSS 5-Fu-urea powders obtained: with methanol (top), and without methanol (bottom). Heating rate 5 K/min. ....	119
<b>Fig. 5.20</b> FTIR spectra of CSS 5-Fu-urea powders obtained: without methanol (top), and with methanol (bottom). ....	120
<b>Fig. 5.21</b> SEM images of 5-Fu-urea CSS powders obtained without methanol (a,b), and with methanol (c,d). ....	120
<b>Fig. 5.22</b> PXRD patterns of: SAS processed thiourea (top), orthorhombic thiourea calculated from CIF (middle), and commercial thiourea (bottom).....	122
<b>Fig. 5.23</b> PXRD patterns of the 5-Fu-thiourea co-crystal obtained through: SAS (top), and.....	122
<b>Fig. 5.24</b> DSC thermograms of: SAS processed 5-Fu-thiourea (top), commercial thiourea (middle), and commercial 5-Fu (bottom). Heating rate 5 K/min.....	123
<b>Fig. 5.25</b> TGA and DSC thermogram of SAS processed 5-Fu-thiourea. Heating rate 5 K/min. ....	123
<b>Fig. 5.26</b> DSC thermogram of a 5-Fu-thiourea equimolar physical mixture. Heating rate 5 K/min. ....	124
<b>Fig. 5.27</b> FTIR spectrum of thiourea. ....	125
<b>Fig. 5.28</b> FTIR spectrum of SAS processed 5-Fu-thiourea. ....	126
<b>Fig. 5.29</b> SEM images of commercial and SAS processed thiourea. ....	126
<b>Fig. 5.30</b> SEM images of SAS processed 5-Fu-thiourea.....	127
<b>Fig. 5.31</b> PXRD patterns from top to bottom of: 5-Fu-thiourea CSS powder obtained with methanol, 5-Fu-thiourea CSS powder obtained without methanol, orthorhombic thiourea calculated from CIF, and 5-Fu polymorph I calculated from CIF. ....	127

<b>Fig. 5.32</b> PXRD patterns of the 5-Fu-thiourea co-crystal obtained through: CSS with methanol (top), SAS (middle), and calculated from CIF (bottom).....	128
<b>Fig. 5.33</b> DSC thermograms of: 5-Fu-thiourea powders obtained through CSS: with methanol (top), and without methanol (bottom). Heating rate 5 K/min. ....	128
<b>Fig. 5.34</b> FTIR spectra of: 5-Fu-thiourea powders obtained through CSS: without methanol (top), and with methanol (bottom). ....	129
<b>Fig. 5.35</b> SEM images of: 5-Fu-thiourea CSS powders obtained: without methanol (a,b), and with methanol (c,d). ....	130
<b>Fig. 5.36</b> PXRD patterns of: acridine polymorph III calculated from CIF (top), and commercial acridine (bottom). ....	132
<b>Fig. 5.37</b> PXRD patterns of: 5-Fu polymorph I calculated from CIF (top), and the co-crystal 5-Fu-acridine obtained: through SAS (middle), and calculated from CIF (bottom).....	132
<b>Fig. 5.38</b> PXRD patterns of the 5-Fu-acridine co-crystal obtained: through SAS with an excess of acridine (top), ....	133
<b>Fig. 5.39</b> PXRD patterns from top to bottom: 5-Fu-acridine powder obtained through SAS with an excess of acridine, 5-Fu polymorph I calculated from CIF, acridine polymorph II calculated from CIF, and acridine polymorph III calculated from CIF. ....	133
<b>Fig. 5.40</b> DSC thermograms of: SAS processed 5-Fu-acridine (top), commercial acridine (middle), and commercial 5-Fu (bottom). Heating rate 5 K/min.....	134
<b>Fig. 5.41</b> DSC thermogram of SAS processed 5-Fu-acridine with an excess of acridine. Heating rate 5 K/min. ....	134
<b>Fig. 5.42</b> FTIR spectrum of acridine.....	135
<b>Fig. 5.43</b> FTIR spectra of: commercial 5-Fu (top), SAS processed 5-Fu-acridine in a 2:1 molar ratio (middle) and SAS processed 5-Fu-acridine with an excess of acridine (bottom).....	136
<b>Fig. 5.44</b> SEM images of: SAS processed 5-Fu (a), SAS processed 5-Fu-acridine in a 2:1 molar ratio (b), commercial acridine (c), and SAS processed 5-Fu-acridine with an excess of acridine (d).....	136
<b>Fig. 5.45</b> PXRD patterns of: 5-Fu-acridine powder obtained through CSS without methanol (top), and 5-Fu polymorph I calculated from CIF (bottom). ....	137
<b>Fig. 5.46</b> PXRD patterns from top to bottom of: 5-Fu-acridine powder obtained through CSS with methanol, commercial acridine, 5-Fu polymorph I calculated from CIF, and 5-Fu-acridine co-crystal calculated from CIF. ....	138

<b>Fig. 5.47</b> DSC thermograms of: 5-Fu-acridine powder obtained through CSS with methanol (top), 5-Fu-acridine powder obtained through CSS without methanol (middle), and commercial 5-Fu (bottom). Heating rate 5 K/min.....	138
<b>Fig. 5.48</b> FTIR spectra of: commercial 5-Fu (top) and 5-Fu-acridine powder obtained through CSS without methanol.....	139
<b>Fig. 5.49</b> FTIR spectra of 5-Fu-acridine powders: SAS processed with an excess of acridine (top) and CSS processed with methanol (bottom). ....	140
<b>Fig. 5.50</b> SEM images of CSS 5-Fu-acridine powders processed: without methanol (a,b) and with methanol (c,d). ....	140
<b>Fig. 5.51</b> PXRD patterns of: SAS processed 4HBA (top), commercial 4HBA (middle), and 4HBA polymorph I calculated from CIF (bottom). ....	142
<b>Fig. 5.52</b> PXRD patterns of: SAS processed 5-Fu-4HBA (top), 4HBA polymorph I calculated from CIF (middle) and 5-Fu polymorph I calculated from CIF (bottom). ....	143
<b>Fig. 5.53</b> PXRD patterns of: SAS processed 5-Fu-4HBA (top), 5-Fu-4HBA co-crystal polymorph I calculated from CIF (middle), and 5-Fu-4HBA co-crystal polymorph II calculated from CIF (bottom). ....	144
<b>Fig. 5.54</b> PXRD patterns of: SAS processed 5-Fu-4HBA with an excess of 4HBA (top), and 4HBA polymorph I calculated from CIF (bottom). ....	144
<b>Fig. 5.55</b> DSC thermograms from top to bottom of: SAS 5-Fu-4HBA processed with an excess of 4HBA, SAS 5-Fu-4HBA processed with an equimolar ratio, commercial 4HBA, and commercial 5-Fu. Heating rate 5 K/min.....	145
<b>Fig. 5.56</b> DSC thermograms of 5-Fu-4HBA physical mixtures with molar ratios: 1:2 (top), 1:1 (middle), and 2:1 (bottom). Heating rate 5 K/min.....	145
<b>Fig. 5.57</b> TGA and DSC thermograms of SAS 5-Fu-4HBA processed: with an equimolar ratio (a), and with an excess of 4HBA (b). Heating rate 5 K/min. ....	146
<b>Fig. 5.58</b> FTIR spectrum of 4HBA. ....	147
<b>Fig. 5.59</b> FTIR spectra of : SAS 5-Fu-4HBA processed with an excess of 4HBA (top), and SAS 5-Fu-4HBA processed with an equimolar ratio (bottom). ....	148
<b>Fig. 5.60</b> SEM images of commercial and SAS processed 4HBA. ....	148
<b>Fig. 5.61</b> SEM images of 5-Fu-4HBA SAS precipitates: processed with an equimolar ratio (a), processed with an excess of 4HBA (b), and an amplification of the latter to clearly identify both morphologies present (c). ....	149
<b>Fig. 5.62</b> PXRD patterns from top to bottom of: 5-Fu-4HBA powder obtained through CSS without methanol, 5-Fu-4HBA powder obtained through CSS with methanol, 4HBA (polymorph I) calculated from CIF, and 5-Fu (polymorph I) calculated from CIF. ....	149

<b>Fig. 5.63</b> DSC thermograms of 5-Fu-4HBA powders obtained through CSS: with methanol (top), and without methanol (bottom). Heating rate 5 K/min. ....	150
<b>Fig. 5.64</b> FTIR spectra of: 5-Fu-4HBA powder obtained through CSS without methanol (top), and 5-Fu-4HBA powder obtained through CSS with methanol (bottom). ....	150
<b>Fig. 5.65</b> SEM images of: 5-Fu-4HBA CSS powders processed: without methanol (a,b), and with methanol (c,d). ....	151
<b>Fig. 5.66</b> Images of a 9 mg/mL PZA solution in methanol introduced in a view cell with a CO <sub>2</sub> molar fraction of 0.97 at: 5.0 MPa and 303 K (a); 7.7 MPa and 310 K (b); 10.0 MPa and 313 K (c). ....	152
<b>Fig. 5.67</b> PXRD patterns of: commercial PZA (top), and PZA polymorph $\alpha$ calculated from CIF (bottom). ....	153
<b>Fig. 5.68</b> PXRD patterns from top to bottom of: 5-Fu-PZA powder obtained through CSS with methanol, 5-Fu-PZA powder obtained through CSS without methanol, 5-Fu polymorph I calculated from CIF, and PZA polymorph $\alpha$ calculated from CIF. ....	153
<b>Fig. 5.69</b> DSC thermograms of commercial PZA with heating rates: 20 K/min (top), 5 K/min (middle) and 1 K/min (bottom). ....	154
<b>Fig. 5.70</b> Schematic representation of the solid-solid transition of enantiopric polymorphs $\alpha$ to $\gamma$ at temperature $T_{\alpha \rightarrow \gamma}$ . And melting temperature representation of both polymorphs. ....	154
<b>Fig. 5.71</b> DSC thermograms from top to bottom of: 5-Fu-PZA powder obtained through CSS with methanol, 5-Fu-PZA powder obtained through CSS without methanol, and 5-Fu-PZA physical mixtures with molar ratios: 2:1, 1:1, and 1:2. Heating rate 5 K/min. ....	155
<b>Fig. 5.72</b> TGA thermograms of commercial PZA (top left), and physical mixtures of 5-Fu-PZA with molar ratios: 1:2 (top right), 1:1 ratio (bottom left), and 2:1 ratio (bottom right). Heating rate of 5 K/min. ....	156
<b>Fig. 5.73</b> FTIR spectrum of PZA. ....	157
<b>Fig. 5.74</b> FTIR spectra of 5-FU-PZA powders obtained through CSS: without methanol (top), and with methanol (bottom). ....	158
<b>Fig. 5.75</b> SEM images of: PZA (a,b), 5-Fu-PZA CSS powders processed: without methanol (c,d) and with methanol (e,f). ....	159
<b>Fig. 5.76</b> PXRD patterns of: SAS processed SAC (top), comercial SAC (middle), and SAC calculated from CIF (bottom). ....	160
<b>Fig. 5.77</b> PXRD patterns of: SAS processed 5-Fu-SAC (top), 5-Fu polymorph I calculated from CIF (middle), and SAC calculated from CIF (bottom). ....	160

<b>Fig. 5.78</b> DSC thermograms of: SAS processed 5-Fu-SAC (top), commercial SAC (middle), and commercial 5-Fu (bottom). Heating rate 5 K/min. ....	161
<b>Fig. 5.79</b> DSC thermograms of 5-Fu-SAC physical mixtures with molar ratios: 2:1 (top), 1:1 (middle) and 1:2 (bottom). Heating rate 5 K/min. ....	161
<b>Fig. 5.80</b> FTIR spectrum of SAC. ....	162
<b>Fig. 5.81</b> FTIR spectra of: SAS processed 5-Fu-SAC (top) and commercial 5-Fu (bottom). ....	163
<b>Fig. 5.82</b> SEM images of: SAS processed 5-Fu-SAC (a), and SAS processed SAC <sup>50</sup> (b). .....	163
<b>Fig. 5.83</b> PXRD patterns of: SAC (bottom), 5-Fu polymorph I (middle), CSS 5-Fu-SAC (top). ....	164
<b>Fig. 5.84</b> DSC thermograms of: 5-Fu-SAC powder obtained through CSS (top), and 5-Fu-SAC equimolar physical mixture (bottom). Heating rate 5 K/min. ....	164

## List of abbreviations

API.....	Active pharmaceutical ingredient
ARISE.....	Atomized rapid injection for solvent extraction
ATR.....	Attenuated total reflection
BCS.....	Biopharmaceutics classification system
BPR.....	Back pressure regulator
CAN-BD.....	Carbon dioxide assisted nebulization with a bubble dryer
CCDC.....	Cambridge Crystallographic Data Centre
CBZ.....	Carbamazepine
CFD.....	Computational fluid dynamic
COSMO-RS.....	Conductor-like screening model for real solvents
CPF.....	Concentrated powder form
CIF.....	Crystallographic information file
CSS.....	Co-crystallization with supercritical solvent
DCEP.....	Double critical end points
DCM.....	Dichloromethane
DELOS.....	Depressurization of expanded liquid organic solutions
DIF.....	Diflunisal
DMSO.....	Dimethylsulfoxide
DSC.....	Differential scanning calorimetry
EDX.....	Energy-dispersive detection X-ray
EGA.....	Evolved gas analysis
EMA.....	European Medicines Agency
EMP.....	Expanded microparticle
FDA.....	United States Food and Drug Administration
GAS.....	Gas antisolvent
GRAS.....	Generally recognized as safe
IR.....	Infrared spectroscopy
INA.....	Isonicotinamide
LCEP.....	Lower critical end point
LL.....	Liquid-liquid
LLV.....	Liquid-liquid-vapour
MEPS.....	Molecular electrostatic potential surfaces
MOF.....	Metallic organic framework
NIC.....	Nicotinamide
NSAID.....	Non steroidal anti-inflammatory drug
NVP.....	N-vinylpyrrolidinone
PCA.....	Precipitation by compressed antisolvent
PCL.....	Polycaprolactone
PEG.....	Polyethylene glycol
PLGA.....	Poly-lactide-co-glycolide

PGSS.....	Particles from gas saturated solutions
PLLA.....	Poly(L-lactide)
PSD.....	Particle size distribution
PVP.....	Polyvinylpyrrolidone
PXRD.....	Powder X-ray diffraction
PZA.....	Pyrazinamide
RESS.....	Rapid expansion of supercritical solutions
RESSAS.....	Rapid expansion of supercritical solutions into an aqueous solution
RESS-SC.....	Rapid expansion of supercritical solutions with solid cosolvent
RESOLV.....	Rapid expansion of supercritical solutions into liquids
SAA.....	Supercritical fluid assisted atomization
SAC.....	Saccharin
SAS.....	Supercritical antisolvent
SAS-EM.....	Supercritical antisolvent precipitation with enhanced mass transfer
SCF.....	Supercritical Fluid
SCW.....	Supercritical water
SCXRD.....	Single-crystal X-ray diffraction
SEA.....	Supercritical enhanced atomization
SEDS.....	Solution enhanced dispersion by supercritical fluids
SEM.....	Scanning electron microscopy
SFEE.....	Supercritical fluid extraction of emulsions
SFZ.....	Sulfathiazole
TGA.....	Thermogravimetric analysis
THF.....	Tetrahydrofuran
TS.....	Thymidylate synthase
UCEP.....	Upper critical end point
USP.....	United States pharmacopeia
VLE.....	Vapour liquid equilibrium
4HBA.....	4-hydroxybenzoic acid
5-Fu.....	5-fluorouracil

# Summary

## I. Introduction

The success of a new active pharmaceutical ingredient (API) relies on essential properties such as solubility, bioavailability, dissolution rate, physicochemical stability, and crystallinity. Most of the new APIs brought into the market by the pharmaceutical industry belong to class II in the biopharmaceutics classification system (BCS), i.e., low solubility and high permeability. Researchers are therefore urged to find paths of formulation development that could overcome the APIs drawbacks and enhance their properties. In this thesis we explore some of these paths:

- Micronization: The reduction in size of an API can increase its dissolution rate due to an increase in its surface area and can also improve the intracellular uptake. Size reduction also enables the use of different administration routes.
- Preparation of composites: The dispersion or encapsulation of APIs in a carrier may permit a controlled delivery. Depending on the interaction of the API with the carrier it may also increase the dissolution rate of the API by inducing amorphization of the drug. It can also prevent API degradation and mask unpleasant properties such as taste or odour.
- Co-crystallization: The combination of the API with a suitable coformer in a solid stoichiometric system connected by non-covalent interactions can improve its physicochemical properties and its medical performance.
- Preparation of metal organic frameworks (MOFs): MOFs are formed by transition metal cations that are bond together through organic bridging ligands. Biocompatible MOFs are used for drug storage and controlled release.

A large number of processes exist to produce the above mentioned API formulations. Nevertheless, industrial processes seek to comply with increasing environmental regulations. Supercritical CO<sub>2</sub> based processes generally involve fewer steps, a reduced amount of organic solvents and use innocuous and non-flammable CO<sub>2</sub> that is considered a green solvent, therefore these are more sustainable processes. The supercritical antisolvent (SAS) process in particular is a semi continuous process that has already been scaled up successfully to pilot plant scale, thus presenting for the pharmaceutical industry a real and attractive alternative to



process and simultaneously micronize drugs with a narrow particle size distribution (PSD) in a one-step, environmental friendly and sterile process. Moreover, these microparticles are solvent-free and changes in the operational parameters provide an easy way of controlling the process outcome.

## II. Objectives

This thesis is aimed to exploring the use of supercritical CO<sub>2</sub> in the enhancement and improvement of API properties through co-crystallization, formation of composites and metal adducts.

## III. Methodology

Two supercritical technologies have been used, namely SAS and cocrystallization with supercritical solvent (CSS). For comparison reasons MOFs have been also obtained through slow evaporation. A view cell has been used, depending on the system, to measure solubilities in CO<sub>2</sub>. Dissolution profiles were measured using a paddle apparatus, and dialysis bags. Characterization of the products was performed using: scanning electron microscopy (SEM), powder and single crystal X-ray diffraction (PXRD and SCXRD), thermogravimetric analysis (TGA), differential scanning calorimetry (DSC), mass spectroscopy, Infrared spectroscopy (IR) and microelemental analysis.

The APIs studied in this doctoral thesis were: 5-Fluorouracil (cancer treatment), diflunisal (anti-inflammatory), carbamazepine (epilepsy treatment), and copper propanoate (activity in diverse pharmaceutical fields).

## III. Comprehensive discussion of results

The preparation of pharmaceutical composites via coprecipitation using the SAS technique was explored. Composites of 5-Fluorouracil (5-Fu) and poly(L-lactide) (PLLA) were prepared via SAS in a 1:1 v/v mixture of dichloromethane (DCM) and dimethylsulfoxide (DMSO). Different operational conditions of temperature (308-323 K) and pressure (12-25 MPa) were studied. Composites were characterized using SEM, DSC and PXRD. Drug loading and stability of the composites was established using TGA. The dissolution profile of a chosen composite was compared to that of the pure drug. For the composite material a controlled drug delivery was achieved.

The production of co-crystals using the SAS technique was also explored. Co-crystals of diflunisal (DIF) and nicotinamide (NIC) were prepared via SAS. The influence of operating conditions: temperature (308-313 K), pressure (10-12 MPa) and drug concentration (15-30 mg DIF/mL) was studied following a factorial design of experiments. Influence of solvent was also studied and experiments were carried out in ethanol and acetone. The studied variables had very little effect on the outcome of the SAS process for this particular system and further experimentation in a different system was required to understand these effects. Pure DIF and NIC were also micronized via SAS for comparative purposes. Co-crystals were studied using SEM, PXRD, DSC and IR. Dissolution profile of the SAS obtained co-crystal was compared to that of the pure drug observing a slight dissolution rate improvement in the SAS co-crystal.

To further investigate the influence of operating conditions in the co-crystal formation via SAS and to study the polymorphism in the SAS produced formulations, co-crystals of carbamazepine (CBZ) with saccharin (SAC) in a 1:1 molar ratio were prepared. Influence of solvent selection in the polymorphic outcome of the precipitate was investigated using four different solvents: methanol, ethanol, DCM and DMSO. The influence of pressure (10-15 MPa), temperature (313-333 K) and concentration (15-30 mg CBZ/mL) in experiments carried out in methanol was also investigated. Precipitates were studied using PXRD, SEM, DSC and IR. Except experiments performed in DMSO that failed to produce any precipitate, all experiments led to the formation of the co-crystal. Pressure showed to have an influence in yield and macromorphology of the precipitates, while temperature and solvent showed to have a major influence in the polymorphic outcome. This research pointed out the possible dependence of the SAS outcome on the type of ternary phase diagram for the system formed by the co-crystal components and solvent (i.e., incongruent or congruent saturating phase diagram). The SAS technique was proven once again suitable for the production of an improved drug formulation. Co-crystals of CBZ-SAC polymorph I with yields up to 65 % and free of solvent and homocrystal impurities were obtained in methanol. The undesired dihydrate form of CBZ was avoided.

In the studies described so far only pure co-crystal precipitates with no presence of homocrystals were obtained by SAS. Other researchers though had reported the presence of drug homocrystals in the SAS precipitates. Therefore, further systems were explored to investigate the factors related to homocrystal precipitation. For comparison purposes the use of CO<sub>2</sub> as a solvent in the co-crystallization of different 5-Fu co-crystals was also investigated using the CSS technique. Co-crystals of 5-Fu with and urea, thiourea, acridine, 4-hydroxybenzoic acid (4HBA), pyrazinamide

(PZA) and SAC were attempted via SAS using methanol as a solvent. All experiments were carried at 313 K and 10.0 MPa (conditions above the critical point of CO<sub>2</sub>-methanol mixture). Preparation of the same systems was also attempted by CSS. Conditions used in CSS were 323 K and 20.0 MPa. Experiments were performed in pure CO<sub>2</sub> and in CO<sub>2</sub> modified with a small amount of methanol for 20 hours under stirring. Particles obtained using both techniques were studied with PXRD, DSC, TGA, IR and SEM.

CSS cocrystallization was successful only in the experiments performed using CO<sub>2</sub> modified with methanol. CSS failed to produce pure co-crystals and homocrystals were always present. The particle size control was poor and the micronization was not possible, moreover the scaling up is difficult indicating that this technology is not suitable for co-crystallization. Nevertheless, a 5-Fu and PZA co-crystal that could not be obtained via SAS was obtained via CSS.

The preparation of 5-Fu co-crystals using the SAS technique was possible for all systems studied (except that of 5-Fu and PZA) although homocrystals also appear in the precipitate. Attention must be given to the solubilities of the cofomers in the selected solvent and in CO<sub>2</sub>.

The SAS precipitation of these systems pointed out interesting findings. Co-crystals of 5-Fu with thiourea and urea were obtained via SAS. In this case 5-Fu homocrystals were also present at the studied conditions. The large solubility difference of the co-crystal cofomers in methanol suggests an incongruent saturating ternary phase diagram, what would lead to the formation of homocrystals.

Co-crystals of 5-Fu and acridine were also obtained via SAS. In this case the solubility of acridine in CO<sub>2</sub> is much higher than that of 5-Fu. Increasing the initial concentration of acridine in the solution led to the formation of the co-crystal. These results suggest that increasing the concentration in the feeding solution of the more soluble cofomer in CO<sub>2</sub> may lead to the co-crystal formation. The difficulties of optimizing this process may be challenging though as the final drying step in the SAS process could result in the extraction of the more soluble cofomer.

Co-crystal precipitation of 5-Fu with 4HBA and PZA also posed difficulties under the studied conditions. Although both 5-Fu and PZA have a very low solubility in CO<sub>2</sub> and their solubility in methanol is similar (suggesting a congruent saturating ternary phase diagram), the precipitate obtained via SAS consisted of 5-Fu only indicating that PZA was washed out of the precipitation chamber. A full understanding of the reasons

for this behaviour is still lacking but the possible precipitation of considerably small particles that will not be retained by the 2µm frit is suggested. A similar problem was encountered with 4HBA and although its solubility in CO<sub>2</sub> is even smaller than that of 5-Fu, the amount of 4HBA in the precipitate was smaller than that expected. Similarly, to the 5-Fu and acridine co-crystal, the concentration in the initial solution of 4HBA was increased. This led to the obtention of 4HBA homocrystals and a complex mixture of phases.

The use of the SAS technique in the preparation of MOFs was also assessed. A MOF of copper propanoate and isonicotinamide (INA) in a 1:2 molar ratio was prepared from an ethanol solution via evaporation. Its crystal structure was elucidated using SCXRD and further characterization was accomplished using PXRD, IR, DSC and SEM. The same MOF was prepared via SAS and compared to the one obtained via slow evaporation. Decomposition of the MOFs prepared using both techniques was studied by means of TGA and mass spectrometry. Conditions of SAS precipitation studied were temperature, pressure and molar ratio of components. Two solvents (ethanol and methanol) were studied in the SAS precipitation. Both MOF components were precipitated via SAS for comparative purposes. The successful preparation of the MOF through SAS depends on the operational conditions used. A loss in organic matter in the precipitate was observed. Nevertheless, SAS led to a precipitate with a much smaller particle size where the MOF and an amorphous phase were present, thus, SAS seems to be a suitable method for its synthesis.

#### IV. **Conclusions and further work**

SAS is a promising technique for industrial processing of pharmaceuticals. SAS operates at moderate temperatures and therefore thermosensible drugs and carriers may be processed. Supercritical CO<sub>2</sub> is considered a green solvent and can be recycled. Furthermore, the amount of organic solvents is reduced in SAS and micronization and a narrow size particle distribution are achieved. Sterile solvent-free formulations are obtained in a semi-continuous single step process. Moreover, SAS has been proven to be a suitable process for the production of different enhanced API formulations.

SAS showed to be an adequate process for the production of microparticle composites of 5-Fu and PLLA, the production of a MOF between copper propanoate and INA and the production of several co-crystals (DIF and NIC, CBZ and SAC, and 5-Fu and urea, thiourea, acridine and 4HBA). Operating conditions and the solubilities

of cofomers in the solvent and CO<sub>2</sub> play a key role in the production of MOFs and co-crystals via SAS.

CSS showed to be a technique capable of co-crystallization; a co-crystal of 5-Fu and PZA where the SAS technique had failed was obtained by CSS. Nevertheless, the difficulty of scaling up this technique and the lack of micronization discourages the use of CSS. The rapid expansion of supercritical solutions (RESS) seems to be a more convenient technique if CO<sub>2</sub> is to be used as a solvent.

As further work we propose: A more detailed investigation of the influence of the ternary phase diagram in the SAS co-crystallization, the preparation of MOFs with other copper alkanoates via SAS in order to understand the loss of organic matter, and the formation of co-crystals inside aerogel carriers, an innovative formulation that could combine the improved physicochemical properties of the co-crystal and the controlled release of an aerogel.

# Resumen

## I. Introducción

El éxito de un nuevo principio activo depende de propiedades esenciales tales como: solubilidad, biodisponibilidad, velocidad de disolución, estabilidad fisicoquímica y cristalinidad. La mayoría de los nuevos principios activos que la industria farmacéutica saca al mercado pertenecen a la categoría II del sistema de clasificación biofarmacéutica, es decir, presentan baja solubilidad y alta permeabilidad. Es por ello que los investigadores debemos encontrar vías de mejora en la formulación de los principios activos para que puedan superar estas limitaciones y por tanto, mejorar sus propiedades. En esta tesis se exploran algunas de estas vías:

- Micronización: La reducción del tamaño de partícula de un principio activo puede aumentar su velocidad de disolución debido a un incremento en su área superficial y mejorar su absorción intracelular. La reducción de tamaño del principio activo posibilita también el uso de distintas rutas de administración.
- Preparación de composites: La dispersión o encapsulación de un principio activo con un excipiente puede resultar en una liberación controlada del fármaco. Dependiendo en la interacción del principio activo con el excipiente se puede conseguir acelerar la velocidad de liberación si el principio activo se amorfiza. El excipiente puede también proteger al principio activo de degradación y/o enmascarar propiedades no deseadas del mismo tales como olor o sabor.
- Co-cristalización: La combinación de un principio activo con un coformador adecuado mediante interacciones no covalentes en una estequiometría determinada y en estado sólido puede mejorar las propiedades fisicoquímicas del fármaco y su eficiencia.
- Preparación de redes metal-orgánicas (MOFs): Este tipo de redes están formadas por cationes de un metal de transición que están unidos a través de ligandos puente orgánicos. Los MOFs se usan en la conservación de los principios activos durante su almacenamiento y para conseguir una liberación controlada de los mismos.

Existen un gran número de procesos de preparación de las formulaciones antes descritas. No obstante, la industria busca implementar procesos que satisfagan las cada vez más restrictivas normativas medioambientales. Los procesos basados en la utilización de CO<sub>2</sub> supercrítico requieren generalmente menos etapas y un consumo menor de disolventes orgánicos. El CO<sub>2</sub> es un disolvente inocuo, no inflamable y además es considerado un disolvente verde, ofreciendo por tanto una alternativa de procesado más sostenible. En particular el proceso de micronización de materiales usando CO<sub>2</sub> supercrítico como agente antisolvente (SAS) es un proceso en semicontinuo que ya ha sido escalado con éxito a planta piloto y que presenta por tanto para la industria farmacéutica una alternativa real y atractiva para el procesado y micronización simultánea de principios activos. SAS produce micropartículas con un rango estrecho de distribución de tamaños, en un proceso medioambientalmente sostenible que ocurre en una sola etapa y bajo una atmosfera estéril. Además, las micropartículas obtenidas por SAS están libres de restos de disolvente y sus características pueden ser en principio modificadas mediante cambios en las condiciones de operación.

## II. Objetivos

El objetivo de esta tesis es la investigación del uso de CO<sub>2</sub> supercrítico en el desarrollo y mejora de las propiedades de principios activos a través de la co-cristalización, formación de composites y aductos metálicos.

## III. Metodología

Se han utilizado dos tecnologías supercríticas: SAS y co-cristalización mediante disolvente supercrítico (CSS). Los aductos metálicos también se han preparado por cristalización evaporativa (método tradicional) para poder comparar sus características y propiedades. Para la medida de la solubilidad de algunos compuestos en CO<sub>2</sub> se ha utilizado una celda de visión. Los perfiles de disolución de los principios activos y formulaciones se han medido mediante un equipo con paletas de agitación o utilizando bolsas de diálisis. La caracterización de las muestras se realizó usando: Microscopia electrónica de barrido (SEM), difracción de rayos X en polvo y monocristal (PXRD y SCXRD), análisis termogravimétrico (TGA), calorimetría diferencial de barrido (DSC), espectroscopia de masas, espectroscopia infraroja (IR) y microanálisis elemental.

Los principios activos estudiados en esta tesis son: 5-Fluorouracilo (tratamiento del cáncer), diflunisal (antiinflamatorio), carbamazepina (tratamiento de la epilepsia), y propanoato de cobre (usos farmacéuticos diversos).

#### **IV. Discusión integradora de resultados.**

Se ha investigado la preparación de composites farmacéuticos mediante la coprecipitación usando la técnica SAS. Se prepararon por SAS composites de 5-Fluorouracilo (5-Fu) y ácido poli-L-láctico (PLLA) usando una mezcla 1:1 v/v de diclorometano (DCM) y dimetilsulfóxido (DMSO). Los experimentos se realizaron variando la temperatura (308-323 K) y presión (12-25 MPa). Los composites fueron caracterizados usando SEM, DSC y PXRD. La carga del fármaco en el composite fue determinada mediante TGA. El perfil de disolución de uno de los composites obtenidos fue comparado con el del fármaco puro. El composite logró una liberación controlada del fármaco.

También se investigó la preparación de co-cristales usando la técnica SAS. Se prepararon co-cristales de diflunisal (DIF) y nicotinamida (NIC) por SAS. Se investigó la influencia de la temperatura (308-313 K), presión (10-12 MPa) y concentración del fármaco (15-30 mg DIF/mL) mediante un diseño factorial de experimentos. También se investigó el efecto del disolvente realizando experimentos en etanol y acetona. En este sistema en particular las variables investigadas tuvieron un efecto pequeño en el producto obtenido por SAS. Se optó por utilizar otros sistemas para poder entender mejor la influencia de estas variables. Para poder comparar con el co-cristal y evaluar los cambios producidos en los componentes del co-cristal tras el procesado SAS también se micronizaron por SAS DIF y NIC puros. Los co-cristales se caracterizaron usando SEM, PXRD, DSC e IR. El perfil de disolución del co-cristal obtenido por SAS se comparó con el del fármaco puro observándose un ligero aumento en la velocidad de disolución del co-cristal obtenido por SAS.

Para profundizar más en el efecto de las condiciones de operación en la formación de co-cristales por SAS, y para investigar el poliformismo en las formulaciones farmacéuticas obtenidas por SAS; se prepararon co-cristales de carbamazepina (CBZ) y sacarina (SAC) con una estequiometría 1:1. Se investigó el efecto del disolvente en la forma polimórfica del producto usando cuatro disolventes: metanol, etanol, DCM y DMSO. En los experimentos realizados en metanol se investigó la influencia de presión (10-15 MPa), temperatura (313-333 K) y concentración (15-30 mg CBZ/mL). Los productos se caracterizaron usando PXRD,



SEM, DSC e IR. Salvo los experimentos realizados con DMSO que no produjeron precipitado alguno, todos los experimentos resultaron en la formación del co-cristal. La presión afectó al rendimiento del proceso y a la macromorfología del precipitado, mientras que la temperatura y la elección del disolvente tuvieron un efecto mayor en la forma polimórfica del producto. Esta investigación sugiere la posible dependencia del precipitado obtenido por SAS con el tipo diagrama de fase ternario formado por los componentes del co-cristal y el disolvente (es decir, si es un diagrama con saturación congruente o incongruente). Se pudo observar nuevamente que la técnica SAS es adecuada para preparar formulaciones farmacéuticas. A partir de disoluciones de los fármacos en metanol se obtuvieron por SAS co-cristales de CBZ-SAC en la forma polimórfica I con rendimientos de hasta el 65 %, libres de restos de disolvente e impurezas de homocristales. El procesado por SAS evitó la formación de la menos soluble y no deseada CBZ dihidratada.

En las investigaciones descritas hasta ahora por SAS sólo se obtuvieron precipitados consistentes en co-cristales sin la formación de homocristales. Otros investigadores, sin embargo, han observado la presencia de homocristales en sus precipitados SAS. Por este motivo se decidió explorar otros sistemas e investigar los factores que conducen a la precipitación de homocristales. Por motivos comparativos también se realizó la co-cristalización de diversos co-cristales formados con 5-Fu usando CO<sub>2</sub> como disolvente mediante la técnica CSS. La co-cristalización de 5-Fu con urea, tiourea, acridina, ácido 4-hidroxibenzoico (4HBA), pirazinamida (PZA) y SAC se llevó a cabo usando la técnica SAS y metanol como disolvente. Todos los experimentos se realizaron a 313 K y 10.0 MPa (condiciones por encima del punto crítico de la mezcla CO<sub>2</sub>-metanol). La preparación de los mismos co-cristales fue probada con la técnica CSS. Las condiciones de operación en los experimentos CSS fueron de 323 K y 20.0 MPa. Los experimentos se realizaron en CO<sub>2</sub> puro y en CO<sub>2</sub> modificado con una pequeña cantidad de metanol durante 20 horas y bajo agitación magnética. Los precipitados obtenidos mediante ambas técnicas fueron caracterizados mediante PXRD, DSC, TGA, IR y SEM.

La co-cristalización mediante la técnica CSS se logró sólo en los experimentos en los que se usó CO<sub>2</sub> modificado con metanol. En ningún caso la técnica CSS produjo precipitados consistentes en co-cristales puros y siempre se obtuvieron mezclas con los homocristales. Este método no permite controlar el tamaño de partícula ni micronizar, además es una técnica cuyo escalado es difícil por lo que no

parece idónea para la co-cristalización. Sin embargo, mediante CSS se obtuvo un co-cristal de 5-Fu con PZA que no fue posible obtener usando la técnica SAS.

La preparación de co-cristales de 5-Fu usando la técnica SAS fue posible en todos los sistemas estudiados (salvo el de 5-Fu con PZA) aunque los precipitados también contenían homocristales. Se debe prestar atención a las solubilidades de los componentes del co-cristal en el disolvente elegido y en el CO<sub>2</sub>.

La precipitación SAS de estos sistemas condujo a resultados de interés. La técnica SAS produjo co-cristales de 5-Fu con urea y tiourea. En este caso también se observaron en el precipitado SAS homocristales de 5-Fu. La gran diferencia en las solubilidades de los componentes del co-cristal en metanol sugiere un diagrama de fases ternario con saturación incongruente, lo que llevaría a la formación de homocristales.

También se obtuvieron mediante SAS co-cristales de 5-Fu con acridina. En este caso la solubilidad de acridina en CO<sub>2</sub> es mucho mayor que la del 5-Fu. Aumentando la concentración de acridina en la disolución inicial se obtuvo el co-cristal. Estos resultados sugieren que en mezclas de fármacos de muy distinta solubilidad en CO<sub>2</sub> aumentando la concentración del fármaco más soluble en CO<sub>2</sub> en la disolución inicial a precipitar se favorece la formación del co-cristal. Las dificultades de optimizar este proceso son grandes ya que la etapa de secado final del proceso SAS puede resultar en la extracción del componente más soluble.

La co-cristalización de 5-Fu con 4-HBA y PZA en las condiciones de operación estudiadas también fue compleja. A pesar de que tanto 5-Fu como PZA tienen una solubilidad muy baja en CO<sub>2</sub> y su solubilidad en metanol es similar (sugiriendo por tanto un diagrama de fases ternario con saturación congruente), el precipitado obtenido por SAS contenía solamente 5-Fu lo que sugiere la extracción o el arrastre de la PZA de la cámara de precipitación. Este resultado no es fácil de explicar. Una posibilidad es que la PZA precipite formando partículas muy pequeñas que no queden retenidas en el filtro de 2 µm. Un problema similar se encontró con 4HBA, y aunque la solubilidad de este compuesto en CO<sub>2</sub> es incluso menor que la del 5-Fu, la cantidad de 4HBA en el precipitado SAS era menor de la esperada. De manera similar como se hizo para el co-cristal de 5-Fu con acridina, se aumentó la concentración de 4HBA en la disolución inicial. Esto condujo a la aparición de homocristales de 4HBA junto a una mezcla compleja de fases.

El uso de la técnica SAS en la preparación de MOFs también fue investigada. Un MOF de propanoato de cobre con isonicotinamida (INA) en una proporción molar 1:2 se preparó por cristalización evaporativa a partir de una disolución en etanol. La estructura cristalina del MOF se resolvió usando SCXRD y el material fue caracterizado adicionalmente por PXRD, IR, DSC y SEM. El mismo MOF fue preparado usando la técnica SAS y comparado con el obtenido por cristalización evaporativa. La descomposición del MOF obtenido por ambas técnicas fue estudiada mediante TGA y espectroscopia de masas. Las condiciones de operación estudiadas fueron temperatura (298-313 K), presión (8-25 MPa) y razón molar de los componentes (razones molares de propanoato de cobre a INA de 1:2 y 1:1). Se estudiaron dos disolventes (etanol y metanol) en la precipitación SAS. Además cada uno de los componentes por separado fue procesado por SAS. La preparación del MOF mediante SAS depende de las condiciones de operación utilizadas. Se observó una pérdida en el contenido orgánico del precipitado SAS frente al preparado por evaporación. No obstante, la técnica SAS produjo un precipitado de mucho menor tamaño de partícula en el que el MOF estaba presente junto a una fase amorfa resultando, por tanto, la técnica SAS adecuada para su síntesis.

## **V. Conclusiones y futuras líneas de trabajo.**

SAS es una técnica prometedora para el procesamiento a escala industrial de fármacos. Las temperaturas usadas en el proceso SAS son moderadas y por tanto es apta para el procesamiento de fármacos y excipientes termosensibles. CO<sub>2</sub> supercrítico está considerado un disolvente verde y se puede reciclar, además, la cantidad de disolventes orgánicos usados se ve reducido en SAS y se consigue la micronización con distribuciones estrechas de tamaño de partícula. Se obtienen formulaciones farmacéuticas estériles, libres de disolvente en un proceso que opera en semicontinuo. Además, se ha demostrado que SAS es un proceso apto para la producción de distintas formulaciones farmacéuticas donde se mejoran las propiedades del principio activo.

SAS demostró ser un proceso adecuado para la producción de: micropartículas del composite de 5-Fu y PLLA; la producción de un MOF de propanoato de cobre e INA; y la producción de varios co-cristales (DIF y NIC, CBZ y SAC, y 5-Fu y urea, thiourea, acridina y 4HBA). Las condiciones de operación utilizadas y las solubilidades de los componentes en el disolvente y CO<sub>2</sub> juegan un papel fundamental en la producción de MOFs y co-cristales usando la técnica SAS.

La técnica CSS demostró ser una técnica capaz de lograr la co-cristalización. Un co-cristal de 5-Fu con PZA que no pudo ser obtenido mediante SAS fue obtenido mediante CSS. No obstante, dado que no se consigue una micronización y debido a que el escalado de este proceso es complicado, la técnica CSS no parece ser idónea para la preparación de co-cristales. La expansión rápida de disoluciones supercríticas (RESS) es una técnica que permite micronizar si se va a utilizar el CO<sub>2</sub> como disolvente.

Como futuras líneas de trabajo se proponen: una investigación más detallada de la influencia del diagrama de fase ternario en la co-cristalización usando la técnica SAS, la preparación de MOFs con otros alcanatoatos de cobre mediante SAS para entender la pérdida de contenido orgánico, y la formación de co-cristales dentro de aerogeles, una formulación innovadora que podría combinar la mejora de las propiedades físico-químicas de un co-cristal con la liberación controlada de un aerogel.



# **Chapter 1**

## **Introduction**



# 1 INTRODUCTION

## 1.1 Supercritical fluids

A fluid reaches its supercritical state when temperature and pressure are above the critical point. If we draw a pressure (P) vs. temperature (T) diagram representing the boundaries between the solid, liquid and gas phases (Fig. 1.1), for a pure substance we can observe that as temperature arises, the gas-solid equilibrium line (sublimation curve) reaches the triple point. At this point gas, solid and liquid phases are all in equilibrium. As we further raise the temperature, the liquid-gas equilibrium moves to higher pressures until we reach the critical point. Above this point the vapour-liquid equilibrium curve disappears leading to the supercritical phase. Sometimes the melting curve can merge at very high pressure with the supercritical region leading to an equilibrium curve between the supercritical and the solid phases<sup>1</sup>, in those cases increasing substantially the pressure above the critical value will bring the fluid to the solid phase.

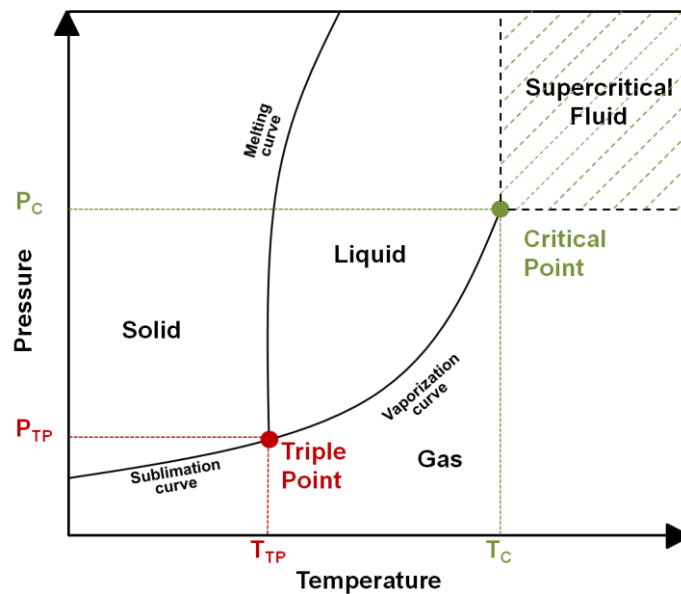


Fig. 1.1 Schematic phase diagram for a pure substance.

A supercritical fluid (SCF) presents physical properties intermediate between those of liquids and gases (Table 1.1).<sup>2</sup> SCFs exhibit gas-like diffusivity and viscosity as well as low surface tension, therefore gas-like mass transfer rates and good penetration into solid matrixes and porous materials, whilst maintaining liquid-like



density and solvating properties. This peculiarity has been used by chemists and engineers to develop and improve numerous processes in the chemical industry.

Table 1.1 Comparison of properties in the gas, supercritical and liquid state.<sup>2</sup>

	Density ( $\text{g}\cdot\text{cm}^{-3}$ )	Diffusivity ( $\text{cm}^2\cdot\text{s}^{-1}$ )	Viscosity ( $\text{g}\cdot\text{cm}^{-1}\cdot\text{s}^{-1}$ )
<b>Gas</b>	$10^{-3}$	$10^{-1}$	$10^{-4}$
<b>SCF</b>	$10^{-1} - 8 \times 10^{-1}$	$10^{-3} - 10^{-4}$	$5 \times 10^{-4} - 10^{-3}$
<b>Liquid</b>	1	$10^{-6}$	$5 \times 10^{-3} - 10^{-2}$

Another important characteristic of SCFs is the lack of an abrupt change in its physical properties when moving from the supercritical phase into the gas or liquid phase. If we observe Fig. 1.1 lowering the pressure isothermally from the liquid phase will move us to the gaseous phase crossing the vaporization curve and leading to an abrupt change in the physical properties. The same abrupt change in the physical properties will be observed if we isobarically raise the temperature to pass from the liquid to the gas region. However, lowering pressure or temperature from the supercritical phase will bring the SCF into the vapour or liquid phase, respectively, without any abrupt change in its physical properties.

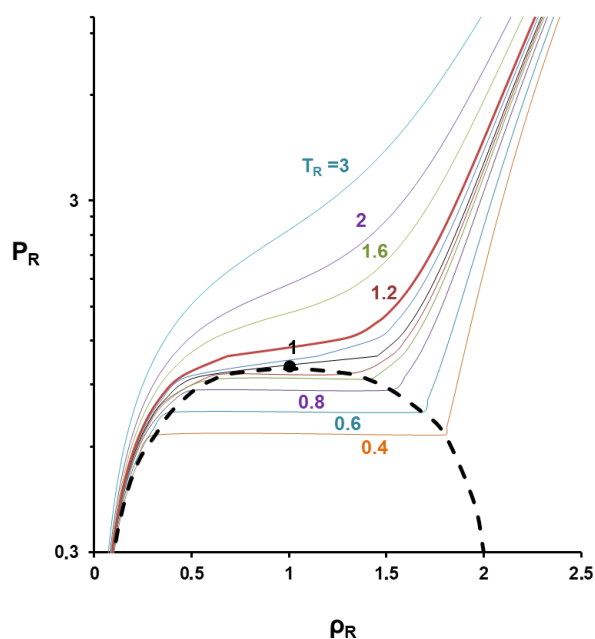


Fig. 1.2 Relationship between reduced pressure ( $P_R$ ) and reduced density ( $\rho_R$ ) at different reduced temperatures ( $T_R$ ) for  $\text{CO}_2$ .<sup>3</sup>

The variation of SCF properties with changes in pressure and temperature can be better observed in Fig. 1.2 where supercritical  $\text{CO}_2$  isotherms are shown in terms of reduced pressure and reduced density.<sup>3</sup> The value of the reduced properties is defined as the ratio between the actual value of the property under consideration and its value

at the critical point. All isotherms below the critical temperature display the same behaviour. As pressure increases, the density of gaseous carbon dioxide increases until we reach the phase transition, then density changes from the low characteristic values from gases to the higher ones of liquids. Afterwards pressure has to be increased significantly in order to achieve an increase in density due to the low compressibility of liquids. If we follow an isotherm above the critical temperature, we can observe that the abrupt change in density characteristic of phase transition does not take place. At temperatures slightly above the critical temperature small changes in pressure or temperature have a marked effect on density. Therefore, in this region we have the capability to change the density of the fluid and therefore its solvation power with slight variations in the operational parameters. As temperature increases further above the critical temperature a bigger increment in pressure is required to raise the density.

Table 1.2 Critical properties of the most commonly used SCFs.<sup>4</sup>

SCF		T <sub>c</sub> (K)	P <sub>c</sub> (MPa)	ρ <sub>c</sub> (g/mL)
<b><i>Inorganic</i></b>				
Carbon dioxide	CO <sub>2</sub>	304.12	7.374	0.468
Water	H <sub>2</sub> O	647.14	22.064	0.322
Nitrogen	N <sub>2</sub>	126.20	3.398	0.311
Nitrous oxide	N <sub>2</sub> O	309.60	7.255	0.454
Ammonia	NH <sub>3</sub>	405.40	11.353	0.235
<b><i>Hydrocarbon</i></b>				
Methane	CH <sub>4</sub>	190.56	4.599	0.163
Ethylene	C <sub>2</sub> H <sub>4</sub>	282.34	5.041	0.214
Ethane	C <sub>2</sub> H <sub>6</sub>	305.32	4.872	0.207
Propene	C <sub>3</sub> H <sub>6</sub>	364.90	4.600	0.228
Propane	C <sub>3</sub> H <sub>8</sub>	369.83	4.248	0.220
n-pentane	C <sub>5</sub> H <sub>12</sub>	469.70	3.370	0.232
n-hexane	C <sub>6</sub> H <sub>14</sub>	507.60	3.025	0.234
Benzene	C <sub>6</sub> H <sub>6</sub>	562.05	4.895	0.305
Toluene	C <sub>7</sub> H <sub>8</sub>	591.75	4.108	0.292
<b><i>Oxygenates</i></b>				
Diethyl ether	C <sub>4</sub> H <sub>10</sub> O	466.70	3.640	0.265
Acetone	C <sub>3</sub> H <sub>6</sub> O	508.10	4.700	0.278
Methanol	CH <sub>4</sub> O	512.64	8.097	0.272
Ethanol	C <sub>2</sub> H <sub>6</sub> O	513.92	6.148	0.276
<b><i>Other Compounds</i></b>				
Chlorotrifluoromethane	CClF <sub>3</sub>	301.84	3.873	0.579
Trichlorofluoromethane	CCl <sub>3</sub> F	471.10	4.472	0.554
Pyridine	C <sub>5</sub> H <sub>5</sub> N	620.00	5.670	0.311

A variety of compounds are used as supercritical fluids for research and industrial purposes. The most commonly used and their critical values are listed in Table 1.2. Some of these solvents present several drawbacks such as toxicity,

corrosive behaviour or a less accessible critical point (which translates in higher operational costs). From this list CO<sub>2</sub> is by far the supercritical fluid most commonly used due to a myriad of reasons. Supercritical CO<sub>2</sub> does not present environmental contamination problems, is inert, non-toxic, non-flammable and non-corrosive, and therefore it is considered a green solvent. It is also easily obtainable at high purities and relatively low prices as a by-product in ethanol and ammonia plants. Supercritical CO<sub>2</sub> also presents interesting transport properties like low viscosity and high diffusivity. The low enthalpy of vaporization of CO<sub>2</sub> near the critical point and its moderate critical temperature and pressure (304.18 K and 7.4 MPa)<sup>5</sup> translate in lower energy requirements. Supercritical CO<sub>2</sub> is easy to remove as it is a gas at ambient conditions (reducing the pressure will be sufficient to separate the CO<sub>2</sub> from the compound of interest). One of the major problems of supercritical CO<sub>2</sub> (associated to its use as a solvent) is its relatively low solvent strength for polar compounds, limiting therefore its extraction applications. This problem is generally overcome by the addition of a small amount of a polar solvent or cosolvent which increases the polarity of the medium and improves the solvation power of CO<sub>2</sub> for polar compounds (cosolvents commonly used are ethanol, methanol, propanol and dichloromethane<sup>6</sup>).

The second most commonly used supercritical fluid is water (SCW). Water critical temperature and pressure are 647 K and 22.060 MPa, respectively.<sup>7</sup> Although these values are quite high and involve greater operational costs, the singular properties of SCW have drawn the attention of researchers and industry. SCW changes from being a polar solvent at ambient conditions to a nearly non-polar fluid at critical and near critical state. Also the dielectric constant reduces its value drastically allowing the solubilisation of hydrocarbons. Main applications of SCW are: coolant in nuclear reactors, supercritical water oxidation of waste effluents, material synthesis and extraction<sup>8</sup>.

## **1.2 Phase diagrams of multicomponent systems involving supercritical fluids**

In all supercritical fluids applications, it is important to understand and have the best possible knowledge of the systems phase behaviour. As the target compound whose extraction is attempted using supercritical technology gets dissolved in the supercritical fluid, or after the addition of a cosolvent, the phase diagram of the mixture may become very complex thus affecting the technical or economic feasibility of the

process. The different phase equilibria that are going to be involved will be strongly influenced by pressure, temperature and composition.

### 1.2.1 Binary mixtures

It is common to start studying binary mixtures and use the knowledge gained to move further in the understanding of more complex mixtures. van Kronynenburg and Scott<sup>9</sup> showed that the van der Waals equation of state was applicable to qualitatively explain the experimentally observed phase behaviour of binary mixtures and classify them in five distinctive types of phase diagrams. A sixth type less commonly observed and not predictable with the van der Waals equation completes the classification.<sup>10</sup> Although ideally the phase behaviour of the mixture should be known, either from experimental data or by application of a thermodynamic model, in reality this is seldomly achieved. Good experimental data are expensive and time consuming, and thermodynamic models show very often discrepancies with experimental data in asymmetric systems.<sup>11</sup> Nevertheless, as remarked previously, the van der Waals equation of state combined with quadratic mixing rules helps to predict qualitatively the phase behaviour of a system at different operational conditions. The understanding of the basic concepts of phase diagrams and the different possible types of phase behaviour is fundamental in supercritical fluid technology. Detailed explanation of the diagrams can be found in the descriptions given by Mc Hugh and Krukoni<sup>12</sup> and de Loos.<sup>13</sup>

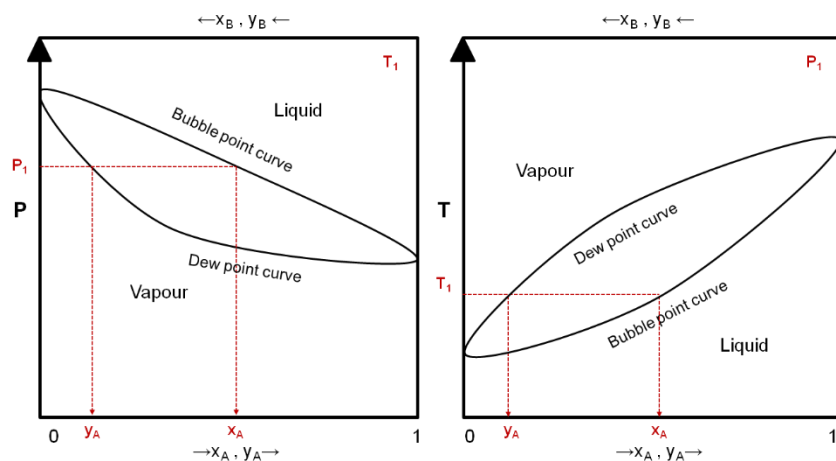


Fig. 1.3 P-x and T-x diagram for a binary mixture with complete miscibility below the critical point.

P-x and T-x diagrams below the critical point of a binary mixture in which the two components are miscible in all proportions in the liquid and gas phases are

represented in Fig. 1.3. In the isothermal P-x diagram at a given pressure  $P_1$  the intersection of a parallel to the composition axis with the lower curve provides the composition of the less volatile compound A in the vapour phase ( $y_A$ ) while the intersection of this line with the upper curve provides the composition of the liquid phase ( $x_A$ ). These two phases are in equilibrium at  $P_1$  and  $T_1$ . Analogous reasoning can be used in the T-x diagram.

Above the critical point of the lighter component ( $C_B$ ) the liquid-vapour equilibrium disappears as it had been observed in Fig. 1.1 and the curves do not merge at the pure component B. The critical point then appears in the P-x or T-x diagrams as a maximum or minimum, respectively (Fig. 1.4). Thus, only a mixture with a given composition will have its critical point at those values of pressure and temperature. For each P, T set the composition at which the critical point is reached and the liquid-vapour equilibrium disappears must be determined. The set of critical points in a P-T diagram defines the so-called critical locus of the mixture.

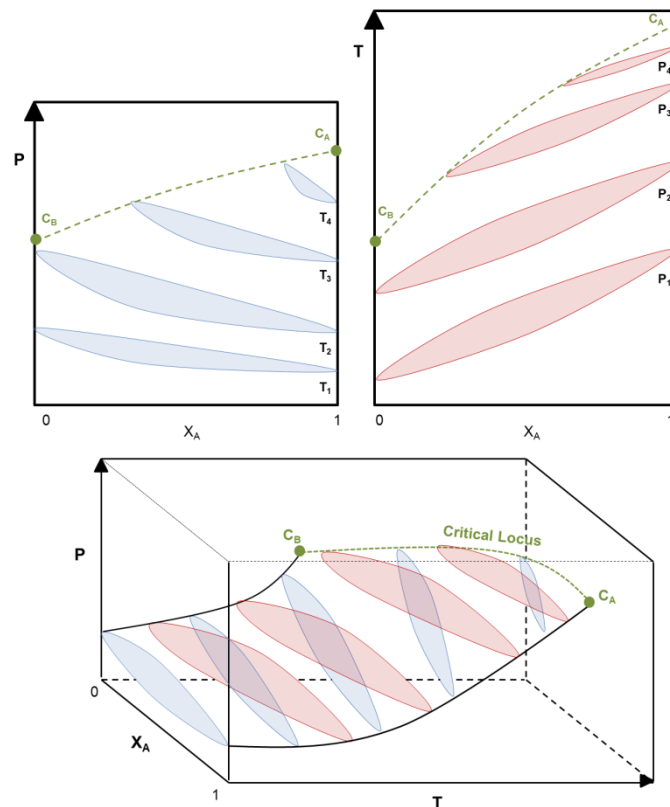


Fig. 1.4 Three dimensional representation of a P-T-x diagram for a two component mixture in which both components are miscible.

As we can see in Fig. 1.4 the critical locus for this simple binary system will connect the critical points of the more volatile compound B ( $C_B$ ) and the heavier

compound A ( $C_A$ ). In both extremes of the diagram corresponding to pure A and B, the vaporization curve of the pure substances is observable, each of them ending in its critical point. The PT projection of the three dimensional diagram is the usual form to represent the different types of phase diagrams. In the case of the studied system shown in Fig. 1.4 (complete miscibility in the liquid and gas phases), this projection will include the vaporization curves of A and B as well as the critical locus. This diagram corresponds to the Type I in the van Konynenburg and Scott classification (see Fig. 1.5).

The second type of phase diagram corresponds to a binary mixture in which there are two liquid phases present in a range of pressure and temperature below the critical points of both components. This will be seen as a liquid-liquid-vapour (LLV) line in the P-T projection of the diagram. As temperature rises, the composition of the two liquid phases in the LLV line approach. The point where this line ends is the so called upper critical end point (UCEP). At temperatures above the UCEP the L-L and L-V region are separated by a homogeneous liquid phase.

If the region of the two liquid phases extends above the critical point of the more volatile compound a type III diagram takes place. The critical line is then divided in two sections. The first one will go from the critical point of the more volatile compound to the UCEP. The second section of the critical line starting at the critical point of the heavier compound reaches high pressures and may exhibit a maximum or minimum in pressure, temperature or both. When temperatures in this critical line section are higher than that of the heavier compound the line is described as a gas-gas critical line.

The fifth type of phase diagram exhibits besides the UCEP a lower critical end point (LCEP). This point is the beginning of a two liquid region. As temperature rises over the LCEP the two liquid region becomes bigger and the difference in the composition of both liquids increases. When temperature rises over the critical value of the more volatile compound the region  $L_1$ -V becomes smaller and it disappears in the UCEP. The critical line will go from the critical point of the more volatile compound to the LCEP and then from the LCEP to the UCEP and then to the critical point of the heavier compound.

The fourth type occurs when the two liquid-liquid phase region described for type II and type V take place.

Type VI is found in binary mixtures where specific chemical interactions take place (for example self association through hydrogen bonds in the system

water-2-butanol). This type displays two critical lines, one connecting the critical points of the pure substances, and another one that connects a LCEP with an UCEP.

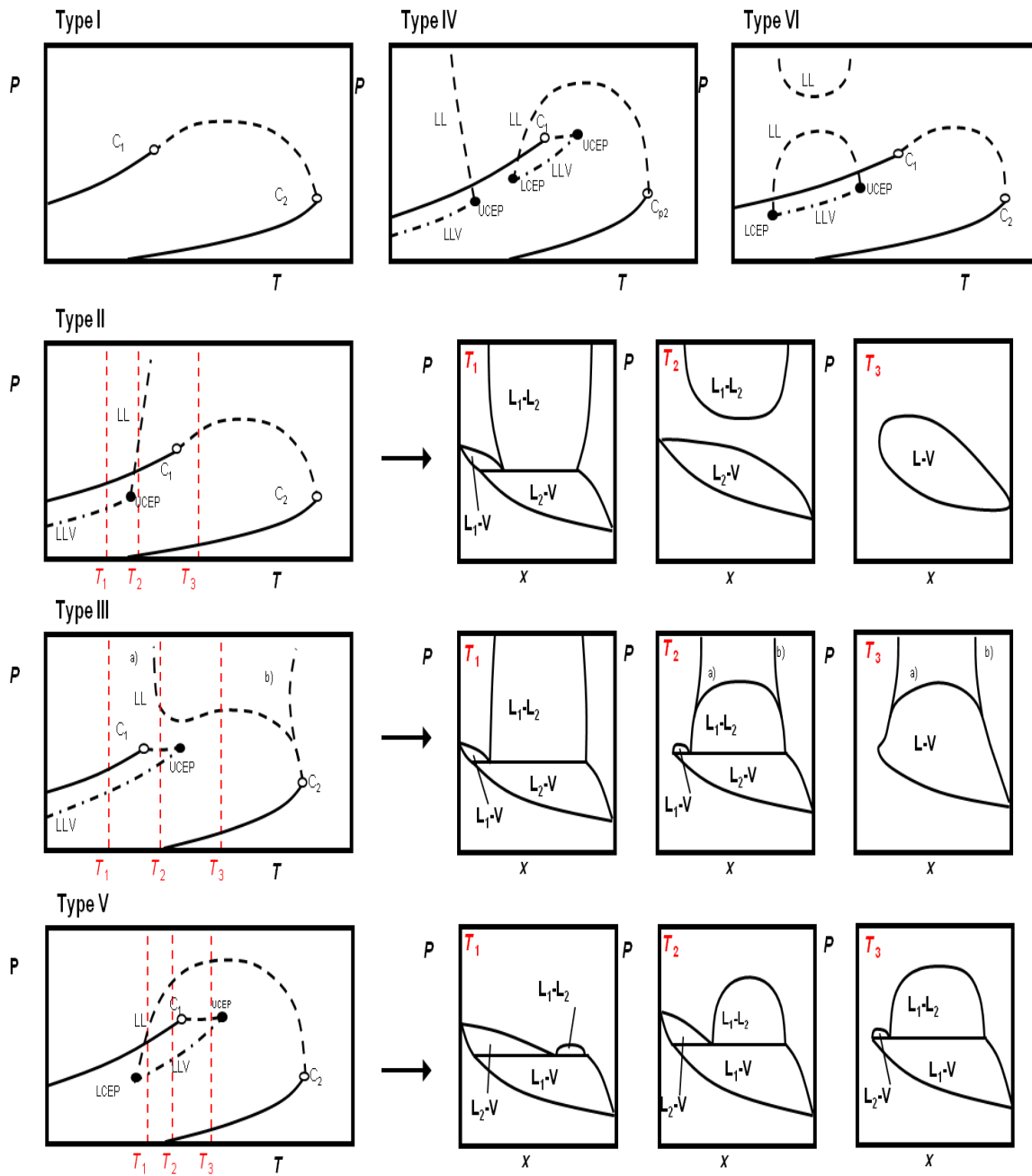


Fig. 1.5 Six types of phase behaviour according to the van Konynenburg and Scott classification<sup>9</sup> in binary fluid systems. Points  $C_1$  and  $C_2$  correspond to the critical points of the pure components. Liquid (L); vapour (V); upper critical end point (UCEP); lower critical end point (LCEP).

### 1.2.2 Ternary mixtures

In ternary systems the critical locus will be a surface that joins the critical points of the pure components. In the simplest case (type 1 behaviour of the binary systems)

this surface may be continuous. In other more complex systems the surface may present discontinuities and holes as it has been observed in the system formed by 1-heptanol, pentadecane and  $\text{CO}_2$ <sup>14</sup>

Some processes using supercritical fluids require the use of multicomponent mixtures formed by three or more components. For example, in the supercritical antisolvent (SAS) technology that will be further detailed in this thesis. In this process a solute dissolved in an organic solvent precipitates from the solution upon addition of  $\text{CO}_2$  to the system. Although the solute or solutes to be precipitated may influence the phase diagram, generally in the SAS technology their presence is not taken into account in the analysis of the vapour-liquid phase equilibria. A requisite for the application of the SAS technology is that the solute should not be soluble in the organic solvent- $\text{CO}_2$  mixture, and therefore the system is usually considered as a pseudo-binary equilibrium.<sup>15</sup>

Sometimes the target solute or mixture of solutes to be precipitated may require more than one organic solvent, leading therefore to a complex mixture of  $\text{CO}_2$ , organic solvents and solutes. The analysis of the critical locus of the mixture may be again simplified if we consider negligible the effect of the solute in the system and by considering the mixture of  $\text{CO}_2$  and organic solvents as a set of pseudo-binary systems. An example of the evolution of the critical point in the ternary system  $\text{CO}_2$ , dimethylsulfoxide (DMSO) and ethanol (solvents commonly used in the SAS processing of pharmaceuticals) with the DMSO/ethanol ratio is shown in Fig. 1.6 adapted from Chui et al.<sup>16</sup>

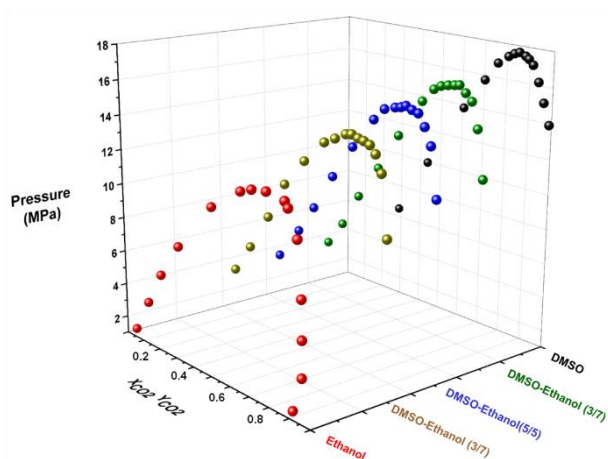


Fig. 1.6 VLE phase diagram at 348.4 K of  $\text{CO}_2$ -ethanol<sup>17</sup> and at 348.15 K of  $\text{CO}_2$ -DMSO, and of  $\text{CO}_2$ -[DMSO/ethanol] for DMSO/ethanol molar ratios: 3/7; 5/5 and 7/3.<sup>18</sup>



Some reports highlight that the solute effect on the phase diagram must be considered when operating at high temperatures and high solute concentrations. Campardelli et al.<sup>19</sup> studied the influence of cefonicid in the phase equilibria for the DMSO-CO<sub>2</sub> system. Operating at constant temperature (313 K), they observed a change in the shape of the vapour-liquid equilibrium curve (VLE) when the concentration of cefonicid was of 90 mg/mL. Same authors have also investigated the effect of Polyvinylpyrrolidone (PVP) in the ethanol-CO<sub>2</sub> and ethanol-acetone-CO<sub>2</sub> systems<sup>20</sup>. Higher PVP concentrations shifted the mixtures critical point to higher pressure. Han and Kang<sup>21</sup> also reported the variation of the phase diagram type in the ethanol-CO<sub>2</sub> system with the addition of the drug arbutin.

As a simple rule the presence of a solute will move the critical point of the mixture towards higher pressures and therefore it is advisable to operate at pressures relatively higher than the critical pressure of the solvent-CO<sub>2</sub> system<sup>22</sup>.

### **1.3 Supercritical fluid technology in the pharmaceutical industry**

First large-scale applications of supercritical fluid technology were coffee decaffeination and hops resin extraction<sup>23</sup>. Since then supercritical fluid technology has been applied in the development of many industrial processes<sup>24</sup> trying to minimize environmental impact, reduce energy consumption, avoid the use of organic solvents (thus reducing toxic residues), and enhance the quality of the final product.

Apart from these mentioned advantages, in the pharmaceutical industry supercritical fluids are a useful tool to achieve crucial aspects of product development, in particular the need of products with controlled particle size and polymorphic purity<sup>25</sup>,<sup>26</sup>. Properties such as bioavailability and dissolution rate are strongly influenced by the size of the particles. The shelf life, stability and performance of a drug may be conditioned by its polymorphic form and crystallinity. The conventional techniques used in the micronization of pharmaceuticals present several drawbacks: milling processes and freeze drying consume a lot of energy and produce a broad particle size distribution (PSD); spray drying requires elevated temperatures and may damage the product due to thermal stress; liquid antisolvent crystallization may contaminate the particles with organic solvents or other toxic substance requiring several post-purification steps. For these reasons several supercritical techniques for the processing and micronization of pharmaceuticals have been developed. A comprehensive review

of the use of supercritical fluid based techniques for the production of drug nanoparticles and nanocrystals has been recently published by Padrela et al<sup>27</sup>. In these techniques the supercritical fluid can be used as:

- Solvent: rapid expansion of supercritical solutions (RESS), RESS with solid cosolvent (RESS-SC), RESS into liquids (RESSOLV) and co-crystallization with supercritical solvent (CSS)
- Cosolvent or solute: particles from gas saturated solutions (PGSS), PGSS-drying, concentrated powder form (CPF) and depressurization of expanded liquid organic solutions (DELOS).
- To generate the solution nebulation: carbon dioxide assisted nebulization with a bubble dryer (CAN-BD) and supercritical fluid assisted atomization (SAA).
- Extraction fluid: supercritical fluid extraction of emulsions (SFEE).
- As an antisolvent: gas antisolvent (GAS), supercritical antisolvent (SAS).

A brief explanation of the most important techniques used in the pharmaceutical industry follows with an especial emphasis in the SAS technique used in this thesis.

### 1.3.1 Micronization techniques using CO<sub>2</sub> as solvent

#### 1.3.1.1 Rapid expansion of supercritical solutions (RESS)

This supercritical technique was patented in 1986 by Smith and Wash<sup>28</sup> shortly after Kurkonis published the first experimental results<sup>29</sup>. It involves a two stage process (Fig. 1.7). In a first stage the solute that is going to be processed is dissolved in a supercritical fluid (generally CO<sub>2</sub>) at a given temperature  $T_s$  and pressure  $P_s$  until saturation. Then it is heated to the desired pre-expansion conditions ( $T_0$ ,  $P_0$ ) and sent through a nozzle to an expansion chamber where the fluid depressurizes to the desired value ( $T_f$ ,  $P_f$ ). This pressure drop generates a large decrease in the solvent power of the fluid and the precipitation of the solute. The high pressure difference between  $P_0$  and  $P_f$  produces a high speed jet as the solute-supercritical fluid solution leaves the nozzle. This translates in high supersaturations that are transmitted rapidly through the fluid and produce small particles with uniform PSD.

The mechanisms involved in the precipitation using the RESS technique have been described in detail in several publications by professor Türk<sup>30-32</sup>. Particle size and morphology may be controlled by changing the operational conditions but caution must

be given to avoid the formation of liquid droplets. Therefore, knowledge of the solute melting point variation with pressure, and the phase behaviour of the binary solute-CO<sub>2</sub> mixture is required.<sup>33</sup> Once the jet leaves the nozzle the density of the supercritical fluid decreases rapidly as mentioned earlier and supersaturation leads to particle nucleation. These nuclei then grow by coagulation (collision of particles) and condensation (deposition of molecules on the surface). CO<sub>2</sub> turns into a gas at lower pressure and it does not leave any residue.

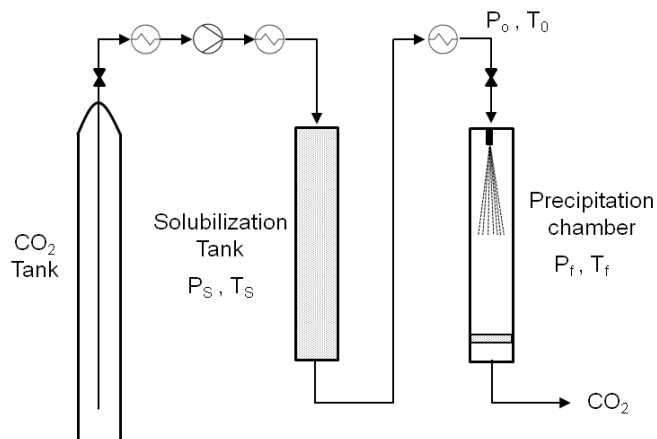


**Fig. 1.7 Schematic diagram of the rapid expansion of supercritical solutions (RESS) process. P and T represent pressure and temperature, respectively at: s (solubilisation tank), 0 (pre-expansion), and f (precipitation chamber).**

RESS is therefore a technique capable of producing solvent-free particles in a narrow range of PSD that do not require post-purification steps. The process can be performed at moderate temperatures making it suitable for the processing of thermal-sensitive drugs and carriers. The variation of morphology and particle size is possible through changes in the operational parameters and its application for small scale is relatively simple. However, the technique also presents some important drawbacks that limit its use in the pharmaceutical processing. Due to their polarity pharmaceuticals often show a very low solubility in supercritical CO<sub>2</sub> (the main solvent used in RESS). This means that large amounts of SCF-solute need to be processed to obtain relatively small amounts of product, and even in favourable situations the production is limited. Furthermore, the scaling up of the process is challenging due to possible nozzle blockages and the size of the formed microparticles is often compromised due to their adhesive nature and agglomeration. For these reasons some variations of the RESS technique have been developed.

### **1.3.1.2 Rapid expansion of supercritical solutions with solid cosolvent (RESS-SC)**

To overcome the problem of pharmaceuticals low solubility in supercritical CO<sub>2</sub>, the use of cosolvents has been proposed. Liquid cosolvents can only be used in small amounts to avoid the dissolution of the particles in the precipitation chamber. Thakur and Gupta<sup>34-36</sup> used menthol as a solid cosolvent to enhance the solubility of the active pharmaceutical ingredient (API) in supercritical CO<sub>2</sub>. They obtained up to 28-fold solubility enhancements what can substantially increase the production of the process. Menthol can afterwards be easily removed by sublimation avoiding the associated problem of liquid cosolvents previously mentioned. Other authors have also obtained good results with menthol<sup>37</sup> and vanillin.<sup>38</sup> The most important features that the solid cosolvent should have are:<sup>34</sup>

- Enhance the solubility of the target solute in supercritical CO<sub>2</sub>.
- Good solubility in supercritical CO<sub>2</sub>.
- Be solid at the nozzle exit temperature (usually 278 to 303 K).
- High vapour pressure to allow its removal through sublimation.

### **1.3.1.3 Rapid expansion of supercritical solutions into liquid solvents (RESOLV)**

This modification consists in the expansion taking place in a liquid solution that may contain stabilizing agents like surfactants. The idea behind is to avoid particle growth in the precipitation chamber due to collision. This variation of the RESS technique is also called RESSAS (rapid expansion of supercritical solutions into an aqueous solution) when the liquid solution is water and a surfactant is added. The surfactants stabilize the small particles formed hindering agglomeration and flocculation. The chosen surfactant should be active at the drug-water interface and non-active at the CO<sub>2</sub>-drug interface<sup>39</sup>. Türk and coworkers<sup>31, 32</sup> have pointed out that particle size depends not only on the RESS operational conditions and solubility of the API in supercritical CO<sub>2</sub>. The adsorption kinetic (i.e. the speed at which the surfactant molecules adsorb to the solute) and the solubility of the drug in the aqueous surfactant solution also play a key role in particle size.

### **1.3.1.4 Co-crystallization with supercritical solvent (CSS)**

This technique was developed by Padrela et al<sup>40, 41</sup> and uses a supercritical fluid as the medium in which two components interact to form a co-crystal. A more detailed description of this technique is given in section 1.8 of this introduction.

### 1.3.2 Micronization techniques using CO<sub>2</sub> as cosolvent or solute

#### 1.3.2.1 Particles from gas saturated solutions (PGSS)

This method developed and patented by Weidner et al.<sup>42, 43</sup>, conversely to the RESS technique does not use the solvent properties of supercritical CO<sub>2</sub> to generate the microparticles. The PGSS uses the large cooling produced by the Joule-Thomson effect when CO<sub>2</sub> is depressurized from a supercritical pressure to ambient conditions to generate fine particles.

In a first step CO<sub>2</sub> is dissolved in a melted solid producing a reduction in its viscosity. The gas saturated melt is then conducted to a depressurization chamber through a nozzle. The expansion will cause the vaporization of the dissolved CO<sub>2</sub> and the volume increase disintegrates the liquid into tiny droplets<sup>44</sup> which solidify rapidly due to the associated cooling effect (Fig. 1.8).

This technique is suitable for compounds where the SCF (usually CO<sub>2</sub>) has a good solubility. In this case, the compound may also swell with the addition of the SCF. Polymers are usually suitable for this technique and as they are common carriers in the pharmaceutical industry, composites of API and polymers can be produced.<sup>45</sup> For amorphous polymers, CO<sub>2</sub> also causes a strong decrease of the glass transition temperature of the polymer facilitating its melting at much lower temperatures than those required at atmospheric pressure.<sup>46</sup>

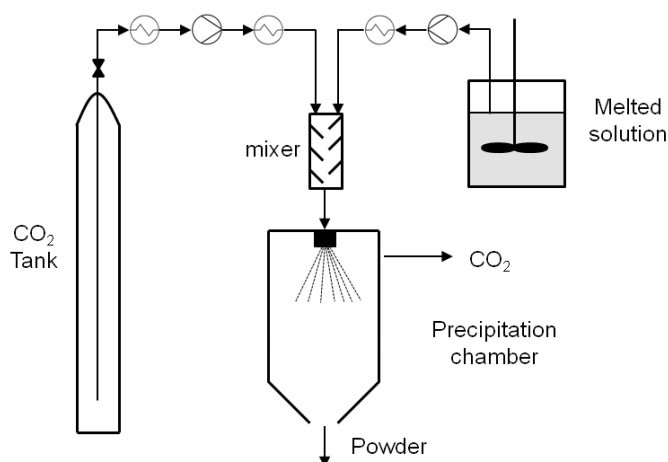


Fig. 1.8 Schematic diagram of the particles from gas saturated solutions (PGSS) process.

Analogously to RESS, the PGSS process does not involve the use of organic solvents, and particles may be obtained employing CO<sub>2</sub> green solvent only. In PGSS

the solute does not have to dissolve in supercritical CO<sub>2</sub> and therefore the high pressure requirements of RESS to generate a dense supercritical phase are not necessary. This means that PGSS can work at much lower pressures, thus, reducing operational costs. The main drawback is the thermal and mechanical stress at which drugs and carriers are exposed and that might rule-out this technology for certain products.

Several variations of the PGSS process have been developed because of the reduced consume of CO<sub>2</sub> compared to other supercritical processes and the lower pressure requirements. Moreover, large scale applications of the PGSS process are already in operation<sup>47, 48</sup>. A brief presentation of the more relevant PGSS developments follows.

### **1.3.2.2 PGSS drying**

This is a modification of the PGSS process developed by Meterc et al.<sup>49</sup> to dry aqueous compounds. The PGSS drying enables the processing of pharmaceuticals and carriers at relatively gentle operational conditions. Although high temperatures, typically of 373 to 393 K, are reached, drugs are exposed to these temperatures only for a short period of time in the static mixer prior to expansion and therefore, the thermal degradation that often occurs in spray drying is avoided. The process is carried out in a closed inert system with CO<sub>2</sub> avoiding product contamination. As in the PGSS process, the SCF is used to saturate a liquid phase. In this case the phase is an aqueous solution. The saturated liquid is sent through a nozzle to the precipitation chamber at ambient pressure and at a temperature over the dew line of the CO<sub>2</sub>-H<sub>2</sub>O mixture. The atomization takes place due to the combination of two different mechanisms<sup>50</sup>: flash-boiling and atomization. When a superheated liquid is expanded through a nozzle there is a partial evaporation of the liquid generating gas bubbles that enhance liquid atomization. On the other hand, the mixture that expands through the nozzle is a mixture of liquid and gas, the expansion of these gas bubbles produces the atomization. Therefore, atomization depends directly to the amount of CO<sub>2</sub> in the liquid. Variation of parameters that lead to an increase of CO<sub>2</sub> in the liquid phase will produce particles of smaller size.

### **1.3.2.3 Concentrated powder form (CPF)**

This method was patented by Weidner et al.<sup>51</sup> to produce powders with a high content in liquids (up to 90 wt.%)<sup>52</sup>. It is mainly used to produce powders rich in liquid extracts of essential oils. This enables the dosing of essential oils in a powder form with

longer shelf life and standardized quality<sup>48</sup>. The saturated solution of a liquid (e.g. essential oil) with SCF is sprayed in the expansion chamber. Simultaneously a solid carrier material is blown into the chamber by means of an inert gas resulting in a high turbulence zone and intensive mixing. The liquid adsorbs to the surface of the carrier (and in the pores). Eventually liquid bridges between carrier particles form and aggregation occurs. This leads to a powder with a high content in liquid that can be collected at the bottom of the expansion chamber. Due to the reduction in viscosity generated by the saturation with the SCF this procedure can be used to spray liquids of high viscosity. Moreover, as very fine droplets are produced in the expansion, non-wetting liquids can fill the carrier pores. The maximum liquid to carrier ratio depends mainly on the physical and chemical properties of the carrier. In principle low bulk densities of the carrier can produce high liquid loadings.

#### **1.3.2.4 Depressurization of expanded liquid organic solutions (DELOS)**

This technology developed and patented by Ventosa et al.<sup>53, 54</sup> is used to micronize a solute from an organic solution in a batch operating process. In DELOS a solution of the target solute in an organic solvent is saturated with a SCF (the SCF, generally CO<sub>2</sub>, has a cosolvent effect). Then, the solution is depressurized through a nozzle in a precipitation chamber causing a rapid cooling and a homogeneous supersaturation of the solution. As a consequence, crystallization of fine particles with a narrow size distribution takes place. In this process the SCF is used as a cosolvent and is completely miscible with the organic solution at the operational conditions (pressure and temperature at which the saturation of the solution solute-organic solvent with SCF occurs). This means that we need to operate under the saturation conditions of the solute in the solute-organic solvent-SCF solution to avoid the precipitation of the solute prior to the expansion chamber. The crucial parameters that affect particle size have been identified by Ventosa et al.<sup>54</sup> Pressure before expansion does not have a significant effect in particle size because initial pressure does not affect the temperature decrease significantly. Thus, lower pressure values may be employed reducing operational costs. Also stirring of the system prior to depressurization is not necessary. The most important parameter in the system is the amount of CO<sub>2</sub> employed. Reducing the ratio of CO<sub>2</sub> relative to saturation in the mixture reduces the yield, and increasing the ratio will give a stronger temperature decrease. The ratio can only be increased until a certain amount though, as in some cases there is a threshold ratio from then on the SCF stops behaving as a cosolvent and starts acting as an antisolvent.

An important DELOS feature is its capability to produce new crystal forms of the same API or polymorphs.<sup>55</sup> New polymorphs generate interest in the pharmaceutical industry due to its different pharmacokinetics and physicochemical properties. A more detailed explanation of polymorphism can be found later in this introduction.

### **1.3.3 Micronization techniques using CO<sub>2</sub> as nebulization agent**

#### **1.3.3.1 Carbon dioxide assisted nebulization with a bubble dryer (CAN-BD)**

CAN-BD was developed and patented by Sievers et al.<sup>56, 57</sup> This micronization technique was developed to process solutes that are soluble in water and non soluble in supercritical CO<sub>2</sub> such as proteins. The solute is dissolved in water and mixed with supercritical CO<sub>2</sub> in a low-dead-volume mixing tee (less than 1 µL) forming an emulsion. The emulsion is sent through a capillary tube to a precipitation chamber where the nebulization occurs. The expansion of the dissolved supercritical CO<sub>2</sub> in the droplets enhances the atomization. In the precipitation chamber heated N<sub>2</sub> is used to dry the droplets.

#### **1.3.3.2 Supercritical fluid assisted atomization (SAA)**

This process is a variation of the CAN-BD process and was developed by Reverchon<sup>58</sup> to avoid the solute precipitation in the capillary and to enhance the mixing of both streams. The mixing tee is substituted by a thermostated packed tower where the equilibrium solubilisation of CO<sub>2</sub> in the liquid is reached. The saturated liquid is expanded by means of a thin wall injector to avoid the capillary blockage. The process is called supercritical enhanced atomization (SEA)<sup>40</sup> when the mixing device is replaced with a smaller one (the solution does not have to be saturated) and a coaxial nozzle is added.

#### **1.3.4 Supercritical fluid extraction of emulsions (SFEE)**

This technology was developed and patented by the Ferro corporation<sup>59</sup> and exploits the advantages of the emulsion processes to produce submicrometric particles with the posterior extraction of the organic solvents using supercritical fluids. In a typical SFEE process first an emulsion of the solute and the coating material (generally biopolymers) dissolved in an organic solvent is created in a water-surfactant medium. The surfactant acts as a stabilizer and avoids the aggregation of the micelles in the described oil in water (o/w) emulsion. It is possible to use different emulsions like oil in oil (o/o), multiple emulsions (e.g. w/o/w) or suspensions to encapsulate hydrophilic or



lipophilic compounds. Then the extraction of the organic solvent is performed using a supercritical fluid (generally  $\text{CO}_2$ ). The extraction of the organic solvent can be carried out in discontinuous or in continuous using a packed tower<sup>60</sup>. In the continuous operation the emulsion is fed from the top of the column and supercritical  $\text{CO}_2$  is fed in countercurrent from the bottom. The continuous operation reduces the amount of solvent required, increases the production capacity and enables lower residual organic solvent concentrations in the raffinate.<sup>61</sup>

### 1.3.5 Micronization techniques using $\text{CO}_2$ as antisolvent

#### 1.3.5.1 Gas antisolvent (GAS)

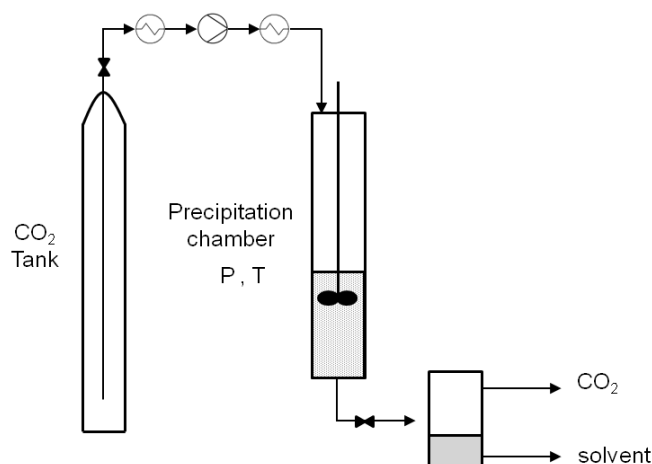


Fig. 1.9 Schematic diagram of gas antisolvent (GAS) process.

This technology uses the properties of the supercritical fluid as an antisolvent. The process operates in discontinuous and the solute whose micronization is desired is firstly dissolved in an organic solvent and placed in a vessel. The vessel is then pressurized with a SCF that has a good solubility with the organic solvent and is a bad solvent of the solute until the desired pressure ( $P_G$ ) is reached. The saturation of the organic solvent with the SCF decreases the solvent power of the liquid mixture causing supersaturation, i.e., the solution contains more dissolved solute than the amount that can be dissolved, and precipitation of the solute takes place. The flow of SCF is continued (maintaining the pressure in the vessel) for a certain amount of time to ensure the complete removal of the solvent. The advantage of using the SCF instead of a liquid antisolvent derives in the good solubility of the SCF in the liquid phase (e.g.  $\text{CO}_2$  in organic solvents at relative moderate pressures) and the favourable transport properties of SCFs that give as a result a quicker mixing and supersaturation.

Moreover, CO<sub>2</sub> is easily removed by depressurization. Mechanical stirring may be necessary when larger volumes are processed (Fig. 1.9).

The key parameter in the GAS technique is the volumetric expansion of the organic solvent. Lower solvent density will generally reduce its solvation power. The classical expression of volumetric expansion given by Kordikowski et al.<sup>62</sup> showed nearly identical expansion curves for different solvents when plotted against CO<sub>2</sub> molar fraction. This fact would imply that the volumetric expansion was the same for the different solvents at a given CO<sub>2</sub> molar fraction and therefore the solubility of the solute to micronize in the solvent was the limiting factor in the crystallization process. De la Fuente et al.<sup>63, 64</sup> adapted the definition of volume expansion to take into consideration the volumetric behaviours of the different solvents for a given antisolvent and considered only molar volumes of the liquid phase of the mixture and of the pure solvent (eq. 1. 1).

$$\frac{\Delta v}{v} = \frac{v_L(T, P, x_1) - v_2(T, P_0)}{v_2(T, P_0)} \quad \text{eq. 1. 1}$$

Where  $v_L$  is the molar volume of the liquid phase of the mixture at a certain temperature (T) and pressure (P) and  $x_1$  represents the molar fraction of antisolvent in the mixture.  $v_2$  is the molar volume of the pure solvent at the same temperature (T) and a reference pressure ( $P_0$ ; usually atmospheric pressure). This expression indicates that positive and negative values of the relative expansion may occur (notice that the total number of moles increases upon CO<sub>2</sub> addition). This definition has been proposed by the authors to select the optimum combination of the solvent-antisolvent mixture,<sup>63, 64</sup> pressure and temperature for the GAS process. The optimum operation pressure will lead to the nearly complete precipitation of the solute. This optimum value is coincident with the pressure where the curve of the relative molar volume change ( $\Delta v/v$ ) according to eq. 1. 1 reaches a minimum.<sup>64</sup> Temperatures close but below the critical temperature of the antisolvent showed a sharper drop in the concentration of solute in the liquid phase leading therefore to a quick and homogeneous precipitation.

### 1.3.6 Supercritical antisolvent (SAS)

This is the main technique studied in this thesis. Basically is an adaption of GAS to a semicontinuous operation (Fig. 1.10). The solute or solutes to be micronized are dissolved in the desired solvent and injected through a nozzle to a precipitation chamber set to the desired pressure and temperature in which supercritical CO<sub>2</sub> flows

continuously. When the solute-solvent mixture atomized drop enters in contact with the supercritical  $\text{CO}_2$  in the precipitation chamber, the latter diffuses in to the solution producing, as in the GAS technique, a volumetric expansion of the solvent, and at the same time, the solvent evaporates from the atomized drops into the antisolvent. This two way mass transfer process produces a fast supersaturation and the precipitation of the solute<sup>65</sup>. This fast supersaturation generally leads to small particles with a narrow PSD. The precipitated solute is retained in a frit at the bottom of the chamber and the solvent- $\text{CO}_2$  mixture is sent to a gas-liquid separator to recover the solvent. After the desired amount of solution has been processed the chamber is purged with supercritical  $\text{CO}_2$  to remove any rests of solvent. The requirements for a successful SAS micronization are the complete miscibility of  $\text{CO}_2$  and the organic solvent and the insolubility of the solute in the  $\text{CO}_2$ -organic solvent mixture at the precipitation conditions.

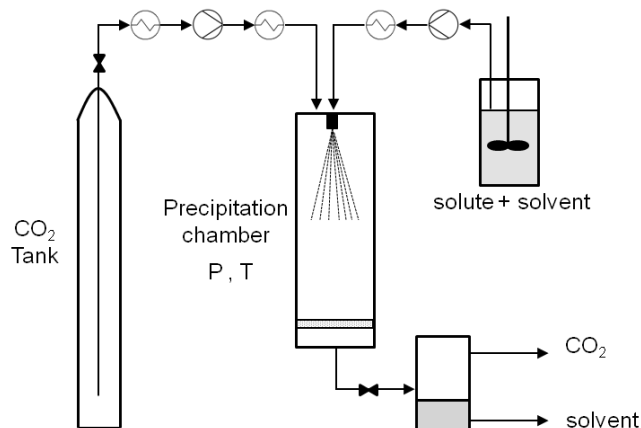


Fig. 1.10 Schematic diagram of the supercritical antisolvent process (SAS).

There are several process parameters involved in the SAS technology that affect the characteristics of the precipitate: pressure, temperature, solute concentration, flow rate of solution and supercritical  $\text{CO}_2$ , molar fraction of  $\text{CO}_2$ , choice of solvent, etc. The interpretation of results is complicated due to the complex interaction between high-pressure vapour liquid equilibria, fluid dynamics, mass transfer and nucleation and growth processes. This interaction makes it difficult to isolate a singular phenomenon as being responsible for the particle characteristics. Several research groups have attempted the analysis and modelling of the SAS process or parts of it and some interesting findings are detailed in the following paragraphs.

An analysis of mass transfer in the supercritical antisolvent process at subcritical and supercritical conditions was performed by Werling and Debenedetti.<sup>65, 66</sup>

Considering the solvent and antisolvent completely miscible at conditions over the critical point of the mixture (surface tension equals zero) a droplet radius was defined based on the density difference between the solvent-rich and antisolvent rich regions. The authors studied the toluene-CO<sub>2</sub> system and simplified the process by considering the droplet stagnant. They concluded that when operational conditions imply a higher density of the solvent phase than that of the antisolvent, droplets will swell, whilst at conditions where the density of the antisolvent is greater than that of the solvent droplets will shrink (Fig. 1.11). Later Elvasorre et al.<sup>67</sup> included the presence of a fictitious solute to the model.

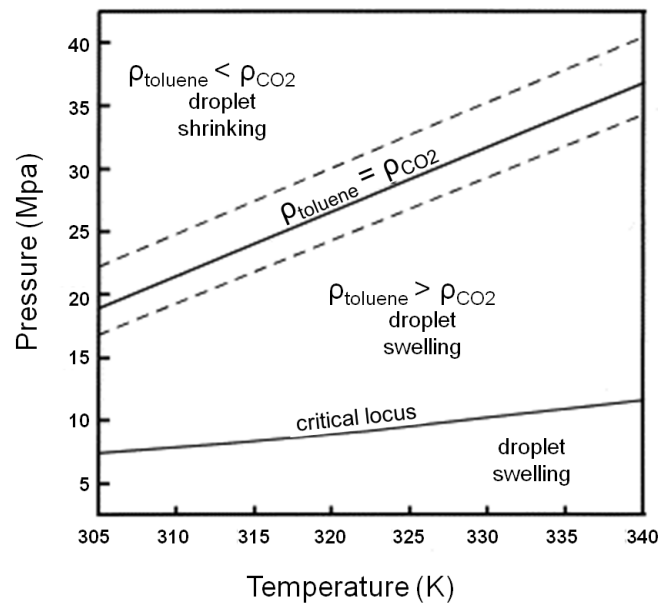


Fig. 1.11 Effect of operating temperature and pressure on droplet behaviour. Figure adapted from Werling and Debendetti<sup>66</sup> The CO<sub>2</sub>-toluene critical locus and the conditions for which densities of toluene and CO<sub>2</sub> are coincident are identified.

The influence of the hydrodynamics in the SAS process has also been investigated by several researchers. Lengsfeld et al.<sup>68</sup> and Dukhin et al.<sup>69</sup> showed that when a liquid jet is fed into a supercritical fluid the vanishing of the dynamic surface tension is not instantaneous. They observed two jet modes (liquid jet and gas-like jet). At conditions below the critical point of the mixture classical jet break theory was applicable and a liquid jet was formed, when conditions were slightly over the critical point of the mixture jet break-up into droplets still took place but at conditions further above the critical point of the mixture the surface tension equalled zero before jet break-up and a gas-like jet was formed.

An interpretation of nucleation and growth of particles in a supercritical CO<sub>2</sub> antisolvent process has been given by Bristow et al.<sup>70</sup> They measured supersaturation

as the defining parameter for nucleation and rapid post-nucleation growth during jet mixing in the ethanol-paracetamol-CO<sub>2</sub> system. At conditions below the mixture critical point the nucleation and precipitation and growth are confined in the solvent rich phase and agglomeration of particles was found and explained due to the precipitation of particles in shrinking ethanol droplets. At conditions above the critical point of the mixture, morphology changed from a spherical to a prismatic one, and the precipitation behaviour in the miscible region was assumed to be similar to that of liquid solution crystallization. Different supersaturation mechanisms were proposed by Dukhin et al.<sup>71</sup> First mechanism is the result of the decrease of the solute equilibrium concentration in the droplet when the antisolvent concentration grows (volumetric expansion). The second is due to the shrinking of the droplet, the solute equilibrium concentration remains constant but the solute concentration increases due to the evaporation of the solvent.

A numerical modelling of the SAS process was proposed by Martín and Cocero.<sup>72</sup> The hydrodynamics and mass transfer calculations considered completely miscible fluids under turbulent mixing and turbulent diffusion. Particle nucleation was presumed homogeneous and growth was a result of coagulation and condensation. The model was compared to results in the SAS precipitation of ascorbic acid dissolved in ethanol and  $\beta$ -carotene dissolved in dichloromethane. Although the model failed to predict the particle size and morphology of the precipitated particles, it predicted correctly the trends in particle size with operational parameters.

Several interesting computational fluid dynamic (CFD) models have been also developed.<sup>73, 74</sup> Cardoso et al.<sup>73</sup> incorporated the effects of buoyancy and of the excess volumes of solvent-antisolvent mixtures to their calculations. The model allowed the authors to identify problems with mixing inside the precipitation chamber and a different chamber geometry (feed of CO<sub>2</sub> from the bottom of the chamber) was proposed for systems in which the excess volume is negative. The same experimental data of the system minocycline-ethanol from the latter authors was used by Erriguible et al.<sup>74</sup> to investigate the effects of injection velocity and concentration in the 3D distribution of solute concentration, supersaturation and particle size using an unsteady turbulent model and a 3D simulation. Their results indicate that higher concentration induces a raise in the attainable supersaturation and particles become smaller whilst velocity of injection had a smaller impact. Existing models to the best of our knowledge present no quantitative results about particle size (or have been applied to a very limited set of experimental evidences) and do not predict possible changes in particle morphology. As mentioned earlier the modelling of the SAS process is challenging due to the large

number of operating parameters and their influence in several phenomena involved in the process. The interaction between these parameters makes it difficult to interpret the results and identify the main mechanisms determining particle morphology and size.

Clercq et al.<sup>75</sup> have investigated the influence of solvent, solute concentration, and flow rates (CO<sub>2</sub> and solution) in the polymorphism and macromorphology of sulfathiazole (SFZ) precipitated by SAS. All experiments were carried at 313 K and 10 MPa. They reported solvent selection as a key factor in the polymorphic outcome of SFZ. Similar to conventional crystallization, different solvents will imply different solute–solvent interactions and different conformations of the solute in solution, that could lead to different polymorphs. They observed that higher concentrations of SFZ, i.e., higher supersaturation of the injected solution and therefore a faster nucleation, lead to the less stable polymorph I. CO<sub>2</sub> molar fraction in the precipitation chamber will also affect the supersaturation and lower molar fractions will lead to lower supersaturations. In the studied conditions they observed that higher solution flow rates (higher Reynolds and therefore better mixing conditions), lead to the less stable form I whilst the effect of the CO<sub>2</sub> flow rate was neglectable.

Reverchon et al.<sup>15, 76</sup> proposed a comprehensive explanation for the mechanisms involved in the SAS process that lead to different particle size and morphology. A key factor determining the characteristics of the obtained particles will be the relation between the two distinctive times introduced by Dukhin et al.<sup>71</sup> i.e. the jet break-up time  $t_{jb}$ , and the time for dynamic surface tension vanishing  $t_s$ . The  $t_{jb}$  quantifies the time elapsed between the exit of the nozzle and the break-up of the jet (transition from laminar to turbulent flow) and  $t_s$  is the time required for vanishing the dynamic surface tension between the injected liquid and the CO<sub>2</sub> to vanish. If  $t_{jb}$  is smaller than  $t_s$  the jet breaks-up into droplets due to the surface tension. On the contrary, if the dynamic surface tension vanishes before jet break-up a gas-like mixing will take place.

When operating below the critical point of the mixture (i.e. in the two phase zone) the surface tension does not disappear and the liquid jet breaks into micrometric droplets inside the precipitation chamber. Mass transfer from CO<sub>2</sub> into the droplet and from solvent into the CO<sub>2</sub> rich phase occurs. The precipitation takes place therefore in a confined droplet (liquid phase) leading frequently to spherical microparticles. Operating below the critical point of the mixture means that the surface tension will never vanish. If the mass transfer from CO<sub>2</sub> into the droplet prevails the drop will continue expanding. Because CO<sub>2</sub> concentration is higher at the surface of the droplet, solute saturation

and precipitation takes place near the droplet surface and leads finally to a hollow balloon structure or expanded microparticle (EMP). If we move slightly over the critical point of the mixture, the dynamic surface tension of the droplet will eventually vanish hindering the large swelling of the droplet and the formation of microparticles instead of EMPs will be favoured. If the pressure is increased further above the critical point of the mixture nanoparticles can be obtained. The vanishing of the surface tension takes place faster at higher pressures. An increase of pressure from 12 to 16 MPa for a DMSO jet injected at 2 mL/s in a SAS chamber resulted in a reduction of  $t_s$  from 15 to 10 ms.<sup>77</sup> Operating at higher pressure values will therefore lead to the vanishing of surface tension before jet break-up ( $t_s < t_{jb}$ ) and gas-like mixing prevails. Under gas-like mixing conditions the precipitation process takes place in the SCF phase. Saturation will generate precipitation and nucleation of the solute but growth is small because there are no solute molecules or very little in the surrounding phase.

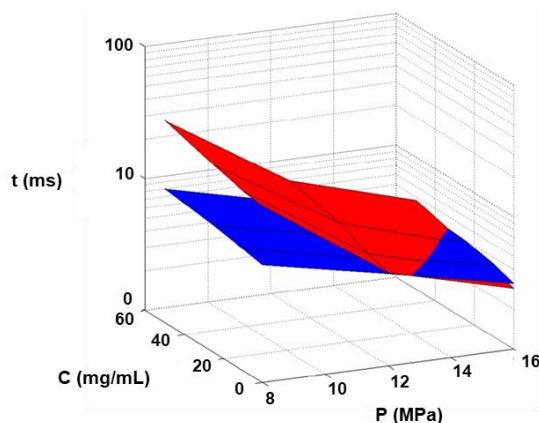


Fig. 1.12 Jet break-up time (blue) and time for dynamic surface tension vanishing (red) as function of pressure and initial concentration in the yttrium acetate-DMSO system. Figure adapted from Marra et al.<sup>78</sup>

The influence that the solute concentration on the liquid phase has on  $t_s$  and  $t_{jb}$  has been studied in the system DMSO and yttrium acetate<sup>78</sup>. A higher concentration will lead to an increase in the viscosity of the solution and a raise in  $t_{jb}$  and  $t_s$  (being more pronounced the increase in the former). This means that when processing more viscous solutions higher pressures must be employed if gas-like mixing wants to be accomplished (see Fig. 1.12)

The effect of the solution flow rate at constant  $\text{CO}_2$  mole fraction in the precipitation chamber showed little influence in the particle size and morphology for the same system (DMSO-yttrium acetate) in the range from 1 to 3 mL/min.<sup>77</sup>

In plenty of examples in the SAS literature though, and in the systems studied in this thesis, the solute precipitates as crystals. These crystals present different morphologies and sizes. Rossmann et al.<sup>79</sup> used light scattering to measure supersaturation levels at the location where the first solid particles were generated during the SAS precipitation of the systems yttrium acetate-DMSO and paracetamol-ethanol. The supersaturation level can be defined as the ratio between the actual molar fraction and the saturation mole fraction of the solute (the latter will be conditioned by the solubility of the solute in the solvent-CO<sub>2</sub> system). Yttrium acetate has a much lower solubility in the CO<sub>2</sub>-DMSO mixture, thus, much higher levels of supersaturation are reached. This leads to the formation of nano, micro or EMPs particles as a function of the  $t_s$  and  $t_{jb}$  relation described earlier. Paracetamol on the contrary had a higher solubility in the ethanol-CO<sub>2</sub> mixture and lower supersaturation levels were achieved leading to the formation of crystals regardless of the  $t_s$ - $t_{jb}$  relation (i.e. crystals formed when precipitation took place in the liquid droplet or in the fluid phase). The saturation solubility of the solute in the solvent-antisolvent mixture was found to be the key factor controlling the formation of crystals in the SAS process. Increasing pressure at constant initial concentration will decrease supersaturation (higher CO<sub>2</sub> densities will enhance the solubility of the solute in the solvent-CO<sub>2</sub> mixture) and crystals will grow (in the specific paracetamol case a change in morphology was also observable). Increasing initial concentration at constant pressure will increase the supersaturation and crystal size will decrease. Changing the operational conditions will still lead to the formation of crystals. If nanoparticles are the target another solvent with a lower solubility of the solute in the solvent-CO<sub>2</sub> mixture should be selected.<sup>79, 80</sup>

Reverchon & de Marco<sup>15</sup> proposed other two scenarios where the formation of crystals was possible. If solutes were believed to have very fast crystallization kinetics the crystallization process could superimpose the precipitation one leading to the crystal formation. The other scenario would also be related to the solubility of the solute in the solvent-CO<sub>2</sub> mixture, but in this case, contrary to the findings of Rossmann,<sup>79</sup> the possible effect of the solute in the phase behaviour of the system is taken into consideration. The presence of the solute could shift the critical point towards higher pressure values and the precipitation in the SAS chamber could take place therefore in the two phase region.

Several processes exist which are similar to SAS. The precipitation by compressed antisolvent (PCA) technique is another name that some authors have used instead of SAS. The solution enhanced dispersion by supercritical fluids (SEDS)<sup>81</sup>



is a modification of SAS using a different nozzle configuration. A two or three way coaxial nozzle is used to improve jet atomization and to avoid solubility problems by feeding solutions separately. In the supercritical antisolvent precipitation with enhanced mass transfer (SAS-EM)<sup>82</sup> the precipitation vessel is provided with an ultrasound device enhancing mass transfer and jet break-up in the vessel. In order to avoid blockage at the nozzle the atomized rapid injection for solvent extraction (ARISE)<sup>83</sup> process was developed. In this process the nozzle is substituted with a bigger orifice (around 1 mm). The solution with target solute is placed in a vessel and pressurized with an inert substance that has no antisolvent effect (typically N<sub>2</sub> or Ar). This vessel is at higher pressure than the precipitation vessel where CO<sub>2</sub> flows. Opening a valve between both vessels creates jet injection due to the pressure difference overcoming the need of the atomization nozzle.

## 1.4 Pharmaceutical co-crystals

The concept and definition of a co-crystal has been an ongoing matter of discussion due to the overlapping with other multicomponent solid forms, namely, solvates and salts. To the best of our knowledge, till today there is not a uniformly accepted definition of co-crystal. A broad and generally accepted working definition of co-crystal would be “a stoichiometric multi-component system connected by non-covalent interactions where all the components present are solid under ambient conditions”<sup>84</sup>. Thus, the co-crystal presents a new crystalline phase different to that of its components. A guidance and regulatory classification for pharmaceutical co-crystals has been recently given by the European Medicines Agency (EMA)<sup>85</sup> and the United States Food and Drug Administration (FDA)<sup>86</sup>.

A pharmaceutical co-crystal involves a system formed by an active pharmaceutical ingredient (API) and a suitable coformer or another API (multi-drug co-crystal)<sup>87</sup>. Coformers commonly used will be substances in the GRAS (generally recognized as safe) list. The aim of co-crystallization is to improve the physicochemical properties of the API and its medical performance which are intimately bond to its solid state.

An API can present several solid states (see Fig. 1.13). It can be in an amorphous state, for example nanoparticles obtained after processing and micronizing using the SAS technique as we have seen earlier. The amorphous API can present a significantly higher solubility than its crystal form improving the in-vitro and in-vivo dissolution behaviour.<sup>88</sup> For this reason several marketed drugs, such as accolate

(asthma treatment), ceftin (antibiotic) and accupril (to control high blood pressure), commercialize the amorphous form of the API. But several drawbacks such as thermodynamic instability and processing difficulties can make the amorphization of the API unpractical. On the other hand, the crystal form of an API can have several polymorphs (different crystal structure but the same chemical composition) which will present different physicochemical properties and stabilities. A specific polymorph of an API can then be desirable due to its enhanced properties. More about polymorphism will be described later on this chapter (section 1.6). As multicomponent crystals we can have solvates (or hydrates), salts and co-crystals.

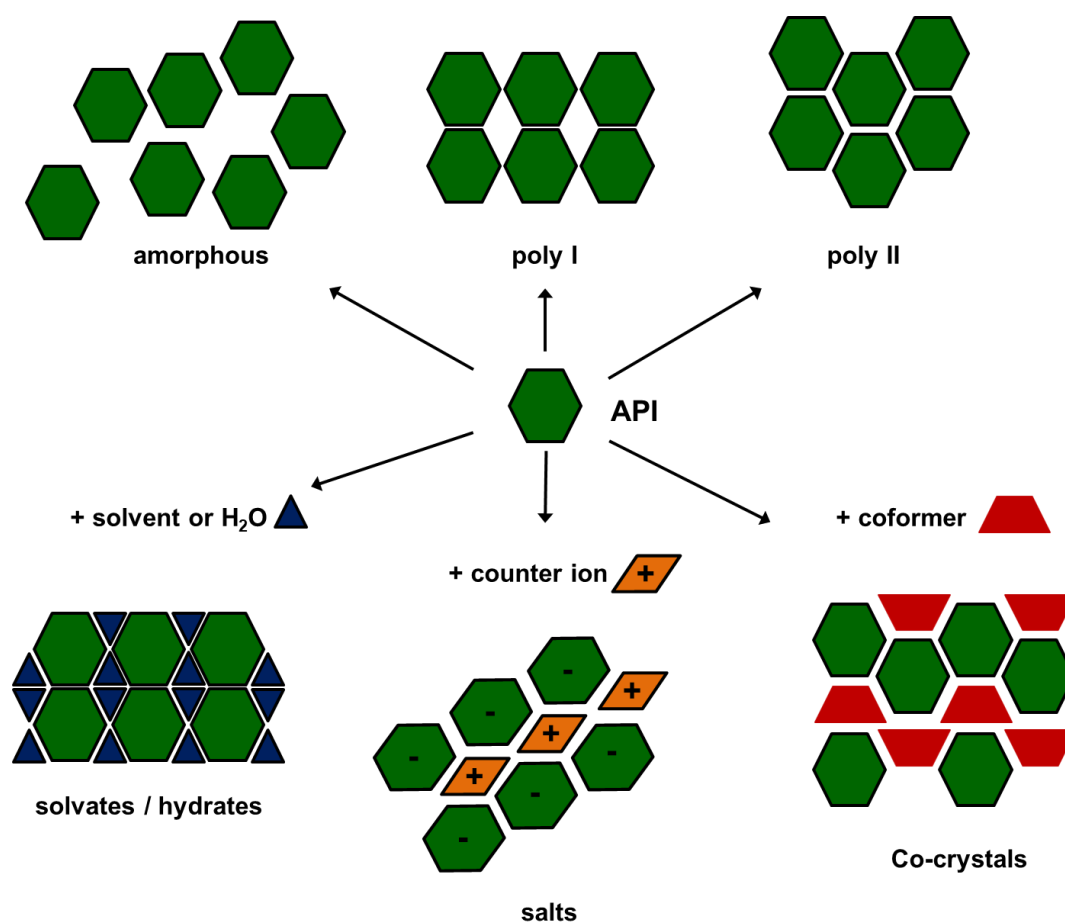


Fig. 1.13 Schematic representation of the possible solid states of an API. Figure adapted from Vioglio et al.<sup>89</sup>

In a solvate the molecules of solvent (water in case of a hydrate) are incorporated into the crystal lattice. The amount of solvent that can be incorporated will depend on the type of solvent and regulation limits. The EMA classifies the solvents in three categories: I (to be avoided), II (to be limited) and III (with low toxic potential)<sup>90</sup> and specifies the permitted amounts. The low physical stability of solvates to elevated temperatures or humidity generally discards its utilization in marketed drugs.<sup>91</sup>

Hydrates are generally also avoided in the pharmaceutical industry and their formation during storage is a problem. Nevertheless, nearly one third of marketed drugs are hydrates.<sup>92</sup>

A pharmaceutical salt will require the ionization of the API (anionic, cationic or zwitterionic) and the atomic or molecular counterion. So the salification of a drug is limited to those APIs with at least one acidic or basic group. For the formation of a salt the value of the  $\Delta pK_a$  (difference in the acid dissociation constant) has to be above 3. Values between  $0 < \Delta pK_a > 3$  can lead to co-crystal or salt formation and when  $\Delta pK_a < 0$  co-crystal formation is expected.<sup>84</sup> The production of pharmaceutical salts is one of the most common ways used in the industry to improve the properties of an API and more than 50% of drugs are commercialized as salts.<sup>93</sup> Like amorphization, the formation of salts also improves the solubility and dissolution rate of an API but conferring a higher physico-chemical stability and manufacturability.<sup>94</sup> A drawback associated to the salification of APIs is that there is in many cases a health limitation in the dose of counterions that can be administrated. Guidance over the most common counterions and the allowed dosis has been given by Saal et al.<sup>95</sup> Other main limitation is that salification is only applicable to those APIs with ionisable groups.

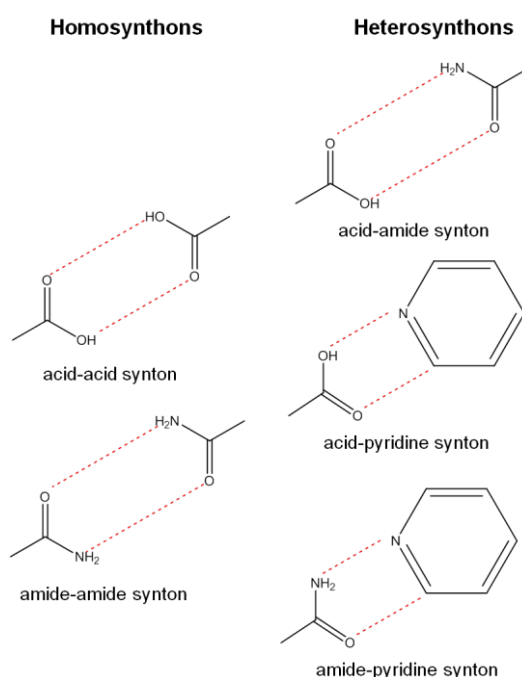


Fig. 1.14 Frequent intramolecular synthons.

Co-crystals present a path of drug development that can overcome the limitations of the solid state forms presented above. The supramolecular crystal

structure will emerge through a non-covalent bonding between the API and the coformer. This means that the main difference between a salt and a co-crystal is the lack of proton transfer what means that there is actually a smooth and overlapping transition between both solid states.<sup>96</sup> Analogously as in salts with counterion selection, by choosing the adequate coformer in co-crystals the properties of the API may be tuned improving dissolution rates, thermal stability, hygroscopicity, mechanical and organoleptic properties.<sup>97</sup> The election of the coformer will be though limited to those molecules that present a functional group capable of forming an interaction with a functional group of the API. This interaction between complementary functional groups leads to the so-called intramolecular synthons. It can be distinguished between homosynthons when the two functional groups involved are the same and heterosynthons when they are different. Fig. 1.14 shows some of the most frequent intramolecular synthons.

The first step in the co-crystal development will be therefore the selection of a coformer with supramolecular compatibility with the API and compliance with drug safety regulation. To assess the compatibility there are several methods that can help. The Fabian's method<sup>98</sup> stipulates that co-crystals are likely to form between molecules of similar polarity and shape. Karamertzanis et al.<sup>99, 100</sup> used lattice energy calculations to predict co-crystal structure. Molecular electrostatic potential surfaces (MPES) have been used to identify H-bond donor and acceptors parameters and through interaction site pairing energy calculations the probability of co-crystal formation was predicted<sup>101</sup>. Also the fluid-phase thermodynamics theory conductor-like screening model for real solvents (COSMO-RS) has been applied in coformer screening.<sup>102</sup>

The development of a marketed co-crystal drug is a long path. After the selection of a suitable coformer the co-crystal has to be obtained experimentally and characterized by several techniques. These techniques are usually single-crystal X-ray diffraction (SCXRD), powder X-ray diffraction (PXRD), Differential scanning calorimetry (DSC), thermogravimetric analysis (TGA) and Infrared and Raman spectroscopies. The composition of the powder is a key issue. The coformers homocrystals could precipitate together with the co-crystal. Also, when organic solvents are used the absence of solvent residues should be confirmed. The physicochemical properties of the co-crystal have to be assessed. These include key drug properties such as physical and chemical stability, aqueous dissolution rate and solubility and manufacturability. Pharmacokinetic studies assessing bioavailability,  $C_{max}$  (maximum concentration that the drug achieves in a test area of the body after the drug has been administrated) and time required to obtain the latter concentration must also be performed. Another

important step once the properties of the co-crystal have been characterized is the formulation of the drug. i.e. which excipients are going to be present in the final formulation. As co-crystals are sustained by hydrogen bonds their stability can be compromised with the presence of excipients which also contain hydrogen bonding groups. Final drug will need to be produced through a suitable process and regulatory approval sought.

## 1.5 Co-crystal phase diagrams

The understanding of the co-crystal phase diagrams and the changes expected as we move along the different areas in these diagrams are of great importance when characterizing the co-crystals.

### 1.5.1 Binary phase diagrams

In a binary phase diagram in which the components A and B form a new co-crystal phase A-B the regions where the different phases are stable can be followed as a function of composition, temperature and pressure. Two different types of phase diagrams with congruent and incongruent melting have been observed.

#### 1.5.1.1 Congruent melting system

Fig. 1.15 depicts the phase diagram at fixed pressure of a co-crystal formed between A and B in an equimolar ratio with congruent melting. The diagram shows the different regions of coexistence of the solid co-crystal (A-B) with the pure crystals A and B at low temperatures. As the temperature increases the solid melts and depending on the composition a liquid phase may coexist with solid A, B or co-crystal A-B. In a congruent melting system a pure co-crystal phase A-B will melt congruently to a homogeneous liquid phase with the same composition when reaching its melting temperature  $T_{AB}$  (arrow 1 in Fig. 1.15).  $T_{AB}$  does not have to be necessarily intermediate between the melting temperatures of A ( $T_A$ ) or B ( $T_B$ ).  $E_1$  and  $E_2$  are the eutectic points at which the mixtures of A and A-B, and B and A-B melt.

If an excess of B with respect to the stoichiometric ratio is present but we are under the composition of the eutectic point  $E_2$  (arrow 2), when the temperature  $T_{E_2}$  is reached the excess B and a small amount of co-crystal will melt, as we keep on raising the temperature the solid phase (co-crystal A-B) will partially melt and the amount of liquid will increase and change its composition until  $T_2$  is reached. When  $T_2$  is reached the solid phase will disappear. If the excess of B is above the composition of the eutectic  $E_2$  (arrow 3), the co-crystal A-B and a small amount of B will melt when

reaching  $T_{E2}$ , as we keep on raising the temperature the solid phase (B) will partially melt and the amount of liquid will increase until we reach  $T_3$ . When  $T_3$  is reached the solid phase will disappear. Analogous reasoning can be applied to the left side of the phase diagram.

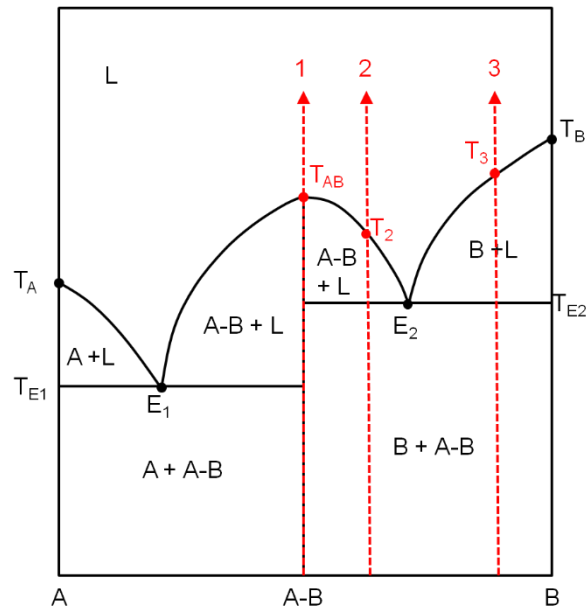


Fig. 1.15 Binary phase diagram of a congruent melting system at constant pressure.

### 1.5.1.2 Incongruent melting system

Fig. 1.16 represents the phase diagram at constant pressure of a co-crystal formed between A and B in an equimolar ratio with incongruent melting. At low temperatures the phase diagram is similar to the previous one and shows regions of coexistence of A or B with the co-crystal A-B. For this system however, when the temperature of a pure co-crystal phase is increased (arrow 1) an incongruent melting occurs. The system exhibits a peritectic point (P). At the peritectic temperature ( $T_P$ ) the co-crystal A-B melts and part of B recrystallizes in equilibrium with a liquid phase of composition P. Increasing the temperature further, component B will then gradually melt until  $T_1$  is reached. The same incongruent melting will be found if there is an excess of B with respect to the stoichiometric ratio (right side of arrow 1 in Fig. 1.16). If we have an excess of A but the composition is over of the peritectic point, when the eutectic temperature ( $T_{E1}$ ) is reached the excess of A and a small amount of the co-crystal will melt. The co-crystal phase A-B will melt gradually as we increase the temperature (increasing therefore also the amount of liquid and varying its composition). At the peritectic temperature ( $T_P$ ) the A-B solid phase will undergo incongruent melting and solid B will appear. At  $T_2$  all B would have melted. In case of

having an excess of A underneath the concentration of the peritectic point (arrow 3) no incongruent melting will take place, A will melt when  $T_E$  is reached and A-B will melt gradually until  $T_3$  is reached.

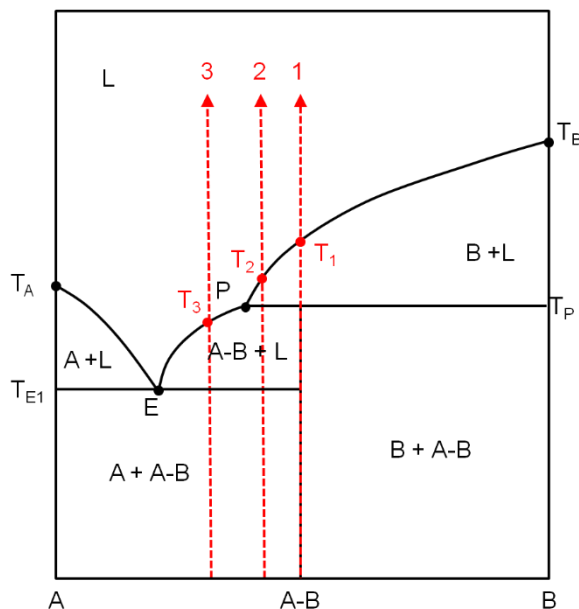


Fig. 1.16 Binary phase diagram of an incongruent melting system at constant pressure.

## 1.5.2 Ternary phase diagrams

In the production of co-crystals and metal adducts in this thesis using solvent evaporation or SAS, the coformers have been previously dissolved in a solvent. The ternary phase diagram formed by the coformers and this solvent is of great importance and can condition the success of the process.

We can distinguish between congruent and incongruent saturating ternary diagrams.

### 1.5.2.1 Congruent saturating system

Fig. 1.17 shows the ternary phase diagram at constant temperature and pressure of a system formed by the compounds A and B and a solvent. A and B form an equimolar A-B co-crystal. This phase diagram corresponds to a system that saturates congruently. The point  $S_A$  represents the solubility of pure A in the solvent and analogously  $S_B$  that of pure B. The line that bonds  $S_A$  with C represents solubility curve of A. Crossing from the liquid region (L) this line will result in the precipitation of

A. Analogously, the solubility curve of B is represented by the line that bonds  $S_B$  with D. C represents the point in the phase diagram where liquid, A and co-crystal A-B are in equilibrium and D is the point where liquid, B and co-crystal A-B are in equilibrium. The line that joins C with D is the solubility curve of the co-crystal. Crossing this line from the liquid phase will render a pure co-crystal precipitate. The dotted line in the diagram represents the stoichiometric ratio line for an equimolar co-crystal. In a congruent saturating system removing the solvent from a solution where A and B are in equimolar ratio will cross only the solubility curve of the co-crystal and will therefore yield a pure co-crystal phase. Precipitation by SAS of an equimolar solution of A and B in this type of system will yield pure co-crystals as long as the saturation curve is crossed.

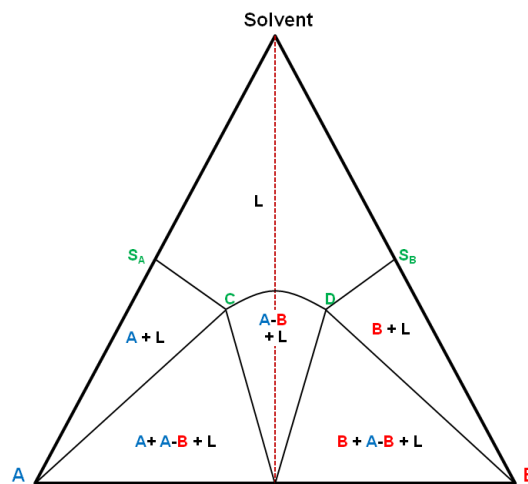


Fig. 1.17 Ternary phase diagram of a congruent saturating system at constant temperature and pressure.

### 1.5.2.2 Incongruent saturating system

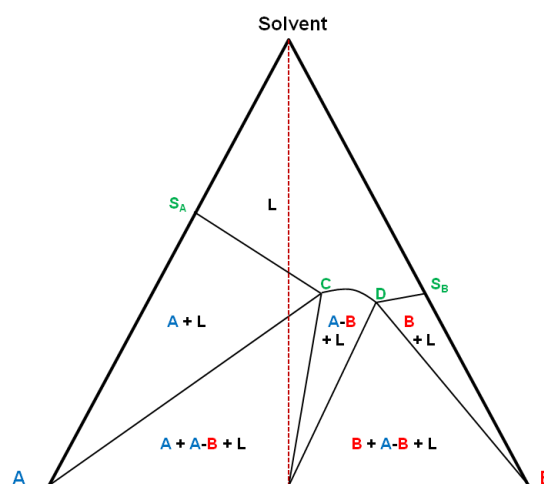


Fig. 1.18 Ternary phase diagram of an incongruent saturating system at constant temperature and pressure.



An incongruent saturating system will take place when the solubilities of pure A and B are very different resulting in a very asymmetrical ternary phase diagram (see Fig. 1.18). In this case the co-crystal stoichiometric ratio line will cross the solubility line of one of the co-crystal components resulting in the precipitation of homocrystals, and eventually the co-crystals but always yielding a mixture of phases.

## 1.6 Polymorphs and co-crystal polymorphs

Polymorphs are different crystalline modifications of the same chemical substance<sup>103</sup>. Polymorphism can be found in any crystalline material and a great number of pharmaceutical drugs show polymorphism. It is no surprise that pharmaceutical drugs are the compounds where more polymorphs have been reported as Mc Crone's law states: "the number of known polymorphic forms for a given compound is proportional to the time and money spent in research on that compound"<sup>104</sup>. Investigating the polymorphic form of an API is crucial because its physicochemical properties (solubility, stability...) can vary significantly from one form to the other affecting the quality, safety and efficacy of the final product formulation. A case that illustrates the importance of polymorphism in the pharmaceutical industry is the one of Ritonavir<sup>105</sup> an antiretroviral drug used to treat HIV that had to be withdrawn from the market because the API changed from the polymorph I to the less soluble and more stable form II during storage. For this reason, generally the most stable polymorphic form of the API is chosen during drug development to avoid its conversion to another polymorphic form during storage that could compromise its performance. A metastable form can be chosen in certain occasions due to its enhanced physicochemical properties but a precise knowledge of the thermodynamic stability relationship between the polymorphs is required to understand the stability of the solid forms.

Ostwald's rule of stages<sup>106</sup> stipulates that when a system leaves a state the transition will be to a more stable one and not necessarily to the most stable one. According to this rule during the crystallization from a solvent generally the first crystal form to assemble is the kinetically favoured or metastable form. As the sample crystallizes the solution becomes less saturated and a thermodynamic equilibrium is re-established producing a solvent mediated phase conversion to the more stable form. However, this is not always true and often the direct crystallization of the stable form

from a solution is observed. The formation of one polymorphic form or another depends on various parameters that affect the crystallization process. Some of the most important would be: solvent in which the crystallization takes place, temperature, degree and rate of supersaturation, agitation and pH.

Thermal methods are usually employed for determining the stability relationship between polymorphs. Polymorphs can be either enantiotropic or monotropic. In enantiotropic polymorphism the stable forms are different above and below the transition temperature (reversible equilibrium). In monotropic polymorphism one polymorph is stable over the entire temperature range and the transition from one to another is irreversible.

Although it was once thought that through co-crystallization, polymorphism and the problems caused by this phenomenon in the pharmaceutical industry could be avoided, analogously to simple components, co-crystals may also show polymorphism. Aitipamula et al.<sup>107</sup> proposed a classification of polymorphism in co-crystals where not only the conformational differences are taken into account but also the intermolecular interactions. The three main different classes of polymorphism in co-crystals described by the latter authors would be:

- **Synthon polymorphs:** The polymorphs present different synthons, thus a different H-bond net.
- **Packing polymorphs:** The overall three dimensional crystal packing is different between polymorphs.
- **Conformational polymorphs:** Polymorphs present different molecular conformations.

## 1.7 Preparation of co-crystals using SAS

Co-crystals can be produced by several methodologies ranging from the traditional solution methods and liquid assisted technologies to more novel ones like hot melt extrusion. The description of these methods is out of the scope of this introduction and for more information on this topic readers are referred to the recent detailed review by Douroumis et al.<sup>108</sup>

Different methodologies involving the use of supercritical fluids have also been employed by several authors in the preparation of co-crystals. Pando, Cabañas and the author of this thesis<sup>109</sup> have recently reviewed these contributions summarizing the

achievements obtained through supercritical methods and discussing their limitations and advantages. As this thesis investigates the co-crystallization using mainly the SAS technique we will like to briefly expose the advances achieved so far in this field.

Pradela et al.<sup>40</sup> reported in 2009 the formation of a 1:1 co-crystal of indomethacin and saccharin using several solvents: ethanol, acetone, tetrahydrofuran (THF), methanol and ethyl acetate. In all experiments equimolar concentration of indomethacin and saccharin were dissolved in the same amount of solvent ( $2.82 \times 10^{-3}$  g of indomethacin/g of solvent). Temperature was maintained constant at 323 K and pressures around 9.0 MPa were used. The solution was introduced through a 200  $\mu\text{m}$  coaxial nozzle allowing the mixture of the solution and the supercritical  $\text{CO}_2$  in a 30  $\mu\text{L}$  chamber prior to full mixing in the precipitation chamber. All experiments led to the formation of the co-crystal with a mixture of needle and block-shaped particles. No difference between samples was remarked by the authors.

Chen et al.<sup>110</sup> in 2015 reported the successful co-crystallization of a 1:1 co-crystal of piracetam and salicylic acid using acetone as a solvent and operating at 318 K and 10 MPa. No variation of the operational conditions was studied and no information of initial solution concentration or  $\text{CO}_2$  molar fraction was given. Dissolution tests were carried out and a controlled release of piracetam was achieved. Controlled release of piracetam through the co-crystallization was achieved and concentration levels were close to half of that for pure piracetam, thus, avoiding the undesired side-effects of this drug.

Hiendrawan et al.<sup>111</sup> obtained in 2016 a 1:1 co-crystal of paracetamol and dipicolinic acid using methanol as a solvent and operating at 313 K and 10 MPa. Initial solution concentration was not given.  $\text{CO}_2$  and solution flow rates were 30 g/min and 1 mL/min, respectively ( $\text{CO}_2$  molar fraction of approximately 0.97). The authors compared the SAS precipitate with the one obtained by slow evaporation and pure paracetamol. The co-crystal obtained using SAS displayed a much smaller particle size (4.18  $\mu\text{m}$ ) than the one obtained by slow evaporation (64.93  $\mu\text{m}$ ) or commercial paracetamol (45.33  $\mu\text{m}$ ). Dissolution rate of the SAS co-crystal was 2.45 times higher than that of pure paracetamol. Co-crystals obtained by both techniques showed improved tableting properties and were more stable than pure paracetamol.

Neurohr et al.<sup>112</sup> in 2016 prepared a 2:1 naproxen-nicotinamide co-crystal using acetone as solvent at 310 K and 10 MPa. The naproxen solution was injected through a 180  $\mu\text{m}$  nozzle to a 320 mL chamber. The authors investigated the influence of  $\text{CO}_2$  and solution ratio in the co-crystallization process and assumed that jet behavior and

hydrodynamics in the precipitation chamber were not significantly changed. Operating with a solution concentration of 40 mg/mL and CO<sub>2</sub> molar fractions between 0.75 and 0.93, they produced precipitates with a co-crystal content over 94 %, yields between 60 to 70 % and large plate-like particles of 20 µm to 1mm. Increasing the solution concentration to 50 mg/mL in an attempt to obtain higher supersaturation levels did not produce changes in the precipitate obtained. The reason given was that the supersaturation level could not exceed 1.5 in the investigated conditions (supersaturation is proportional to the ratio between concentration of the co-crystal formers and the solubility of the co-crystal in the CO<sub>2</sub>-solvent mixture).

The relatively high acetone concentrations used in these experiments imply a greater solubility of the co-crystal in the CO<sub>2</sub>-acetone phase explaining the size of the particles obtained (a weaker antisolvent effect of CO<sub>2</sub>). To reduce solubility and therefore attain higher supersaturation levels and reduced particle size the authors increased the CO<sub>2</sub> molar fraction to 0.98 and processed solutions with 40 and 50 mg/mL. The morphology of the precipitates obtained in these experiments was of aggregated particles consisting of plate-like crystals (similar to the ones obtained in the previous experiments) and needles (similar to the morphology obtained when processing only naproxen). The different characterization techniques confirmed the presence of an excess of naproxen in the precipitate. Reproducibility of experiments done at  $x_{\text{CO}_2}$  of 0.98 was low and co-crystal content varied significantly (4 to 86% in the experiment with higher concentration). The supersaturation levels of naproxen were much higher than those of the co-crystal and nicotinamide. Nicotinamide did not precipitate and left the precipitation chamber along with the CO<sub>2</sub>-acetone mixture.

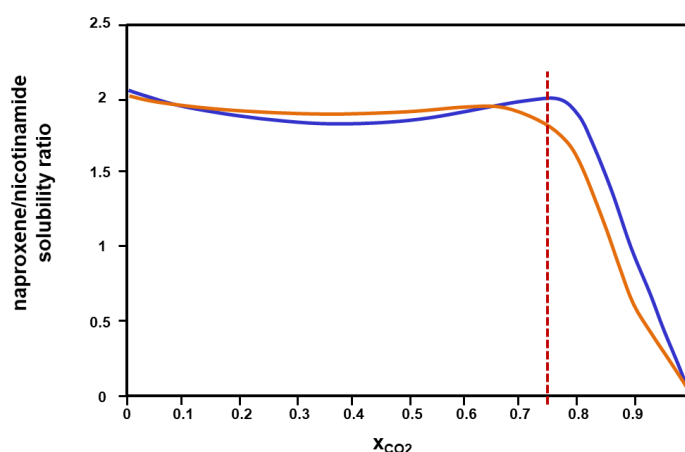


Fig. 1.19 Evolution of naproxen-nicotinamide (NIC) solubility ratio with CO<sub>2</sub> molar fraction in (acetone-CO<sub>2</sub>) mixtures at 10 MPa and — 298.15 K; — 310.65 K. Figure adapted from Ryelli et al.<sup>113</sup>

By doubling the content of nicotinamide in the initial solution and using a 1:1 molar ratio (naproxen-nicotinamide) solution 99% pure co-crystals were obtained. These results indicate that the relative solubilities of the crystal formers in the CO<sub>2</sub>-acetone mixture play a key role in the production of pure co-crystal powders. As we can observe in figure Fig. 1.19<sup>113</sup> as the acetone content in the CO<sub>2</sub>-acetone mixture decreases the solubility difference of both co-crystal formers increases. This solubility difference explains the formation of naproxen homocrystals in the experiments carried out with  $x_{\text{CO}_2} = 0.98$  and a 2:1 (naproxen-nicotinamide) molar ratio.

A CFD modeling of the process was also developed by these authors to obtain supersaturation distribution profiles in the precipitation chamber<sup>112</sup>.

Paracetamol was also the API used in 2018 by Zhao et al.<sup>114</sup> to prepare a 1:1 co-crystal with trimethylglycine. As solvent they used a methanol-DCM mixture and an orthogonal array design of experiments with 5 variables (pressure, temperature, volume ratio of DCM and methanol, solution concentration and solution flow rate) and 4 levels was employed to optimize the process. The chosen optimal operational conditions were those that led to the sample with higher paracetamol content. Optimized conditions were 10 MPa, 318 K, 50% volume DCM, solution concentration of 30 mg/mL and a solution flow rate of 1.2 mL/min (CO<sub>2</sub> flow rate of 30 g/min was held constant in all experiments, thus the optimized molar fraction of CO<sub>2</sub> was 0.97). The fact that the optimal sample presents a paracetamol content of approximately 61 % combined with the results of PXRD, FTIR, DSC, TGA and Raman spectroscopy indicates the presence of homocrystals in the samples. The optimal sample showed better tableability and dissolution rate than that of pure paracetamol or the same co-crystal obtained through ball milling.

The PCA technique, which is basically identical to SAS, was used by Hermann et al.<sup>115</sup> in 2009 to obtain co-crystals of paracetamol and caffeine. They used a 1:1 molar ratio of the co-crystal formers in a methanol-dichloromethane (DCM) mixture at pressures between 5 and 20 MPa. Temperature, solvent ratio, concentration of initial solution and molar fraction of CO<sub>2</sub> in the precipitation chamber were not specified. Scanning electron microscopy (SEM) images of the experiments show agglomerates of different particles. PXRD analysis revealed that samples contained mixtures of new phases identified as paracetamol-caffeine co-crystals accompanied with homocrystals of caffeine, caffeine hydrate and paracetamol.

## 1.8 Preparation of co-crystals using CSS

This technique has been assessed in this thesis as a complementary technique to SAS.

In this technique supercritical CO<sub>2</sub> is used as a solvent. Solvent power and molecular mobility enhancement provided by supercritical CO<sub>2</sub> will promote the co-crystallization of the API and the coformer. Moreover, solvents play an important role in co-crystal outcome<sup>116</sup> and new molecular interactions with CO<sub>2</sub> may lead to the nucleation and growth of different co-crystal polymorphs or co-crystal stoichiometries.

The first co-crystallization equipment used by the authors<sup>40</sup> consisted of two high-pressure vessels (6 and 9 mL) inside a temperature-controlled air chamber set at 313 K. The smaller vessel had an independent heating jacket and its temperature was set to 323 K. The temperature gradient between both vessels allowed CO<sub>2</sub> recirculation by thermosiphon. Approximately 0.25 mmol of each substance was placed in a paper cup inside the smaller vessel. After hours of co-crystallization the vessels were slowly depressurized and the precipitate was collected from the paper cup (approximately 100%). This equipment design was unsuccessful in the co-crystallization of a 1:1 (indomethacin-saccharin) molar mixture. Experiments were performed at 14 to 22 MPa and co-crystallization times from 3.5 to 90 hours. Subsequent equipment design (Fig. 1.20) consisted in a temperature-controlled chamber where a CO<sub>2</sub> storage vessel and a high-pressure vessel of 8 mL were placed. Magnetic stirring ensured a better mixing of the co-crystal components inside the high-pressure vessel.

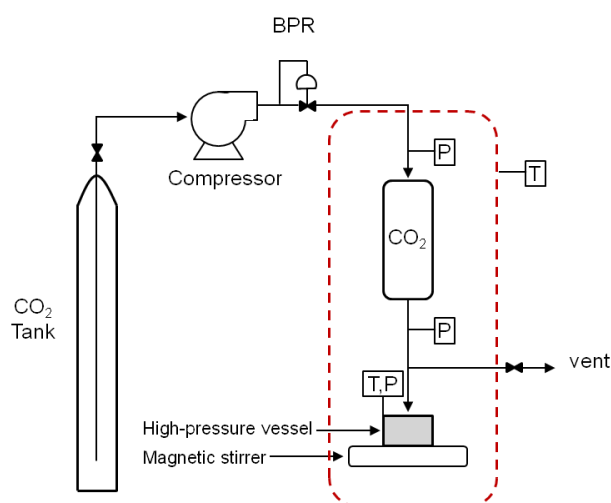


Fig. 1.20 Schematic description of the co-crystallization with supercritical solvent (CSS) setup used by Padrela et al.<sup>41</sup>

Co-crystallization of theophylline, carbamazepine, indomethacin, caffeine, sulfamethazine and acetyl salicylic acid with the coformer saccharin was studied. The successful co-crystallization of the indomethacin-saccharin co-crystal with the modified equipment (processing 400 mg of co-crystal components in an equimolar ratio at 323 K, 20 MPa, 300 rpm stirring rate and a co-crystallization time of 2 hours) validated the new setup. A significant amount of experimental work was performed from which the most important findings are described next.

Although co-crystal components have low solubility in CO<sub>2</sub>, results suggest that the co-crystallization is mediated by the dissolution of the substances in CO<sub>2</sub>. Nevertheless, co-crystallization was also observed when gaseous CO<sub>2</sub> and N<sub>2</sub> were employed, so a significant drop in solvation power would still enable co-crystallization. Stirring plays a key role in the process as it promotes the mass transfer by convection (otherwise limited to the solutes diffusivity in CO<sub>2</sub>) and facilitates the molecular interactions between the two coformers. The co-crystallization kinetics are enhanced at higher CO<sub>2</sub> densities. The fact that co-crystallization curves show a zero order reaction (concentration increases linearly with time) suggests that CO<sub>2</sub> is always saturated in both components. As in conventional solution methods co-crystal formation is strongly influenced by the nature of the solvent. For example, despite both APIs are relatively soluble in CO<sub>2</sub>, the co-crystallization of sulfamethazine and caffeine was unsuccessful. Only with the addition of ethanol as cosolvent (0.4 mL) the co-crystallization was successful. The process seems to be conditioned by the overall balance between the affinity of the substances for the solvent or for each other.

## **1.9 Metallic organic frameworks (MOFs) as pharmaceuticals and their preparation using supercritical CO<sub>2</sub>**

MOFs are formed by transition metal cations that are bonded together through organic bridging ligands. As crystalline porous materials they have raised the interest of scientific research and industry in areas like gas storage, separation and catalysis.<sup>117</sup> In the scope of this thesis their applications in the pharmaceutical industry are relevant.

Preparation of biocompatible MOFs for drug storage and controlled release of several APIs has been described by several authors. Readers are referred to two recent reviews from Wu et al.<sup>118</sup> and Wang et al.<sup>119</sup> for a detailed description of achievements in this field.

The use of supercritical fluids in the processing of MOFs has recently been reviewed by Matsuyama.<sup>120</sup> The role of the SCF in the MOFs processing is classified as:

**1. Supercritical drying and activation:** The solvent molecules imbedded in the MOF structure are removed from the pores through supercritical CO<sub>2</sub> drying. The absence of surface tension and capillary stress of supercritical drying permits this removal conserving the porous structure. In some cases excess of linkers used in the MOF preparation can also be removed. Many researchers refer to this supercritical drying process as activation.

**2. Synthesis in supercritical CO<sub>2</sub> and compressed CO<sub>2</sub> mixtures:** In this case supercritical CO<sub>2</sub> or compressed CO<sub>2</sub> mixtures are used as the solvent media in which the crystallization between the metal salt and the organic linker takes place (supercritical reactive crystallization). Due to the low solubility of polar and heavy molecules in supercritical CO<sub>2</sub> the solvent media may be substituted by a CO<sub>2</sub> expanded liquid.

**3. Supercritical-fluid-assisted immobilization of nanoparticles:** In this case supercritical impregnation is used to load the MOF with nanoparticles.

In this thesis supercritical CO<sub>2</sub> is used as an antisolvent for the production of a copper MOF. The linking of the metal salt (copper propanoate) with an organic linker (isonicotinamide) is performed in an ethanol solution. This solution is then processed using the semicontinuous SAS technique. Up to the best of our knowledge this is the first time that a MOF is obtained using SAS.

## **1.10 Pharmaceutical composite microparticles and their preparation using supercritical CO<sub>2</sub>**

The benefits of drug micronization have already been briefly discussed within this introduction and include benefits such as improved drug bioavailability and enabling more suitable administration routes. The coprecipitation of drugs to produce composites is sought to improve the pharmaceutical properties of an API, or to confer them additional properties to prevent their degradation, to mask their unpleasant taste or odour and/or to achieve a controlled delivery. Moreover, composites are easier to handle and dose than the pure API particles.



Pharmaceutical composites involve the coprecipitation of an API with a suitable material. Ideally this material should be biodegradable, biocompatible, non-toxic, compatible with the API, targeting, and stimulus responsive. The materials more extensively used for this sake are biopolymers.

Composites are generally classified in either microspheres or microcapsules. In microcapsules the API is surrounded by a polymeric shell whilst in the microspheres the polymer and drug are dispersed in the same particle.

There are several conventional processes that are used to produce composites, from which the most common are: spray drying, jet milling, extrusion-spheronization, coprecipitation methods (liquid antisolvent or evaporation), and emulsification. These methods may submit the composite components to thermal and/or mechanical stress, can have little control on the particle size, morphology and PSD, and may require further purification steps to remove residual solvent. To overcome these drawbacks several supercritical fluid processes have been employed for the production of composites. A description of the different supercritical processes used can be encountered in a review from Cocero et al.<sup>121</sup> And a more specific review of the SAS process has been recently published by Prosapio et al.<sup>122</sup> The SAS precipitation of composites has led to the formation of microparticles, nanoparticles, sub-microparticles, crystals and other morphologies. Although further research work needs to be performed in order to draw general rules of SAS coprecipitation outcome, some findings have been identified.<sup>122</sup>

- SAS operating conditions and precipitation mechanisms are similar to those of single compounds detailed earlier in this introduction.
- In the case of microparticles, successful precipitation of the API and polymer separately does not guarantee a successful coprecipitation.
- The selection of the polymer and the polymer to drug ratio can influence the precipitation mechanism and a successful obtention of composite microparticles.
- Compounds whose micronization was unsuccessful with SAS (i.e. large crystals were obtained) can be successfully micronized when processed with a polymer (the coprecipitation seems to block the tendency of the API to produce crystals).
- The production of composite nanoparticles is questioned and a more likely precipitation of separate nanoparticles is suggested.

## References

1. Iota, V.; Yoo, C., Phase Diagram of Carbon Dioxide: Evidence for a New Associated Phase. *Physical review letters* **2001**, 86 (26), 5922-5925.
2. Erkey, C., *Supercritical fluids and organometallic compounds: from recovery of trace metals to synthesis of nanostructured materials*. **2011**; Vol. 1, p 1-233.
3. NIST Standard Reference Database Number 69, which can be accessed electronically through the NIST Chemistry Web Book (<http://webbook.nist.gov/chemistry>).
4. Bruce E. Poling, J. M. P., John P. O'Connell, *The Properties of Gases and Liquids*. 5th Edition ed.; McGraw-Hill: New York, **2001**; p 768.
5. Suehiro, Y.; Nakajima, M.; Yamada, K., Critical parameters of  $\{x\text{CO}_2+(1-x)\text{CHF}_3\}$  for  $x=(1.0000, 0.7496, 0.5013, \text{ and } 0.2522)$ . *Journal of Chemical Thermodynamics* **1996**, 28 (10), 1153-1164.
6. Dean, J. R., *Applications of Supercritical Fluids in Industrial Analysis*. **2012**.
7. Brunner, E., Fluid mixtures at high pressures IX. Phase separation and critical phenomena in 23 (n-alkane + water) mixtures. *Journal of Chemical Thermodynamics* **1990**, 22 (4), 335-353.
8. Cocero, M. J., Supercritical water processes: Future prospects. *The Journal of Supercritical Fluids* **2018**, 134, 124-132.
9. van Konynenburg, P. H.; Scott, R. L., Critical lines and phase-equilibria in binary van der Waals mixtures. *Philosophical Transactions of the Royal Society a-Mathematical Physical and Engineering Sciences* **1980**, 298 (1442), 495-540.
10. Streett, W. B., Phase behavior in fluid and solid mixtures at high pressures. *Pure and Applied Chemistry* **1989**, 61 (2), 143-152.
11. Gardeler, H.; Gmehling, J., Experimental determination of phase equilibria and comprehensive examination of the predictive capabilities of group contribution equations of state with a view to the synthesis of supercritical extraction processes. In *Supercritical fluids as solvents and reaction media*, Brunner, G., Ed. **2004**; pp 3-38.
12. Mc Hugh. M. A; Krukonis. Val J, *Supercritical fluid extraction: principles and practice*. 2 ed.; **1994**.
13. De Loos. Th. W, Understanding phase diagrams. In *Supercritical fluids fundamentals for application*, E. Kiran; Levelt Sengers. J. M. H, Eds. Kluwer academic publishers: Netherlands, **1994**; pp 65-89.
14. Geana, D., Phase Equilibria in Ternary Systems Carbon Dioxide+1-Hexanol + n-Pentadecane and Carbon Dioxide+1-Heptanol + n-Pentadecane: Modeling of Holes in Critical Surface and Miscibility Windows. *Journal of Chemical and Engineering Data* **2018**, 63 (4), 994-1005.
15. Reverchon, E.; De Marco, I., Mechanisms controlling supercritical antisolvent precipitate morphology. *Chemical Engineering Journal* **2011**, 169 (1-3), 358-370.
16. Chiu, H. Y.; Lin, H. M.; Lee, M. J., Vapor-liquid phase equilibrium of carbon dioxide with mixed solvents of DMSO plus ethanol and chloroform plus methanol including near critical regions. *Journal of Supercritical Fluids* **2013**, 82, 146-150.
17. Galicia-Luna, L. A.; Ortega-Rodriguez, A.; Richon, D., New apparatus for the fast determination of high-pressure vapor-liquid equilibria of mixtures and of accurate critical pressures. *Journal of Chemical and Engineering Data* **2000**, 45 (2), 265-271.
18. Chiu, H. Y.; Jung, R. F.; Lee, M. J.; Lin, H. M., Vapor-liquid phase equilibrium behavior of mixtures containing supercritical carbon dioxide near critical region. *Journal of Supercritical Fluids* **2008**, 44 (3), 273-278.
19. Campardelli, R.; Reverchon, E.; De Marco, I., Dependence of SAS particle morphologies on the ternary phase equilibria. *Journal of Supercritical Fluids* **2017**, 130, 273-281.

20. Campardelli, R.; Reverchon, E.; De Marco, I., PVP microparticles precipitation from acetone-ethanol mixtures using SAS process: Effect of phase behavior. *Journal of Supercritical Fluids* **2019**, *143*, 321-329.
21. Han, C. N.; Kang, C. H., Phase behavior of arbutin/ethanol/supercritical CO<sub>2</sub> at elevated pressures. *Korean J. Chem. Eng.* **2017**, *34* (6), 1781-1785.
22. Reverchon, E.; De Marco, I.; Torino, E., Nanoparticles production by supercritical antisolvent precipitation: A general interpretation. *Journal of Supercritical Fluids* **2007**, *43* (1), 126-138.
23. Perrut, M., Supercritical fluid applications: Industrial developments and economic issues. *Industrial & Engineering Chemistry Research* **2000**, *39* (12), 4531-4535.
24. Knez, Z.; Markocic, E.; Leitgeb, M.; Primožic, M.; Hrncic, M. K.; Skerget, M., Industrial applications of supercritical fluids: A review. *Energy* **2014**, *77*, 235-243.
25. Tabernero, A.; del Valle, E. M. M.; Galan, M. A., Supercritical fluids for pharmaceutical particle engineering: Methods, basic fundamentals and modelling. *Chemical Engineering and Processing* **2012**, *60*, 9-25.
26. Martin, A.; Cocero, M. J., Micronization processes with supercritical fluids: Fundamentals and mechanisms. *Advanced Drug Delivery Reviews* **2008**, *60* (3), 339-350.
27. Padrela, L.; Rodrigues, M. A.; Duarte, A.; Dias, A. M. A.; Braga, M. E. M.; de Sousa, H. C., Supercritical carbon dioxide-based technologies for the production of drug nanoparticles/nanocrystals - A comprehensive review. *Advanced Drug Delivery Reviews* **2018**, *131*, 22-78.
28. Smith, R. D.; Wash, R. Supercritical fluid molecular spray film deposition and powder formation. Patent US 4582731. **1986**.
29. Kurkonis, V., Supercritical nucleation of difficult to comminute solids. *AIChE meeting, San Francisco* **1984**.
30. Helfgen, B.; Türk, M.; Schaber, K., Hydrodynamic and aerosol modelling of the rapid expansion of supercritical solutions (RESS-process). *Journal of Supercritical Fluids* **2003**, *26* (3), 225-242.
31. Türk, M., Manufacture of submicron drug particles with enhanced dissolution behaviour by rapid expansion processes. *Journal of Supercritical Fluids* **2009**, *47* (3), 537-545.
32. Türk, M., Formation of organic particles using supercritical fluid as solvent. In *Particle formation with supercritical fluids challenges and limitations*, Kiran, E., Ed. Elsevier: **2014**; Vol. 6, pp 57-75.
33. Türk, M., Influence of thermodynamic behaviour and solute properties on homogeneous nucleation in supercritical solutions. *Journal of Supercritical Fluids* **2000**, *18* (3), 169-184.
34. Thakur, R.; Gupta, R. B., Rapid expansion of supercritical solution with solid cosolvent (RESS-SC) process: Formation of griseofulvin nanoparticles. *Industrial & Engineering Chemistry Research* **2005**, *44* (19), 7380-7387.
35. Thakur, R.; Gupta, R. B., Rapid expansion of supercritical solution with solid cosolvent (RESS-SC) process: Formation of 2-aminobenzoic acid nanoparticle. *Journal of Supercritical Fluids* **2006**, *37* (3), 307-315.
36. Thakur, R.; Gupta, R. B., Formation of phenytoin nanoparticles using rapid expansion of supercritical solution with solid cosolvent (RESS-SC) process. *International Journal of Pharmaceutics* **2006**, *308* (1-2), 190-199.
37. Sodeifian, G.; Sajadian, S. A., Solubility measurement and preparation of nanoparticles of an anticancer drug (Letrozole) using rapid expansion of supercritical solutions with solid cosolvent (RESS-SC). *Journal of Supercritical Fluids* **2018**, *133*, 239-252.
38. Uchida, H.; Nishijima, M.; Sano, K.; Demoto, K.; Sakabe, J.; Shimoyama, Y., Production of theophylline nanoparticles using rapid expansion of supercritical

- solutions with a solid cosolvent (RESS-SC) technique. *Journal of Supercritical Fluids* **2015**, *105*, 128-135.
39. Young, T. J.; Mawson, S.; Johnston, K. P.; Henriksen, I. B.; Pace, G. W.; Mishra, A. K., Rapid expansion from supercritical to aqueous solution to produce submicron suspensions of water-insoluble drugs. *Biotechnology Progress* **2000**, *16* (3), 402-407.
40. Padrela, L.; Rodrigues, M. A.; Velaga, S. R.; Matos, H. A.; de Azevedo, E. G., Formation of indomethacin-saccharin cocrystals using supercritical fluid technology. *European Journal of Pharmaceutical Sciences* **2009**, *38* (1), 9-17.
41. Padrela, L.; Rodrigues, M. A.; Tiago, J.; Velaga, S. P.; Matos, H. A.; de Azevedo, E. G., Insight into the Mechanisms of Cocrystallization of Pharmaceuticals in Supercritical Solvents. *Crystal Growth & Design* **2015**, *15* (7), 3175-3181.
42. Weidner, E.; Steiner, R.; Knez, Z. In *Powder generation from polyethyleneglycols with compressible fluids*, 3rd International Symposium on High Pressure Chemical Engineering, Eth, Zurich, Switzerland, Oct 07-09; Elsevier Science Publ B V: Eth, Zurich, Switzerland, **1996**; pp 223-228.
43. Weidner, E.; Knez, Z.; Novak, Z. A process and equipment for production and fractionation of fine particles from gas saturated solutions, Patent WO 95/21688. **1994**.
44. Weidner, E.; Petermann, M.; Knez, Z., Multifunctional composites by high-pressure spray processes. *Current opinion in solid state & materials science* **2003**, *7* (4-5), 385-390.
45. Pestieau, A.; Krier, F.; Lebrun, P.; Brouwers, A.; Streeel, B.; Evrard, B., Optimization of a PGSS (particles from gas saturated solutions) process for a fenofibrate lipid-based solid dispersion formulation. *International Journal of Pharmaceutics* **2015**, *485* (1-2), 295-305.
46. Tomasko, D. L.; Li, H. B.; Liu, D. H.; Han, X. M.; Wingert, M. J.; Lee, L. J.; Koelling, K. W., A review of CO<sub>2</sub> applications in the processing of polymers. *Industrial & Engineering Chemistry Research* **2003**, *42* (25), 6431-6456.
47. Yeo, S. D.; Kiran, E., Formation of polymer particles with supercritical fluids: A review. *Journal of Supercritical Fluids* **2005**, *34* (3), 287-308.
48. Weidner, E., High pressure micronization for food applications. *Journal of Supercritical Fluids* **2009**, *47* (3), 556-565.
49. Meterc, D.; Petermann, M.; Weidner, E., Drying of aqueous green tea extracts using a supercritical fluid spray process. *Journal of Supercritical Fluids* **2008**, *45* (2), 253-259.
50. Martin, A.; Weidner, E., PGSS-drying: Mechanisms and modeling. *Journal of Supercritical Fluids* **2010**, *55* (1), 271-281.
51. Weidner, E.; Steiner, R.; Dirscherl, H.; Weinreich, B. Method for producing a powder product from a liquid substance or mixture of substances, Patent EP 9705484 **1997**.
52. Grüner, S.; Otto, F.; Weinreich, B. In *proceedings of the 6th international symposium on supercritical fluids*, CPF-technology a new cryogenic spraying process for pulverization of liquids, Versailles, **2003**.
53. Ventosa, N.; Sala, S.; Veciana, J., DELOS process: a crystallization technique using compressed fluids - 1. Comparison to the GAS crystallization method. *Journal of Supercritical Fluids* **2003**, *26* (1), 33-45.
54. Ventosa, N.; Sala, S.; Veciana, J.; Torres, J.; Llibre, J., Depressurization of an expanded liquid organic solution (DELLOS): A new procedure for obtaining submicron- or micron-sized crystalline particles. *Crystal Growth & Design* **2001**, *1* (4), 299-303.
55. Sala, S.; Elizondo, E.; Moreno, E.; Calvet, T.; Cuevas-Diarte, M. A.; Ventosa, N.; Veciana, J., Kinetically Driven Crystallization of a Pure Polymorphic Phase of Stearic Acid from CO<sub>2</sub>-Expanded Solutions. *Crystal Growth & Design* **2010**, *10* (3), 1226-1232.

56. Sievers, R. E.; Karst, U.; Milewski, P. D.; Sellers, S. P.; Miles, B. A.; Schaefer, J. D.; Stoldt, C. R.; Xu, C. Y., Formation of aqueous small droplet aerosols assisted by supercritical carbon dioxide. *Aerosol Sci. Technol.* **1999**, *30* (1), 3-15.
57. Sievers, R. E.; Sellers, S. P.; Carpenter, J. F. Supercritical fluid assisted nebulization and bubble drying, Patent WO 00/75281 **2000**.
58. Reverchon, E., Supercritical-assisted atomization to produce micro- and/or nanoparticles of controlled size and distribution. *Industrial & Engineering Chemistry Research* **2002**, *41* (10), 2405-2411.
59. Chattopadhyay, P.; Shekunov, B. Y.; Seitzinger, J. S.; Huff, R. W. Particles from supercritical fluid extraction of emulsions, U.S. Patent 2004026319 (A1). **2004**.
60. Della Porta, G.; Falco, N.; Reverchon, E., Continuous Supercritical Emulsions Extraction: A New Technology for Biopolymer Microparticles Production. *Biotechnol. Bioeng.* **2011**, *108* (3), 676-686.
61. Prieto, C.; Calvo, L.; Duarte, C. M. M., Continuous supercritical fluid extraction of emulsions to produce nanocapsules of vitamin E in polycaprolactone. *Journal of Supercritical Fluids* **2017**, *124*, 72-79.
62. Kordikowski, A.; Schenk, A. P.; VanNielen, R. M.; Peters, C. J., Volume expansions and vapor-liquid equilibria of binary mixtures of a variety of polar solvents and certain near-critical solvents. *Journal of Supercritical Fluids* **1995**, *8* (3), 205-216.
63. de la Fuente, J. C.; Peters, C. J.; Arons, J. D., Volume expansion in relation to the gas-antisolvent process. *Journal of Supercritical Fluids* **2000**, *17* (1), 13-23.
64. de la Fuente, J. C.; Shariati, A.; Peters, C. J., On the selection of optimum thermodynamic conditions for the GAS process. *Journal of Supercritical Fluids* **2004**, *32* (1-3), 55-61.
65. Werling, J. O.; Debenedetti, P. G., Numerical modeling of mass transfer in the supercritical antisolvent process. *Journal of Supercritical Fluids* **1999**, *16* (2), 167-181.
66. Werling, J. O.; Debenedetti, P. G., Numerical modeling of mass transfer in the supercritical antisolvent process: miscible conditions. *Journal of Supercritical Fluids* **2000**, *18* (1), 11-24.
67. Elvassore, N.; Cozzi, F.; Bertucco, A., Mass transport modeling in a gas antisolvent process. *Industrial & Engineering Chemistry Research* **2004**, *43* (16), 4935-4943.
68. Lengsfeld, C. S.; Delplanque, J. P.; Barocas, V. H.; Randolph, T. W., Mechanism governing microparticle morphology during precipitation by a compressed antisolvent: Atomization vs nucleation and growth. *Journal of Physical Chemistry B* **2000**, *104* (12), 2725-2735.
69. Dukhin, S. S.; Zhu, C.; Dave, R.; Pfeffer, R.; Luo, J. J.; Chavez, F.; Shen, Y., Dynamic interfacial tension near critical point of a solvent-antisolvent mixture and laminar jet stabilization. *Colloid Surf. A-Physicochem. Eng. Asp.* **2003**, *229* (1-3), 181-199.
70. Bristow, S.; Shekunov, T.; Shekunov, B. Y.; York, P., Analysis of the supersaturation and precipitation process with supercritical CO<sub>2</sub>. *Journal of Supercritical Fluids* **2001**, *21* (3), 257-271.
71. Dukhin, S. S.; Shen, Y.; Dave, R.; Pfeffer, R., Droplet mass transfer, intradroplet nucleation and submicron particle production in two-phase flow of solvent-supercritical antisolvent emulsion. *Colloid Surf. A-Physicochem. Eng. Asp.* **2005**, *261* (1-3), 163-176.
72. Martin, A.; Cocero, M. J., Numerical modeling of jet hydrodynamics, mass transfer, and crystallization kinetics in the supercritical antisolvent (SAS) process. *Journal of Supercritical Fluids* **2004**, *32* (1-3), 203-219.
73. Cardoso, M. A. T.; Cabral, J. M. S.; Palavra, A. M. F.; Geraldes, V., CFD analysis of supercritical antisolvent (SAS) micronization of minocycline hydrochloride. *Journal of Supercritical Fluids* **2008**, *47* (2), 247-258.

74. Erriguible, A.; Fadli, T.; Subra-Paternault, P., A complete 3D simulation of a crystallization process induced by supercritical CO<sub>2</sub> to predict particle size. *Comput. Chem. Eng.* **2013**, *52*, 1-9.
75. Clercq, S.; Mouahid, A.; Gerard, P.; Badens, E., Investigation of crystallization mechanisms for polymorphic and habit control from the Supercritical AntiSolvent process. *Journal of Supercritical Fluids* **2018**, *141*, 29-38.
76. De Marco, I.; Knauer, O.; Cice, F.; Braeuer, A.; Reverchon, E., Interactions of phase equilibria, jet fluid dynamics and mass transfer during supercritical antisolvent micronization: The influence of solvents. *Chemical Engineering Journal* **2012**, *203*, 71-80.
77. Braeuer, A.; Dowy, S.; Torino, E.; Rossmann, M.; Luther, S. K.; Schluucker, E.; Leipertz, A.; Reverchon, E., Analysis of the supercritical antisolvent mechanisms governing particles precipitation and morphology by in situ laser scattering techniques. *Chemical Engineering Journal* **2011**, *173* (1), 258-266.
78. Marra, F.; De Marco, I.; Reverchon, E., Numerical analysis of the characteristic times controlling supercritical antisolvent micronization. *Chem. Eng. Sci.* **2012**, *71*, 39-45.
79. Rossmann, M.; Braeuer, A.; Dowy, S.; Gallinger, T. G.; Leipertz, A.; Schluucker, E., Solute solubility as criterion for the appearance of amorphous particle precipitation or crystallization in the supercritical antisolvent (SAS) process. *Journal of Supercritical Fluids* **2012**, *66*, 350-358.
80. De Marco, I.; Rossmann, M.; Prosapio, V.; Reverchon, E.; Braeuer, A., Control of particle size, at micrometric and nanometric range, using supercritical antisolvent precipitation from solvent mixtures: Application to PVP. *Chemical Engineering Journal* **2015**, *273*, 344-352.
81. Hanna, M.; York, P. Method and apparatus for the formation of particles, Patent WO 95/01221 **1994**.
82. Gupta, R. B.; Chattopadhyay, P. Method of forming nanoparticles and microparticles of controllable size using supercritical fluids with enhanced mass transfer, Patent US 6620351(B2). **2003**.
83. Foster, N. R.; Sih, R. P. T. Process for producing particles via atomized rapid injection for solvent extraction, Patent WO 04/0094. **2008**.
84. Thakuria, R.; Delori, A.; Jones, W.; Lipert, M. P.; Roy, L.; Rodriguez-Hornedo, N., Pharmaceutical cocrystals and poorly soluble drugs. *International Journal of Pharmaceutics* **2013**, *453* (1), 101-125.
85. EMA, Reflection paper on the use of cocrystals and other solid state forms of active substances in medicinal products, **2015**. ([http://www.ema.europa.eu/docs/en\\_GB/document\\_library/Scientific\\_guideline/2015/07/WC500189927.pdf](http://www.ema.europa.eu/docs/en_GB/document_library/Scientific_guideline/2015/07/WC500189927.pdf)).
86. FDA, Guidance for industry: regulatory classification of pharmaceutical cocrystals, **2011**. (<https://www.fda.gov/downloads/Drugs/GuidanceComplianceRegulatoryInformation/Guidance1054s/UCM281764.pdf>).
87. Thipparaboina, R.; Kumar, D.; Chavan, R. B.; Shastri, N. R., Multidrug cocrystals: towards the development of effective therapeutic hybrids. *Drug Discovery Today* **2016**, *21* (3), 481-490.
88. Hancock, B. C.; Parks, M., What is the true solubility advantage for amorphous pharmaceuticals? *Pharmaceutical Research* **2000**, *17* (4), 397-404.
89. Cerreia Vioglio, P.; Chierotti, M. R.; Gobetto, R., Pharmaceutical aspects of salt and cocrystal forms of APIs and characterization challenges. *Advanced Drug Delivery Reviews* **2017**, *117*, 86-110.
90. EMA, ICH guideline Q3C (R6) on impurities: guideline for residual solvents, **2016**. ([http://www.ema.europa.eu/docs/en\\_GB/document\\_library/Scientific\\_guideline/2011/03/WC500104258.pdf](http://www.ema.europa.eu/docs/en_GB/document_library/Scientific_guideline/2011/03/WC500104258.pdf)).

91. Loschen, C.; Klamt, A., Computational Screening of Drug Solvates. *Pharmaceutical Research* **2016**, *33* (11), 2794-2804.
92. Vippagunta, S. R.; Brittain, H. G.; Grant, D. J. W., Crystalline solids. *Advanced Drug Delivery Reviews* **2001**, *48* (1), 3-26.
93. Serajuddin, A. T. M., Salt formation to improve drug solubility. *Advanced Drug Delivery Reviews* **2007**, *59* (7), 603-616.
94. Collman, B. M.; Miller, J. M.; Seadeek, C.; Stambek, J. A.; Blackburn, A. C., Comparison of a rational vs. high throughput approach for rapid salt screening and selection. *Drug Dev. Ind. Pharm.* **2013**, *39* (1), 29-38.
95. Saal, C.; Becker, A., Pharmaceutical salts: A summary on doses of salt formers from the Orange Book. *European Journal of Pharmaceutical Sciences* **2013**, *49* (4), 614-623.
96. Childs, S. L.; Stahly, G. P.; Park, A., The salt-cocrystal continuum: The influence of crystal structure on ionization state. *Molecular Pharmaceutics* **2007**, *4* (3), 323-338.
97. Sun, C. C., Cocrystallization for successful drug delivery. *Expert Opinion on Drug Delivery* **2013**, *10* (2), 201-213.
98. Fabian, L., Cambridge Structural Database Analysis of Molecular Complementarity in Cocrystals. *Crystal Growth & Design* **2009**, *9* (3), 1436-1443.
99. Issa, N.; Karamertzanis, P. G.; Welch, G. W. A.; Price, S. L., Can the Formation of Pharmaceutical Cocrystals Be Computationally Predicted? I. Comparison of Lattice Energies. *Crystal Growth & Design* **2009**, *9* (1), 442-453.
100. Karamertzanis, P. G.; Kazantsev, A. V.; Issa, N.; Welch, G. W. A.; Adjiman, C. S.; Pantelides, C. C.; Price, S. L., Can the Formation of Pharmaceutical Cocrystals Be Computationally Predicted? 2. Crystal Structure Prediction. *J. Chem. Theory Comput.* **2009**, *5* (5), 1432-1448.
101. Musumeci, D.; Hunter, C. A.; Prohens, R.; Scuderi, S.; McCabe, J. F., Virtual cocrystal screening. *Chem. Sci.* **2011**, *2* (5), 883-890.
102. Abramov, Y. A.; Loschen, C.; Klamt, A., Rational coformer or solvent selection for pharmaceutical cocrystallization or desolvation. *Journal of Pharmaceutical Sciences* **2012**, *101* (10), 3687-3697.
103. Nangia, A., Conformational polymorphism in organic crystals. *Accounts Chem. Res.* **2008**, *41* (5), 595-604.
104. W.C. McCrone, Polymorphism. In *Physics and chemistry of the organic solid state*, D. Fox; M.M Labes; A. Weissberger, Eds. Interscience publishers: London, **1965**; Vol. 2, pp 725-767.
105. Bauer, J.; Spanton, S.; Henry, R.; Quick, J.; Dziki, W.; Porter, W.; Morris, J., Ritonavir: An extraordinary example of conformational polymorphism. *Pharmaceutical Research* **2001**, *18* (6), 859-866.
106. Ostwald, V. W., Studien über die Bildung und Umwandlung fester Körper. 1. Abhandlung: Übersättigung und Überkaltung. *Zeltschrift f. physic. Chemie* **1897**, *XXII*, 289-330.
107. Aitipamula, S.; Chow, P. S.; Tan, R. B. H., Polymorphism in cocrystals: a review and assessment of its significance. *Crystengcomm* **2014**, *16* (17), 3451-3465.
108. Douroumis, D.; Ross, S. A.; Nokhodchi, A., Advanced methodologies for cocrystal synthesis. *Advanced Drug Delivery Reviews* **2017**, DOI 10.1016/j.addr.2017.07.008.
109. Pando, C.; Cabañas, A.; Cuadra, I. A., Preparation of pharmaceutical cocrystals through sustainable processes using supercritical carbon dioxide: a review. *RSC Advances* **2016**, *6* (75), 71134-71150.
110. Chen, C. T.; Tang, M.; Chen, Y. P. *Proceedings 11th International Symposium on Supercritical Fluids*, 2015.
111. Hiendrawan, S.; Veriansyah, B.; Widjojokusumo, E.; Soewandhi, S. N.; Tjandrawinata, R. R., Simultaneous cocrystallization and micronization of paracetamol-

- dipionic acid cocrystal by supercritical antisolvent (SAS). *International Journal of Pharmacy and Pharmaceutical Sciences* **2016**, 8 (2), 89-98.
112. Neurohr, C.; Erriguible, A.; Laugier, S.; Subra-Paternault, P., Challenge of the supercritical antisolvent technique SAS to prepare cocrystal-pure powders of naproxen-nicotinamide. *Chemical Engineering Journal* **2016**, 303, 238-251.
113. Ryelli, A. L.; Laugier, S.; Erriguible, A.; Subra-Paternault, P., High-pressure solubility of naproxen, nicotinamide in acetone with supercritical CO<sub>2</sub> as an antisolvent. *Fluid Phase Equilibria* **2014**, 373, 29-33.
114. Zhao, Z. Y.; Liu, G. J.; Lin, Q.; Jiang, Y. B., Co-Crystal of Paracetamol and Trimethylglycine Prepared by a Supercritical CO<sub>2</sub> Anti-Solvent Process. *Chemical Engineering & Technology* **2018**, 41 (6), 1122-1131.
115. Herrmann, M.; Forter-Barth, U.; Krober, H.; Kempa, P. B.; Juez-Lorenzo, M. D.; Doyle, S., Co-Crystallization and Characterization of Pharmaceutical Ingredients. *Part. Part. Syst. Charact.* **2009**, 26 (3), 151-156.
116. Chiarella, R. A.; Davey, R. J.; Peterson, M. L., Making co-crystals - The utility of ternary phase diagrams. *Crystal Growth & Design* **2007**, 7 (7), 1223-1226.
117. Stock, N.; Biswas, S., Synthesis of Metal-Organic Frameworks (MOFs): Routes to Various MOF Topologies, Morphologies, and Composites. *Chem. Rev.* **2012**, 112 (2), 933-969.
118. Wu, M. X.; Yang, Y. W., Metal-Organic Framework (MOF)-Based Drug/Cargo Delivery and Cancer Therapy. *Advanced Materials* **2017**, 29 (23), 20.
119. Wang, L.; Zheng, M.; Xie, Z. G., Nanoscale metal-organic frameworks for drug delivery: a conventional platform with new promise. *J. Mat. Chem. B* **2018**, 6 (5), 707-717.
120. Matsuyama, K., Supercritical fluid processing for metal-organic frameworks, porous coordination polymers, and covalent organic frameworks. *Journal of Supercritical Fluids* **2018**, 134, 197-203.
121. Cocero, M. J.; Martin, A.; Mattea, F.; Varona, S., Encapsulation and coprecipitation processes with supercritical fluids: Fundamentals and applications. *Journal of Supercritical Fluids* **2009**, 47 (3), 546-555.
122. Prosapio, V.; De Marco, I.; Reverchon, E., Supercritical antisolvent coprecipitation mechanisms. *Journal of Supercritical Fluids* **2018**, 138, 247-258.





# **Chapter 2**

## **Objectives**



## 2 OBJECTIVES

This thesis is aimed to exploring the use of supercritical CO<sub>2</sub> in the enhancement and improvement of the properties of a given active pharmaceutical ingredient (API) through co-crystallization or coprecipitation with a suitable coformer or carrier.

Mainly the supercritical antisolvent technology (SAS) is investigated due to its proven capacity to generate micro and nanoparticles with unique properties. Moreover, SAS is a semi continuous process that has already been scaled up successfully to pilot plant scale, thus presenting for the pharmaceutical industry a real and attractive alternative to process drugs in a one-step, environmental friendly and sterile process. The co-crystallization using supercritical solvents (CSS) technology is also investigated as a complementary technology in which CO<sub>2</sub> acts as a solvent.

A few drugs are studied in this thesis, namely: the anticancer drug 5-fluorouracil (5-Fu), the anti-inflammatory drug diflunisal (DIF) and carbamazepine (CBZ), a drug used primarily in the treatment of epilepsy and trigeminal neuralgia. Copper propanoate as a molecule with pharmaceutical and fungicidal activity is also used in this thesis. All of them present low solubility in supercritical CO<sub>2</sub> and are therefore good candidates for SAS processing.

The specific objectives of this thesis are:

### I. Preparation and characterization of 5-Fu-polymer composites via SAS coprecipitation

In a previous thesis carried out in our laboratory<sup>1</sup> microparticles of 5-Fu were successfully prepared by SAS using dimethylsulfoxide (DMSO) as solvent. The drug micronization enhances the direct delivery of 5-Fu in an aerosol therapy or an ointment. Nevertheless, the drug is usually given orally or intravenously due to its poor water solubility. To this end, a composite in which the drug is embedded or encapsulated in a biodegradable polymeric matrix is the appropriate choice: this formulation allows a better control dosage and the reduction of side effects. Thanks to its biocompatibility and biodegradability, Poly(L-lactide) (PLLA) is a good candidate as carrier. The solvent and conditions for SAS experiments (pressure, temperature, etc.) have to be explored. Composites need to be fully characterized (SEM, PXRD, DSC, TGA) and the controlled delivery must be demonstrated.

## **II. Preparation and characterization of pharmaceutical co-crystals via SAS**

As explained in the introduction co-crystallization is a powerful tool to improve the API properties that may benefit from the advantages of supercritical technologies. The main aim of this thesis is to prepare via SAS several co-crystals carrying out a full characterization (SEM, PXRD, DSC, TGA, IR) and comparing them with co-crystals obtained through conventional methods. The solvent and conditions for SAS experiments (pressure, temperature, etc.) have to be explored. The presence of homocrystals in the precipitate is a key issue. The pure API and the coformer are also micronized via SAS for comparative purposes. Co-crystals prepared are those formed by DIF and nicotinamide, CBZ and saccharin, and 5-Fu and urea, thiourea, acridine, 4-hydroxybenzoic acid (4HBA), pyrazinamide (PZA) and saccharin (SAC).

## **III. Polymorphic control in SAS co-crystals**

As indicated in the introduction, the API polymorphism is a key issue in pharmaceuticals that also affects co-crystals. On the other hand, SAS has been shown to be an effective tool to control the polymorphic form mainly through the solvent selection. The 1:1 co-crystal of CBZ and saccharin exhibits two polymorphs and an investigation using the SAS method, four different solvents (methanol, ethanol, DCM and DMSO) and different conditions of pressure, temperature and concentration is designed to establish the operational parameters that allow the preparation of a pure polymorph (without the presence of any homocrystal). Precipitates are studied using PXRD, SEM, DSC and IR.

## **IV. Comparison of co-crystals obtained using supercritical CO<sub>2</sub> as an antisolvent (SAS) and as a solvent (CSS).**

The co-crystals of 5-Fu with urea, thiourea, acridine, 4-hydroxybenzoic acid (4HBA), pyrazinamide (PZA) and saccharin (SAC) already attempted via SAS are also prepared via CSS. CSS precipitates are characterized by PXRD, DSC, TGA, IR and SEM. Outcomes of both techniques are compared.

## **V. SAS preparation of metal organic frameworks (MOFs) with pharmaceutical activity**

The capability of SAS to obtain adducts is explored. A new MOF of copper propanoate and isonicotinamide in a 1:2 molar ratio is prepared from an ethanol

solution via evaporation. Its crystal structure is elucidated using single crystal X-ray diffraction (SCXRD) and further characterization is accomplished using PXRD, IR, DSC and SEM. The same MOF is prepared via SAS and (after characterization using the same techniques and micro-elemental analysis) is compared to that obtained via slow evaporation. Conditions of SAS precipitation (solvent, temperature, pressure and molar ratio of components) are explored. Both MOF components are also precipitated via SAS for comparative purposes. This opens a new range of application of the SAS method.

## References

1. Zahran., F. R. F. Microparticles precipitation using supercritical CO<sub>2</sub> as an Antisolvent. Role of thermal effects and phase equilibria. Universidad Complutense de Madrid, Madrid, **2012**.

# **Chapter 3**

## **Methodology**





### 3 Methodology

The experimental devices used in this thesis and the methods employed are described here.

#### 3.1 Supercritical antisolvent precipitation

A SAS apparatus has been used for the micronization of pharmaceuticals and the production of composites, co-crystals and metallic organic frameworks (MOFs) via co-precipitation. The SAS equipment and the schematic diagram of the laboratory plant is depicted in Fig. 3.1 and Fig. 3.2. Details of the set up and validation of the plant can be found in a previous thesis defended in our research group.<sup>1</sup>



Fig. 3.1 SAS apparatus.

A description of the supercritical antisolvent process and phenomena involved can be found in the introduction of this thesis. In this section we will detail the equipment used and the experimental procedure.

First the desired amount of the target solute (or mixture of solutes) is weighed in an A&D GR-200 analytical balance (precision  $\pm 0.1$  mg). The solute is then dissolved in the chosen solvent or mixture of solvents ( $\pm 1$  mL). The beaker with the solution is placed into a bath on a hot and stirring plate (Fischer scientific Isotemp, precision  $\pm 0.1$  K). Stirring is set to 250 rpm and bath temperature is set to the precipitation temperature.

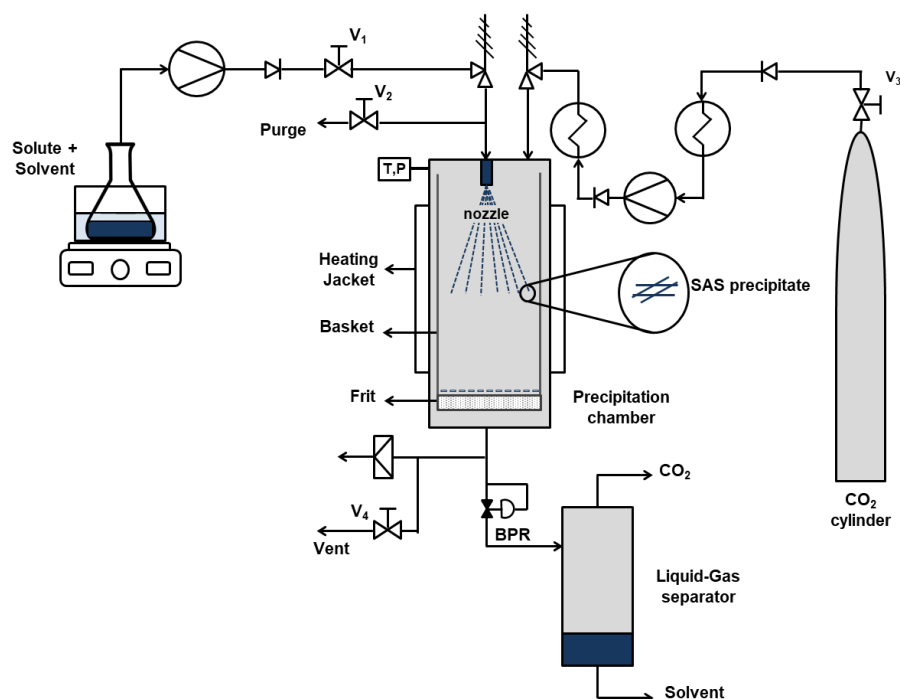


Fig. 3.2 Schematic diagram of the SAS equipment.

Valve  $V_3$  is open and  $\text{CO}_2$  (Air liquide 99.998 or 99.98 mol % pure) enters the system. A check valve (Swagelok SS-CHS2-25) to avoid backward flow and a filter (15  $\mu\text{m}$ , Swagelok SS-4TF-15) to protect the equipment down stream are installed in the line that feeds  $\text{CO}_2$  to the system. A pressure gauge (Swagelok, EN-837-1 Class 2.5) is used to measure the pressure inside the  $\text{CO}_2$  tank.  $\text{CO}_2$  then flows through a 3 m long helix coil (swagelok 1/8 in outside diameter and 0,028 in wall thickness tubing) inside a chiller (Julabo F 25) set at 276 K. This ensures that  $\text{CO}_2$  will be in the liquid phase when it reaches the high-pressure pump avoiding therefore pump cavitation and improving its efficiency. The high pressure pump (Thar-SCF P-50) has two pistons to provide a pulse-free delivery of  $\text{CO}_2$ . As the piston moves backwards the lower check valve opens and fluid enters the chamber.

When the piston moves forward the lower check valve closes and once the pressure in the chamber exceeds the operating pressure the upper check valve opens permitting the flow of CO<sub>2</sub> in the system. Flow rates can be set between 1 and 50 g/min in 1g/min increments. A check valve (Swagelok SS-CHS2-25) is positioned after the pump to avoid backward flow. The CO<sub>2</sub> stream runs then through a 5 m helix coil (swagelok 1/8 in outside diameter and 0,028 in wall thickness tubing) placed inside a heating bath (Selecta thermostat, Tectron 3000543) set to the precipitation temperature.

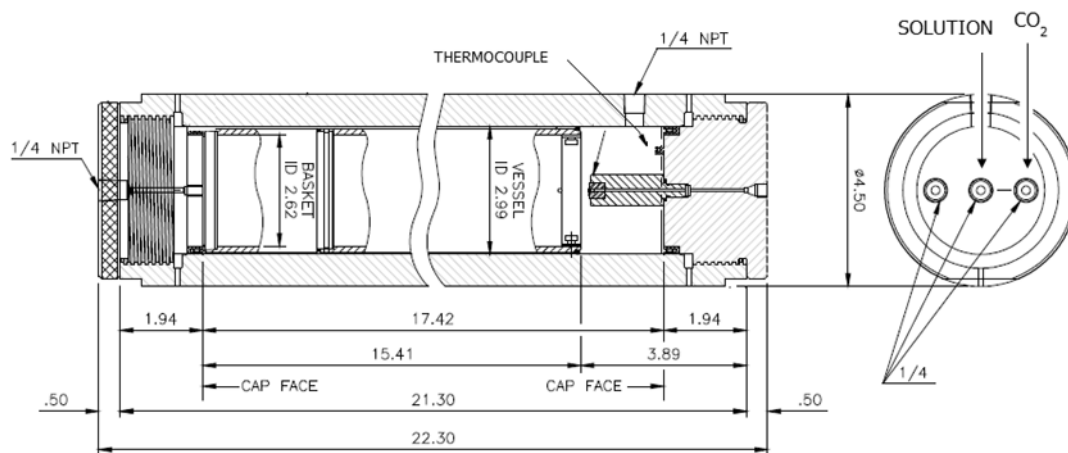


Fig. 3.3 Diagram of the precipitation chamber provided by Thar-SCF. Dimensions in inches.

The preheated CO<sub>2</sub> stream enters the precipitation chamber. Both, precipitation chamber and cyclone separator, have been purchased from Thar-SCF. The precipitation chamber is a stainless steel cylinder of 500 mL (see Fig. 3.3). Inside of it there is a removable basket with a 2 $\mu$ m filter (frit) where the precipitate is collected. To avoid contact with the bottom of the chamber a 4.5 x 2.5 x 0.2 cm (external diameter, height and width, respectively) aluminium cylinder is placed between the basket and the bottom of the chamber. To restrict the movement of the frit inside the basket an aluminium cylinder (4.4 x 1.2 x 0.2 cm) is placed on top of the frit inside the basket. The chamber is heated with an electrical jacket whose temperature is controlled using a temperature controller (CAL 9400). Temperature and pressure inside the precipitation chamber are measured using a digital thermocouple and a pressure transducer (Wika A-10).

The pressure is controlled at the exit of the chamber by means of a Thar-SCF ABPR-20 back pressure regulator (BPR). This BPR consists of a precision valve attached to a motor and a pressure transducer. The needle position (range from 0 to 6000) will move

accordingly to maintain the desired experimental pressure. In order to protect the BPR from any solids that may form in the precipitation chamber a 5  $\mu\text{m}$  filter (Swagelok SS-2TF-LE) is placed between the chamber and the BPR. The outlet stream from the BPR is then conducted to a cyclone separator. This connecting line is heated with an electrical heating coil to avoid the formation of dry ice due to the Joule-Thompson cooling effect during expansion.

The cyclone separator is also a 500 mL stainless steel vessel. The  $\text{CO}_2$  flow exits the separator continuously during operation through the top of the vessel and is released to the atmosphere. The liquid solvent is forced to the bottom by centrifugal forces where it accumulates and is recolected at the end of the experiment.

At the beginning of the SAS experiments only  $\text{CO}_2$  flows through the system until steady state conditions are reached. This takes between 30 and 45 minutes. Once steady conditions are reached the solution is pumped in the precipitation chamber using a HPLC pump (Lab Alliance, Series III 10 mL pump). This pump incorporates a diaphragm-type pulse damper to reduce pulsation. Flow rates can be set between 0.01 and 10 mL/min in 0.01 mL/min increments. Valve  $V_1$  is opened when the pressure in the line equals that in the precipitation chamber and approximately 30 mL of solution are processed at each experiment. The solution enters the precipitation chamber through a 100  $\mu\text{m}$  nozzle to improve jet atomization. After the desired amount of solution has been pumped into the precipitation chamber the pump is stopped and valve  $V_1$  closed. Valve  $V_2$  is then slightly opened to purge any liquid remaining in the line in order to avoid dripping of the liquid into the precipitation chamber. When gas starts coming out of the purge  $V_2$  is closed.

After stopping the solution pump,  $\text{CO}_2$  flows continuously through the precipitation chamber to remove the solvent that has solubilized in the supercritical fluid. This washing step has been previously optimized as the time required to fill three times the precipitation chamber.<sup>1</sup>

$$t_{\text{washing}} = \frac{1500 \cdot \rho_{\text{CO}_2}}{F} \quad \text{eq. 3.1}$$

Where  $t_{\text{washing}}$  is the washing time in minutes,  $\rho_{\text{CO}_2}$  is the  $\text{CO}_2$  density in mg/mL and  $F$  is the  $\text{CO}_2$  flow rate in g/min. For the usual experimental conditions this step takes approximately 60 min.

After the washing step a depressurization step follows (at a rate of approximately 0.25 MPa/min).

The product in the reactor is carefully recollected and weighed. The liquid in the separator is also collected and weighed after evaporation of the solvent in a fume hood. A mass balance between injected solute and collected precipitate was used to calculate the yield ( $Y_P$ ). The yield was also calculated by the mass balance between the injected solute and the waste collected in the cyclon separator ( $Y_W$ ). The average between  $Y_P$  and  $Y_W$  was considered as yield ( $Y$ ). The discrepancies between injected solute and the amount of solute weighed in precipitation chamber and waste were between 5 to 10 %.

$$Y_p(\%) = 100 \cdot \frac{P}{Q \cdot C \cdot t} \quad \text{eq. 3.2}$$

$$Y_w(\%) = 100 \cdot \left(1 - \frac{W}{Q \cdot C \cdot t}\right) \quad \text{eq. 3.3}$$

$$Y(\%) = \frac{Y_p + Y_w}{2} \quad \text{eq. 3.4}$$

Where P is the amount of precipitate (mg), W is the amount of dry waste (mg), Q is the solution flow rate (mL/min), C is the solution concentration (mg/mL) and t is the time required to pump the solution into the precipitation chamber (min). The purge from  $V_2$  and the washing of the lines downstream of the precipitation chamber were added to the waste.

The SAS plant has two relief valves (Swagelok, SS-4R3A) placed in the  $\text{CO}_2$  and solution feeding lines to the precipitation chamber. A manual vent valve ( $V_4$ ) and a rupture disc (Zook, PB 1/4 "; 48.0 MPa) are placed between the precipitation chamber and the BPR . All connecting lines are 1/8 " chemically clean and passivated stainless steel tubing of 0.05 " wall thickness and 0.052 " inside diameter (Autoclave Engineers, MS 15-200 316 SS).

The SAS laboratory plant limiting conditions are 25.0 MPa and 343 K. A summary of the different components and specifications of the SAS equipment is displayed in Table 3.1.

Table 3.1 Equipment employed in the SAS laboratory plant.

Equipment	Manufacturer / model	Specifications	
<b>Temperature measuring</b>			
Thermocouples	RS Type J (Iron-Constantan)	Precision:	$\pm 0.1$ K
<b>Temperature control/display</b>			
Heating jacket Precipitation chamber	CAL 9400		
<b>Pressure measuring</b>			
Pressure sensor Precipitation chamber	Wika A-10	Range:	0 – 40.0 MPa
Pressure gauge CO <sub>2</sub> feeding line	Swagelok, EN-837-1 Class 2.5	Range:	0 – 25.0 MPa
<b>Vessels</b>			
Precipitation chamber	Thar-SCF	P <sub>max</sub> Volume	69.0 MPa 500 mL
Separator chamber	Thar-SCF	P <sub>max</sub> Volume	40.0 MPa 500 mL
<b>Pumps</b>			
CO <sub>2</sub> Pump	Thar-SCF P-50	Range:	0 – 65.0 MPa
HPLC Pump	Lab Alliance, Series III 10 mL	Range:	0 – 41.0 MPa
BPR	Thar-SCF ABPR-20	Range:	0 – 68.0 MPa
<b>Pressure relief</b>			
Rupture Disc	Zook, PB 1/4 "		48.0 MPa (295 K)
Relief valve	Swagelok, SS-4R3A		41.3 MPa (310 K)

## 3.2 High-pressure variable volume view cell

For some systems, the solubility of the active pharmaceutical ingredients (APIs) in  $\text{CO}_2$  and  $\text{CO}_2$ -cosolvent mixtures has been studied using a high-pressure variable-volume view cell. An image of the high-pressure view cell used in our laboratory and a schematic diagram of the set up are presented in Fig. 3.4.

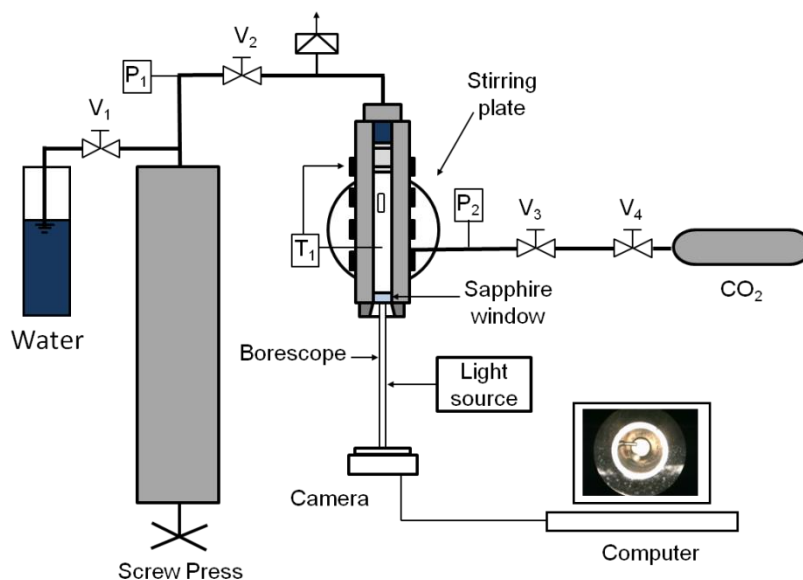
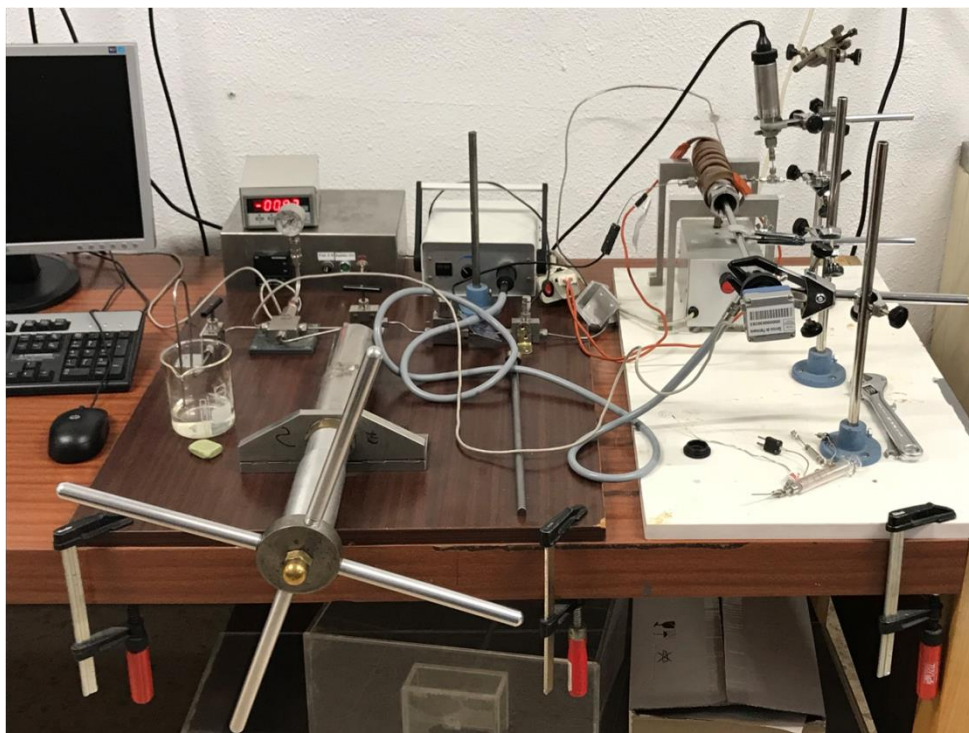


Fig. 3.4 Image of the high-pressure view cell and schematic diagram of the set up in our laboratory



A detailed description of the set-up and equipment validation can be found in a doctoral thesis defended in our research group<sup>2</sup>. A brief description of the equipment and experimental procedure is presented next.

The solid or solution whose solubility in supercritical CO<sub>2</sub> wants to be measured is weighed in a high precision balance (A&D GR-200, precision  $\pm 0.1$  mg) and placed inside the cell together with a magnetic stirrer. The cell is sealed with a sapphire window from the front and a mobile piston at the back. If a solution is to be introduced a syringe is used to weigh and introduce the solution.

The cylindrical high-pressure view cell is made of stainless steel and its inner volume is approximately 15 mL. The rear of the cell is connected to a screw press (manual high pressure pump filled with H<sub>2</sub>O as hydrostatic fluid). In the front of the cell a sapphire window allows us to observe the inside of the cell. Light is introduced in the cell by means of a borescope (Fiegert Endotech) to which a digital camera (Moticam 2000) is attached. The camera signal is sent to a computer to monitor and record the events that take place inside the view cell.

The high-pressure cell is heated with a silicon heating band (Omegalux SRT051-040) whose temperature is controlled using a temperature controller (Micromega CN77000 series). Temperature and pressure inside the precipitation chamber are measured using a thermocouple and a pressure transducer (Druck PTX7511-1). A rupture disc (ZOOK, PB 1/4 ") is placed between the screw press and the cell as a safety measurement.

CO<sub>2</sub> is introduced into the cell using a small tank of ca 20 mL filled with liquid CO<sub>2</sub>. This tank is then connected to the high-pressure cell and heated using a heat gun (the pressure gradient generated upon heating is used to fill the high-pressure cell). The small CO<sub>2</sub> tank is weighed before and after the filling (A&D GX-200, precision  $\pm 1$  mg) in order to determine the amount of CO<sub>2</sub> introduced into the cell.

Opening  $V_1$  and moving the screw press backwards fills the press with water.  $V_1$  is then closed and  $V_2$  opened. Moving the screw press forward will displace the mobile piston inside the cell, The cell volume is then decreased and at constant temperature pressure increases. Isothermal pressurization of the cell is continued until complete solubilization of the target solute or liquid in CO<sub>2</sub> is achieved. A stirring magnet is employed to ensure homogenization inside the cell at all time. Solubility measurements are then performed by slowly decreasing the pressure until the cloud point is reached and the liquid or solid phase appears. Measurements are repeated several times to improve accuracy. A brief summary of equipment and features can be found in Table 3.2.

Table 3.2 Equipment employed in the high pressure view cell.

Equipment	Manufacturer / model	Specifications	
<b>Temperature measuring</b>			
Thermocouples	RS Type J (Iron-Constantan)	Precision:	$\pm 0.1$ K
<b>Temperature control/display</b>			
Temperature controller	Micromega CN77000 series		
Heating band	Omegalux SRT051-040	$T_{\max}$	503 K
<b>Pressure measuring</b>			
Pressure sensor High pressure cell	Druck PTX7511-1	Range:	0 – 30.0 MPa
Pressure gauge	Swagelok, EN-837-1 Class 2.5	Range: Precision:	0 – 34.4 MPa $\pm 2.0$ MPa
<b>Vessels</b>			
High pressure cell	mechanical workshop (Universidad Complutense de Madrid)	$P_{\max}$ Volume	30.0 MPa 15 mL
CO <sub>2</sub> tank	mechanical workshop (Universidad Complutense de Madrid)	$P_{\max}$ Volume	15.0 MPa 20 mL
<b>Pressure relief</b>			
Rupture Disc	Zook, PB 1/4 "	31.8 MPa (295 K)	

### 3.3 Co-crystallization with supercritical solvent

CSS experiments were performed at the “Institut für Technische Thermodynamik und Kältetechnik” (ITTK) at the Karlsruher Institut für Technologie (KIT). A scheme of the CSS equipment is shown in Fig. 3.5.

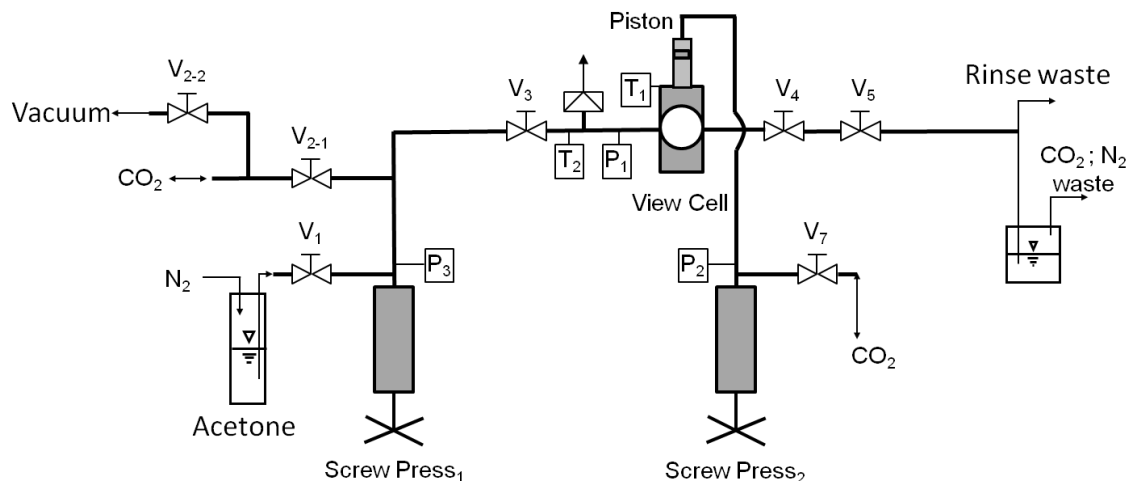


Fig. 3.5 Schematic representation of the CSS laboratory plant.

Equipment was designed to resist up to 65.0 MPa ( $\pm 5\%$  burst pressure of the SITEC rupture disc) and temperatures up to 423 K. Pressure was achieved by means of two screw presses (manual high-pressure pump systems) from Nova Swiss. Co-crystallization took place inside a view cell of maximum volume 7.3 mL equipped with a sapphire window. A piston maneuvered with screw press<sub>2</sub> was attached to the view cell enabling the variation of its volume from 3.3 to 7.3 mL. The view cell, piston volume, and pipes between V<sub>3</sub> and V<sub>4</sub> have heating bands to provide optimal temperature control. Temperature was measured using thermocouples from THERMOCOAX and pressure was measured by means of piezoresistive pressure sensors from WIKA. A brief summary of the different components of this equipment is provided in Table 3.3.

In the experimental procedure a defined amount of an API was weighed in a black PTFE carbon pan using a Mettler Toledo XS105DU balance (precision  $\pm 0.02$  mg). The same balance was used to weigh the cofomer that was then added to the pan. A stirring magnet ball was placed in the pan, it was then covered with a metal grid and another stirring ball was placed on the top to enhance mixing and avoid spillage in the cell (Fig. 3.6).

Table 3.3 Equipment employed in the CSS laboratory plant at the ITTK

Equipment	Manufacturer / model	Specifications / precision	
<b>Temperature measuring</b>			
Thermocouples	Thermocoax Type K (NiCrNi)	Precision: $\pm 0.3$ K (41 $\mu$ V/K)	
<b>Temperature control/display</b>			
Pipes	Eurotherm / 2116		
View cell	Eurotherm / 2116		
Piston	Eurotherm / 3216		
<b>Pressure measuring</b>			
Pressure sensor P <sub>1</sub> view cell	WIKA / 891.20.501	Range:	0 – 60.0 MPa
Pressure sensor, P <sub>2</sub> and P <sub>3</sub>	WIKA	Range:	0 – 60.0 MPa
<b>Screw Press</b>			
Screw Press <sub>1</sub>	Nova Swiss/ 550.0400.2	P <sub>max</sub>	70.0 MPa
		V <sub>piston</sub>	2.5 mL
		V <sub>∅</sub>	0.08 mL
Screw Press <sub>2</sub>	Nova Swiss/ 550.0301.1	P <sub>max</sub>	40.0 MPa
		V <sub>piston</sub>	5 mL
		V <sub>∅</sub>	0.15 mL
<b>Vacuum</b>			
Pump	Leybold / Trivac D 2.5 E	Suction:	3.2 m <sup>3</sup> /h
		capacity:	< 5·10 <sup>-4</sup> mbar
Display	Leybold /Thermovac TM 200	Range:	1·10 <sup>-4</sup> / 1·10 <sup>+3</sup> mbar
Magnet stirrer	Komet /H&P Variomac Power direct		
Weight balance	Denver Instruments/ 4102	Precision:	$\pm 0.05$ g
	Mettler Toledo/ XS 105 DU	Precision::	$\pm 0.02$ mg
Rupture Disc	SITEC / 720.5032	65.0 MPa $\pm 5$ % (293 K )	

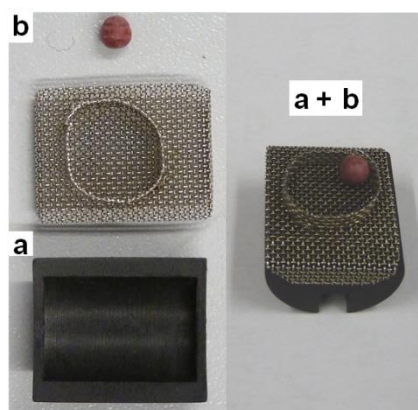


Fig. 3.6 PTFE carbon pan (a), stirring ball and metal grid (b) used in the co-crystallization experiments.

Temperature of the equipment was set to the desired experimental value and vacuum was applied. Valves  $V_3$  and  $V_4$  were closed and the view cell was opened to introduce the pan with the API and cofomer. Subsequently the cell was closed and tightened to 40 N using a torque wrench. Valve  $V_3$  was opened again until vacuum was restored and then valve  $V_{2-2}$  and  $V_3$  were closed. Piston was moved to its intermediate position with the screw press<sub>2</sub>. A CO<sub>2</sub> tank was submerged in a heating bath to elevate its pressure and connected to the line at  $V_{2-1}$ . Tank valve and  $V_{2-1}$  valve were opened and screw press drawn back in order to fill the press with CO<sub>2</sub>. Valve  $V_{2-1}$  was closed and screw press was drawn forward. After a positive pressure difference between  $P_1$  and  $P_3$  was achieved  $V_3$  was opened carefully and CO<sub>2</sub> was pumped slowly into the view cell to avoid major temperature fluctuations. Once the desired pressure in the view cell was reached the stirrer was turned on and experiment time count began.

In order to know the exact amount of CO<sub>2</sub> used in the experiment the CO<sub>2</sub> tank was weighed before and after use (Denver Instruments 4102 balance with precision  $\pm 0.05$  g). The remaining CO<sub>2</sub> in the lines and screw press<sub>1</sub> was recollected in another tank submerged in liquid N<sub>2</sub> and was also weighed to correct the mass balance.

After the desired experimental time the stirrer and the heating bands were turned off. First pressure was decreased slowly moving the piston backwards with the screw press<sub>2</sub> until full retraction. Pressure was further decreased till atmospheric value by moving slowly valves  $V_4$  and  $V_5$  (ensuring no abrupt pressure drop takes place and hindering particles being dragged out of the view cell). PTFE carbon pan was weighed to assess loss of cofomer or API during the experiment.

After each experiment the plant was washed out with acetone. N<sub>2</sub> was used to fill the pipes, view cell and screw press<sub>1</sub> with acetone. Temperature was set to 343 K and pressure was increased to 25.0 MPa with screw press<sub>1</sub>. After a couple of minutes valves V<sub>4</sub> and V<sub>5</sub> were opened and acetone removed. This procedure was repeated four times and nitrogen was used to drag out any acetone residues.

### **3.4 Particle characterization**

A brief description of the different characterization techniques used to establish the properties of the particles obtained in this thesis is presented.

#### **3.4.1 Dissolution profiles**

All the pharmaceuticals prepared were intended for solid oral dosage form. The particle dissolution profiles at constant pH were obtained using two different methods in two different equipments. All tests were performed at sink conditions.

##### **Dissolution profiles using a membrane diffusion method**

This is the method normally used for carrier based drugs. To measure the dissolution profile of 5-Fluorouracil (5-Fu) – Poly(L-lactide) (PLLA) composites a membrane diffusion method was employed. 20 mg of the 5-Fu samples were suspended in 5 mL of a pH 7.4 buffer solution (Sigma Aldrich P3813, 0.01M phosphate buffer). The suspension was then introduced in dialysis sacks (Sigma Aldrich D6066-25EA, molecular weight cut-off 12,000 Da) and sealed with dialysis tubing closures (Sigma Aldrich Z7371092-10EA). The bag was suspended in a flask containing 250 mL buffer solution at 310 K and stirred at 250 rpm.

1 mL aliquots of solution were taken at time intervals during 4 days. To keep the solution volume constant, 1 mL of buffer solution was added each time an aliquot was withdrawn. The content in 5-Fu of the samples was analysed using a UV/Vis Perkin-Elmer spectrophotometer model Lambda 35 at 265 nm.

##### **Dissolution profiles using a paddle apparatus**

For co-crystals, the dissolution profile was obtained using a standardized paddle apparatus. To measure the dissolution profile of diflunisal (DIF) the United States pharmacopeia (USP) monograph for DIF was followed. 13 mm diameter tablets of 100 mg of DIF were prepared using an hydraulic press at 5000 kg/cm<sup>2</sup>. Tablets were introduced in a Sotax USP apparatus 2 (vertical paddle apparatus with stirring set at 50 rpm) that contained

0.9 L of a 7.4 pH buffer solution (Sigma Aldrich P3813, 0.01M phosphate buffer) at 310 K. 5 mL aliquots were taken at time intervals during 8 hours, and analogously as in the membrane method, 5 mL of buffer solution were added after each sample was taken. The DIF content in the samples was analysed using a UV/Vis Perkin-Elmer spectrophotometer model Lambda 35 at 306 nm.

### 3.4.2 Powder X-ray diffraction (PXRD)

Diffraction patterns of the samples were measured prior and after processing to assess changes in their crystal structure. Samples were measured in a Philips X'pert, model MPD diffractometer on reflection mode. A Cu anode X-ray tube with two goniometers was powered at 40 kV and 40 mA ( $K_{\alpha 1}$  1.54056 Å). Samples were scanned between 5 ° to 50 ° 2 $\theta$  with a step size of 0.016 ° 2 $\theta$  using the Bragg-Bentano geometry. Measurements were performed at the X-ray facilities of Universidad Compluense de Madrid.

### 3.4.3 Micro-elemental analysis

This technique provides a sensitive method to determine the sample content in C, H, N and S. The sample undergoes an instantaneous and complete combustion, followed by selective reduction of nitrogen oxides, and being the elements transformed into CO<sub>2</sub>, H<sub>2</sub>O, N<sub>2</sub> and SO<sub>2</sub>. The effluents are then transported to independent sensors. Equipment used to measure our samples was a LECO CHNS-932 with a  $\pm$  0.35 precision for C and S and a  $\pm$  0.3 precision for N and H. Samples were measured at the Micro-elemental analysis facilities of Universidad Complutense de Madrid. The C to N or S ratio of the products was used to study the composition of the precipitates.

### 3.4.4 Scanning Electron Microscopy (SEM) and energy-dispersive detection X-ray (EDX)

SEM uses a focused beam of high-energy electrons to generate a variety of signals at the surface of a sample. The electron-sample interaction signals provide information about the morphology, topography and chemical composition. Data collected over a selected area is used to generate a two dimensional image. The SEM is also capable of performing EDX analysis of selected locations of the sample permitting qualitatively or semi-quantitatively determination of chemical compositions. SEM images were taken in a Jeol 6335F electron microscope with an accelerating voltage of the electron beam of 10, 15 or 20 kV. Samples were previously coated with gold in a Q150RS Rotary-Pumped Sputter Coater. Analyses were performed in the National Centre of Electron Microscopy located at Universidad Complutense de Madrid.

### 3.4.5 Infrared Spectroscopy (IR)

Molecules absorb specific frequencies that are characteristic of their structure. IR is a useful tool in co-crystal characterization because the functional groups in the co-crystal spectrum show differences in the wavenumbers and intensity of the vibrational modes in comparison to those of the two cofomers individual spectra. The synthons established will present characteristic bands.

Most instruments nowadays are Fourier transformed infrared (FTIR) spectrometers which simultaneously collect data over a wide spectral range at a time. Radiation in the infrared region (instruments usually work in the mid infrared radiation from 4000 to 400  $\text{cm}^{-1}$ ) is passed through a sample and uses a detector to measure the percent transmission of the radiation through the sample. In a representation of the transmittance versus the wavenumber of the radiation, a downward peak will reveal the wavenumber at which the radiation absorption is taking place.

Infrared spectra of the samples were obtained using the spectrum 100 Fourier-transform infrared spectrometer from Perkin Elmer with the universal attenuated total reflection (ATR) sampling accessory at a resolution of 4  $\text{cm}^{-1}$ . Samples were measured in the 4000-650  $\text{cm}^{-1}$  range.

### 3.4.6 Thermogravimetric Analysis (TGA)

TGA analysis measures the changes in weight of a sample as function of temperature, as it undergoes a controlled temperature program in a controlled atmosphere. This allows the determination of the temperature of decomposition and the weight change associated to it, what can lead to quantitative analysis of composition. It can also determine the content in water or residual solvents. TGA measurements in this thesis were performed in two different instruments.

**1** TA Instruments Q500 thermobalance equipped with an evolved gas analysis (EGA) oven connected to a ThermoStar Omnistar GSD 301 O/301T mass spectrometer. Samples were placed in open Pt containers and heated at 10 K/min under a 100 mL/min  $\text{N}_2$  flow from room temperature to the desired value. These measurements were performed at the thermal analysis facilities of Universidad Autónoma de Madrid.

**2** TA SDT Q600 (simultaneous DSC and TGA). Samples were placed in open Pt or Al pans and heated at 5 K/min under a 100 mL/min  $\text{N}_2$  flow from room temperature to the desired value.



### 3.4.7 Differential scanning calorimetry (DSC)

DSC is a technique that observes how the heat capacity of a material ( $C_p$ ) is affected by temperature. This allows the detection of several transitions such as melting, glass transitions and other phase changes. The temperature of the sample and a reference are maintained equal and the heat flow required to achieve this is measured. DSC curves of untreated and processed materials were measured in a TA Instruments DSC Q 20 modulated DSC connected to a refrigerating cooling system (RCS). Experiments were run with a nitrogen flow of 50 mL/min. Samples were contained in tightly sealed aluminium pans and weighed using a MT5 Mettler microbalance (error of  $\pm 0.001$  mg). Temperature and enthalpy of the calorimeter were previously calibrated using standard samples of In (purity > 99.999%), Sn (>99.9%) and benzoic acid (>99.97%).

DSC analysis is a useful characterization technique that in scope of this thesis can be applied to:

Polymorph identification: DSC can identify polymorphs through the differences in their melting points. However, the endothermic peak associated to the melt might be followed by an exothermic peak associated to the crystallization to a more stable polymorph. This endo-exo event can overlap and be difficult to identify. Reducing the heating rate generally increases resolution but reduces sensitivity. For example, if we had a sample consistent of the metastable form A only, using a fast heating rate can avoid the recrystallization of form B during the melt and give us therefore a better view of the real content of our sample. Conversely, a slower heating rate will separate the melting and recrystallization peaks making them easier to identify, but form B might not be present at all in our original sample and be formed during the scan only.

Amorphous phase identification: The transition from the amorphous glassy state (state at which molecules have no mobility) to a rubbery state (molecules exhibit a certain degree of mobility) takes place over a range of temperatures and is known as the glass transition ( $T_g$ ). DSC is often use to measure this transition. If the amorphous material is dispersed in another material the recrystallization of the amorphous material might not take place<sup>3</sup> and a recrystallization exotherm will not be observed.

Co-crystal phase diagram identification: Different thermal transitions will take place in our sample upon heating depending on the composition of our sample as it can be seen in Fig. 3.7. Heating pure A, co-crystal A-B, or B will show a single endothermic peak with onset at  $T_A$ ,  $T_{A-B}$ , or  $T_B$ , respectively. Other compositions with mixture of phases A, B, and/or A-B will result in thermograms with several peaks. In the case of a congruent melting system like

the one represented in Fig. 3.7, with good sample homogenization a first peak will take place with onset at one of the eutectic points. The base line will recover when the melting is completed and only a liquid phase (L) is left.

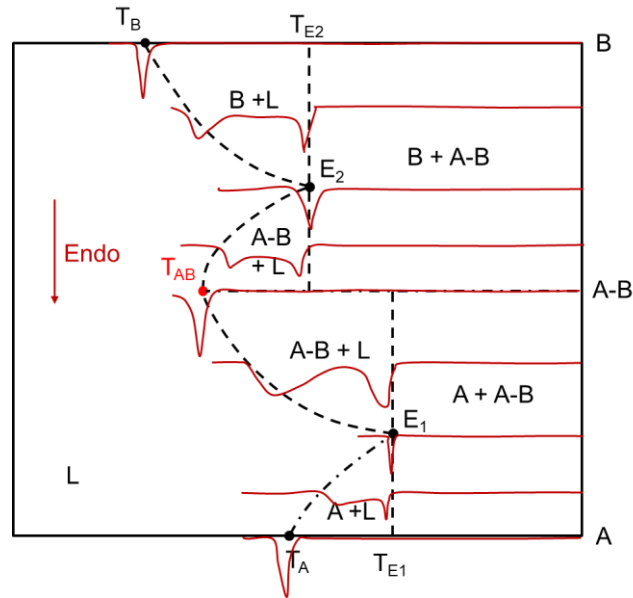


Fig. 3.7 Representation of DSC curves in the binary phase diagram of a congruent melting system.

## References

1. Zahran, F. R. Microparticles precipitation using supercritical CO<sub>2</sub> as an Antisolvent. Role of thermal effects and phase equilibria. Universidad Complutense de Madrid, Madrid, **2012**.
2. Pérez, E. V. Equilibrio de fases y solubilidades en fluídos supercríticos. Universidad Complutense de Madrid, Madrid, **2008**.
3. Balani, P. N.; Wong, S. Y.; Ng, W. K.; Widjaja, E.; Tan, R. B. H.; Chan, S. Y., Influence of polymer content on stabilizing milled amorphous salbutamol sulphate. *International Journal of Pharmaceutics* **2010**, 391 (1-2), 125-136.

# **Chapter 4**

## **Comprehensive discussion of results**



## 4 COMPREHENSIVE DISCUSSION OF RESULTS

The most relevant results obtained in this doctoral thesis are summarized in a comprehensive way in this chapter. Some of these results have been published in four peer reviewed publications that can be found attached in the publications section of this thesis. Other unpublished work can be found in chapter 5 of this thesis: “*Co-crystallization of 5-fluorouracil using supercritical CO<sub>2</sub>*”. The unifying discussion of results will be structured in the following blocks:

- Preparation and characterization of 5-Fu-polymer composites using the supercritical antisolvent technique (SAS). Controlled drug delivery through supercritical CO<sub>2</sub> processing. Publication I.
- Preparation of pharmaceutical co-crystals via SAS. Evaluation of the influence of SAS parameters in the co-crystal production. Publication II.
- Influence of SAS operating parameters in co-crystal polymorphism. Publication III.
- Limiting parameters in the successful preparation of co-crystals using supercritical CO<sub>2</sub>. Chapter 4: Co-crystallization of 5-Fluorouracil (5-Fu) using supercritical CO<sub>2</sub>.
- Preparation of metal organic frameworks (MOFs) via SAS. Evaluation of the SAS technique. Publication IV.

### 4.1 Preparation and characterization of 5-Fu-polymer composites using the SAS technique. Controlled drug delivery through supercritical CO<sub>2</sub> processing

Drug micronization can increase the bioavailability of an active pharmaceutical ingredient (API), facilitate the use of different administration routes and reduce the required dosage. The production of composites of drugs with biocompatible polymers for controlled delivery has raised a great interest in the last decade<sup>1</sup>. Especially in the treatments which involve the use of drugs with a high toxicity, like the treatment of cancer with chemotherapy<sup>2</sup>. A controlled drug release can milder the side effects of the API and reduce the amount of drug required for the treatment.

Due to the benefits presented by the composites of a drug and a biocompatible polymer the aim of this first work was to explore the production of composites for

controlled drug delivery using the SAS technique. 5-Fu was chosen as the target drug due to its proven antitumoral properties. Poly(L-lactic acid) (PLLA) was chosen as the suitable carrier because it is a biocompatible polymer (produced from biobased raw materials such as corn starch) and has been used in the encapsulation and preparation of composites of several drug formulations<sup>3</sup>.

A 1:1 v/v % mixture of dimethylsulfoxide (DMSO) and dichloromethane (DCM) was chosen as the solvent. Influence of temperature and pressure was studied (see Table 4.1). Concentration (5 mg/mL for both composite components), solution flow rate (1 mL/min) and CO<sub>2</sub> flow rate (20 g/min) were kept constant.

**Table 4.1 Temperature and pressure conditions for 5-Fu and PLLA composite preparation using SAS and drug loading.**

Experiment	Temperature (K)	Pressure (MPa)	5-Fu loading (% w)
9	308	12.0	35
10		18.0	32
11	323	12.0	42
12		18.0	36
13		25.0	18

In the range of temperatures and pressures studied the influence of these parameters on particle morphology was low. SAS composites presented in all cases a similar morphology (see Fig. 4.1): large crystals of 5-Fu (lengths range from 10 to over 100  $\mu\text{m}$ ) coated by a layer of PLLA spheres. The size of the spheres increased with operating temperature from 600  $\pm$  200 nm at 308 K to 1200  $\pm$  300 nm at 323 K. Composite components were precipitated separately at 323 K and 18.0 MPa (conditions that led to optimal particles in the precipitation of 5-Fu in DMSO<sup>4</sup>). These conditions led to large 5-Fu crystals and small aggregated PLLA particles.

Loadings of 5-Fu in the composites were measured using thermal gravimetric analysis (TGA) as 5-Fu and PLLA decompose at very different temperatures. Pressure increase seemed to have a negative influence on drug loading with a clear descent of 5-Fu content in the experiment at 25.0 MPa. Analysis was repeated after 5 months and no changes were observable indicating composite material stability.

The dissolution profile of the composite was measured and compared to that of the pure drug in order to assess if controlled drug delivery was achieved. The

cumulative release rates of the composite showed to be much slower than those of the pure drug (see Fig. 4.2), thus a successful 5-Fu drug formulation was achieved.

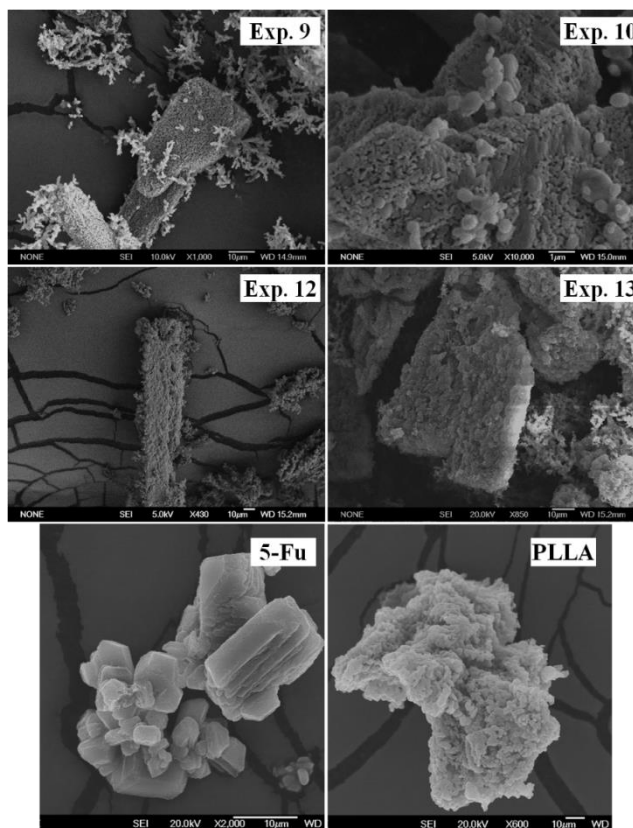


Fig. 4.1 SEM images of the 5-Fu composites and of pure 5-Fu and PLLA processed by SAS at 323 K and 18.0 MPa using as a solvent a 1:1 v/v % DMSO + DCM mixture.

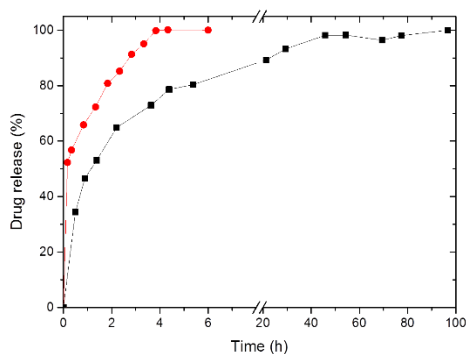


Fig. 4.2 Dissolution profiles of pure 5-Fu (●) and the 5-Fu-PLLA composite (■) obtained by SAS precipitation at 323 K and 18.0 MPa.

SAS was proven to be capable of producing 5-Fu-PLLA composites in a one-step process. These composites presented no change in the polymorphic form of the API and EDX analysis showed that complete removal of DMSO and DCM was



accomplished. Despite an initial burst release of approximately 37 % in the first hour, over four days were required to achieve a full release of 5-Fu.

## 4.2 Preparation of pharmaceutical co-crystals via SAS. Evaluation of the influence of SAS parameters in the co-crystal production

Co-crystallization is an emerging technique used in the pharmaceutical industry to improve important properties of new produced drugs such as solubility, dissolution profiles, shelf life and mechanical or organoleptic properties<sup>5</sup>. Moreover, co-crystallization of two APIs is becoming an important field of research in the treatment of complex disorders<sup>6</sup>. To the best of our knowledge SAS co-crystallization had been attempted only twice.<sup>7, 8</sup>

**Table 4.2** Values for factors used in the SAS co-crystallization and the factorial design of experiments used. solution flow rate (1 mL/min), CO<sub>2</sub> flow rate (20 g/min), nozzle diameter (100 µm) were kept constant.

Factor	Unit	Low level (-)	High level(+)	
Temperature	K	308	313	
Pressure	MPa	10.0	12.0	
DIF concentration	mg/mL	15	30	
Experiment	Temperature	Pressure	Concentration	Solvent
1	-	-	-	Acetone
2	-	+	-	Acetone
3	+	-	-	Acetone
4	+	+	-	Acetone
5	-	-	+	Acetone
6	-	+	+	Acetone
7	+	-	+	Acetone
8	+	+	+	Acetone
9	-	-	-	Ethanol

After studying the production of a composite using the SAS technology, we decided to explore the formation of co-crystals using this technology. For this purpose, we chose a co-crystal formed by diflunisal (DIF) and nicotinamide (NIC) (in a 2:1 molar

ratio). DIF is a non steroidal anti-inflammatory drug (NSAID) with analgesic activity that belongs to class II in the biopharmaceutics classification system (BCS). This means DIF has low solubility and high permeability. NIC is a form of vitamin B3 and is a molecule belonging to the generally recognized as safe (GRAS) list. Through the co-crystallization of DIF and NIC a faster release rate is aimed so that patients can feel a quicker relief of pain.

A factorial design of experiments at two levels was used to assess the influence of temperature, pressure and concentration (see Table 4.2). Experiments were performed using acetone as solvent. All the experiments were carried out using the corresponding stoichiometric amount of NIC.

An additional experiment at 308 K, 10.0 MPa and 15 mg/mL DIF concentration was made in ethanol to investigate the influence of solvent. The same conditions of pressure and temperature were used to precipitate DIF and NIC separately.

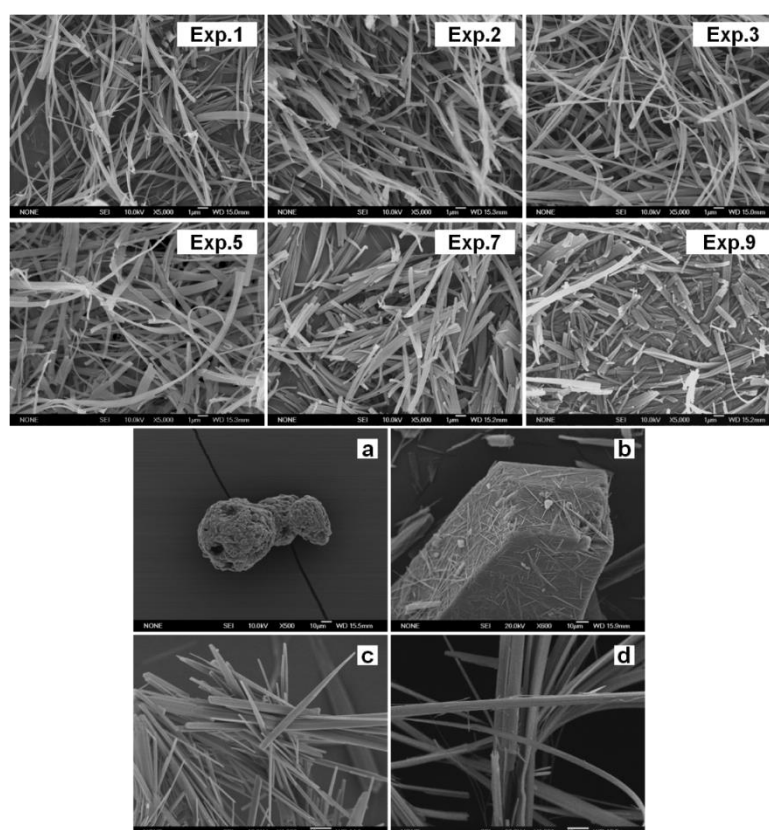
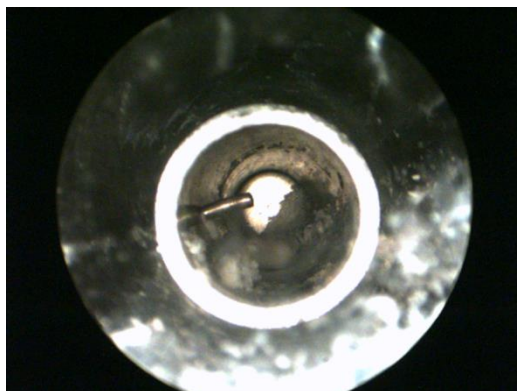


Fig. 4.3 SEM images of the co-crystals obtained in experiments 1-3, 5, 7 and 9; commercial NIC (a) and DIF (b) and SAS processed NIC (c) and DIF (d).

As it may be seen in Fig. 4.3 the effect of temperature, pressure, concentration and solvent in the co-crystal morphology showed a weak influence and narrow needle-like microparticles were obtained. Same kind of morphology was exhibited by the SAS processed NIC and DIF (see Fig. 4.3). Nevertheless, a considerable particle size reduction with a homogeneous size distribution was achieved.

The needle-like morphology could be explained by a possible solubilisation of the solutes in the solvent-CO<sub>2</sub> mixture. Nucleation and crystal growth will then take place following a liquid-like mechanism leading to larger particles. Another possible explanation would be the solute influence on the phase diagram. In a first approximation, we considered this effect negligible but this does not have to be necessary true. Planned pressure and temperature conditions were above the critical point of the binary mixture and in the one-phase region, but a shifting of this point to higher values could mean that we had been operating with a liquid phase in the precipitation chamber. To rule out this possibility, the NIC-DIF solution in acetone of experiment one was introduced together with CO<sub>2</sub> in the view cell with the same CO<sub>2</sub> molar fraction as that used in the experiments (0.98). As it can be seen in Fig. 4.4, no liquid phase was observable in the cell so we can confirm that experiments were therefore performed in a one-phase region.



**Fig. 4.4** View cell with the DIF-NIC solution at the concentration used in experiment 1 and a CO<sub>2</sub> molar fraction equal to 0.98 at 313 K and 10.0 MPa.

Several characterization techniques were employed to analyse the precipitates obtained via SAS. All of them indicated co-crystal formation without homocrystals detected. Powder X-ray diffraction (PXRD) patterns presented the diffraction peaks at  $2\theta$ : 6.6, 8.2, 14.0 and 16.5 ° (see Fig. 4.5) that had been previously described by Évora et al.<sup>9</sup> and Wang et al.<sup>10</sup> for this co-crystal. Differential scanning calorimetry (DSC) showed a sharp peak with onset at 467.5 K. This fusion temperature was intermediate

between those of pure NIC (402.6 K) and pure DIF (485.5 K). As a consequence of DIF processing via SAS, pure DIF changed its polymorphic form.

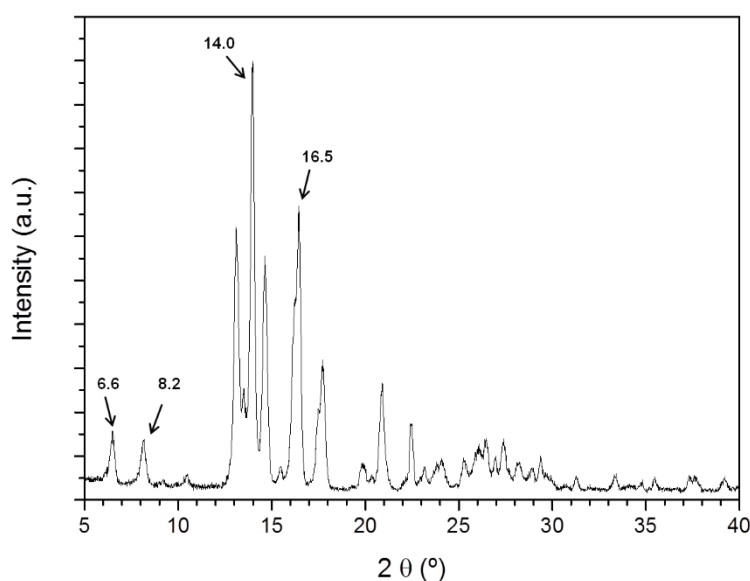


Fig. 4.5 PXRD pattern of the DIF-NIC co-crystal obtained by SAS in experiment 1.

The dissolution profile of the DIF-NIC SAS co-crystal obtained in experiment 1 was compared to that of pure DIF. Measurements were made following the U.S. Pharmacopeia (USP) monograph for DIF in a U.S. Food and Drug Administration (FDA) paddle apparatus at the Pharmacy Faculty of Universidad Complutense de Madrid. A slight improvement in the cumulative release rate was observed (see Fig. 4.6). Larger improvements had been measured for this co-crystal by other authors<sup>9, 10</sup> using smaller and coated tablets. Further dosage forms of the co-crystal apart from tableting could be investigated. Despite not having achieved a substantial improvement in the release rate, the obtained drug formulation may also be considered an improved drug formulation due to additional synergistic therapeutic benefits that the pharmaceutical activity of NIC in combination to that of DIC may offer.

Because the window of operating conditions used in the factorial design of experiments was too narrow further operating conditions different from those described in the publication were studied. Experiments at 333 K and 15.0 MPa were performed and no change in particle morphology was observable.

Microelemental analysis indicated that purities of the co-crystals were over 99%. TGA showed no mass loss associated to the evaporation of residual solvent from the SAS obtained co-crystals. The SAS technique was employed to produce a pure

co-crystal phase of the 2:1 DIF-NIC co-crystal in a single step, semicontinuous process. The influence of the studied variables had very little effect on the outcome of the SAS process in this particular system and further experimentation was required to understand these effects. Sections 4.4 and 4.5 of this chapter are aimed to explain these effects.

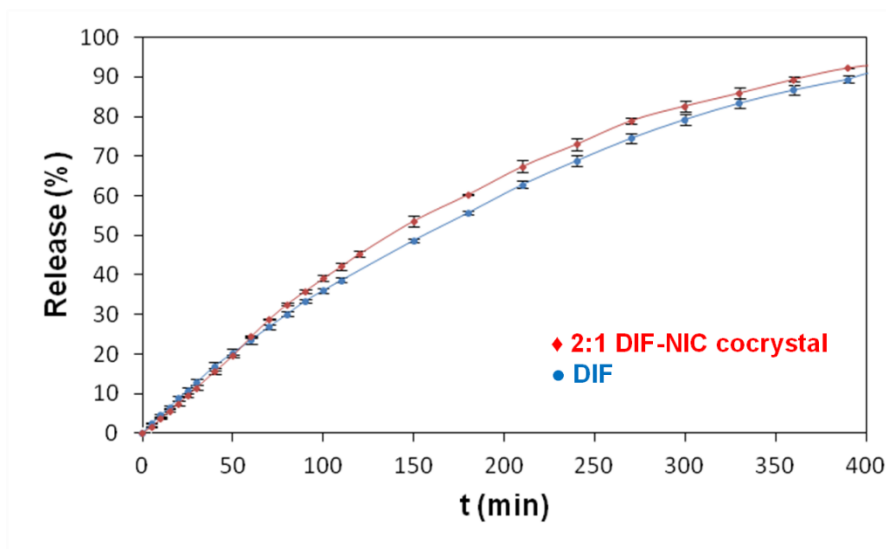


Fig. 4.6 Dissolution profiles of the untreated diflunisal (●), and the DIF-NIC co-crystal obtained by SAS in experiment 1 (♦).

### 4.3 Influence of SAS operating parameters in co-crystal polymorphism

As stated earlier in the introduction of this thesis, distinct polymorphic forms of an API can present different physicochemical properties (solubility, stability...) affecting the quality, safety and effectiveness of the final product formulation. Drug formulations seek API purity and therefore, the API should be in a distinctive solid form. Changes in the polymorphic form of an API upon SAS precipitation had been observed previously in publication I. Commercial DIF is a mixture of polymorphs with a main content of form I. After SAS processing in acetone at 308 K and 10.0 MPa DIF exhibited the form V. If SAS is going to be used in the formation of co-crystals for enhanced drug formulations, we should investigate the formation of different polymorphs of a co-crystal.

The co-crystal chosen for this purpose was that formed by carbamazepine (CBZ) and saccharin (SAC). CBZ is an anticonvulsant drug used in the treatment of epilepsy and a BCS class II drug (low solubility and high permeability). CBZ forms a

co-crystal with SAC (compound frequently used as an excipient in drug formulations) with a 1:1 molar ratio. Through its co-crystallization with saccharin an improvement in the solubility<sup>11</sup> and shelf life<sup>12</sup> of CBZ has been reported. Moreover, this co-crystal has two well known polymorph forms, whose crystallographic information file (CIF) is available in the Cambridge crystallographic data centre (CCDC).<sup>13, 14</sup> Hence, it seemed as an optimal candidate to investigate polymorphism of co-crystals via SAS and study the conditions that will allow us obtain an improved CBZ formulation.

First the influence of the solvent was assessed. In crystal and co-crystal preparation through conventional methods the solvent election has proved to be a key factor in the polymorphic outcome<sup>15</sup>. Experiments were performed at 10.0 MPa and 313 K (conditions above the critical point of all the CO<sub>2</sub>-solvent binary mixtures employed). Concentrations of CBZ and SAC were chosen in order to be relatively close to the saturation value of the less soluble cofomer in the corresponding solvent and always maintaining the 1:1 CBZ-SAC molar ratio of the co-crystal. Solution flow rate was 1 mL/min and CO<sub>2</sub> flow rate was 20 g/min. A summary of conditions and results is presented in Table 4.3.

**Table 4.3 Summary of conditions and results for the 1:1 CBZ-SAC co-crystallization by SAS using several solvents at 313 K and 10.0 MPa.**

Run	Solvent	CBZ (mg/mL)	Yield (%)	Polymorph	Melting point (K)	Morphology
1	Methanol	30	65	I	447.9	Plate-like
2	Ethanol	15	55	I+II	437.1; 445.3	Plate-like and Needle-like
3	DCM	2.6	40	I+II	445.3	Plate-like and Needle-like
4	DMSO	65	*	*	*	*

PXRD analysis of the different samples showed that only experiments performed in methanol produced a precipitate consisting in a pure polymorph I phase (see Fig. 4.7). Polymorph I of the CBZ-SAC co-crystal presents characteristic diffraction peaks at  $2\theta$ : 7.0, 14.1, 23.9, 15.7, 28.3 and 28.3 ° whilst characteristic diffraction peaks of the polymorph II are at  $2\theta$ : 5.0, 11.5, 12.8, 15.0 and 25.7 °. Co-crystals obtained using methanol as a solvent presented the characteristic diffraction peaks of polymorph I at  $2\theta$ : 7.0, 14.1 and 28.3 only. Co-crystals produced with ethanol and DCM presented diffraction peaks of both polymorphs in their

respective PXRD patterns, indicating a mixture of polymorphs in their compositions. In no case homocrystals were detected.

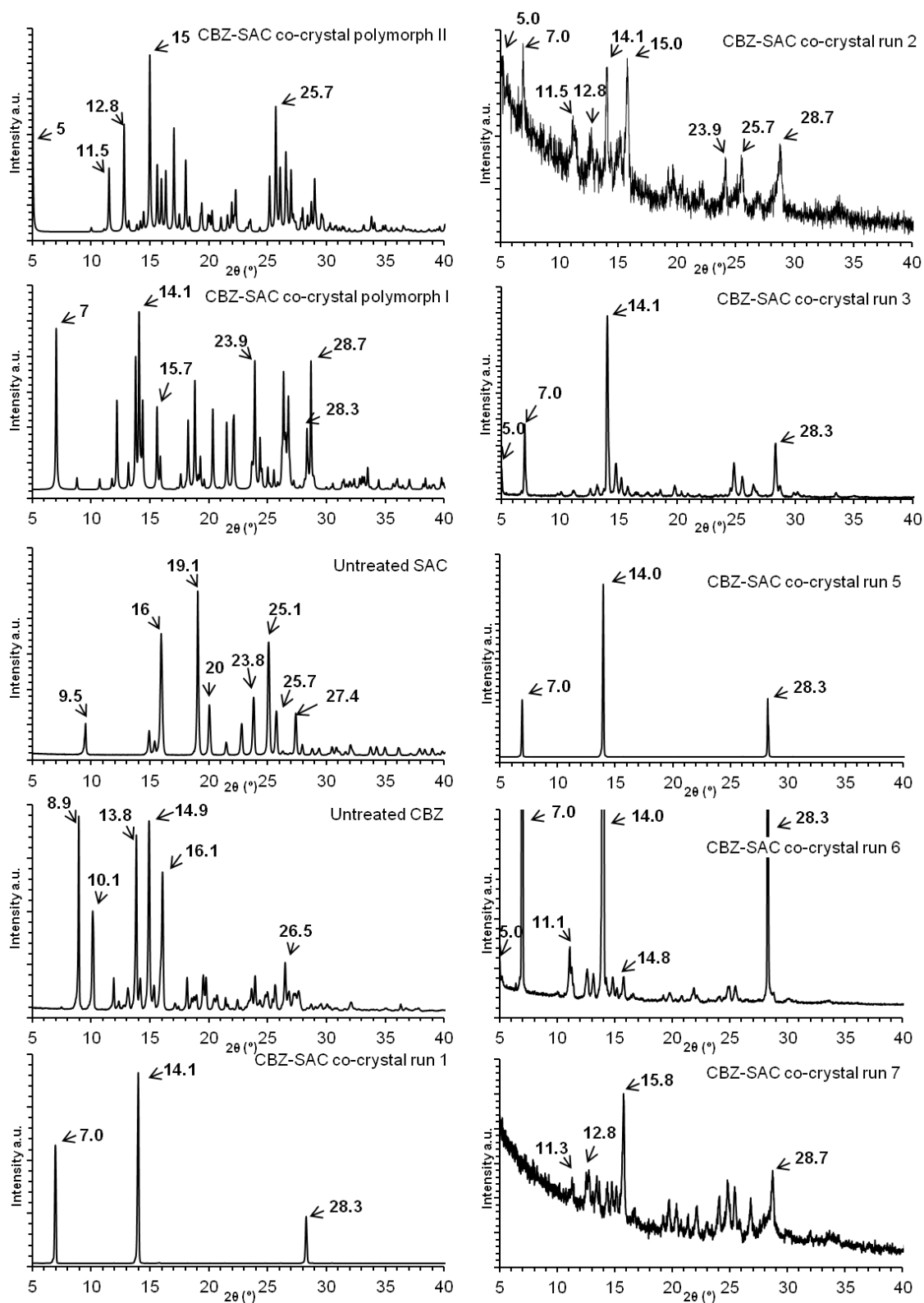


Fig. 4.7 PXRD patterns of CBZ-SAC co-crystals polymorphs I and II simulated from crystallographic information file. Experimental PXRD patterns of untreated CBZ, SAC and co-crystals of CBZ-SAC obtained in runs 1, 2, 3, 5, 6 and 7.

These findings were corroborated by FTIR and DSC analysis. Polymorph I presents characteristic absorption bands of the amide stretching at 3500 and 3434  $\text{cm}^{-1}$ , and of the amide carbonyl group at 1645  $\text{cm}^{-1}$ .<sup>14</sup> These same absorption bands were found in the co-crystals obtained using methanol. Co-crystals obtained using ethanol and DCM exhibit absorption bands at frequencies similar to those of polymorph II<sup>14</sup> (3430 and 3350  $\text{cm}^{-1}$  for the amide stretching and 1668  $\text{cm}^{-1}$  for the amide carbonyl group).

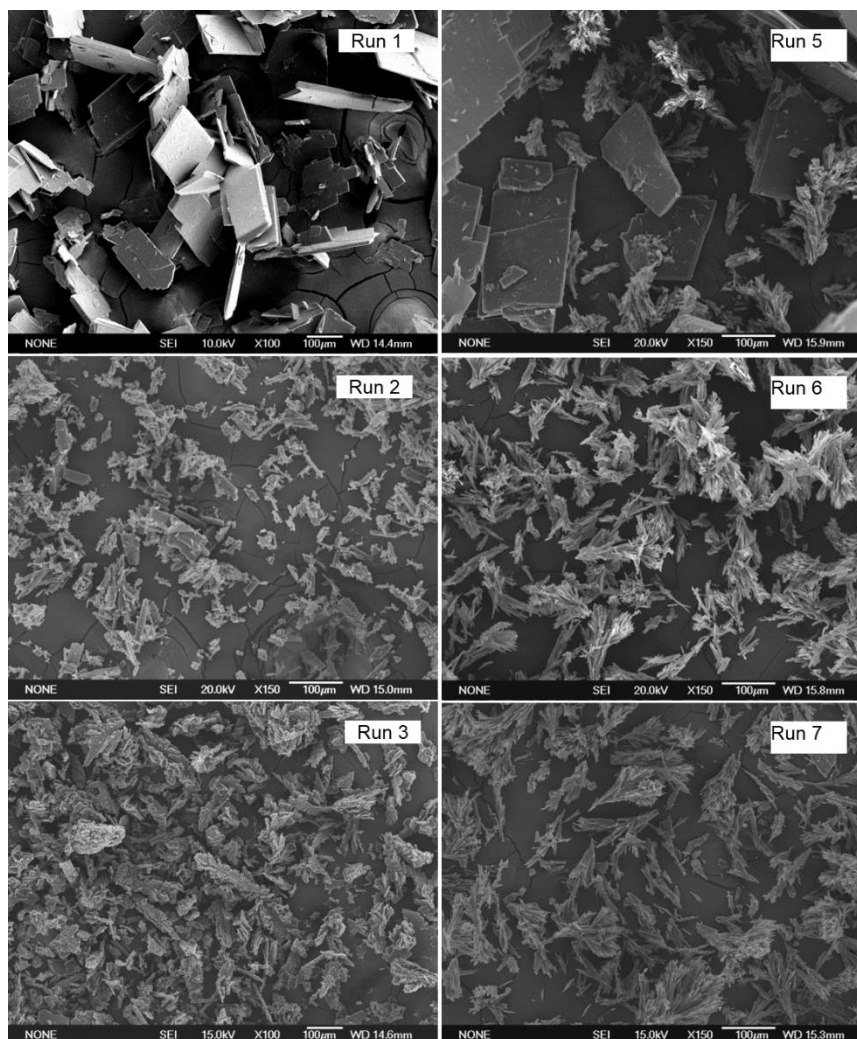


Fig. 4.8 SEM images of CBZ-SAC co-crystals obtained in runs 1,2,3,5,6 and 7.

DSC analysis showed only one endothermic peak for the co-crystal obtained using methanol with onset at 447.9 K (similar to the one described for polymorph I at 445 K<sup>14</sup>). The thermogram of polymorph II exhibited two transitions at 441 K and 445 K.<sup>14</sup> Co-crystals obtained using ethanol presented two transitions with onsets at 437.1 and 445.3 K and co-crystals obtained in DCM only one at 445.3 K.



SEM images of the precipitates (see Fig. 4.8) also backed these findings. For this co-crystal a plate-like morphology for form I and a needle-like one for form II have been reported.<sup>14</sup> The co-crystal obtained in methanol presents a plate-like morphology accompanied by plate-like agglomerates (heterogeneous sizes with widths between 5 and 10  $\mu\text{m}$ ). Co-crystals obtained using ethanol present a mixture of agglomerated plate-like and agglomerated needle-like morphologies and those obtained using DCM present a plate-like morphology and seem to agglomerate in one direction. In both cases a much smaller size is obtained through SAS processing.

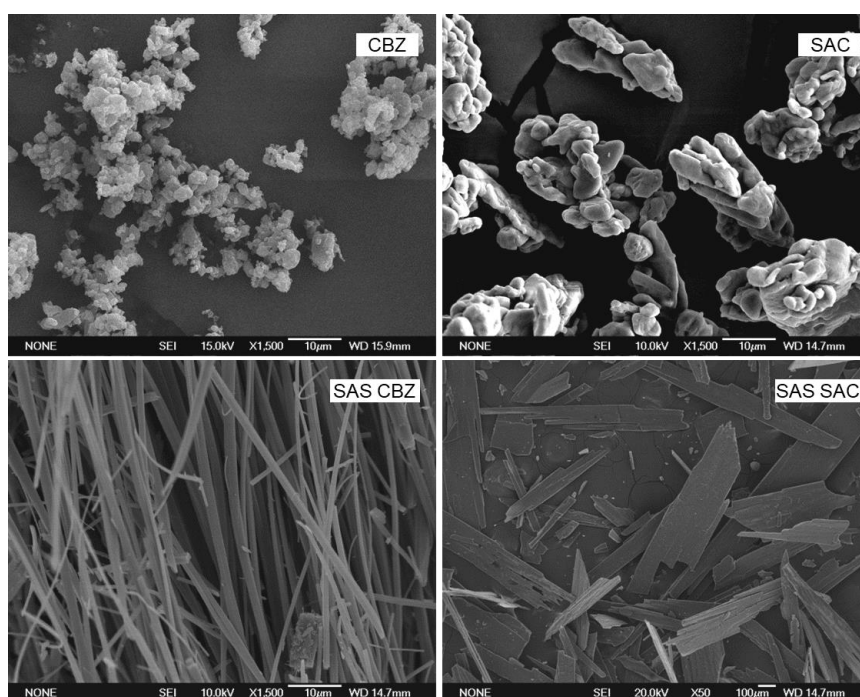


Fig. 4.9 SEM images of comercial CBZ and SAC, and SAS processed CBZ and SAC using conditions of run 1.

For comparison purposes pure CBZ and SAC were also precipitated in methanol at the conditions of run 1. Commercial CBZ consisted in a mixture of polymorphs I and III. After SAS processing only form I was detectable. SAC kept its monoclinic form. The morphology of both components changed from agglomerated particles to fine needles in the case of CBZ and to thin fragmented plates of heterogeneous size in the case of SAC (see Fig. 4.9). Both components presented a larger surface area after SAS processing. The SAS crystals and co-crystals obtained in this study demonstrate the reduction of size through SAS.

Experiments performed in DMSO failed to produce any precipitate and generated clogging in the back pressure regulator (BPR). A partial solubilisation of the

co-crystal components in the CO<sub>2</sub>-DMSO mixture might have been the reason of this behaviour.

We then proceeded to observe the influence of operating parameters. We chose as solvent methanol and pressure, temperature and concentration were varied (see Table 4.4).

**Table 4.4 Summary of conditions and results for the 1:1 CBZ-SAC co-crystallization using methanol as a solvent. CO<sub>2</sub> density for runs 1, 5, 6 and 7 was 0.63, 0.78, 0.6 and 0.6 (mg/mL), respectively.**

Run	T (K)	P (MPa)	CBZ (mg/mL)	Yield (%)	Polymorph	Melting point (K)	Morphology
1	313	10.0	30	65	I	447.9	Plate-like
5	313	15.0	30	50	I	447.9	Plate-like
6	333	15.0	30	60	I+II	438.1; 443.2	Needle-like
7	333	15.0	15	45	I+II	439.2; 444.7	Needle-like

Increasing the pressure from 10.0 to 15.0 MPa did not change the polymorphic outcome. The PXRD pattern of run 5 showed the same reflections peaks as that of run 1, i.e., polymorph I (see Fig. 4.7). An increase in temperature led to a mixture of polymorphs (run 6). Reducing the concentration of the component at the highest temperature and pressure (run 7) produced a significant change in the PXRD pattern. Diffraction peaks of both polymorphs were present with increased intensity in the reflection peaks of form II and decreased intensity in those of form I. The pattern though showed low crystallinity and conclusions about the phases present were difficult. FTIR and DSC analysis of the samples confirmed the PXRD results.

SEM images (see Fig. 4.8) revealed that an increase in pressure resulted in a higher amount of agglomerate in the sample. A plate-like morphology was still present. Samples from runs 6 and 7 at higher temperatures presented a needle-like agglomerated morphology.

From this study we could withdraw some findings. The increase in pressure of 5.0 MPa at constant temperature and therefore in density (increase of 0.15 mg/mL) did not influence the polymorphic outcome. This suggests that the density of the antisolvent does not have a major role in the polymorphic outcome. Macromorphology

and yield though were influenced by pressure. Higher pressures reduced the yield of the process and produced a higher amount of agglomerate.

The solvent showed to be a crucial factor in the polymorphic outcome. Solute-solvent interactions have been described as a key factor in the preparation of different polymorphs using conventional crystallization via solution and evaporation<sup>15</sup>. Also the solubilities of the coformers are different in each solvent. Very different solubilities of the co-crystal components in the solvent could lead to an incongruent saturating diagram and the formation of different polymorphs and even homocrystals. Fig. 1.17 and Fig. 1.18 show two ternary phase diagrams of a 1:1 co-crystal formed by an API (A) and a coformer (B) at constant temperature and pressure. Fig. 1.17 corresponds to a congruent saturating diagram and Fig. 1.18 to an incongruent one. These diagrams correspond to the simplest situation in which the co-crystal A-B shows only one polymorph. In a congruent saturating system the co-crystal stoichiometric ratio line will cross the solubility curve of the co-crystal only (C-D line), and a pure co-crystal precipitate may be obtained by solvent evaporation. When solubilities of the co-crystal components in the solvent are very different an incongruent saturating system might take place. In this case the co-crystal stoichiometric ratio line will cross the solubility line of one of the co-crystal components (in Fig. 1.18  $S_{A-C}$  line) resulting in the precipitation of homocrystals.

Temperature also had a marked effect on the polymorphic outcome; polymorph II was formed at higher temperature. In this case, the phase diagram will be more complex as different regions of coexistence for each polymorph will be found. If the solubility of each compound changes differently with temperature, a congruent saturating system may become incongruent at higher temperature.

The SAS technique was proven once again suitable for the production of an improved drug formulation. Co-crystals of CBZ-SAC polymorph I with yields up to 65 % and free of solvent and homocrystal impurities were obtained. The undesired dehydrate form of CBZ obtained together with the co-crystal by conventional methods was avoided.

#### 4.4 Limiting parameters in the successful preparation of co-crystals using supercritical CO<sub>2</sub>

The previous research centred in the DIF-NIC and CBZ-SAC co-crystals left some queries still unresolved. In these cases we have not found the presence of homocrystals, suggesting therefore that the stoichiometric amount of coformers could always be used in the starting solution. Other researchers though had found the presence of mixed phases at the stoichiometric ratios, such as in the SAS precipitation of the naproxen-nicotinamide system.<sup>16</sup> The different solubilities of the co-crystal components in the CO<sub>2</sub> solvent system and the incongruent saturating system phase diagram may be the reasons. To investigate the influence of the different coformer solubilities in the solvent and in the supercritical CO<sub>2</sub> phase, we decided to study the co-crystal systems formed by 5-Fu and several coformers: urea, thiourea, acridine, 4-hydroxybenzoic acid (4HBA) and pyrazinamide (PZA). Moreover, we decided to investigate the use of CO<sub>2</sub> as a solvent in the co-crystallization and compare the results to those in which CO<sub>2</sub> has played the antisolvent role.

**Table 4.5 Summary of conditions and results of the SAS 5-Fu co-crystallization experiments with several coformers.**

Co-crystal	Stoichiometry	Thermal transition (K)	Product
5-Fu-urea	1:1	480.2	co-crystal + 5Fu
5-Fu-thiourea	1:1	470.7	co-crystal + 5Fu
5-Fu-acridine	2:1	553.5	5Fu
5-Fu-acridine	1:13.4	433.7 <sup>a)</sup>	unknown phase
5-Fu-4HBA	1:1	488.3	mixture of phases + 5-Fu
5-Fu-4HBA	1:3	475.0	mixture of phases + 4HBA
5-Fu-Pyrazinamide	2:1	556.4	5-Fu

a) Onset of an exothermic event.

Co-crystals of 5-Fu were selected because improved formulations of 5-Fu had already been prepared using SAS in our laboratory. Therefore, 5-Fu seemed a good candidate to explore additional improved formulations with the use of supercritical CO<sub>2</sub>. Enhancement of 5-Fu pharmacological properties through co-crystallization has been investigated by several researchers (detailed description will be given in chapter 5) and several patents have been submitted. The study of co-crystals of one API with several coformers that present different solubilities in the solvent and the CO<sub>2</sub> phase fits our

research purposes. By processing the same co-crystals using the co-crystallization with supercritical solvent (CSS) technique we aim to compare the differences in the co-crystals obtained with CO<sub>2</sub> as an antisolvent and as a solvent.

All SAS experiments were carried using methanol as a solvent and the operating conditions were kept constant: temperature (313 K), pressure (10.0 MPa), solution flow rate (1 mL/min), 5-Fu solution concentration (5 mg/mL) and CO<sub>2</sub> flow rate (20 g/min). A brief summary of the SAS experiments conditions and results is presented in Table 4.5. Thermal transitions of the SAS precipitates are also reported.

Full detailed characterization data for the co-crystals discussed in this section can be found in chapter 5 of this thesis. For the sake of simplicity we will only discuss the main observations and conclusions withdrawn from these results.

PXRD analysis of the 5-Fu-urea and the 5-Fu-thiourea SAS precipitates revealed the formation of the co-crystal, nevertheless, 5-Fu homocrystals were also present. The solubilities of 5-Fu and urea in supercritical CO<sub>2</sub> are very low and in the same order of magnitude ( $2.81 \times 10^{-6}$  mol 5-Fu/mol CO<sub>2</sub> at 10.0 MPa and 313 K<sup>17</sup>, and  $3.6 \times 10^{-6}$  mol urea/mol CO<sub>2</sub> at 15.0 MPa and 313 K<sup>18</sup>). There are no data available for thiourea. On the other hand, the very different solubilities of 5-Fu, urea and thiourea in methanol (5, 166 and 94.25 mg/mL, respectively<sup>19, 20</sup>) suggest that these homocrystals could have an incongruent saturating system. TGA showed that the SAS samples had the stoichiometric amount of the cofomers. On the other hand, DSC did not show any thermal transition for homocrystals of urea or thiourea. These latter analyses suggest that SAS powders have a relatively high content in the co-crystal phase. The presence of 5-Fu homocrystals though confirm the influence of the ternary phase diagram in the SAS process. Therefore, in systems in which the solubility of the cofomers in the solvent is large and very different from that of the drug in the same solvent, it would be advisable to dedicate time to study the ternary phase diagram prior to selecting the operating conditions.

The co-crystal of 5-Fu and acridine showed the same problems due to the large solubility differences in supercritical CO<sub>2</sub>. Experiments ran for solutions with the stoichiometric co-crystal ratio (2:1 molar ratio) produced a precipitate in which only 5-Fu was detectable using PXRD analysis. Acridine did not precipitate or was completely washed out of the precipitation chamber. An additional experiment was ran in which the concentration of acridine was increased taking into account its solubility in supercritical CO<sub>2</sub> ( $1.18 \times 10^{-4}$  mol acridine/mol CO<sub>2</sub> at 10.2 MPa and 318 K<sup>21</sup>). The

PXRD pattern of this precipitate presented the diffraction peaks of the reported co-crystal structure plus some unidentified peaks. DSC and TGA analysis confirm the presence of a different phase. These results suggest that increasing the concentration in the feeding solution of the more soluble coformer in CO<sub>2</sub> or the CO<sub>2</sub>-cosolvent mixture may lead to the co-crystal formation. The difficulties of optimizing this process may be considerable though, as the supercritical drying step that follows the SAS precipitation could result in the extraction of the most soluble coformer.

The co-crystal of 5-Fu and 4-HBA has two known polymorphs<sup>22</sup>. This co-crystal seemed to have a problem similar to the one previously explained for 5-Fu and acridine, i.e., after SAS precipitation the content of 4-HBA in the precipitate was smaller than the expected. In this case though, the solubility of 4-HBA in supercritical CO<sub>2</sub> ( $4.52 \times 10^{-7}$  mol 4HBA/ mol CO<sub>2</sub> at 10.1 MPa and 318 K<sup>23</sup>) is even smaller than that of 5-Fu. Solubility measurements of 4-HBA in CO<sub>2</sub> with methanol as cosolvent were performed using a view cell (see chapter 5). However, the solubilities of both coformers in CO<sub>2</sub>-cosolvent mixtures were similar. In the first experiments with a 1:1 molar ratio of 5-Fu and 4-HBA, PXRD analysis revealed that a complex mixture of phases was obtained after SAS precipitation. No homocrystals were detectable in this precipitate. Precipitation of both coformers separately under the same operating conditions revealed a 3 fold yield difference. Because the precipitation yield of 5-Fu was higher, the SAS co-crystallization experiment was repeated increasing the 4HBA content, and an initial 1:3 molar ratio (5-Fu-4-HBA) in the feeding solution was used. In the experiments performed with this increased concentration of 4-HBA in the feeding solution, PXRD analysis revealed the presence of 4-HBA homocrystals and other crystalline phases. Solubility of 4-HBA in methanol (389.9 mg/mL<sup>24</sup>) is substantially larger than that of 5-Fu. Therefore, an incongruent saturating system is expected. Different crystalline phases were obtained through SAS but a better knowledge of the ternary phase diagram would be necessary if pure phases want to be produced. The presence of different polymorphic forms can not be ruled out.

Finally, the co-crystallization of 5-Fu and pyrazinamide using SAS was not achieved. Solubility of pyrazinamide in methanol (13,8 mg/mL<sup>20</sup>) is not very different from that of 5-FU, and a congruent saturating system could be expected. On the other hand, solubility of PZA in supercritical CO<sub>2</sub> is very low (attempts to measure the solubility in our laboratory indicated that it was less than  $1.37 \times 10^{-4}$  mol pyrazinamide/mol CO<sub>2</sub> at 25.0 MPa and 313 K). Nevertheless, pyrazinamide was not detectable in the precipitates obtained via SAS. The attempt to precipitate

pyrazinamide alone failed to produce any precipitate. A full understanding of the reasons for this behaviour is still lacking.

Because some of these systems could not be successfully precipitated by SAS, the CSS technique was also used. Only the CSS 5-Fu co-crystals experiments in which methanol was used as a cosolvent produced new crystalline phases. In the experiments performed in pure CO<sub>2</sub> only homocrystals were obtained. This confirms the importance of the solubilization of the cofomers in CO<sub>2</sub> to achieve a successful CSS co-crystallization. The 5-Fu and pyrazinamide co-crystal that could not be obtained via SAS was obtained via CSS. Nevertheless, the control of particle size is poor for the CSS technology and micronization is not possible, moreover the scaling up is difficult. An interesting technology to investigate in the co-crystal production using CO<sub>2</sub> as a solvent that overcomes the CSS problems would be RESS.

## 4.5 Preparation of metal organic frameworks (MOFs) via SAS. Evaluation of the SAS technique.

MOFs are a type of adducts that have been explored in the recent decade as suitable pharmaceutical formulations for controlled drug release and/or prolonged shelf life<sup>25</sup>. To the best of our knowledge, up to date the SAS technique has never been used in the production of MOFs and we decided to investigate its feasibility.

Table 4.6 Operating conditions used in the preparation of MOFs using SAS.

Experiment	Solvent	Temperature (K)	Pressure (MPa)	Cu(C <sub>3</sub> ) <sub>2</sub> :INA molar ratio
1	Ethanol	313	10.0	1:2
2	Ethanol	313	10.0	1:1
3	Ethanol	298	10.0	1:2
4	Ethanol	298	8.0	1:2
5	Ethanol	313	25.0	1:2
6	Methanol	313	10.0	1:2

We decided to prepare a MOF formed by copper (II) propanoate (Cu(C<sub>3</sub>)<sub>2</sub>) and isonicotinamide (INA). Cu(C<sub>3</sub>)<sub>2</sub> was chosen due to the extensive knowledge about of this molecule in our laboratory<sup>26</sup> and its proven pharmaceutical activity<sup>27</sup>. INA was

chosen as organic ligand because it also presents pharmacological properties<sup>28</sup> and it is known to behave as a high-yielding supramolecular reagent<sup>29</sup>.

First MOFs were obtained using slow evaporation crystallization. Experiments in ethanol with different molar ratios of  $\text{Cu}(\text{C}_3)_2$  and INA were carried out and pure crystals were obtained in experiments performed with a 1:2 molar ratio of  $\text{Cu}(\text{C}_3)_2$  and INA. These crystals were of good quality and allowed us to obtain crystal structure of the MOF (deposited in the CCDC, number 1846632 for the solid structure measured at 100 K and 1846633 for the one measured at 320 K), hence the theoretical PXRD pattern. Other information gathered from these crystals was the fusion temperature (onset at 482.2 K) and the FTIR spectrum (identification of main absorption bands).

The SAS experiments were carried under several operating conditions (see Table 4.6).  $\text{Cu}(\text{C}_3)_2$  concentration was kept to 3.3 mg/mL (close to its saturation level in ethanol). Solution flow rate (1 mL/min) and  $\text{CO}_2$  flow rate (20 g/min) were also kept constant.

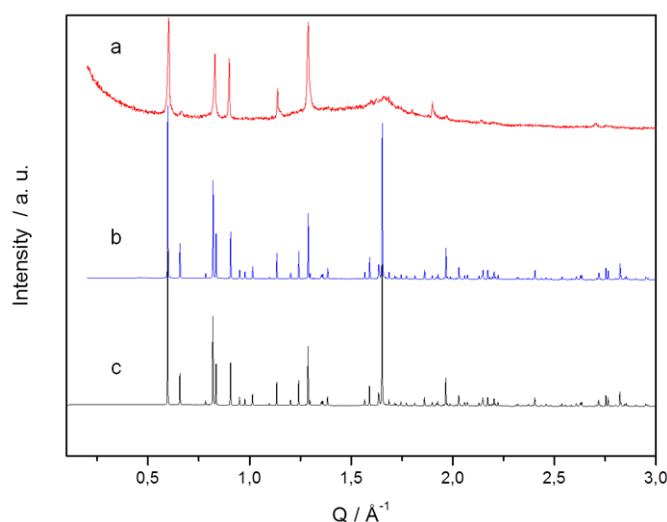


Fig. 4.10 PXRD pattern of the  $\text{Cu}(\text{C}_3)_2$ -INA MOF obtained via: a) SAS experiment 1; b) slow evaporation; c) calculation from the Rietveld refinement at room temperature.

PXRD patterns of the SAS precipitates were compared to the patterns of the crystals obtained via slow evaporation (experimental and calculated from the adduct crystal structure at 320 K). Only the patterns of the samples obtained at 313 K, 10.0 MPa and a 1:2 molar ratio of  $\text{Cu}(\text{C}_3)_2$  to INA (experiments 1 and 6 of Table 4.6) matched the experimental and calculated pattern of the adduct. The rest of the experiments produced samples with complex PXRD patterns that did not match neither those of the pure components nor of the adduct. This showed that both pressure and



temperature had a significant effect in the adduct formation via SAS. For experiment 1 a PXRD measurement in transmission mode was performed and fitted by Rietveld refinement using the crystal structure of the adduct at 320 K. The microstructure of the SAS sample was studied. The average crystal domain corresponded to a platelet very narrow in the direction (010). Fig. 4.10 shows the PXRD patterns measured in transmission mode of the adduct obtained via slow evaporation. Adduct obtained in experiment 1 and the calculated pattern from the crystal structure of the adduct at 320 K.

Fig. 4.11 shows the SEM images of the precipitated adducts, and the untreated and SAS processed  $\text{Cu}(\text{C}_3)_2$  and INA. These images demonstrate once again the reduction of size and the narrow size distribution obtained through SAS. Adduct crystals obtained via SAS were up to 100 times smaller than those obtained via slow evaporation.

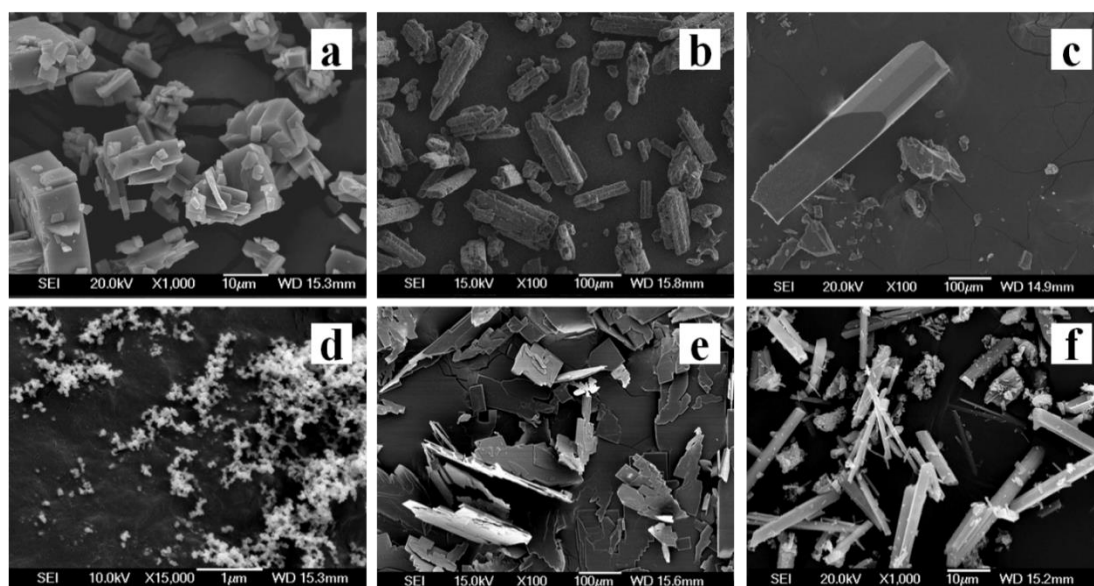
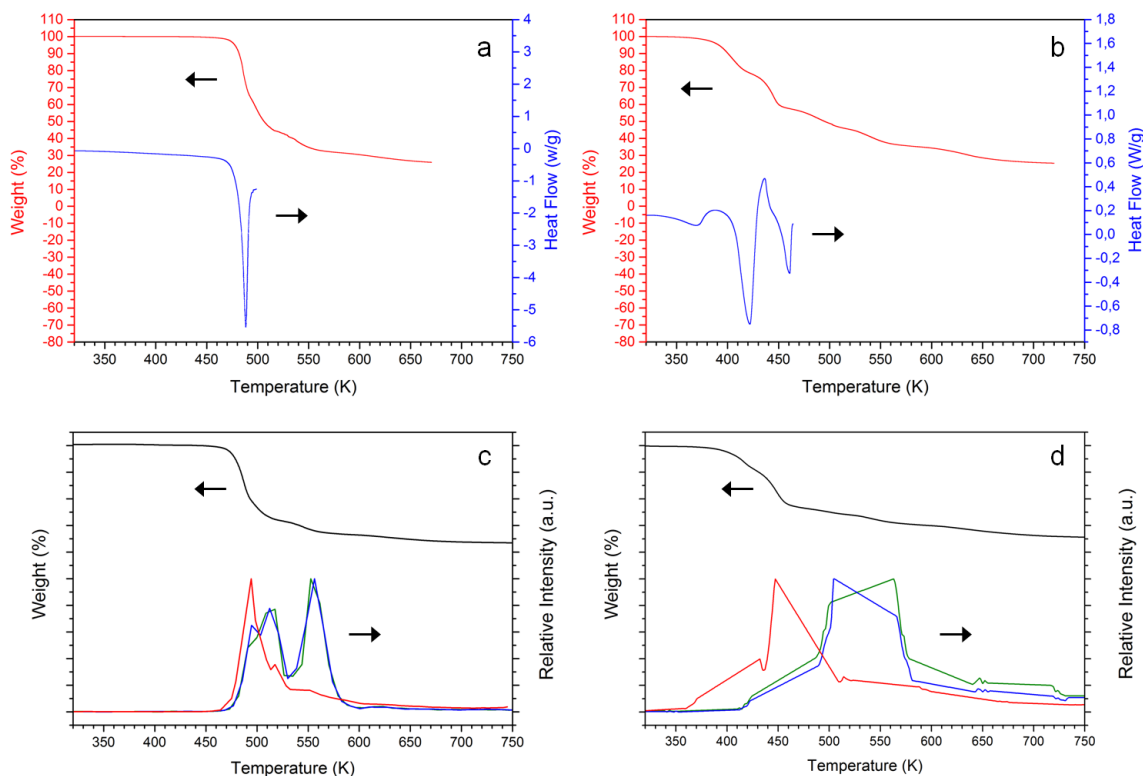


Fig. 4.11 SEM images of: a)  $\text{Cu}(\text{C}_3)_2$  prepared at our laboratory; b) commercial INA; c)  $\text{Cu}(\text{C}_3)_2$ -INA formed by slow evaporation; d)  $\text{Cu}(\text{C}_3)_2$  processed by SAS; e) INA processed by SAS; f) MOF formed by SAS.

The adduct precipitate showed a mixture of morphologies. Whilst most particles were around 3  $\mu\text{m}$  wide and 30 to 50  $\mu\text{m}$  long crystals, nano-fibers and small agglomerates were also present. Similar mixture of morphologies was encountered in the sample obtained via SAS from methanol. This mixture of morphologies could indicate the presence of amorphous impurities (Only the adduct phase was observable by PXRD). Differences in the FTIR spectra from the adduct obtained from slow

evaporation and the one obtained in experiment 1 also suggest the presence of impurities.



**Fig. 4.12** Thermal analysis data: a) TGA and DSC (5 K/min) of the adduct obtained by slow evaporation; b) TGA and DSC (5 K/min) of the adduct obtained by SAS in experiment 1; c) TGA (10 K/min) and mass spectroscopy results for 44 m/z (red), 77 m/z (green) and 104 m/z (blue) of the adduct obtained by slow evaporation; d) TGA (10 K/min) and mass spectroscopy results for 44 m/z (red), 77 m/z (green) and 104 m/z (blue) of the adduct obtained by SAS in experiment 1.

Thermal analysis of the samples showed a different behavior between the SAS adduct and the one obtained via slow evaporation. The latter showed a phase transition between the two different solid forms of the adduct with onset at 235.7 K (after cooling to 183 K and subsequently heating at 10 K/min). This transition was not observable in the SAS adduct. The adduct obtained via slow evaporation had an onset temperature on melting of 482 K (see Fig. 4.12 a). This temperature is intermediate between the sublimation/evaporation temperature of INA (429 K) and the decomposition temperature of  $\text{Cu}(\text{C}_3)_2$  (503 K). INA was therefore stabilized in the adduct until 482 K. When 482 K is reached sample mass loss starts (see Fig. 4.12 c) and the characteristic mass to charge ratios ( $m/z$ ) of INA at 77  $m/z$  and 104  $m/z$  are observed. In the adduct obtained via SAS mass loss measured using TGA starts at a lower temperature (394 K) and the mass to charge ratio characteristic of  $\text{CO}_2$  at 44 ( $m/z$ ) is observed (see Fig. 4.12 d). Although the release of INA starts at 429 K, the

highest concentration is reached after 482 K, suggesting that most of the INA in the SAS precipitate is in the adduct structure. The difference in the thermal behavior between samples could be explained by the much smaller particle size that could prompt adduct decomposition at much lower temperature.

Micro-elemental analysis of the samples also showed a difference between the adducts obtained via SAS and slow evaporation. The carbon content of the former was smaller than the theoretical content. Also when processing  $\text{Cu}(\text{C}_3)_2$  only via SAS the content in carbon was less than the theoretical value. This suggests a possible partial decomposition of the  $\text{Cu}(\text{C}_3)_2$  alkyl chain during the SAS processing.

All these results seem to indicate that the SAS process leads to a mixture of phases where the adduct is the major component, thus, SAS seems to be a suitable method to synthesize mixed-ligand adducts with all the advantages that the SAS technology carries. In the studied adduct further purification strategies should be implemented in order to remove the amorphous impurities.

## References

1. Liechty, W. B.; Kryscio, D. R.; Slaughter, B. V.; Peppas, N. A., Polymers for Drug Delivery Systems. In *Annual Review of Chemical and Biomolecular Engineering, Vol 1*, Prausnitz, J. M.; Doherty, M. F.; Segalman, R. A., Eds. Annual Reviews: Palo Alto, **2010**; Vol. 1, pp 149-173.
2. Kumari, A.; Yadav, S. K.; Yadav, S. C., Biodegradable polymeric nanoparticles based drug delivery systems. *Colloids and Surfaces B-Biointerfaces* **2010**, *75* (1), 1-18.
3. R. Auras; L-T. Lim; S. E. M. Selke; H. Tsuji, *Poly(lactic acid): Synthesis, Structures, Properties, Processing, and Applications (Wiley Series on Polymer Engineering and Technology)*. NJ, **2010**.
4. Zahran., F. R. F. Microparticles precipitation using supercritical CO<sub>2</sub> as an Antisolvent. Role of thermal effects and phase equilibria. Universidad Complutense de Madrid, Madrid, **2012**.
5. Sun, C. C., CocrySTALLIZATION for successful drug delivery. *Expert Opinion on Drug Delivery* **2013**, *10* (2), 201-213.
6. Thipparaboina, R.; Kumar, D.; Chavan, R. B.; Shastri, N. R., Multidrug co-crystals: towards the development of effective therapeutic hybrids. *Drug Discovery Today* **2016**, *21* (3), 481-490.
7. Padrela, L.; Rodrigues, M. A.; Velaga, S. R.; Matos, H. A.; de Azevedo, E. G., Formation of indomethacin-saccharin cocrySTALLS using supercritical fluid technology. *European Journal of Pharmaceutical Sciences* **2009**, *38* (1), 9-17.
8. Chen, C. T.; Tang, M.; Chen, Y. P. *Proceedings 11th International Symposium on Supercritical Fluids*, 2015.
9. Evora, A. O. L.; Castro, R. A. E.; Maria, T. M. R.; Silva, M. R.; ter Horst, J. H.; Canotilho, J.; Eusebio, M. E. S., A thermodynamic based approach on the investigation of a diflunisal pharmaceutical co-crystal with improved intrinsic dissolution rate. *International Journal of Pharmaceutics* **2014**, *466* (1-2), 68-75.
10. Wang, L.; Tan, B.; Zhang, H.; Deng, Z., Pharmaceutical CocrySTALLS of Diflunisal with Nicotinamide or Isonicotinamide. *Organic Process Research & Development* **2013**, *17* (11), 1413-1418.
11. Moradiya, H.; Islam, M. T.; Woollam, G. R.; Slipper, I. J.; Halsey, S.; Snowden, M. J.; Douroumis, D., Continuous CocrySTALLIZATION for Dissolution Rate Optimization of a Poorly Water-Soluble Drug. *Crystal Growth & Design* **2014**, *14* (1), 189-198.
12. Rahman, Z.; Samy, R.; Sayeed, V. A.; Khan, M. A., Physicochemical and mechanical properties of carbamazepine cocrySTALLS with saccharin. *Pharmaceutical Development and Technology* **2012**, *17* (4), 457-465.
13. Fleischman, S. G.; Kuduva, S. S.; McMahon, J. A.; Moulton, B.; Walsh, R. D. B.; Rodriguez-Hornedo, N.; Zaworotko, M. J., Crystal engineering of the composition of pharmaceutical phases: Multiple-component crystalline solids involving carbamazepine. *Crystal Growth & Design* **2003**, *3* (6), 909-919.
14. Porter, W. W., III; Elie, S. C.; Matzger, A. J., Polymorphism in carbamazepine cocrySTALLS. *Crystal Growth & Design* **2008**, *8* (1), 14-16.
15. Weissbuch, I.; Torbeev, V. Y.; Leiserowitz, L.; Lahav, M., Solvent effect on crystal polymorphism: Why addition of methanol or ethanol to aqueous solutions induces the precipitation of the least stable beta form of glycine. *Angewandte Chemie-International Edition* **2005**, *44* (21), 3226-3229.
16. Neurohr, C.; Erriguible, A.; Laugier, S.; Subra-Paternault, P., Challenge of the supercritical antisolvent technique SAS to prepare cocrySTALL-pure powders of naproxen-nicotinamide. *Chemical Engineering Journal* **2016**, *303*, 238-251.
17. Zhan, S. P.; Zhao, Q. C.; Chen, S. H.; Wang, J. C.; Liu, Z. J.; Chen, C., Solubility and Partition Coefficients of 5-Fluorouracil in ScCO<sub>2</sub> and ScCO<sub>2</sub>/Poly(L-lactic acid). *Journal of Chemical and Engineering Data* **2014**, *59* (4), 1158-1164.

18. Catchpole, O. J.; Tallon, S. J.; Dyer, P. J.; Lan, J. S.; Jensen, B.; Rasmussen, O. K.; Grey, J. B., Measurement and modelling of urea solubility in supercritical CO<sub>2</sub> and CO<sub>2</sub>+ethanol mixtures. *Fluid Phase Equilibria* **2005**, *237* (1-2), 212-218.
19. Lawrence, H. K.; Douglas, B. W., *National toxicology program's chemical solubility compendium*. **1991**; p 448.
20. NCBI National center for biotechnological information, which can be accessed electronically through Web (<https://pubchem.ncbi.nlm.nih.gov>).
21. Schmitt, W. J.; Reid, R. C., Solubility of monofunctional organic solids in chemically diverse supercritical fluids. *Journal of Chemical and Engineering Data* **1986**, *31* (2), 204-212.
22. Li, S.; Chen, J.-M.; Lu, T.-B., Synthon polymorphs of 1: 1 co-crystal of 5-fluorouracil and 4-hydroxybenzoic acid: their relative stability and solvent polarity dependence of grinding outcomes. *Crystengcomm* **2014**, *16* (28), 6450-6458.
23. Lucien, F. P.; Foster, N. R., Influence of matrix composition on the solubility of hydroxybenzoic acid isomers in supercritical carbon dioxide. *Industrial & Engineering Chemistry Research* **1996**, *35* (12), 4686-4699.
24. A. Martin; P. L. Wu; Beerbower, A., Expanded Solubility Parameter Approach II: P-Hydroxybenzoic Acid and Methyl P-Hydroxybenzoate in Individual Solvents. *Journal of Pharmaceutical Sciences* **1984**, *73* (2), 188-194.
25. Khan, N. A.; Hasan, Z.; Jhung, S. H., Beyond pristine metal-organic frameworks: Preparation and application of nanostructured, nanosized, and analogous MOFs. *Coordination Chemistry Reviews* **2018**, *376*, 20-45.
26. Riesco, M. R.; Martinez-Casado, F. J.; Cheda, J. A. R.; Yelamos, M. I. R.; da Silva, I.; Plivelic, T. S.; Lopez-Andres, S.; Ferloni, P., New Advances in the One-Dimensional Coordination Polymer Copper(II) Alkanoates Series: Monotropic Polymorphism and Mesomorphism. *Crystal Growth & Design* **2015**, *15* (4), 2005-2016.
27. Dillon, C. T.; Hambley, T. W.; Kennedy, B. J.; Lay, P. A.; Zhou, Q. D.; Davies, N. M.; Biffin, J. R.; Regtop, H. L., Gastrointestinal toxicity, antiinflammatory activity, and superoxide dismutase activity of copper and zinc complexes of the antiinflammatory drug indomethacin. *Chemical Research in Toxicology* **2003**, *16* (1), 28-37.
28. de Souza, R. A.; Stevanato, A.; Treu, O.; Netto, A. V. G.; Mauro, A. E.; Castellano, E. E.; Carlos, I. Z.; Pavan, F. R.; Leite, C. Q. F., Antimycobacterial and antitumor activities of Palladium(II) complexes containing isonicotinamide (isn): X-ray structure of trans-[Pd(N<sub>3</sub>)<sub>2</sub>(isn)<sub>2</sub>]. *European Journal of Medicinal Chemistry* **2010**, *45* (11), 4863-4868.
29. Aakeroy, C. B.; Beatty, A. M.; Desper, J.; O'Shea, M.; Valdes-Martinez, J., Directed assembly of dinuclear and mononuclear copper(II)-carboxylates into infinite 1-D motifs using isonicotinamide as a high-yielding supramolecular reagent. *Dalton Transactions* **2003**, (20), 3956-3962.

**Chapter 5**  
**Co-crystallization of**  
**5-Fu using**  
**SAS and CSS**



## 5 CO-CRYSTALLIZATION OF 5-FLUOROURACIL USING SAS AND CSS

### 5.1 INTRODUCTION

5-Fluorouracil (5-Fu) is a long known BCS (biopharmaceutics classification system) class III drug (high solubility and low permeability) used in chemotherapy for the treatment of cancer. There are two different polymorphs reported for 5-Fu: polymorph I<sup>1</sup> (triclinic) and polymorph II<sup>2</sup> (monoclinic). In polymorph I (the most stable form) the molecules adopt a hydrogen bond sheet structure whilst in polymorph II the hydrogen bond has a ribbon motif (see Fig. 5.1).

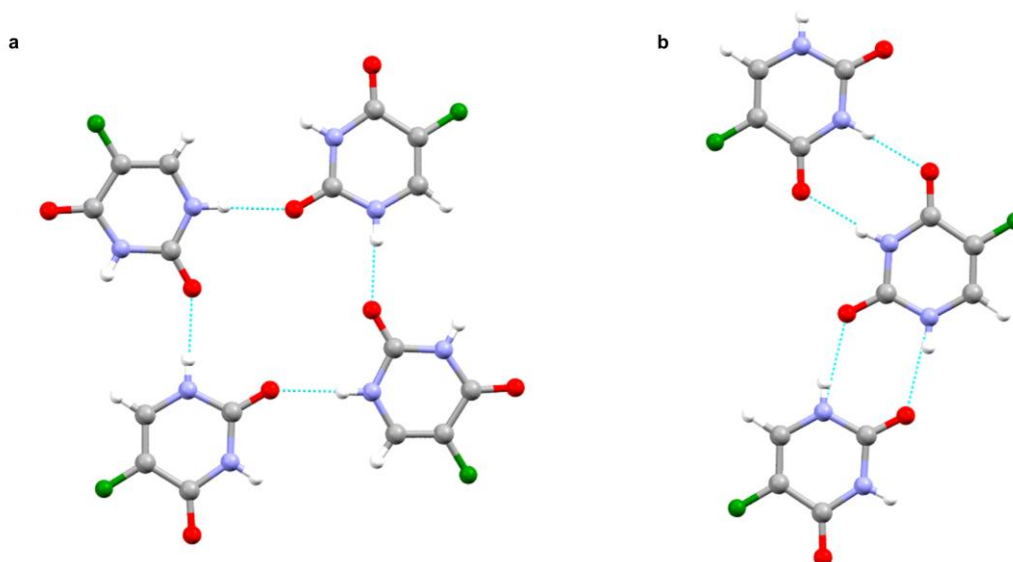


Fig. 5.1 Molecular structures displaying the H-bond connections of: a) 5-Fu polymorph I and b) 5-Fu polymorph II. Nitrogen (purple), oxygen (red), fluorine (green), carbon (grey) and hydrogen (white).

5-Fu was first designed and synthesized by Heidelberger et al.<sup>3</sup> in 1957 based on the research from Rutman et al.<sup>4</sup> This research revealed that uracil had a higher uptake by rat hepatomas than by non-malignant tissues. The similarity of 5-Fu to uracil and thymine, both nucleobases in RNA and DNA respectively, allows 5-Fu to serve as a substrate for the same transport processes and enzymes involved in anabolism and catabolism of nucleobases. 5-Fu had therefore a potential as an antimetabolite drug (drugs that inhibit essential biosynthetic processes and hinder the normal function of DNA and RNA). 5-Fu will enter the cell (higher uptake in the tumour cells) where it will be converted to several active metabolites that obstruct RNA and DNA synthesis and inhibit the enzyme thymidylate synthase (TS).<sup>5</sup>



Due to its antimetabolite action 5-Fu is one of the most commonly used drugs to treat a wide range of cancers, including: head and neck cancer<sup>6</sup>, some skin cancers<sup>7</sup>, and breast cancer<sup>8</sup>. It is though in colorectal cancer where it has demonstrated a higher impact with increased overall and disease-free survival of patients undergoing 5-Fu based chemotherapy<sup>9</sup>. Nevertheless, response rates to 5-Fu based chemotherapy are still relatively low (10-15% in advanced colorectal cancer<sup>9</sup>), and although it has improved when combined with newer chemotherapies (40-50%<sup>10</sup>) there is still a need to overcome its main drawbacks such as tumours developing resistance, lack of selectivity, toxicity and effectiveness (more than 80% of the administered 5-Fu catabolizes in the liver limiting its bioavailability in normal and tumour cells).

The main research paths that have been taken to improve the performance of 5-Fu are:

- Polychemootherapy: Combining more than one drug in the therapy. Specific example would be the combination of the mixture 5-Fu-leucovorin (considered a standard chemotherapy for colon cancer) with oxaliplatin or irinotecan<sup>11</sup>.
- Attempts to identify the pathways that are involved in tumour cell response to 5-Fu in order to enhance its cytotoxic activity<sup>12</sup>.
- Development of 5-Fu derivatives<sup>13</sup> to improve its selectivity and toxicity towards tumour cell, and to enhance cell absorption and metabolic stability. The development of 5-Fu derivatives by conjugation with other molecules is usually done by the attachment of the desired molecule to one or both of the nitrogen atoms present in the 5-Fu pyrimidinic ring. This conjugation generates the so called “prodrugs” that such as capecitabine<sup>14</sup> activate in specific cells by a biological mediator.
- Enhancement of bioavailability and physicochemical properties of 5-Fu through co-crystallization.<sup>15-23</sup> This approach is followed in this chapter of the Thesis.
- Developing enhanced drug delivery systems. 5-Fu derivatives have been conjugated with N-vinylpyrrolidinone (NVP)<sup>24</sup> and a biodegradable graft copolymer<sup>25</sup> achieving slower release rates. In this thesis we have also described the preparation of a composite with poly(L-lactide) (PLLA) that also achieves a slower release rate<sup>26</sup>.

Supercritical fluid technology has been mainly employed in researching novel, enhanced delivery systems for 5-Fu. To the best of our knowledge the techniques and

achievements that have been accomplished in this field with the aid of supercritical fluids are those outlined next.

First reported studies are from Guney and Akgerman<sup>27</sup>, who impregnated 5-Fu in poly-lactide-co-glycolide (PLGA) using supercritical CO<sub>2</sub> to achieve a controlled release of the drug.

Chen et al.<sup>28</sup> prepared microparticles of 5-Fu and PLLA using the Solution enhanced dispersion by supercritical fluids (SEDS) technique. First a 5-Fu saturated solution in ethanol and DCM (volume ratio 4:1) was micronized. The micronized 5-Fu was then dissolved again in an ethanol-DCM mixture (facilitating through the previous micronization 5-Fu solubilization in the organic solution) with PLLA and micronized together. Particles of partly spherical shape and mean size of 980 nm with an average drug load of 3.05 % were obtained. These authors also used the SEDS technology to prepare 5-Fu-SiO<sub>2</sub>-PLLA microcapsules<sup>29</sup>. In this case 5-Fu was loaded to SiO<sub>2</sub> nanoparticles in an ethanol solution. The loaded particles were then dispersed with an ultrasonic method in a PLLA-DCM solution that was subsequently micronized using SEDS. Smooth spherical shape particles of 536 nm mean size and drug load of 0.18% were achieved.

Kalantarian et al.<sup>30</sup> produced partly spherical 5-Fu nanoparticles of approximately 248 nm using the SAS technique from a solvent mixture of methanol and DCM (50:50). The so obtained nanoparticles were mixed with lactose in order to prepare a dry powder that could be administered through direct inhalation in the respiratory route. The same authors used the Gas antisolvent (GAS) and supercritical antisolvent (SAS) techniques to produce co-precipitates of 5-Fu and PLGA<sup>31</sup> accomplishing long term release profiles with partial burst effect.

A “reverse emulsion-SEDS” technique was employed by Zhang et al.<sup>32</sup> to prepare nanoparticles of 5-Fu-PLLA-polyethylene glycol (PEG). A solution of 5-Fu and PEG in water was added dropwise into a solution of PLLA and PEG in acetone and DCM. Nanoparticles were formed immediately in a reverse emulsion, and the SEDS process was then used to dry the emulsion. Smooth spherical nanoparticles of 175 nm mean size and drug load of 18.4 % were produced.

The SAS technique combined with the supercritical impregnation was used by Zhan et al.<sup>33</sup> to generate 5-Fu loaded microparticles of PLLA with a mean size of 680 nm. PLLA microparticles were obtained by SAS precipitation from an acetone-DCM

mixture. They were then loaded (6 %) with 5-Fu using supercritical CO<sub>2</sub> impregnation and ethanol as a cosolvent.

Cabezas et al.<sup>34, 35</sup> used supercritical CO<sub>2</sub> to simultaneously foam a polymeric support of poly-d-l-lactide and PLGA, and impregnate it with 5-Fu (20 % loading). Drug and polymer were placed in an autoclave with stirring. CO<sub>2</sub> was pumped until the desired pressure was reached and the autoclave was heated to the desired temperature. Enough time was allowed to ensure a complete saturation of 5-Fu in supercritical CO<sub>2</sub>. The foaming process took place due to the absorption of gas in the polymer decreasing its T<sub>g</sub> and generating the swelling of the polymer chains. Posterior depressurization generated nucleation and growth of bubbles in the polymer matrix. A similar technique was used by Salerno et al.<sup>36, 37</sup> In this case the polymer used was polycaprolactone (PCL) and impregnation with 5-Fu was carried out by mixing the PCL with a 5-Fu-DMSO solution previous to the foaming step with supercritical CO<sub>2</sub><sup>36</sup>. Unfortunately controlled release of the drug was not achieved and 80% of the drug was released within the first 5 min. Impregnation was then done with less DMSO and two steps, freeze drying followed by a 303 K drying previous to the foaming step were added<sup>37</sup>. Slower depressurization rates were also employed and the drug amount, process temperature and depressurization rate were optimized achieving a progressive release over six days.

The GAS technique was used by Esfandiari and Ghoreishi<sup>38, 39</sup> to micronize 5-Fu. The solvent used was DMSO and mean particles size ranged from 260 to 600 nm. The studied parameters revealed that particle size reduction was favoured at higher antisolvent flow rates and pressure and lower temperatures and 5-Fu concentrations.

Hao et al.<sup>40</sup> used supercritical carbon dioxide to entrap 5-Fu into a mesocellular silica foam modified with thermal and pH functional groups.

As mentioned earlier our research group has also used the SAS technique to micronize 5-Fu and to prepare a 5-Fu-PLLA composite<sup>26</sup> (publication I).

Although several supercritical techniques have been employed in the processing of 5-Fu, none of them was used to prepare 5-Fu co-crystals. As stated in the introduction, co-crystals present several advantages that could improve the overall bioavailability and performance of 5-Fu. Several authors have therefore investigated different co-crystals of 5-Fu by conventional methods and they reported interesting findings.

Singh et al.<sup>15</sup> studied the co-crystallization of 5-Fu with adenosine (one of the four main bases found in DNA and RNA). An equimolar mixture of adenosine and 5-Fu was mixed in a chloroform, ethanol and water solution. After eight hours reflux co-crystals were obtained by slow evaporation. The antitumor activity of the co-crystal against breast cancer was measured. In this example however, 5-Fu activity decreased in the presence of adenosine.

Veverka et al.<sup>16</sup> used 5-Fu to create a co-crystal with the chemotherapeutic agent Imatibin mesylate in order to improve the solid state properties of the latter. The co-crystal was produced through co-grinding and slurry methods.

The production of three co-crystals of 5-Fu with acridine, phenazine and 4,4-bispyridylethylene has been reported by Delori et al.<sup>17</sup> Co-crystals were produced by solvent evaporation using methanol.

An interesting case of polymorphism in 5-Fu co-crystals was published by Li et al.<sup>18</sup> These authors obtained by applying different methodologies and solvents, two different polymorphs of a 5-Fu co-crystal with 4-hydroxybenzoic acid (4HBA). 4HBA is recognized as a good co-crystal cofomer due to its hydroxyl and carboxyl functional groups and low toxicity.

In order to attempt a better solubility and bioavailability of 5-Fu, Da Silva et al.<sup>19</sup> synthesized a co-crystal of 5-Fu and 5-fluorocytosine using slow evaporation from water solutions. 5-Fluorocytosine is an antimetabolite drug currently used in cancer treatments as it is a BCS class I (high solubility and permeability).

Nadzri et al.<sup>20</sup> researched the formation of four different co-crystals of 5-Fu with urea, thiourea, 2,2-bipyridine and 4,4-bipyridine through co-grinding followed by solvent evaporation. They investigated the potential anti-cancer activities and found these co-crystals as promising compounds in the treatment of colorectal cancer.

Improved membrane permeability of 5-Fu was achieved by Dai et al.<sup>21</sup> They co-crystallized 5-Fu with 3-hydroxybenzoic acid, 4-aminobenzoic acid and cinnamic acid using two different methods: liquid assisted grinding and slurry crystallization.

Mohana et al.<sup>22, 23</sup> obtained co-crystals of 5-Fu with 4-methylbenzoic acid, 3-nitrobenzoic acid, 5-bromothiophene-2-carboxylic acid and thiophene-2-carboxylic acid from solutions in methanol.

There are also several patents of 5-Fu co-crystals with: urea (WO2004078161(A1)—2004-09-16), nicotinamide (NIC) (CN104557732(A)—2015-

04-29), pyrazinamide (PZA) (CN104557733(A)—2015-04-29) and 2-aminopyridine (CN105330606(A)—2016-02-17).

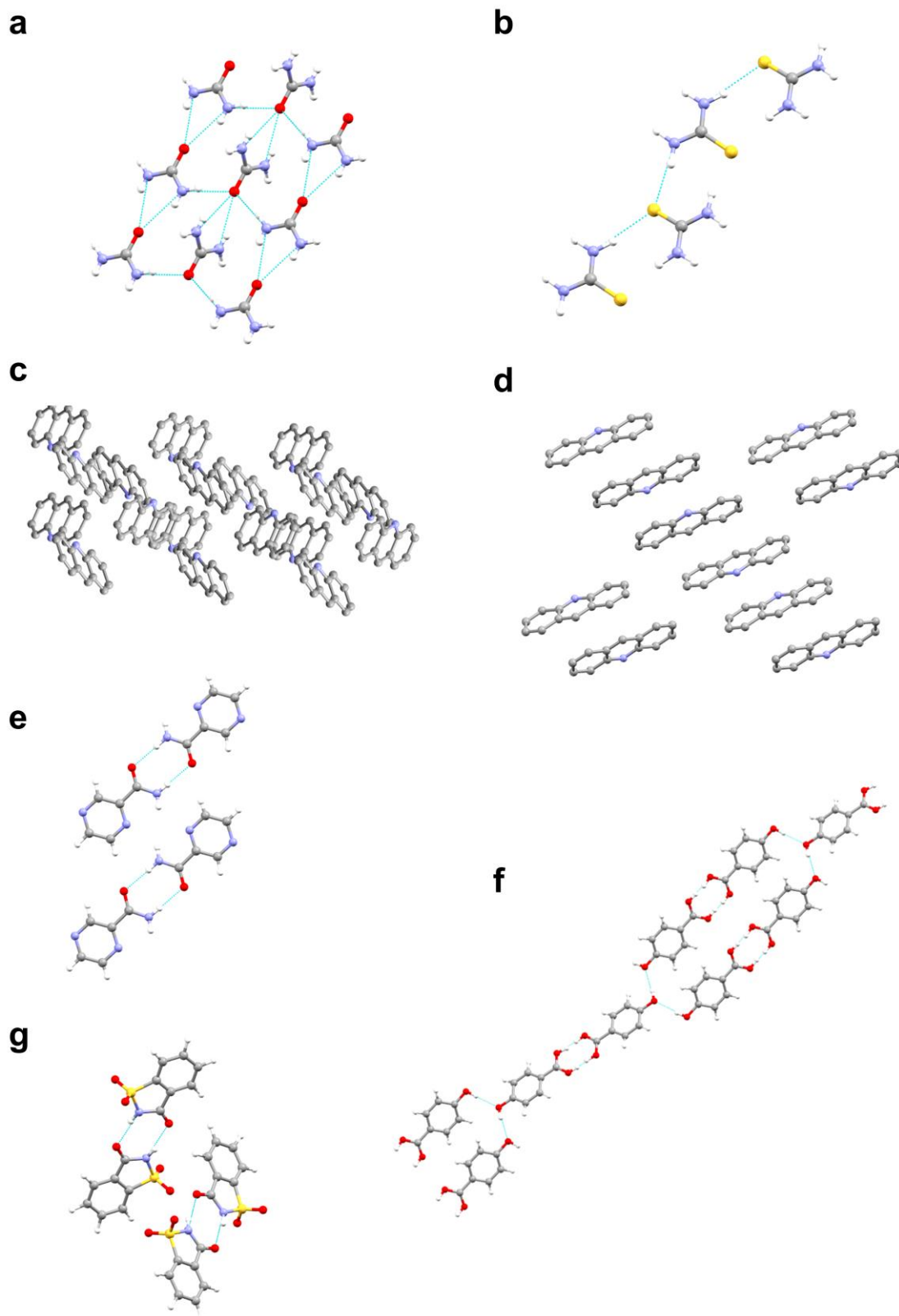


Fig. 5.2 Molecular structure displaying the H-bond connections of the coformers: a) urea polymorph I, b) orthorhombic thiourea, c) ACR polymorph III, d) ACR polymorph II, e) PZA polymorph  $\alpha$ , f) 4HBA polymorph I and g) SAC. Nitrogen (purple), oxygen (red), sulphur (yellow), carbon (grey) and hydrogen (white).

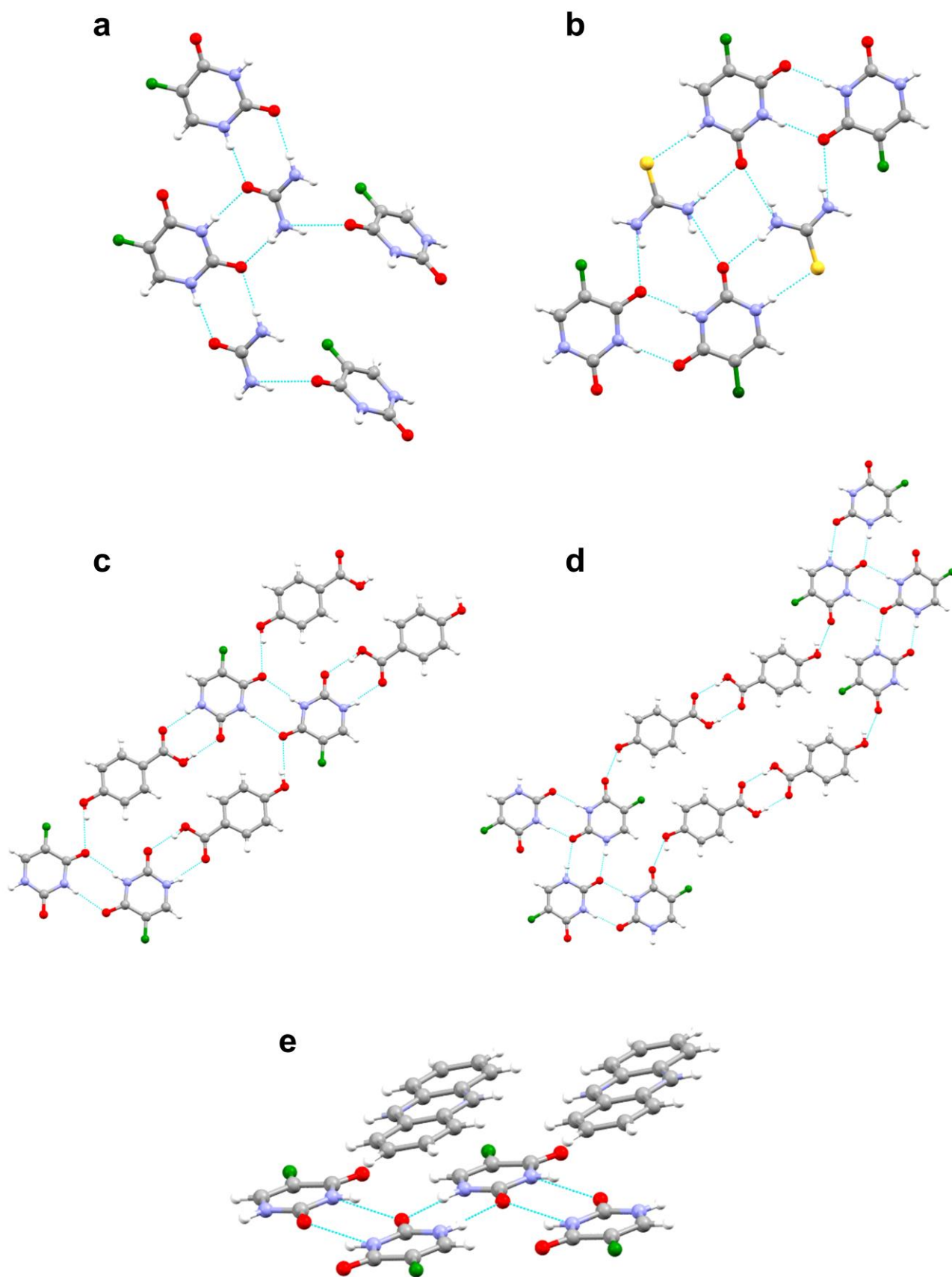


Fig. 5.3 Molecular structure displaying the H-bond connections of the co-crystals: a) 5-Fu-urea, b) 5-Fu-thiourea, c) 5-Fu-4HBA polymorph I, d) 5-Fu-4HBA polymorph II, e) 5-Fu-ACR. Nitrogen (purple), oxygen (red), fluorine (green) sulphur (yellow), carbon (grey) and hydrogen (white).

In order to overcome the difficulties of conventional co-crystallization methods, supercritical precipitation using the SAS technique is a promising process. In this chapter we study the feasibility of the SAS technique in producing co-crystals of 5-Fu with the cofomers urea, thiourea, acridine, 4HBA (for which crystallographic data are already available,<sup>17, 18, 20</sup>), PZA (a co-crystal for which limited crystallographic data are available; patented by the Harbin Medical University), and saccharin (SAC) (a co-crystal that up to our knowledge has not yet been attempted). The production of these co-crystals was also attempted through co-crystallization with supercritical solvent (CSS) in order to compare both supercritical techniques. In the SAS technique CO<sub>2</sub> plays the role of the antisolvent while in the CSS technique CO<sub>2</sub> plays the role of the solvent.

A representation of the molecular structures of the cofomers and co-crystals for which there is crystallographic data is given in Fig. 5.2 and Fig. 5.3, respectively.

## 5.2 EXPERIMENTAL PROCEDURE

### 5.2.1 Materials

Table 5.1 Data of the compounds used in the co-crystallization experiments.

	Formula	Purity (% mol)	Molecular weight (g/mol)	Solubility CO <sub>2</sub> (mol/mol) at $\approx$ CSS conditions		Solubility CO <sub>2</sub> (mol/mol) at $\approx$ SAS conditions	
CO <sub>2</sub>	CO <sub>2</sub>	99.999	44.01	*		*	
Methanol	CH <sub>4</sub> O	99.99	32.04	*		*	
5-Fu	C <sub>4</sub> H <sub>3</sub> N <sub>2</sub> FO <sub>2</sub>	100	130.08	5.25E-06	20.0 MPa; 328 K <sup>41</sup>	2.81E-06	10.0 MPa; 313 K <sup>41</sup>
Acridine	C <sub>13</sub> H <sub>9</sub> N	100	179.22	1.17E-03	20.1 MPa; 328 K <sup>42</sup>	1.18E-04	10.2 MPa; 318 K <sup>42</sup>
Thiourea	CH <sub>4</sub> N <sub>2</sub> SO <sub>3</sub>	99.03	76.12	*		*	
Urea	CH <sub>4</sub> N <sub>2</sub> O	100	60.06	4.80E-06	15.0 MPa; 333 K <sup>43</sup>	3.60E-06	15.0 MPa; 313 K <sup>43</sup>
4HBA	C <sub>7</sub> H <sub>6</sub> O <sub>3</sub>	99.9	138.12	3.72E-06	20.3 MPa; 328 K <sup>44</sup>	4.52E-07	10.1 MPa 318 K <sup>44</sup>
SAC	C <sub>7</sub> H <sub>5</sub> NO <sub>3</sub> S	100	183.18	3.32E-05	20.0 MPa; 323 K <sup>45</sup>	2.45E-05	8.0 MPa; 323 K <sup>45</sup>
PZA	C <sub>5</sub> H <sub>5</sub> N <sub>3</sub> O	100	123.11	>1.37E-04	25.0 MPa; 323 K	>1.37E-04	10.0 MPa; 313 K
CBZ	C <sub>15</sub> H <sub>12</sub> N <sub>2</sub> O	99.6	236.27	1.0E-05	20.0 MPa; 328 K <sup>46</sup>	1.5E-06	10.0 MPa; 313 K <sup>46</sup>

The following reactants were supplied by Sigma Aldrich: 5-fluorouracil (100 % mol pure), carbamazepine (meets USP testing specifications, 99,6 % mol pure), acridine (100 % mol pure), SAC (100 % mol pure), urea (meets USP testing

specifications, 100 % mol pure), thiourea (99.03 % mol pure), pyrazinamide (100 % mol pure), 4-hydroxybenzoic acid (99.9% mol pure). Methanol used in the SAS experiments was supplied by Fischer chemical ( $\geq 99.9$  % mol pure) and in the CSS experiments by Carl Roth ( $\geq 99.95\%$  mol pure). CO<sub>2</sub> used in the SAS experiments was supplied by Air Liquide (99.99 % mol pure) and in the CSS experiments by Linde (99.99 % mol pure). Table 5.1 displays relevant information of the materials employed.

## 5.2.2 Design of SAS experiments

**Table 5.2 Summary of conditions and results in the SAS experiments (solvent used methanol, concentration of 5-Fu 5 mg/mL, pressure 10.0 MPa and temperature 313 K).**

<b>SAS experiments</b>		
Co-crystal (A-B)	Molar ratio employed (A:B)	Product
5-Fu-Urea	1:1	co-crystal + 5-Fu
5-Fu-Thiourea	1:1	co-crystal + 5-Fu
5-Fu-ACR	2:1	5-Fu
5-Fu-ACR	1:13.4	co-crystal + unknown phase
5-Fu-4HBA	1:1	mixture of phases + 5-Fu
5-Fu-4HBA	1:3	mixture of phases + 4HBA
5-Fu-PZA	2:1	5-Fu
5-Fu-SAC	1:1	amorphous phase + 5-Fu

SAS experiments were performed in the equipment available at the Universidad Complutense de Madrid. A full description of the equipment and experimental procedure is given in chapter 3 (section 3.1). The solvent chosen for the co-crystallization of 5-Fu using the SAS technique was methanol. For the majority of the co-crystals studied in this work, methanol was the solvent used in their production through conventional methods. Furthermore, methanol and mixtures of methanol with dichloromethane and acetone have been successfully employed in the preparation of 5-Fu nanoparticles using the SAS technique.<sup>30</sup> Temperature was set at 313 K which is slightly above the critical temperature of CO<sub>2</sub> (304.2 K). Lower operating temperatures will translate in reduced energetic costs and will also help avoid thermal degradation of the pharmaceutical components. Pressure was fixed at 10.0 MPa to ensure conditions above the critical point of the methanol-CO<sub>2</sub> mixture<sup>47, 48</sup> (neglecting the influence that 5-Fu and the different cofomers could have in the phase equilibria diagram of the binary mixture). Other conditions were CO<sub>2</sub> flow rate (20 g/min) and solution flow rate (1 mL/min). At 313 K the critical pressure of the methanol CO<sub>2</sub> mixture is of 7.7 MPa, thus working at 10.0 MPa ensured that we were operating in the supercritical phase.



The concentration of the active pharmaceutical ingredient (API) in the methanol solution was 5 mg/mL. The same concentration had been previously used in the SAS micronization of 5-Fu<sup>30</sup> and its close to the saturation level of 5-Fu in methanol (solubility values from 1 to 5 mg/mL at 293 K<sup>49</sup>). Operating at concentrations close to the saturation level will allow a faster supersaturation of the solute in the precipitation chamber and generally leads to a reduced particle size. The coformer was used in the co-crystal stoichiometric ratio unless stated otherwise. The resulting CO<sub>2</sub> molar fraction in the precipitation chamber was higher than 0.95. A summary of conditions and results of the SAS experiments is given in Table 5.2.

5-Fu and the different coformers studied were also precipitated separately at the same conditions in order to study changes that the API and coformers may undergo in the SAS process.

### 5.2.3 Equipment validation and design of CSS experiments

Experiments were performed using a view cell available at the Institut für Technische Thermodynamik und Kältetechnik (ITTK) at the Karlsruher Institut für Technologie (KIT), group of Prof. Türk. The equipment and the experimental procedure have been previously described in chapter 3 (section 3.3). For the validation of the CSS equipment and experimental procedure the preparation of the 1:1 CBZ-SAC co-crystal was attempted. This co-crystal has been previously employed by Padrela et al.<sup>45</sup> to study the influence of several parameters (stirring, supercritical gas, cosolvent addition, pressure, temperature and time) in the co-crystal formation and its kinetics using the CSS technique. Also, this is a well studied co-crystal at our laboratory<sup>50</sup>.

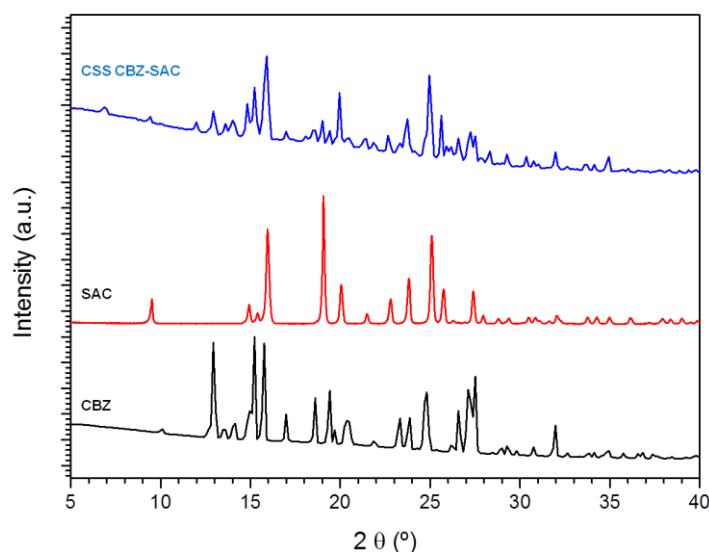


Fig. 5.4 PXRD patterns of: CSS co-crystallization powder of CBZ and SAC after 3 hours (top), commercial SAC (middle) and commercial CBZ (bottom).

In the set-up employed by Padrela et al.<sup>45</sup> 400 mg of CBZ and the stoichiometric amount of SAC were placed in a 8 mL high pressure vessel at 20.0 MPa and 323 K ( $1.2 \times 10^{-3}$  mol CBZ/mol  $\text{CO}_2$ ) and stirred at 300 rpm. Under these conditions co-crystallization took place after 2 hours. In this research the effects of mixing time, pressure and temperature were studied. Higher pressure enhanced the co-crystallization process (co-crystallization below the critical pressure of  $\text{CO}_2$  was unsuccessful in the systems studied by these authors). Conversely, temperature had the reverse effect reducing co-crystal formation as temperature raised, thus higher  $\text{CO}_2$  densities favoured the process. In all experiments stirring was crucial in the production of co-crystals and the co-crystallization rate was shown to be strongly dependent on the solubility of the API and coformer in supercritical  $\text{CO}_2$ .

Experiments in the Prof. Türk laboratory set-up were carried out with a lower quantity of CBZ (9 mg) due to the limiting size of the carbon pan. This translated in a lower CBZ molar ratio in the reactor ( $2.2 \times 10^{-4}$  mol CBZ/mol  $\text{CO}_2$ ) that in principle should facilitate CBZ dissolution and therefore co-crystallization. All the experiments were performed with magnetic stirring at 300 rpm. In contrast to Pradela's report, samples ran using a co-crystallization time of three hours showed the presence of homocrystals (see Fig. 5.4). To achieve full co-crystallization time was increased to 20 hours. PXRD pattern of the sample obtained after 20 hours displayed only the diffraction peaks of the co-crystal polymorph I (see Fig. 5.5). The rest of experiments were then carried out with a co-crystallization time of 20 h.

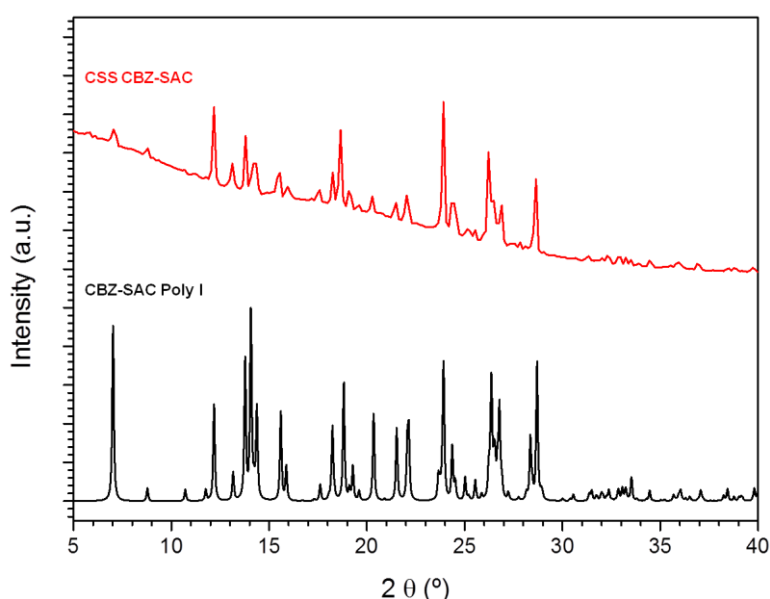


Fig. 5.5 PXRD patterns of: CSS co-crystallization powder of CBZ and SAC after 20 hours (top), and CBZ-SAC co-crystal polymorph I calculated from CIF (bottom).

As to the amounts of 5-Fu and coformers, approximately 9 mg of 5-Fu and the amount of coformer corresponding to the stoichiometric ratio of the co-crystal were weighed and deposit in a PTFE pan. The pan was then introduced in the small variable-volume view cell with a magnetic stirrer and CO<sub>2</sub> was introduced in the system (to ensure a molar fraction of CO<sub>2</sub> of 0.999 approximately 7 g of CO<sub>2</sub> were used). Temperature was raised to 323 K and the system was pressurized to 20.0 MPa. The effects that temperature and pressure have on the process were not explored and these values were kept constant. The sample was stirred at 300 rpm for approximately 20 hours. These values of pressure, temperature and stirring were chosen to reproduce the operating conditions previously used in co-crystallization experiments carried out with this technique.<sup>45</sup>

The solubility of 5-Fu in supercritical CO<sub>2</sub> has been measured at conditions similar to those used in our experiments by several authors. Values (expressed in mol 5-Fu/mol CO<sub>2</sub>) are:  $1.04 \times 10^{-5}$  at 20.0 MPa and 328 K (Suleiman et al.<sup>51</sup>);  $5.25 \times 10^{-6}$  at 20.0 MPa and 328 K (Zhan et al.<sup>41</sup>); and  $9.68 \times 10^{-7}$  at 21.0 MPa and 328 K (Guney and Akgerman<sup>52</sup>). In comparison, the solubility of CBZ in supercritical CO<sub>2</sub> at 328 K and 20.0 MPa is  $1.0 \times 10^{-5}$  mol CBZ/mol CO<sub>2</sub>.<sup>46</sup> The solubility of the different coformers is given in Table 5.1. Due to the low solubility of 5-Fu in supercritical CO<sub>2</sub> and the pan size limitations a higher molar fraction of CO<sub>2</sub> than that employed by Padrela et al.<sup>45</sup> was used in our experiments. Because the co-crystallization rate showed to be much slower than in Padrela's set-up,<sup>45</sup> the contact time of the API, coformer and supercritical CO<sub>2</sub> in the chamber was extended to 20 hours. The effect of cosolvent in the formation of co-crystals through the CSS technique was also assessed and experiments were repeated adding 20  $\mu$ L of methanol as cosolvent (molar fraction of methanol in the mixture of 0.32 %). The influence of cosolvents in the solubility of 5-Fu in supercritical CO<sub>2</sub> has been studied by Zhan et al.<sup>41</sup>. They measured the effect of ethanol and found out that the solubility increased as much as two orders of magnitude (an increase in the solubility could also be expected with the addition of cosolvent methanol). In our experiments methanol was the chosen cosolvent because, like ethanol, it is a cosolvent commonly used to improve the polarity of supercritical CO<sub>2</sub>, and because methanol was also the solvent used to obtain most of the co-crystals by solution conventional methods and in our SAS experiments.

A brief summary of the experimental conditions used and the results of the CSS experiments is given in Table 5.3.

**Table 5.3 Summary of conditions and results in the CSS experiments (pressure 20.0 MPa, temperature 323 K, stirring rate 300 rpm and co-crystallization time of 20 h)**

CSS experiments						
System (A-B)	stoichiometry (A:B)	m <sub>A</sub> (mg)	m <sub>B</sub> (mg)	V <sub>methanol</sub> (μL)	m <sub>CO2</sub> (mg)	Product
CBZ-SAC	1:1	9.09	7.07	0	7680	co-crystal polymorph I
CBZ-SAC	1:1	9.03	7.03	20	6780	co-crystal polymorph I
5-Fu-urea	1:1	9.08	4.41	0	7210	5-Fu + urea
5-Fu-urea	1:1	9.20	4.24	20	6810	co-crystal + 5-Fu + urea
5-Fu-thiourea	1:1	9.07	5.27	0	7600	5-Fu + thiourea
5-Fu-thiourea	1:1	9.00	5.34	20	6750	co-crystal + 5-Fu + thiourea
5-Fu-ACR	2:1	9.00	5.83	0	6800	5-Fu
5-Fu-ACR	2:1	9.08	6.27	20	6750	5-Fu + co-crystal
5-Fu-4HBA	1:1	9.37	9.80	0	7440	5-Fu + 4HBA
5-Fu-4HBA	1:1	9.07	9.76	20	6720	5-Fu + 4HBA
5-Fu-PZA	2:1	9.33	4.36	0	7380	5-Fu + PZA
5-Fu-PZA	2:1	9.07	4.37	20	6730	5-Fu + PZA + unknown phase
5-Fu-SAC	1:1	9.28	12.83	0	6900	5-Fu + SAC

## 5.3 5-Fu-UREA CO-CRYSTAL

### 5.3.1 SAS co-crystallization

This co-crystal (molecular structure can be seen in Fig. 5.3 a) was previously prepared by equimolar co-grinding using a mortar and pestle followed by dissolution in a minimum amount of methanol and subsequent evaporation<sup>20</sup>. The solubility of urea in supercritical CO<sub>2</sub> is small ( $3.6 \times 10^{-6}$  mol urea/mol CO<sub>2</sub> at 15.0 MPa and 313 K<sup>43</sup>) and in the same order of magnitude as that of 5-Fu ( $2.81 \times 10^{-6}$  mol 5-Fu/mol CO<sub>2</sub> at 10.0 MPa and 313 K<sup>41</sup>). The same authors<sup>43</sup> also measured the solubility of urea in supercritical CO<sub>2</sub> modified with ethanol and observed that solubility increased exponentially with the ethanol concentration at fixed temperature and pressure.

### PXRD characterization

PXRD patterns of the commercial and SAS processed 5-Fu were compared in order to assess crystallinity and possible changes in polymorphism of our samples.

Commercial 5-Fu was found to be the monoclinic form I with a marked preferential orientation along the plane (200) at  $2\theta$  28.6°. SAS processed 5-Fu presented no change in polymorphism and a less marked preferential orientation. In Fig. 5.6 the PXRD pattern of commercial 5-Fu, SAS processed 5-Fu and the calculated diffraction pattern from the crystallographic information file (CIF) for 5-Fu polymorph I<sup>1</sup> are compared.

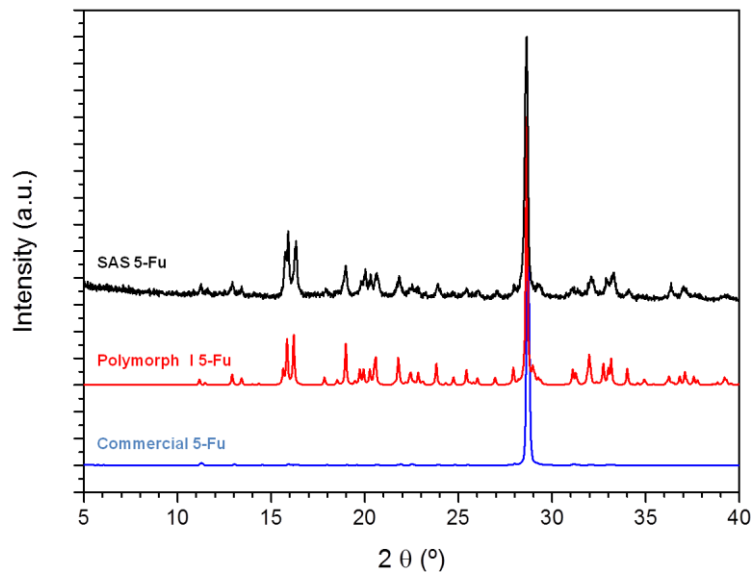


Fig. 5.6 PXRD patterns of: SAS processed 5-Fu (top), 5-Fu polymorph I calculated from CIF (middle) and commercial 5-Fu (bottom).

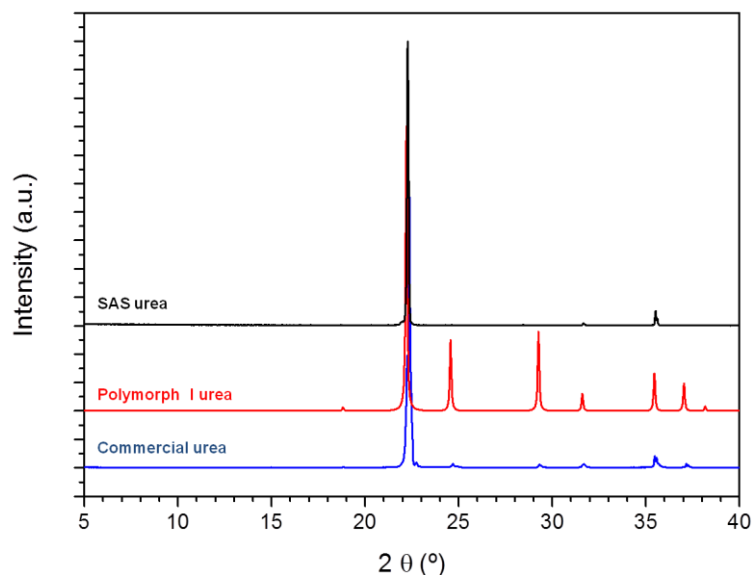


Fig. 5.7 PXRD patterns of: SAS processed urea (top), urea polymorph I calculated from CIF (middle), and commercial urea (bottom).

Same comparison of the PXRD patterns is made for urea (Fig. 5.7). Commercial urea was found to be the orthorhombic polymorph I and no change in polymorphism was observed after SAS processing. Both urea samples (commercial and SAS processed) presented a marked preferential orientation with a very intense peak in the plane (110) at  $2\theta$  22.2 °.

The PXRD pattern of the precipitate obtained from the SAS co-crystallization experiments and the one calculated from the crystallographic information file (CIF) published for this co-crystal<sup>20</sup> are compared in Fig. 5.8.

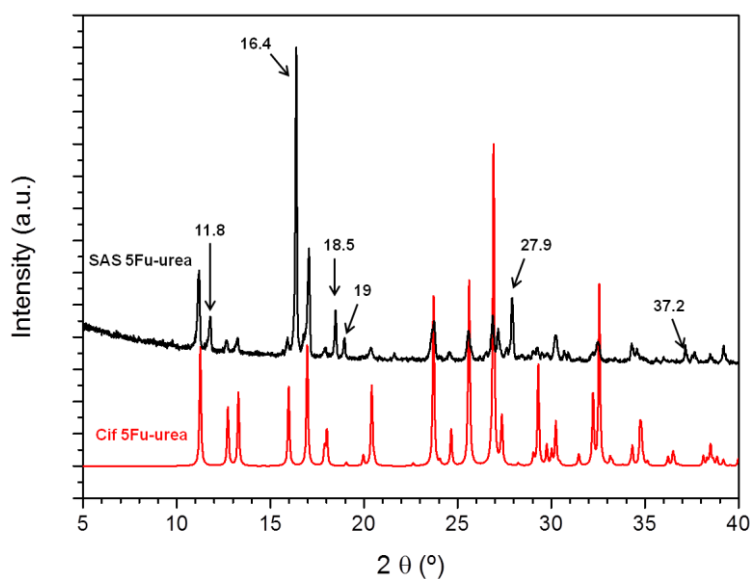


Fig. 5.8 PXRD patterns of the 5-Fu-urea co-crystal obtained through: SAS (top), and calculated from CIF (bottom).

PXRD pattern of the SAS precipitate showed diffraction peaks that were not present in the diffraction patterns of 5-Fu and urea at  $2\theta$ : 11.8, 17.1, 25.6, 26.8, 27.2, 30.2 and 34.3 °. These peaks confirm the presence of a different phase in our powder. In Fig. 5.8 we can observe that these diffraction peaks of the SAS powder are all present in the calculated pattern of the reported co-crystal structure<sup>20</sup> except the one at  $2\theta$  11.8 °. Moreover, the SAS powder also showed diffraction peaks associated to the diffraction pattern of 5-Fu polymorph I at  $2\theta$ : 16.4, 18.5, 19.0, 27.1, 27.9 and 37.2 °. These results indicated that precipitation by SAS at these conditions yielded the 5-Fu-urea co-crystal and 5-Fu homocrystals.

### Thermal characterization

SAS samples were analyzed using DSC and the results confirmed the presence of the co-crystal phase (see Fig. 5.9). The SAS precipitate presented an endothermic

transition at 480.15 K a temperature intermediate between the measured melting transitions of commercial 5-Fu (556.4 K) and commercial urea (407.3 K). Unfortunately, mass loss in the sample started with this endothermic transition, thus the calculation of the heat of fusion via peak integration was not possible, nor a further heating to identify the 5-Fu melting. The overlapping of melting and decomposition processes also called apparent melting<sup>53</sup> is a phenomenon usual in pharmaceutical drugs (the loss of the crystalline structure can be caused by numerous processes other than thermodynamic melting). Apparent melting is usually referred though as melting.

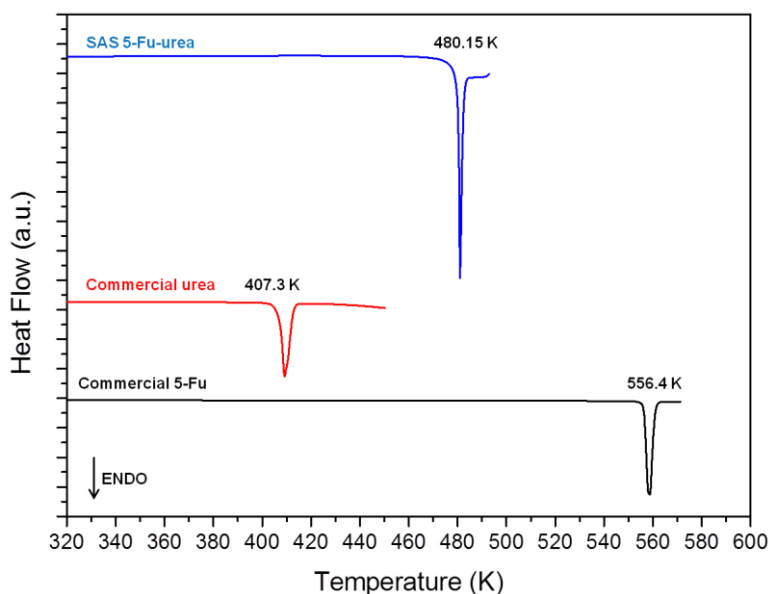


Fig. 5.9 DSC thermograms of: SAS processed 5-Fu-urea (top), commercial urea (middle), and commercial 5-Fu (bottom). Heating rate 5 K/min.

Fig. 5.10 shows the TGA thermogram of the SAS precipitate. It can be observed that mass loss took place in two steps. The first step took place simultaneously to the first endothermic transition which corresponds to the apparent melting of the co-crystal at 480.15 K. The percentage of mass loss measured in this first step was approximately 32% close to the 31.6% content of urea in a 1:1 5-Fu-urea co-crystal. Urea seems to be stabilized in the co-crystal structure above its decomposition temperature (which presents an onset at 460.7 K measured using TGA) so when the co-crystal melts urea decomposes completely. The second step appeared at the same temperature as the apparent melting of 5-Fu (at ca. 550 K). At ca. 550 K 5-Fu starts to decompose. Micro-elemental analysis confirmed the 1:1 stoichiometrical ratio of 5-Fu to urea. The fact that 5-Fu and urea were present in the stoichiometric ratio in the SAS precipitate but no XRD or DSC peaks associated to urea were observed indicates the amorphization of urea upon SAS precipitation.

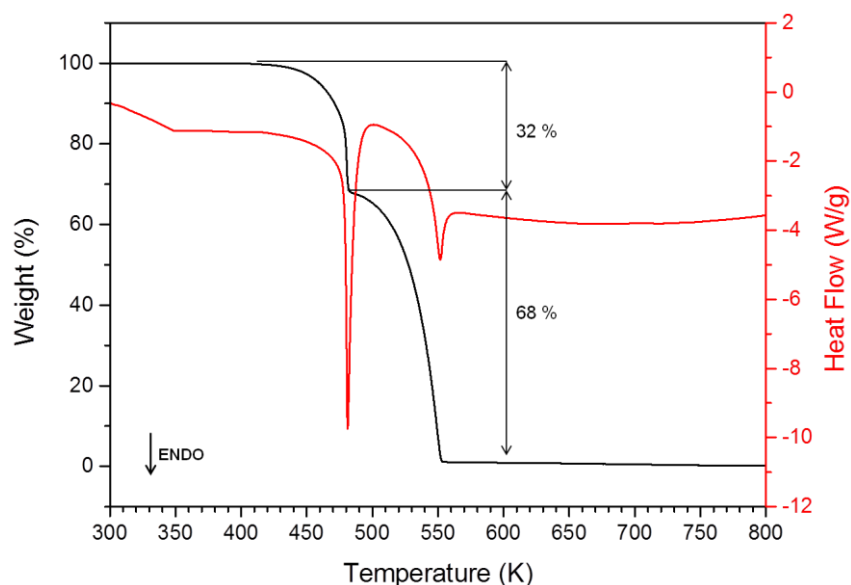


Fig. 5.10 TGA and DSC thermograms of SAS processed 5-Fu-urea. Heating rate 5 K/min.

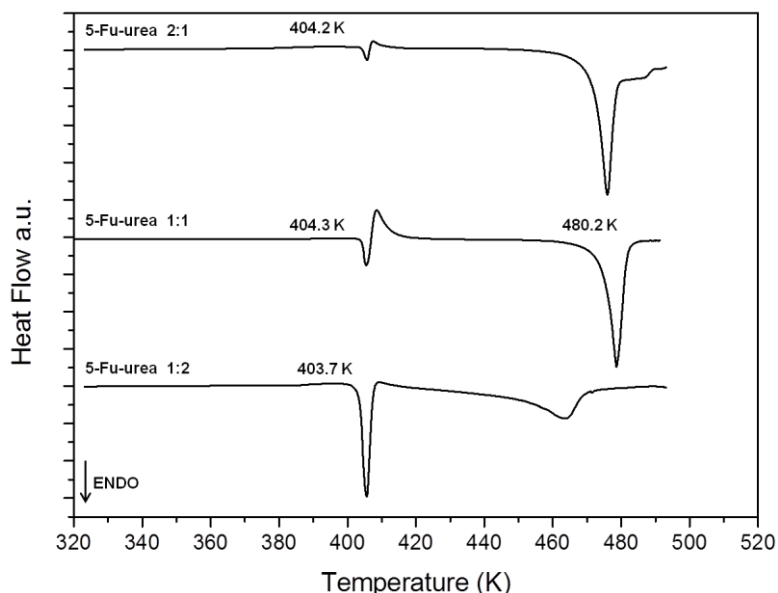


Fig. 5.11 DSC thermograms of 5-Fu-urea physical mixtures with molar ratios: 2:1 (top), 1:1 (middle), and 1:2 (bottom). Heating rate 5 K/min.

In order to ensure that the co-crystal is not being formed during the heating ramp in the DSC analysis, physical mixtures of 5-Fu and urea were submitted to analysis. Different molar ratios of 5-Fu to urea were tested (2:1, 1:1, 1:2). Results can be observed in Fig. 5.11. We can observe a first endothermic peak with onset close to the melting point of urea (at ca. 404.3 K) followed by an exothermic peak that probably corresponds to the formation of the co-crystal and a subsequent endothermic peak at the apparent melting temperature of the co-crystal (480.2 K).



The area of this fusion peak becomes smaller when the relative amount of urea is reduced as it can be observed in Fig. 5.11. The fact that this transition did not appear in the SAS precipitate prior to the apparent melting of the co-crystal confirmed that there were no urea homocrystals present and that the 5-Fu-urea co-crystal was present in the SAS precipitate.

### FTIR characterization

FTIR spectra of the samples were analyzed for further characterization. The FTIR spectrum of 5-Fu has been previously detailed by several authors.<sup>54-56</sup> Experimental characteristic absorption bands of commercial 5-Fu polymorph I can be seen in Fig. 5.12 and are described in Table 5.4 (assignment of fundamental absorption bands based on previous publications<sup>54-56</sup>).

**Table 5.4 Infrared peaks (cm<sup>-1</sup>) of commercial 5-Fu and their assignments:  $\nu$  stretching;  $\delta$  bending;  $\gamma$  torsion;  $\omega$  wagging;  $\tau$  twisting;  $\rho$  rocking.**

Experimental IR wavenumbers (cm <sup>-1</sup> )	Band assignment	Experimental IR wavenumbers (cm <sup>-1</sup> )	Band assignment
3115	$\nu$ (NH)	1243	$\nu$ (C-F); $\nu$ (ring)
3066	$\nu$ (NH)	1180	$\delta$ (C-H); $\delta$ (N-H);
2995	$\nu$ (CH)		$\delta$ (ring)
1720	$\nu$ (C=O); $\delta$ (N-H)	950	$\delta$ (N-H); $\delta$ (C-H);
1644	$\nu$ (C=C); $\nu$ (ring)		$\delta$ (ring)
1501	$\delta$ (N-H); $\nu$ (ring)	868	$\gamma$ (C-H)
1428	$\nu$ (ring); $\delta$ (N-H)	803	$\delta$ (ring)
1348	$\delta$ (N-H); $\delta$ (ring)	747	$\gamma$ (C=O); $\gamma$ (ring)

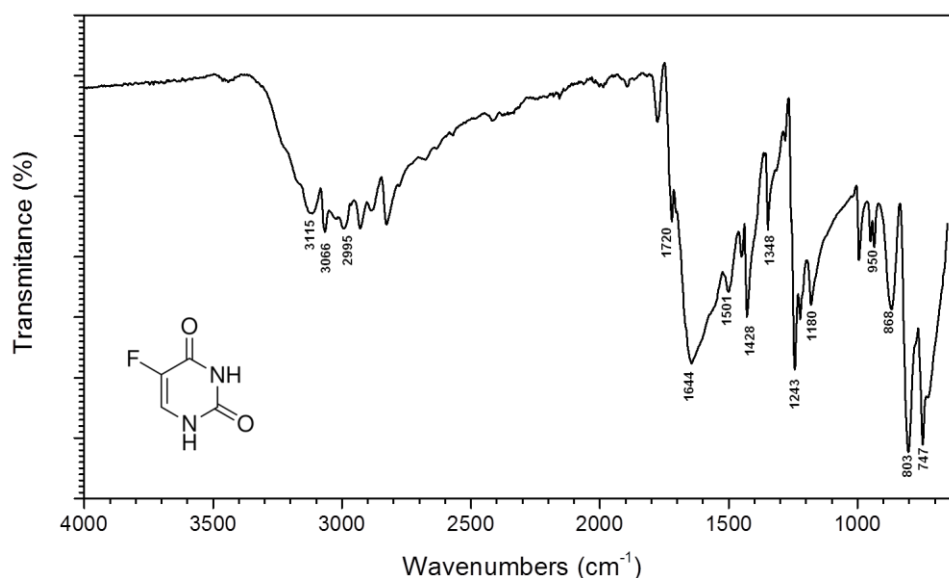


**Fig. 5.12 FTIR spectrum of 5-Fu.**

The spectrum of commercial urea was also measured (see Fig. 5.13) and assignment of the main absorption bands was also carried out with the aid of previous publications<sup>57, 58</sup> (see Table 5.5).

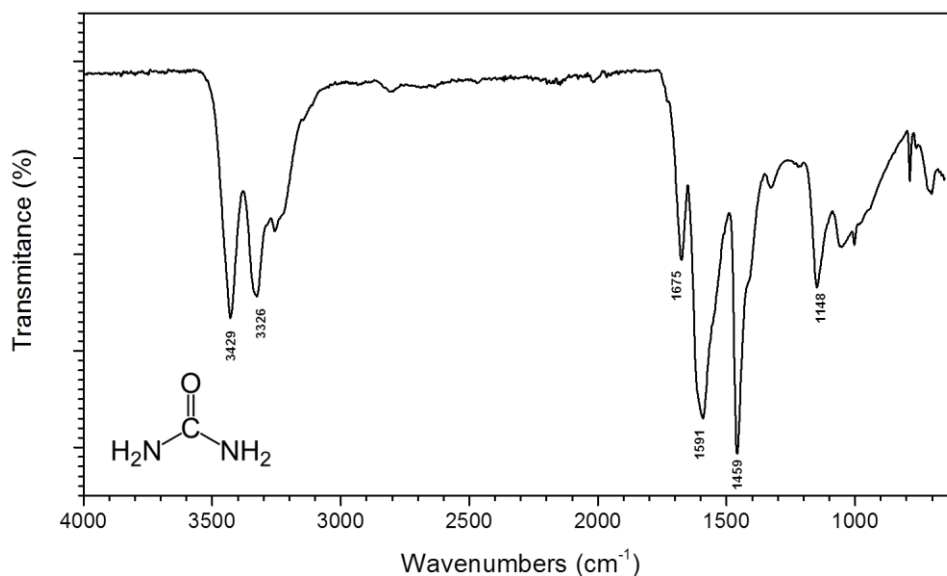


Fig. 5.13 FTIR spectrum of urea.

Table 5.5 Infrared peaks ( $\text{cm}^{-1}$ ) of commercial urea and their assignments:  $\nu$  stretching;  $\delta$  bending;  $\gamma$  torsion;  $\omega$  wagging;  $\text{tw}$  twisting;  $\rho$  rocking.

Experimental IR wavenumbers ( $\text{cm}^{-1}$ )	Band assignment	Experimental IR wavenumbers ( $\text{cm}^{-1}$ )	Band assignment
3429	$\nu$ ( $\text{NH}_2$ )	1591	$\nu$ ( $\text{C}=\text{O}$ )
3326	$\nu$ ( $\text{NH}_2$ )	1459	$\nu$ ( $\text{C}-\text{N}$ )
1675	$\delta$ ( $\text{NH}_2$ )	1148	$\rho$ ( $\text{NH}_2$ )

FTIR spectrum of the SAS precipitate is shown in Fig. 5.14. In comparison to FTIR spectra of pure components a shift of the absorption frequency of several bands was observed in the SAS precipitate. This confirmed a new molecular arrangement with a different H-bond network rather than a mixture of both phases. We can highlight the following shifts in absorption frequencies: the  $\text{NH}_2$  stretching frequency at  $3429 \text{ cm}^{-1}$  of urea blue shifted to  $3442 \text{ cm}^{-1}$ , the  $\text{C}=\text{O}$  stretching vibration of 5-Fu at  $1720 \text{ cm}^{-1}$  red shifted to  $1711 \text{ cm}^{-1}$  and the  $\text{C}=\text{O}$  stretching of urea at  $1591 \text{ cm}^{-1}$  red shifted to  $1567 \text{ cm}^{-1}$ . These shifts in the absorption frequencies in the  $\text{NH}_2$  groups of the urea and the carbonyl groups of 5-Fu and urea indicated an interaction between these functional groups probably forming amide-amide synthons similar to those reported by Nadzri et al.<sup>20</sup> (see Fig. 5.3 a).

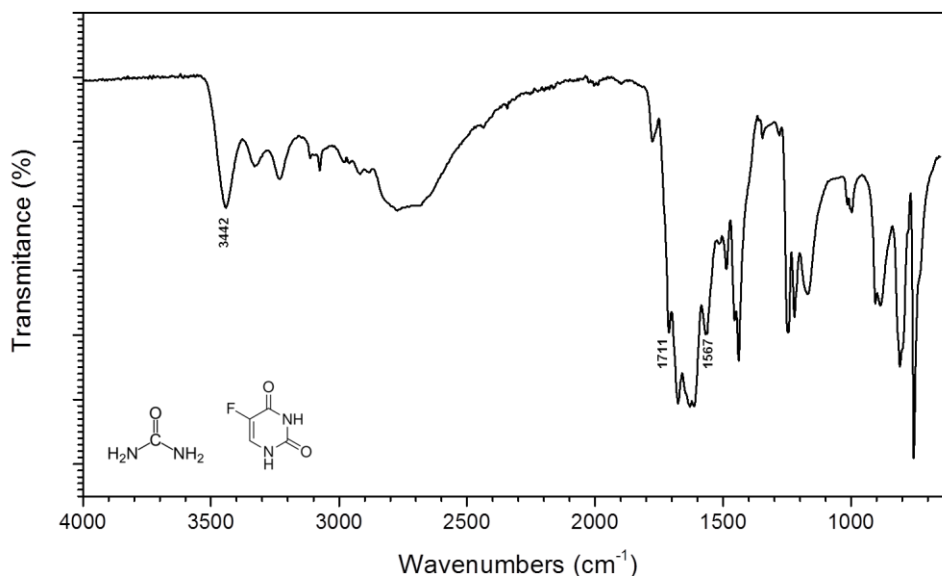


Fig. 5.14 FTIR spectrum of SAS processed 5-Fu-urea.

## SEM characterization

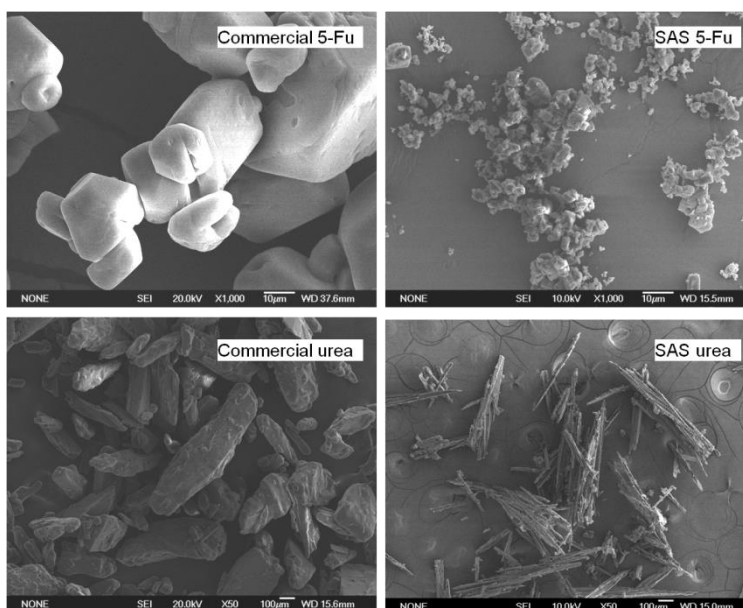


Fig. 5.15 SEM images of commercial and SAS processed 5-Fu and urea.

SEM images of commercial and SAS processed 5-Fu and urea are shown in Fig. 5.15. Commercial 5-Fu presented prismatic particles of heterogeneous size ranging from 50 to 300 µm. Particles of SAS processed 5-Fu presented the same prismatic morphology but with sizes ranging from 0.5 to 5 µm (similar to the 3 µm particles obtained when operating only with methanol by Kalantarian et al.<sup>30</sup>). Commercial urea presented a heterogeneous size distribution with large pieces ranging

from 0.1 up to 1.5 mm. SAS processed urea though presented a needle-like morphology. Needles of around 20  $\mu\text{m}$  wide and lengths ranging from 0.1 to 1 mm were agglomerated in clusters.

SEM images of the 5-Fu-urea SAS precipitate (Fig. 5.16) revealed a different morphology to those previously described. The SAS precipitate consisted mainly of fragmented rectangular plates or wide needles of around 0.5  $\mu\text{m}$  thick, 2 to 6  $\mu\text{m}$  wide and 10 to 60  $\mu\text{m}$  long.

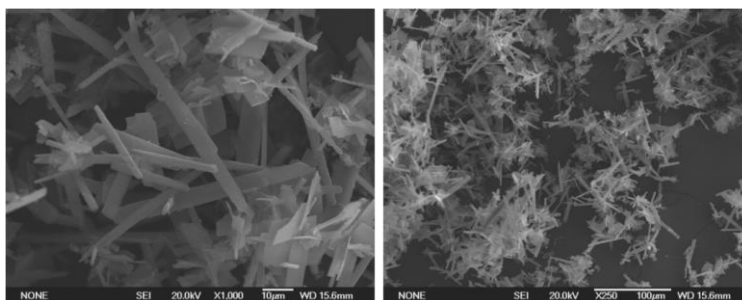


Fig. 5.16 SEM images of SAS processed 5-Fu-urea.

### 5.3.2 CSS co-crystallization

The differences in co-crystallization when  $\text{CO}_2$  acts as the solvent was assessed using the CSS technique.

#### PXRD characterization

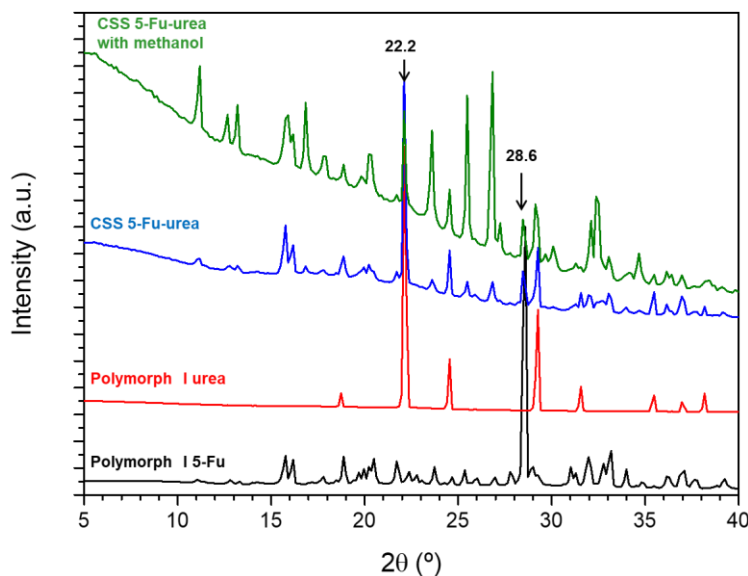


Fig. 5.17 PXRD patterns from top to bottom of: 5-Fu-urea CSS powder obtained using methanol, 5-Fu-urea CSS powder obtained without methanol, urea polymorph I calculated from CIF, and 5-Fu polymorph I calculated from CIF.

PXRD patterns of the CSS samples are shown in Fig. 5.17 along with the patterns of commercial 5-Fu and urea. The sample obtained without cosolvent consisted of a mere mixture of both initial phases and displayed the diffraction peaks of both co-crystal components. Therefore, the formation of a new co-crystal phase at these conditions was unsuccessful.

When methanol was used as cosolvent the PXRD pattern of the powder clearly showed the presence of another phase (see Fig. 5.17). This pattern also revealed the presence of 5-Fu and urea homocrystals. The main reflection peaks of 5-FU at  $2\theta$   $28.6^\circ$  corresponding to plane (2,0,0) and of urea at  $2\theta$   $22.2^\circ$  corresponding to plane (1,1,0) are clearly visible in Fig. 5.17.

Fig. 5.18 compares the PXRD patterns of the 5-Fu-urea powder obtained via CSS with methanol, the 5-Fu-urea SAS precipitate and the calculated pattern from the CIF published by Nadzri et al.<sup>20</sup> The new diffraction peaks of the sample obtained via CSS with methanol matched those calculated from the crystal structure reported by Nadzri et al.<sup>20</sup> for this co-crystal. 5-Fu and urea were also present. Both SAS and CSS seem suitable techniques for the preparation of the 5-Fu-urea co-crystal although none of them rendered a pure phase. The limited solubility of 5-Fu and urea in  $\text{CO}_2$  modified with methanol hindered the complete conversion of the components to the co-crystal.

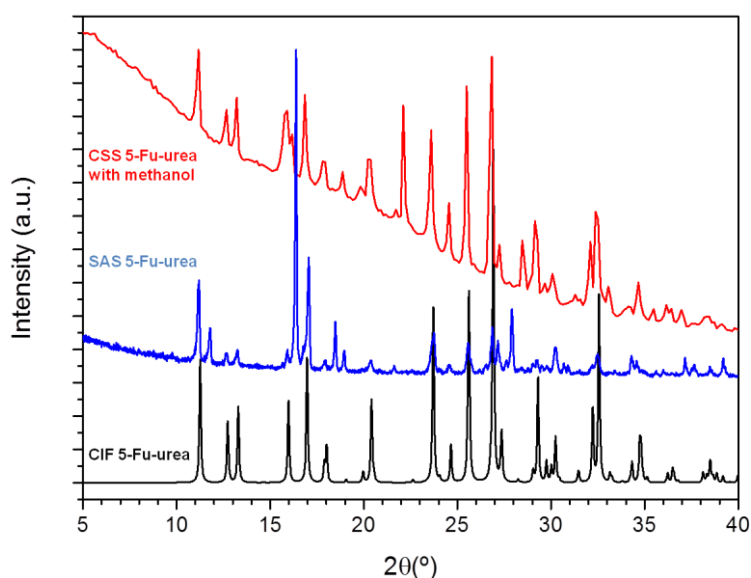


Fig. 5.18 PXRD patterns of the 5-Fu-urea co-crystal obtained through: CSS with methanol (top), SAS (middle), and calculated from CIF (bottom).

### Thermal characterization

CSS samples were also analysed using DSC. Thermogram of the sample prepared without methanol confirmed that the powder was a mere physical mixture of

5-Fu and urea. The endo-exo event corresponding to the melting of urea followed by the co-crystallization that was observed in the thermogram of the physical mixture at ca. 404 K (Fig. 5.11) was also found in the thermogram of this sample (Fig. 5.19).

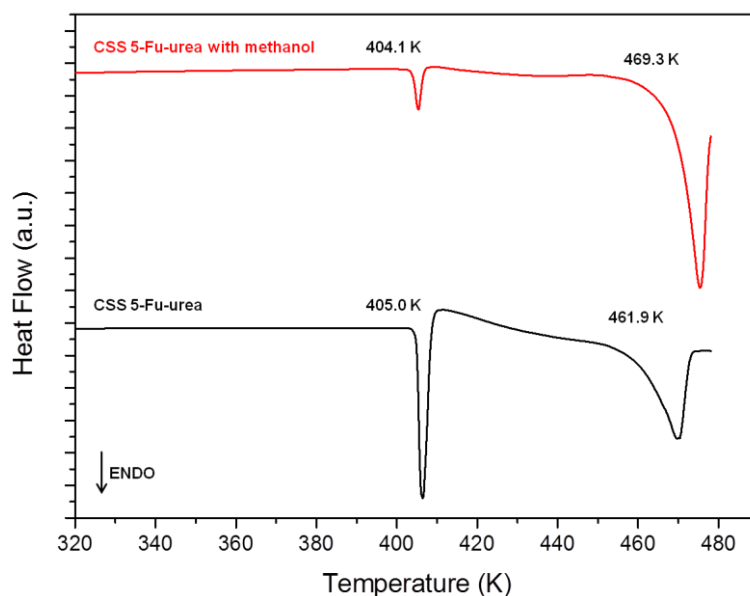


Fig. 5.19 DSC thermogram of CSS 5-Fu-urea powders obtained: with methanol (top), and without methanol (bottom). Heating rate 5 K/min.

The DSC thermogram of the CSS sample prepared with methanol also confirmed the presence of urea homocrystals in the sample (as the PXRD had revealed). The endothermic peak corresponding to the fusion of urea could be clearly identified and was followed by what appeared to be a very weak exothermic event (a small amount of free 5-Fu and urea seemed to co-crystallize). Decomposition of urea has an onset temperature of around 460.7 K, thus, no valid information could be obtained from the following peaks in the thermogram. The first endothermic peak took place at 404-405 K. This temperature is slightly lower than that measured for pure urea (407.3 K) which could be an indication of an eutectic point around 404 K in the phase diagram of the co-crystal. However, further experimentation would be required to clarify the phase diagram of this system.

### FTIR characterization

FTIR spectra of the CSS samples is presented in Fig. 5.20. Spectra of the CSS samples prepared with cosolvent also presented the shifts in the urea  $\text{NH}_2$  and  $\text{C}=\text{O}$  stretchings previously observed for the SAS precipitate. The shift in the  $\text{C}=\text{O}$  stretching of the 5-Fu observed in the SAS precipitate from 1720 to 1711  $\text{cm}^{-1}$  was not clear in the CSS samples though.

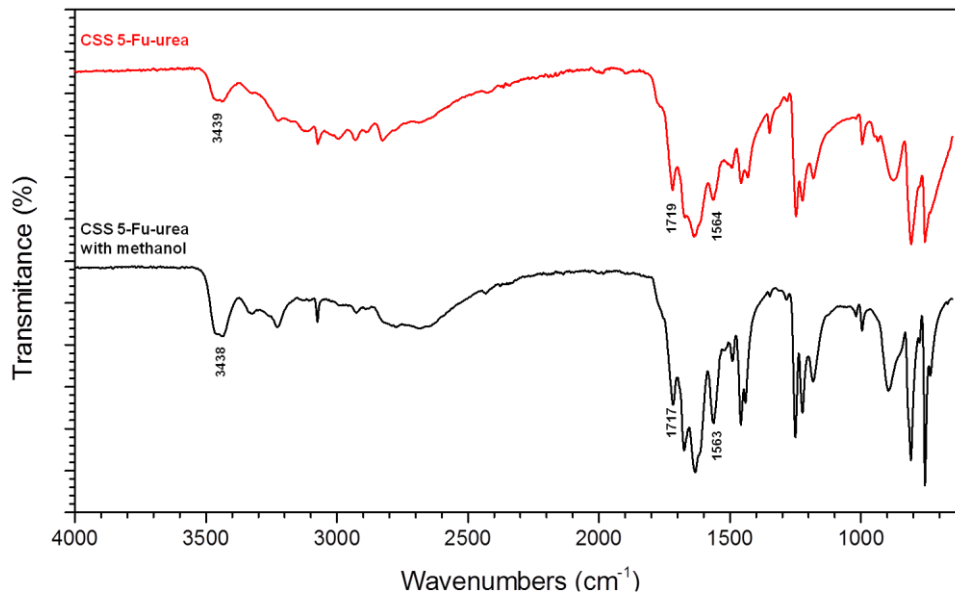


Fig. 5.20 FTIR spectra of CSS 5-Fu-urea powders obtained: without methanol (top), and with methanol (bottom).

### SEM characterization

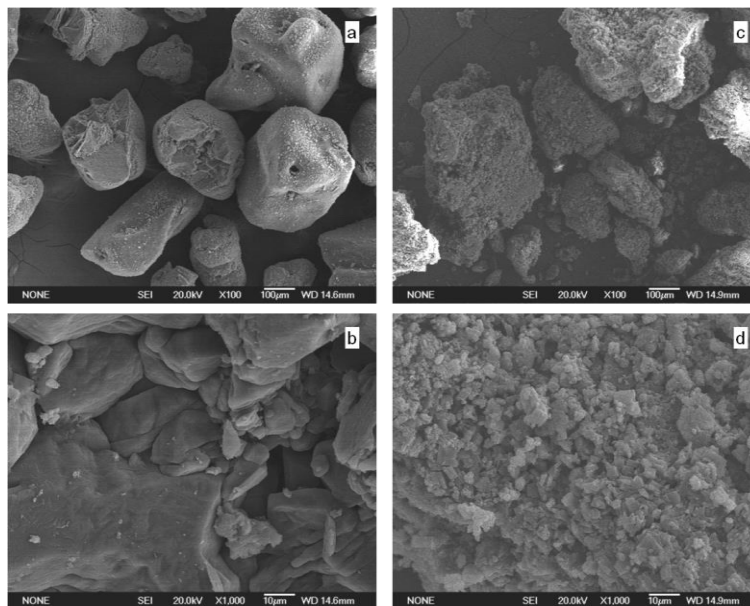


Fig. 5.21 SEM images of 5-Fu-urea CSS powders obtained without methanol (a,b), and with methanol (c,d).

The SEM images of the CSS samples from the experiments ran without methanol showed big prismatic particles of heterogeneous sizes similar to those of commercial 5-Fu but with larger dimensions ranging from 150 to 600 µm. The surface of these big prismatic particles was not smooth like in pure 5-Fu but rough. It seems as if the urea had attached to the walls of the 5-Fu particles (see Fig. 5.21). In the

experiments ran with methanol the roughness of the surface was even more pronounced, suggesting a higher interaction between both cofomers. This closer interaction between the cofomers revealed in the SEM images is in accordance with the results obtained by the other characterization techniques that confirmed the presence of the co-crystal in the experiments run with methanol. Particles of these latter experiments also presented heterogeneous sizes ranging from 50 to 600  $\mu\text{m}$ . Therefore, the advantageous particle size reduction that was achieved with the SAS technique was not reached with the CSS technique. The very low solubility of 5-Fu and urea in  $\text{CO}_2$  (pure and modified with methanol) hindered co-crystal formation in a large extent.

## 5.4 5-Fu-THIOUREA CO-CRYSTAL

### 5.4.1 SAS co-crystallization

Methanol was the solvent used by Nadzri et al.<sup>20</sup> in the preparation of 5-Fu-thiourea co-crystals through conventional methods: mortar and pestle co-grinding followed by dissolution in a minimum amount of methanol and subsequent evaporation. Molecular structure of the co-crystal is showed in Fig. 5.3 b.

#### PXRD characterization

PXRD patterns of the commercial and SAS processed thiourea were also compared in order to assess crystallinity and possible changes in polymorphism after SAS processing. Commercial thiourea was in the orthorhombic form with a marked preferential orientation along the plane (020) at  $2\theta$  20.7 °. SAS processed thiourea presented no change in polymorphism but an even stronger preferential orientation at  $2\theta$  20.7 ° as we can see in Fig. 5.22.

The PXRD pattern of the 5-Fu-thiourea co-crystal obtained using the SAS technique is shown in Fig. 5.23 where it is compared with the calculated pattern from the co-crystal structure described by Nadzri et al.<sup>20</sup> The peak at  $2\theta$  17.4 ° was the most intense peak and it was not found in any of the co-crystal components (5-Fu or thiourea), thus indicating the presence of a different crystal phase. Other much less intense peaks that appeared in the PXRD pattern of the SAS powder and are not present in the diffraction patterns of the co-crystal components are at  $2\theta$  26.3 and 33.6 °. These three peaks are present in the calculated PXRD pattern of the 5-Fu-thiourea co-crystal<sup>20</sup> indicating the presence of this structure in the SAS powder.



Some diffraction peaks that are not present in the calculated pattern from Nadzri et al.<sup>20</sup> were found at  $2\theta$  25.3, 27.1 and 27.9°. These peaks can be found in the pattern of commercial 5-Fu polymorph I (although the relative intensity of these peaks in the pattern of 5-Fu polymorph I are weak). This seems to indicate that the powder obtained via SAS contained the 5-Fu-thiourea co-crystal but could also contain 5-Fu homocrystals. Similar to the 5-Fu and urea coprecipitation by SAS, 5-Fu peaks were identified in the PXRD.

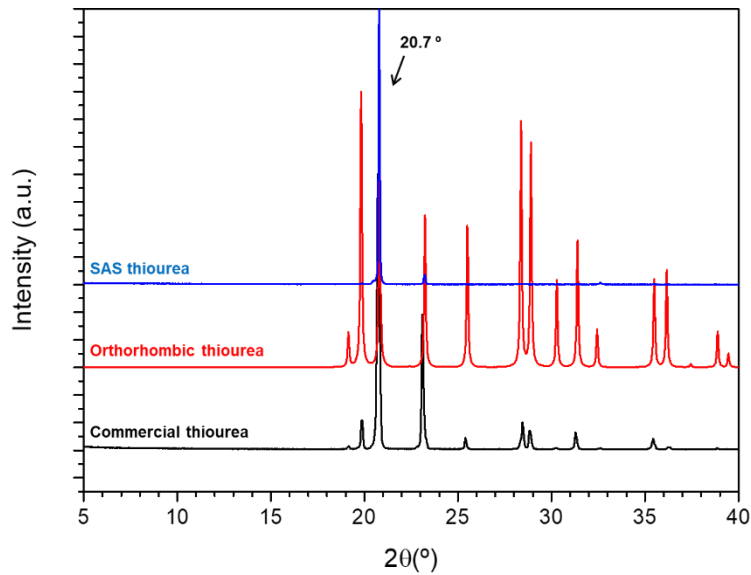


Fig. 5.22 PXRD patterns of: SAS processed thiourea (top), orthorhombic thiourea calculated from CIF (middle), and commercial thiourea (bottom).

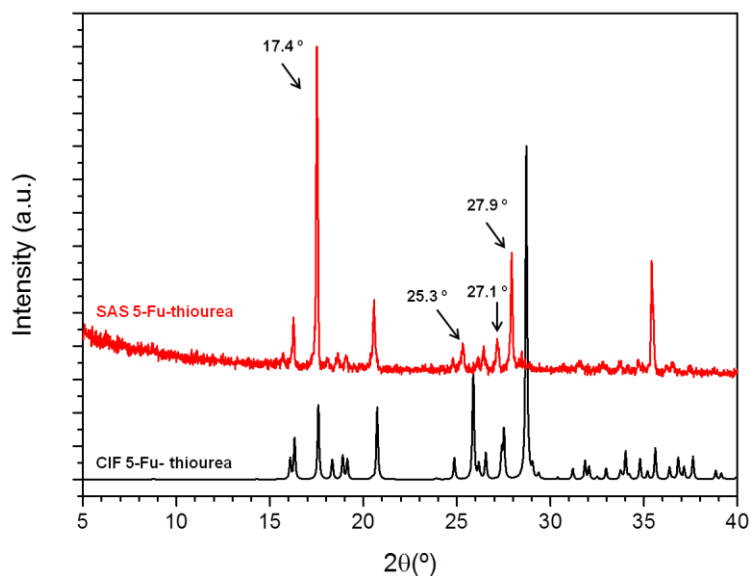


Fig. 5.23 PXRD patterns of the 5-Fu-thiourea co-crystal obtained through: SAS (top), and calculated from CIF (bottom).

## Thermal characterization

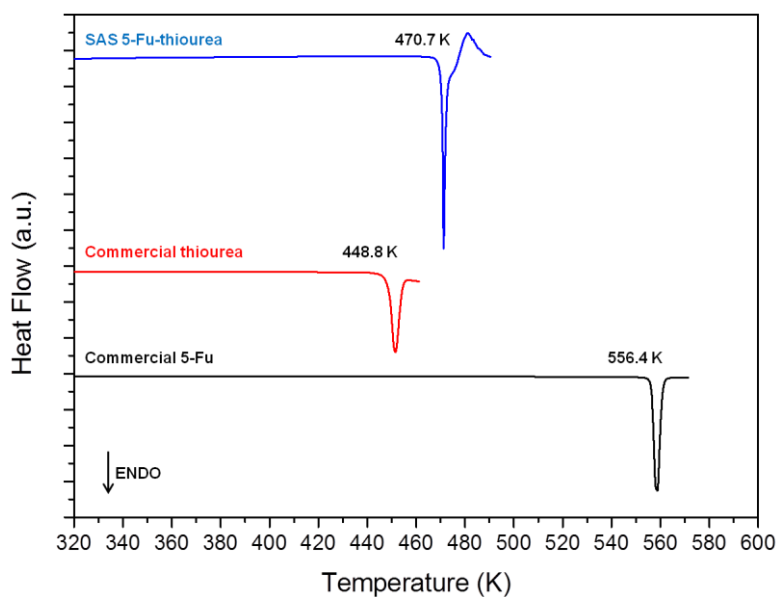


Fig. 5.24 DSC thermograms of: SAS processed 5-Fu-thiourea (top), commercial thiourea (middle), and commercial 5-Fu (bottom). Heating rate 5 K/min.

The analysis of SAS samples using DSC confirmed the presence of a new crystal phase. As it can be seen in Fig. 5.24 the powder obtained in the SAS experiments showed a melting transition at 470.7 K. This melting temperature is (like in the 5-Fu-urea co-crystal) intermediate between the melting transitions of both cofomers, 5-Fu (556.4 K) and thiourea (448.8 K). Mass loss took place simultaneously with the melting transition so the calculation of the heat of fusion via peak integration was again not recommended.

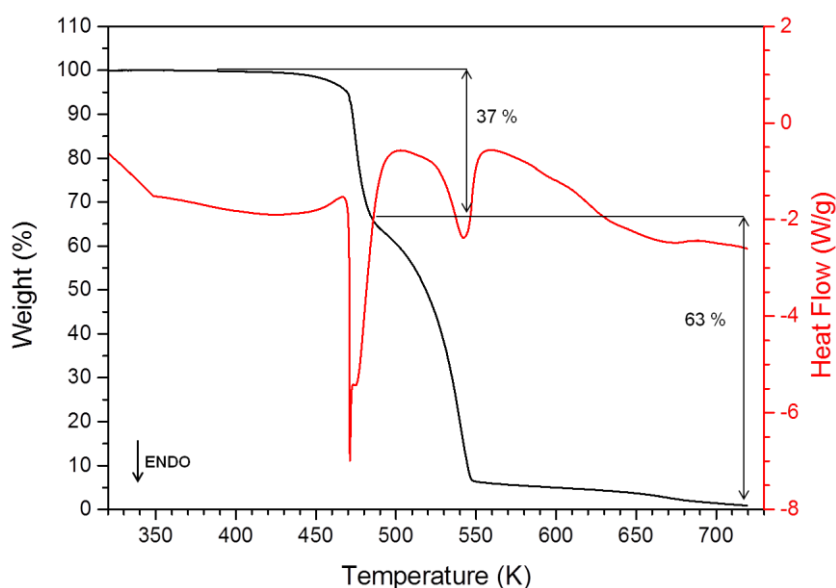


Fig. 5.25 TGA and DSC thermogram of SAS processed 5-Fu-thiourea. Heating rate 5 K/min.

TGA of the SAS precipitate was also similar to that obtained for the 5-Fu-urea co-crystal and mass loss took place in two steps. The first step presented a mass loss of 37% that agrees with the mass percentage of thiourea in the co-crystal (36.9%). Therefore, thiourea was stabilized in the co-crystal over its decomposition temperature (which presents an onset at 474.3 K measured using TGA) and seemed to decompose completely after co-crystal melting took place (see Fig. 5.25). The second step can be associated to the decomposition of 5-Fu. Micro-elemental analysis confirmed the presence of 5-Fu and thiourea in a 1:1 molar ratio in the SAS precipitate.

DSC analysis of the equimolar physical mixture of both co-crystal cofomers (Fig. 5.26) was carried out to warrant that the co-crystal formation is not a result of the heating ramp during the DSC experiment. In the analysis of the equimolar mixture we could observe that the first endothermic transition had an onset at ca. 443.2 K (lower than the pure thiourea melting onset at 448.8 K) and was subsequently followed by a second endothermic transition, therefore describing a decomposition behaviour similar to that previously reported for thiourea<sup>59</sup>. In comparison to the 5-Fu and urea physical mixture, the exothermic event associated to co-crystal formation was not visible after the melting of thiourea as the decomposition takes place. Experiment was stopped at this temperature to avoid fume formation in the apparatus.

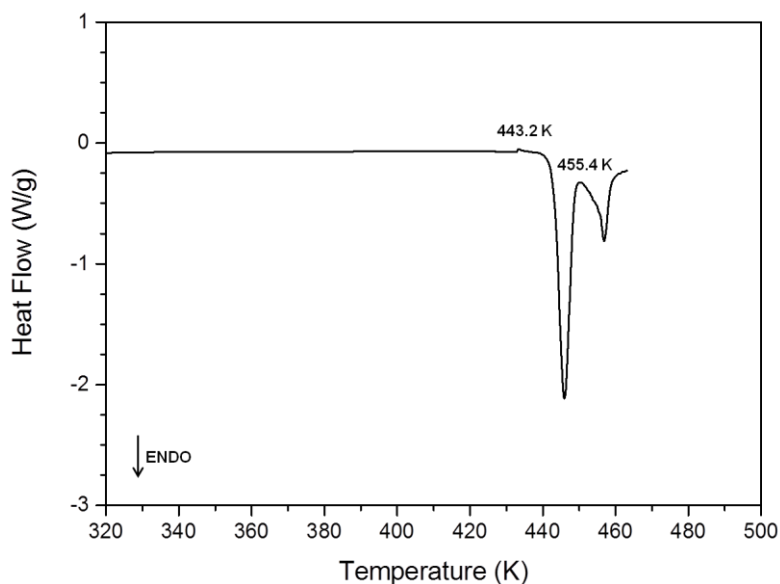


Fig. 5.26 DSC thermogram of a 5-Fu-thiourea equimolar physical mixture. Heating rate 5 K/min.

### FTIR characterization

The spectrum of commercial thiourea was measured in order to analyse possible shifts in the absorption bands. Experimental spectrum is plotted in Fig. 5.27

and the band assignments made with aid of previous publications<sup>60</sup> can be found in Table 5.6.

**Table 5.6 Infrared peaks (cm<sup>-1</sup>) of commercial thiourea and their assignments:  $\nu$  stretching;  $\delta$  bending;  $\gamma$  torsion;  $\omega$  wagging;  $\tau$ w twisting;  $\rho$  rocking.**

Experimental IR wavenumbers (cm <sup>-1</sup> )	Band assignment	Experimental IR wavenumbers (cm <sup>-1</sup> )	Band assignment
3367	$\nu$ (NH <sub>2</sub> )	1461	$\nu$ (C-N)
3266	$\nu$ (NH <sub>2</sub> )	1405	$\nu$ (C=S)
3158	$\nu$ (NH <sub>2</sub> )	1080	$\rho$ (NH <sub>2</sub> )
2685	$\nu$ (C=S)	728	$\nu$ (C-N)
1602	$\delta$ (NH <sub>2</sub> )		

When we compared the FTIR spectra of 5-Fu and thiourea to the experimental spectrum of the SAS processed 5-Fu-thiourea mixture (Fig. 5.28) we detected displacements of the absorption bands of thiourea in the region of the NH<sub>2</sub> stretching (3367, 3266 and 3158 cm<sup>-1</sup>) and of 5-Fu in the NH stretching (3115 and 3066 cm<sup>-1</sup>) where we now find two major absorption peaks at 3387 and 3202 cm<sup>-1</sup>. In the region of the C=S stretching the absorption band at 2685 cm<sup>-1</sup> shifted to 2674 cm<sup>-1</sup> and reduced considerably its intensity and the one at 1405 cm<sup>-1</sup> shifted to 1396 cm<sup>-1</sup> and also reduced its intensity substantially. The C=O stretching of 5-Fu (1720 cm<sup>-1</sup>) shifted to 1690 cm<sup>-1</sup> and reduced its intensity as well. This indicated that these functional groups form a different H-bond network in the precipitate and confirmed the co-crystal formation by SAS. The molecular structure proposed for this co-crystal<sup>20</sup> is shown in Fig. 5.3 b.

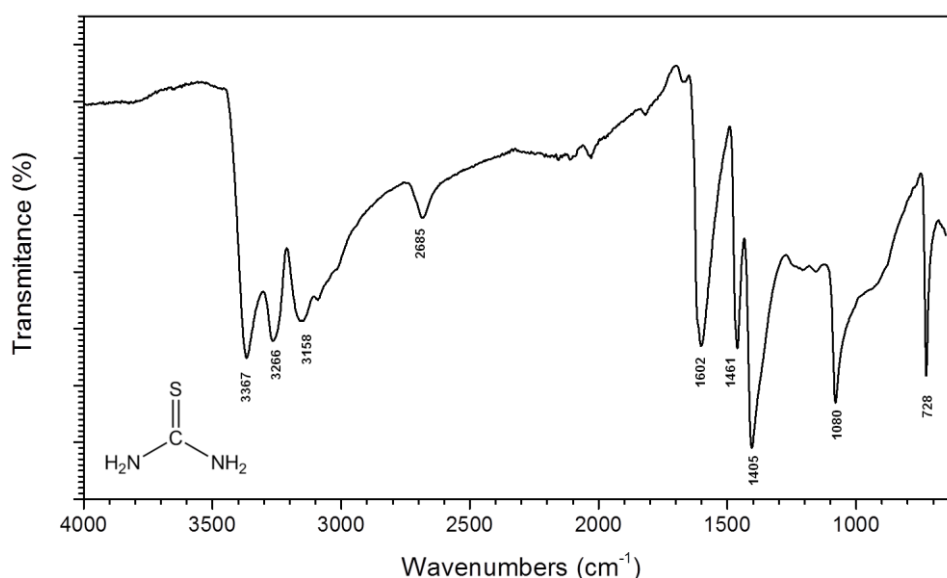


**Fig. 5.27 FTIR spectrum of thiourea.**

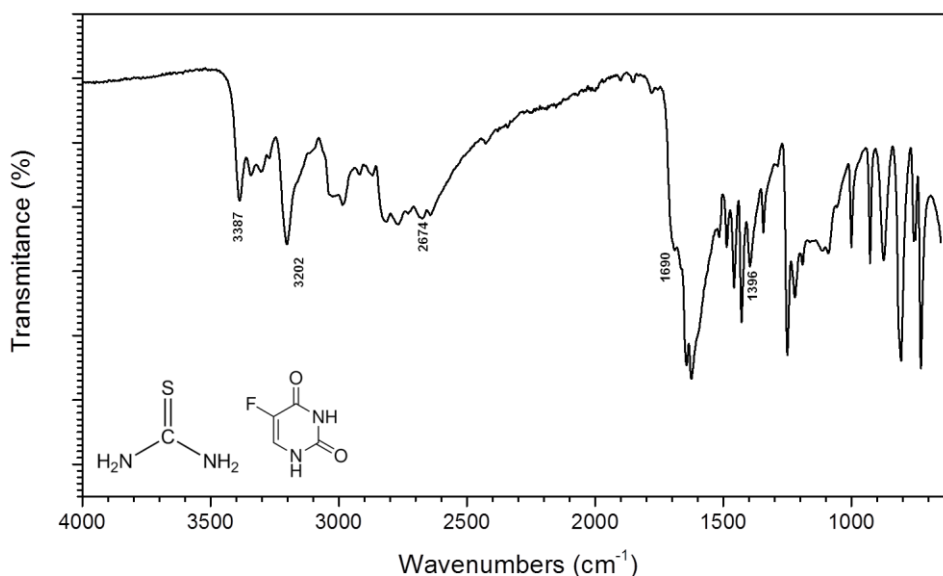


Fig. 5.28 FTIR spectrum of SAS processed 5-Fu-thiourea.

### SEM characterization

Images of SAS processed and commercial thiourea (Fig. 5.29) revealed an important particle size reduction as a result of SAS processing. The macromorphology of commercial thiourea consisted in heterogeneous large particles of smooth surface and sizes ranging from 40 to 350  $\mu\text{m}$ . Once processed via SAS, the morphology observed resembled a net of fragmented thin needles with widths ranging from 1 to 4  $\mu\text{m}$  and lengths from 1 to 40  $\mu\text{m}$ .

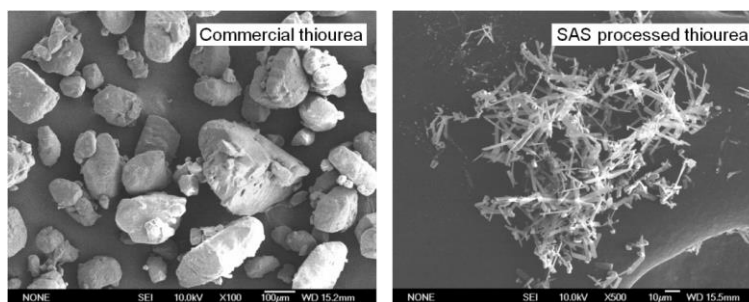


Fig. 5.29 SEM images of commercial and SAS processed thiourea.

The morphology observed in the SEM images of the 5-Fu-thiourea SAS precipitate (Fig. 5.30) was relatively similar to that obtained for the 5-Fu-urea precipitate. It consisted of aggregated rectangular plates which were 0.5 to 3  $\mu\text{m}$  thick, 4 to 8  $\mu\text{m}$  wide and 5 to 65  $\mu\text{m}$  long.

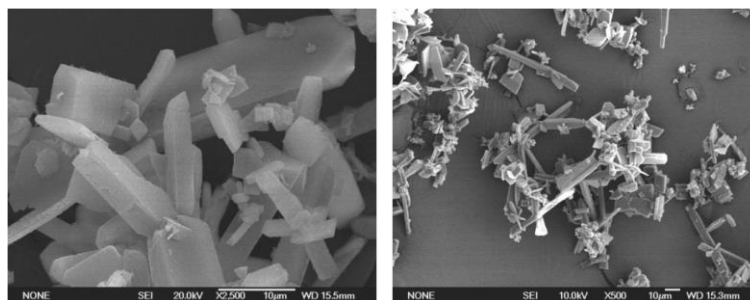


Fig. 5.30 SEM images of SAS processed 5-Fu-thiourea.

## 5.4.2 CSS co-crystallization

### PXRD characterization

The PXRD patterns of the samples obtained using the CSS technique were compared to the patterns of the co-crystal components to assess co-crystal formation (Fig. 5.31). We could observe that when the cosolvent was not used, co-crystal formation was not achieved and the powder obtained displayed the diffraction peaks of both coformers indicating that the powder was a physical mixture of them.

The PXRD pattern of the CSS powder obtained with methanol (Fig. 5.31) showed similar results and most diffraction peaks of the CSS powder were also present in the PXRD patterns of the co-crystal components indicating the presence of homocrystals of both thiourea and 5-Fu. Some new diffraction peaks were present though (peaks at  $2\theta$  17.4, 26.3 and 33.6) indicating the presence of a different phase.

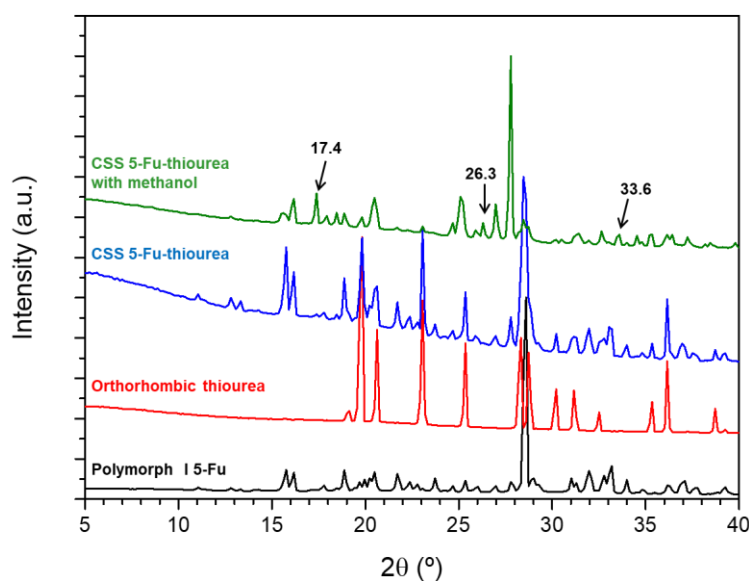


Fig. 5.31 PXRD patterns from top to bottom of: 5-Fu-thiourea CSS powder obtained with methanol, 5-Fu-thiourea CSS powder obtained without methanol, orthorhombic thiourea calculated from CIF, and 5-Fu polymorph I calculated from CIF.

When we compared the diffraction pattern with the patterns of the SAS precipitate and the co-crystal structure calculated from the CIF<sup>20</sup> (Fig. 5.32) we observed that these peaks are present in both patterns. This indicated that the third phase present in the powder was the same co-crystal form that had been obtained using the SAS technique.

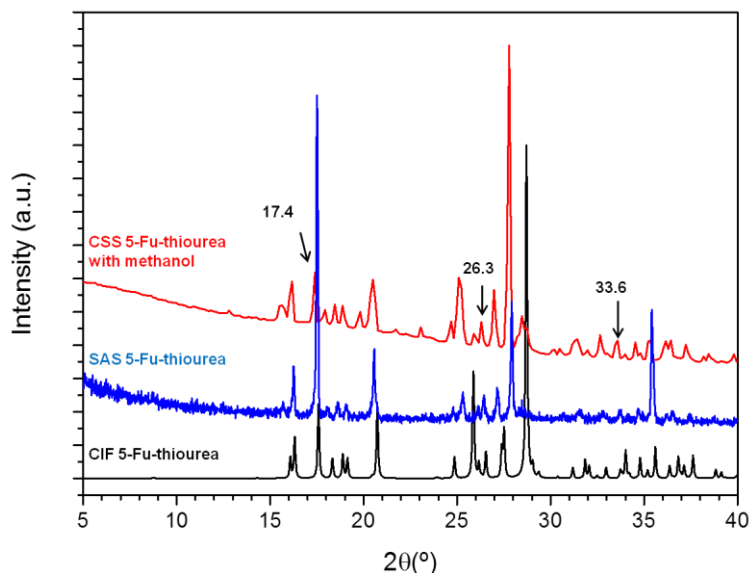


Fig. 5.32 PXRD patterns of the 5-Fu-thiourea co-crystal obtained through: CSS with methanol (top), SAS (middle), and calculated from CIF (bottom).

### Thermal characterization

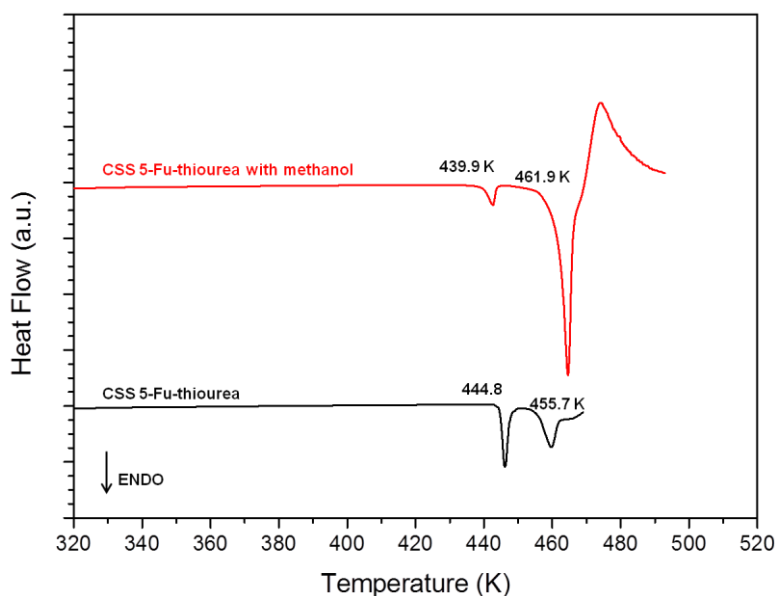


Fig. 5.33 DSC thermograms of: 5-Fu-thiourea powders obtained through CSS: with methanol (top), and without methanol (bottom). Heating rate 5 K/min.

The analysis of CSS samples using DSC confirmed the presence of thiourea homocrystals (endothermic peak around 440 K) in the powders of both CSS experiments. In Fig. 5.33 we could observe again how the presence of methanol enhanced the co-crystallization process and reduced therefore, the amount of thiourea homocrystals which translated in a reduction in the area of the first endothermic peak. In the experiment without methanol the thermogram obtained resembled that previously displayed for an equimolar physical mixture (Fig. 5.26). Therefore, this corroborated the findings obtained from the PXRD pattern confirming again that no co-crystallization was achieved in the absence of cosolvent. We could observe that the onset temperature of the first endothermic transition took place at temperatures lower than the melting onset temperature of pure thiourea suggesting a possible eutectic point in the phase diagram.

### FTIR characterization

FTIR spectra of the CSS samples were also analyzed and are presented in Fig. 5.34. Spectrum of the CSS sample produced without methanol showed the absorption bands of the 5-Fu-thiourea SAS precipitate in the  $\text{NH}_2$  stretching region ( $3387$  and  $3202\text{ cm}^{-1}$  in Fig. 5.28) at  $3386$  and  $3196\text{ cm}^{-1}$  but with less intensity. The thiourea  $\text{C}=\text{S}$  stretching band at  $2685\text{ cm}^{-1}$  also showed a displacement to  $2674\text{ cm}^{-1}$  and a reduction in its intensity and the stretching band at  $1405\text{ cm}^{-1}$  was seen as a shoulder at  $1396\text{ cm}^{-1}$ . In this case we observed no displacement in the 5-Fu  $\text{C}=\text{O}$  stretching that remained at  $1719\text{ cm}^{-1}$ .

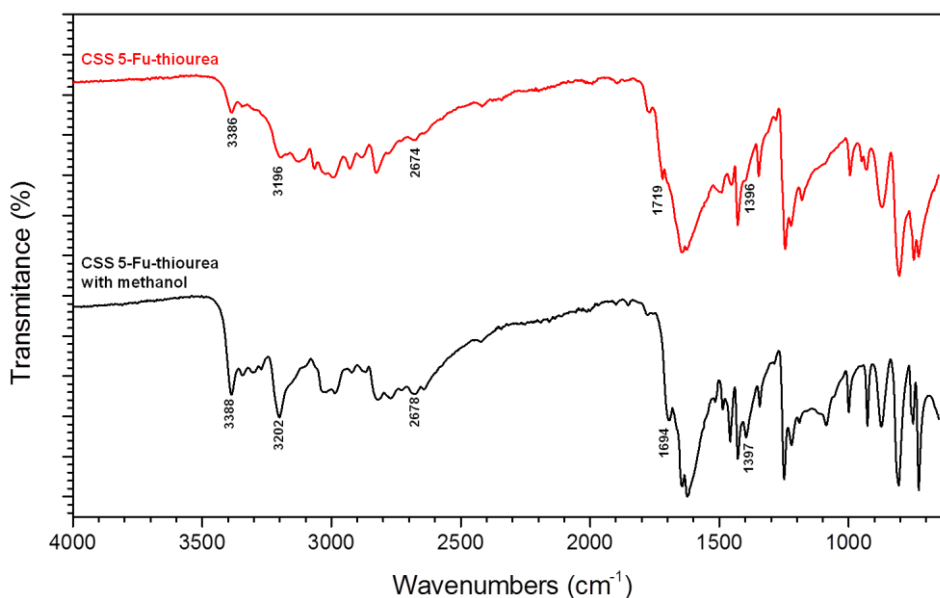


Fig. 5.34 FTIR spectra of: 5-Fu-thiourea powders obtained through CSS: without methanol (top), and with methanol (bottom).



The FTIR spectrum of the CSS experiment carried with methanol showed the same absorption bands with similar peak intensities than those of the 5-Fu-thiourea SAS precipitate in the  $\text{NH}_2$  stretching region (bands at  $3388$  and  $3202\text{ cm}^{-1}$ ). The thiourea  $\text{C}=\text{S}$  stretching absorption band at  $2685\text{ cm}^{-1}$  also presented a displacement to  $2678\text{ cm}^{-1}$  and reduction in its intensity. The other thiourea  $\text{C}=\text{S}$  absorption band at  $1405\text{ cm}^{-1}$  was displaced to  $1397\text{ cm}^{-1}$  and presented again a form and intensity similar to that of the 5-Fu-thiourea SAS precipitate. In this case, as in the 5-Fu-thiourea SAS precipitate, a displacement in the 5-Fu  $\text{C}=\text{O}$  stretching to  $1694\text{ cm}^{-1}$  was observed.

### SEM characterization

Images of CSS experiments (see Fig. 5.35) were similar to those previously obtained in the 5-Fu-urea co-crystallization. In the experiments carried out without methanol we found once again big particles of heterogeneous sizes whose morphology resembled those of both 5-Fu and thiourea with sizes ranging from  $200$  to  $400\text{ }\mu\text{m}$ . The surface of these particles was mostly smooth but we could see patches that were coated with a distinctive different morphology (smaller fragmented cubes ranging from  $10$  to  $25\text{ }\mu\text{m}$ ). When we used methanol in the experiment, the amount of fragmented cubes in the particle surface increased, suggesting again a higher interaction between both cofomers. CSS experiments did not lead to the substantial particle size reduction that was reached using the SAS technique.

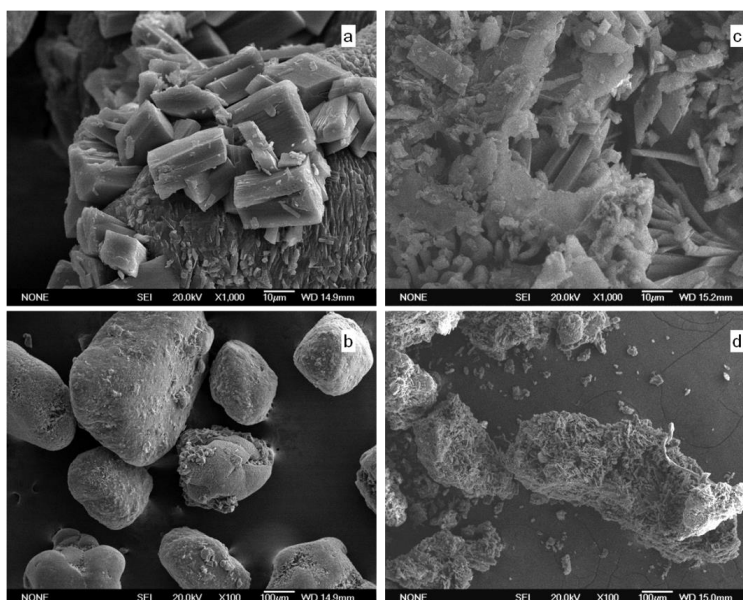


Fig. 5.35 SEM images of: 5-Fu-thiourea CSS powders obtained: without methanol (a,b), and with methanol (c,d).

As in the previous co-crystal, the low solubility of the cofomers at the experimental conditions seems to be the major limitation in the co-crystal formation via CSS.

## 5.5 5-Fu-ACRIDINE CO-CRYSTAL

### 5.5.1 SAS co-crystallization

Methanol was the solvent previously employed by Delori et al.<sup>17</sup> to obtain this co-crystal through slow evaporation. The molecular structure can be seen in Fig. 5.3 e.

The stoichiometry of the reported co-crystal between 5-Fluorouracil and acridine is 2:1<sup>17</sup>. Therefore, first SAS experiments were planned with this molar ratio and a 5 mg/mL concentration of 5-Fu. The experiments failed to form the co-crystal and the obtained powder seemed to be mainly 5-Fu. The suspected reason for this behaviour was the difference in solubility of both cofomers in supercritical CO<sub>2</sub>. The solubility of 5-Fu at the employed conditions (10.0 MPa and 313 K) is  $2.81 \times 10^{-6}$  mol 5-Fu/mol CO<sub>2</sub>,<sup>41</sup> while the solubility of acridine at similar conditions (10.2 MPa and 318 K) is  $1.18 \times 10^{-4}$  mol acridine/mol CO<sub>2</sub>,<sup>42</sup> a value around 100 times higher. Moreover, the solubility of acridine in CO<sub>2</sub> modified with methanol increases as it has been reported by van Alsten et al.<sup>61, 62</sup> A solubility of  $8.54 \times 10^{-4}$  mol acridine/ mol CO<sub>2</sub> at 10.4 MPa, 323 K and 3.9 mol % methanol has been reported by these authors. There are no solubility data for the system methanol-5-Fu-CO<sub>2</sub> but the solubility of 5-Fu in CO<sub>2</sub> is expected to increase with the addition of methanol. Solubility of 5-Fu in CO<sub>2</sub> modified with ethanol at 323 K, 10.0 MPa and 4% ethanol increased to  $2.5 \times 10^{-4}$  (mol 5-Fu/mol CO<sub>2</sub>).<sup>41</sup> For this reason SAS experiments were repeated with an acridine excess of two orders of magnitude.

### PXRD characterization

PXRD pattern of commercial acridine (Fig. 5.36) was coincident with that of the monoclinic form poly III. Although this form is stable at room temperature, increasing the temperature over 318 K will convert it to the most stable polymorph II.<sup>63, 64</sup>

Fig. 5.37 presents the PXRD pattern of the SAS experiment carried out with a 2:1 molar ratio of 5-Fu-acridine and it compares it to the diffraction patterns of the 5-Fu polymorph I and the reported crystal structure for the 5-Fu-acridine co-crystal.<sup>17</sup> In this figure we can clearly observe that the diffraction peaks associated to 5-Fu are present. Moreover, none of the characteristic diffraction peaks of acridine are present in the

diffraction pattern of the SAS precipitate, suggesting a complete solubilisation of acridine in the supercritical CO<sub>2</sub>-methanol mixture.

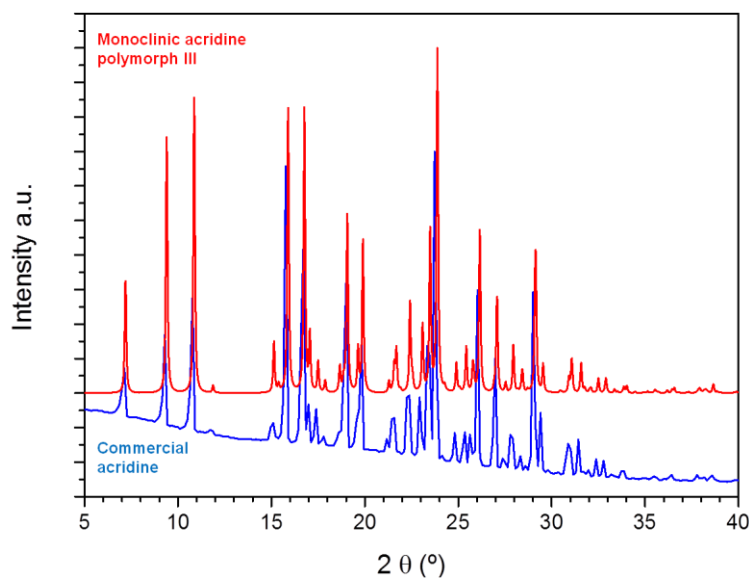


Fig. 5.36 PXRD patterns of: acridine polymorph III calculated from CIF (top), and commercial acridine (bottom).

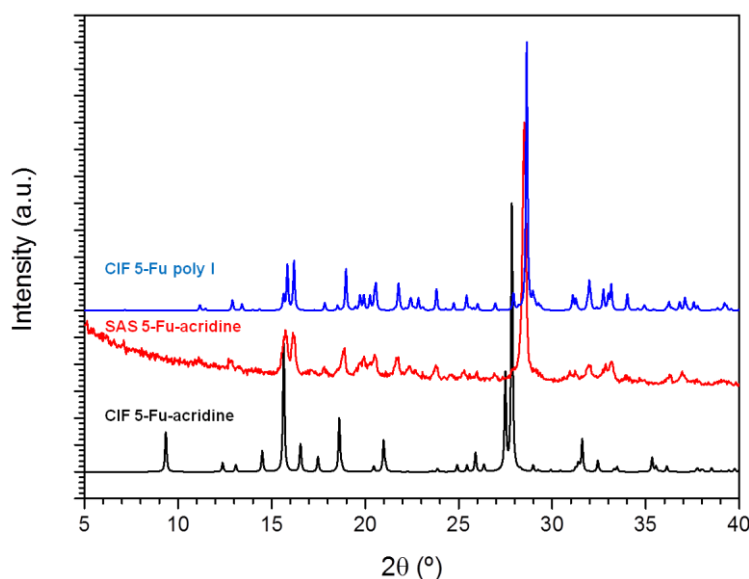


Fig. 5.37 PXRD patterns of: 5-Fu polymorph I calculated from CIF (top), and the co-crystal 5-Fu-acridine obtained: through SAS (middle), and calculated from CIF (bottom).

It seems that partial co-crystallization has been achieved in the experiment carried with an excess of acridine in the feeding solution (molar ratio 5-Fu to acridine of 1:13.4) and the PXRD pattern of the SAS precipitate displayed new diffraction peaks at  $2\theta$ : 9.4, 15.6, 18.6, 27.5 and 27.8 that match the main diffraction peaks of the published co-crystal structure<sup>17</sup>. Nevertheless, it also presented diffraction peaks at  $2\theta$  6.2, 9.7, 11.2 and 19.6 ° that do not match the calculated pattern obtained from the

published structure as it can be seen in Fig. 5.38. These peaks are not present either in the diffraction patterns of acridine polymorph II or III, nor in the diffraction pattern of 5-Fu polymorph I (Fig. 5.39). This seems to indicate that a different phase was present in the powder obtained in this experiment.

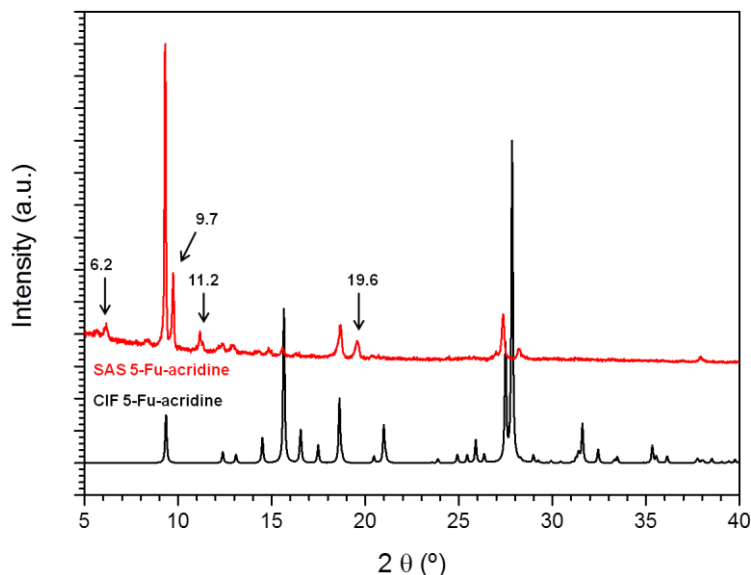


Fig. 5.38 PXRD patterns of the 5-Fu-acridine co-crystal obtained: through SAS with an excess of acridine (top), and calculated from CIF (bottom).

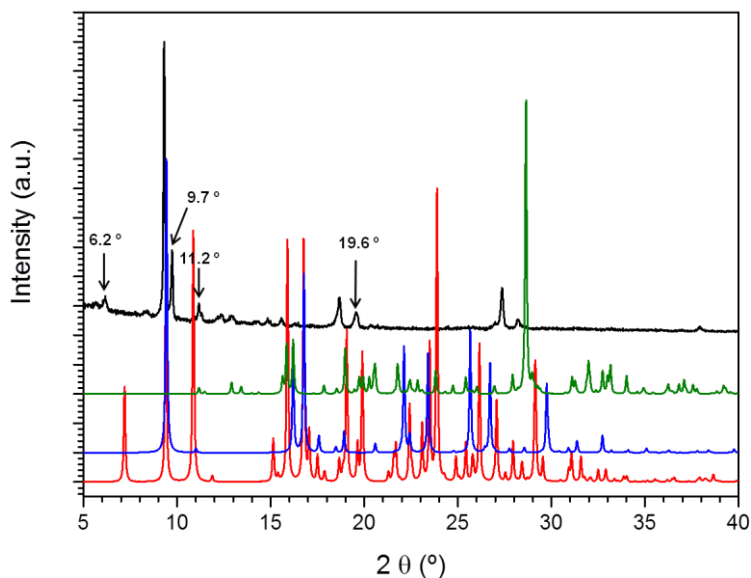


Fig. 5.39 PXRD patterns from top to bottom: 5-Fu-acridine powder obtained through SAS with an excess of acridine, 5-Fu polymorph I calculated from CIF, acridine polymorph II calculated from CIF, and acridine polymorph III calculated from CIF.

Attempts to precipitate acridine alone with a concentration in solution equal to that used in the experiment with an excess of this coformer (90 mg/mL) failed to produce any precipitate in the chamber and acridine was washed away and found in the liquid-gas separator. These results indicate that the SAS technique may not be

effective to produce co-crystals in compounds where the solubility difference in CO<sub>2</sub> is so large.

### Thermal characterization

DSC and TGA analyses of the SAS precipitate obtained with the co-crystal stoichiometric ratio 5-Fu-acridine 2:1 confirmed the PXRD results and no thermal event at the fusion temperature of acridine (379.8 K) could be found (Fig. 5.40). The melting peak of the SAS sample is wider in comparison to that of commercial 5-Fu and has an onset at lower temperature suggesting less purity in the sample. In a material with only a small amount of impurity (that dissolves in the melt, but not in the solid) the melting point is usually depressed and the melting range is broadened.

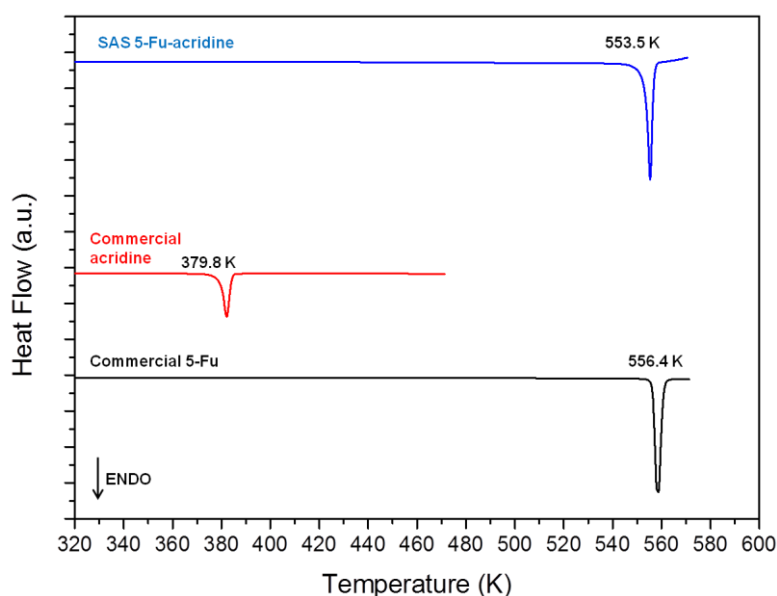


Fig. 5.40 DSC thermograms of: SAS processed 5-Fu-acridine (top), commercial acridine (middle), and commercial 5-Fu (bottom). Heating rate 5 K/min.

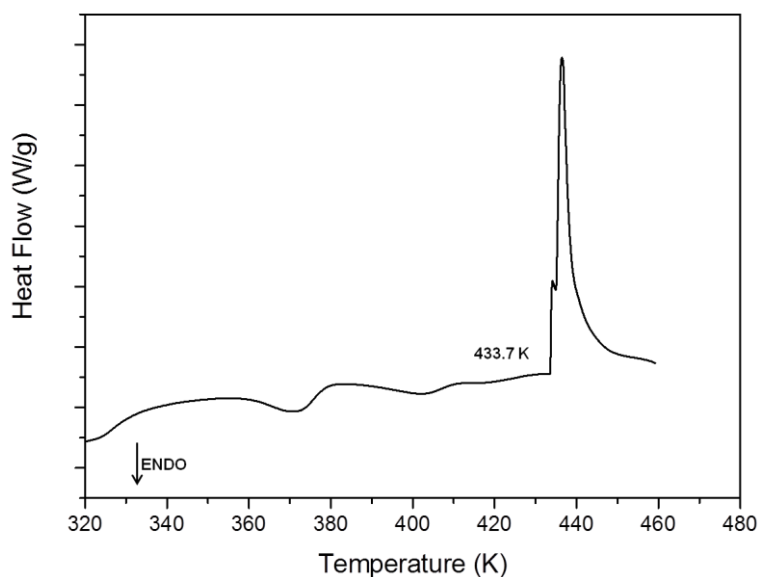


Fig. 5.41 DSC thermogram of SAS processed 5-Fu-acridine with an excess of acridine. Heating rate 5 K/min.

The DSC analysis of the SAS precipitate obtained with an excess of acridine (Fig. 5.41) displayed a sinuous base line and an exothermic peak with onset at 433.7 K. This is a temperature similar to the onset temperature of mass loss in the TGA (432.9 K) and corresponds to a temperature lower than the experimental mass loss onset of commercial acridine (455.0 K) or commercial 5-Fu (556.4 K). This suggests (as the PXRD findings showed) the presence of a different phase in the precipitate.

### FTIR characterization

FTIR spectrum of commercial acridine and the assignment of the main absorption bands<sup>65, 66</sup> are detailed in Fig. 5.42 and Table 5.7.

**Table 5.7 Infrared peaks (cm<sup>-1</sup>) of commercial acridine and their assignments :  $\nu$  stretching;  $\delta$  bending;  $\nu$  torsion;  $\omega$  wagging;  $\tau$  twisting;  $\rho$  rocking.**

Experimental IR wavenumbers (cm <sup>-1</sup> )	Band assignment	Experimental IR wavenumbers (cm <sup>-1</sup> )	Band assignment
3052	$\nu$ (C-H)	911	$\delta$ (C-H)
1513	$\nu$ (C-N-C)	859	$\delta$ (C-H)
1401	$\rho$ (C-N-C)	814	$\nu$ (C-C)
958	$\delta$ (C-H)	732	$\delta$ (C-H)

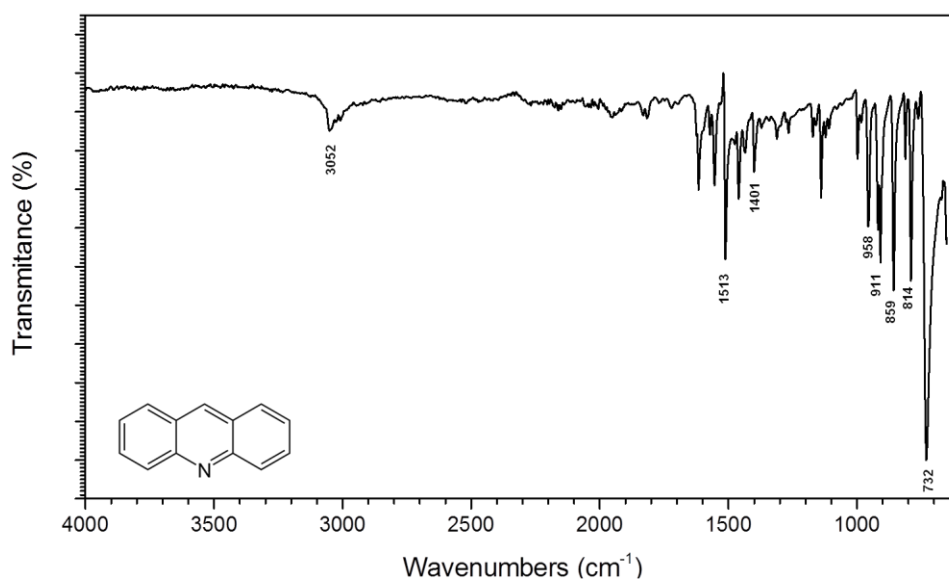


**Fig. 5.42 FTIR spectrum of acridine.**

The FTIR spectrum of the SAS precipitate performed with a 2:1 5-Fu-acridine molar ratio (Fig. 5.43) displayed the same absorption peaks as the FTIR spectrum of commercial 5-Fu, confirming therefore that no acridine was present in the precipitate, in agreement with the other characterization techniques.

The FTIR spectrum of the precipitate obtained in the SAS experiment carried out with an excess of acridine showed displacement of several absorption bands. The absorption band of the NH stretching at  $3115\text{ cm}^{-1}$  in 5-Fu seemed to shift to  $3189\text{ cm}^{-1}$  what would confirm a different intermolecular bonding of this functional group.

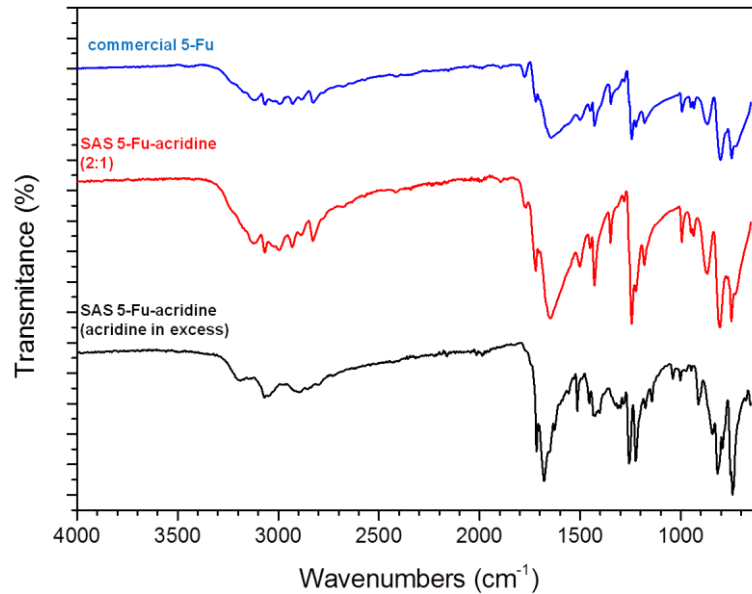


Fig. 5.43 FTIR spectra of: commercial 5-Fu (top), SAS processed 5-Fu-acridine in a 2:1 molar ratio (middle) and SAS processed 5-Fu-acridine with an excess of acridine (bottom).

### SEM characterization

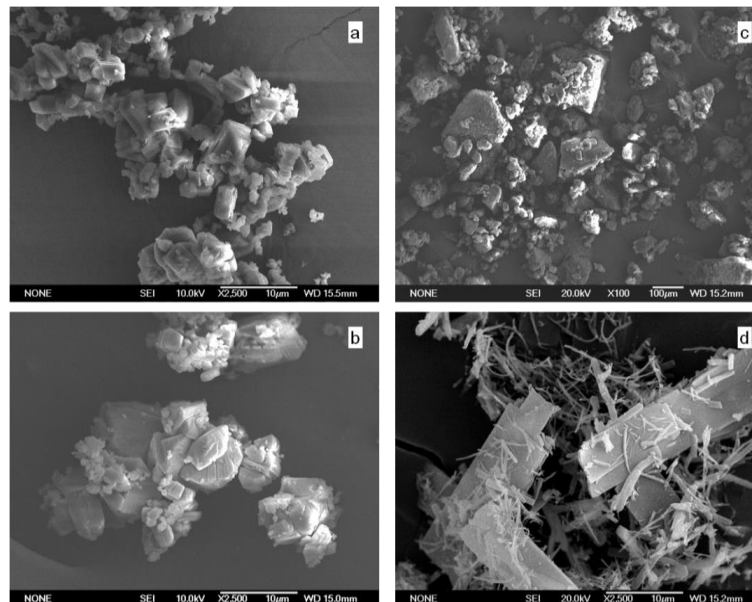


Fig. 5.44 SEM images of: SAS processed 5-Fu (a), SAS processed 5-Fu-acridine in a 2:1 molar ratio (b), commercial acridine (c), and SAS processed 5-Fu-acridine with an excess of acridine (d).

Comparison of the SEM images of the different samples led to the same conclusions that the other characterization techniques. In Fig. 5.44 we can see that the powder obtained from the SAS experiment carried out with the 2:1 molar ratio of the co-crystal presented the same morphology as SAS precipitated 5-Fu (prismatic morphology with sizes ranging 0.5 to 5  $\mu\text{m}$ ). The precipitate obtained in the SAS experiments carried out with an excess of acridine presented however a different morphology than that of commercial acridine (heterogeneous blocks from 50 to 300  $\mu\text{m}$ ) and SAS processed 5-Fu. We could observe agglomeration of thin rectangular plates of 0.2  $\mu\text{m}$  thickness, which are 3 to 7  $\mu\text{m}$  wide and 8 to 30  $\mu\text{m}$  long, surrounded by thin nano fibres.

### 5.5.2 CSS co-crystallization

Due to the larger solubility of acridine in supercritical  $\text{CO}_2$ , CSS may be a suitable technique for co-crystal formation.

#### PXRD characterization

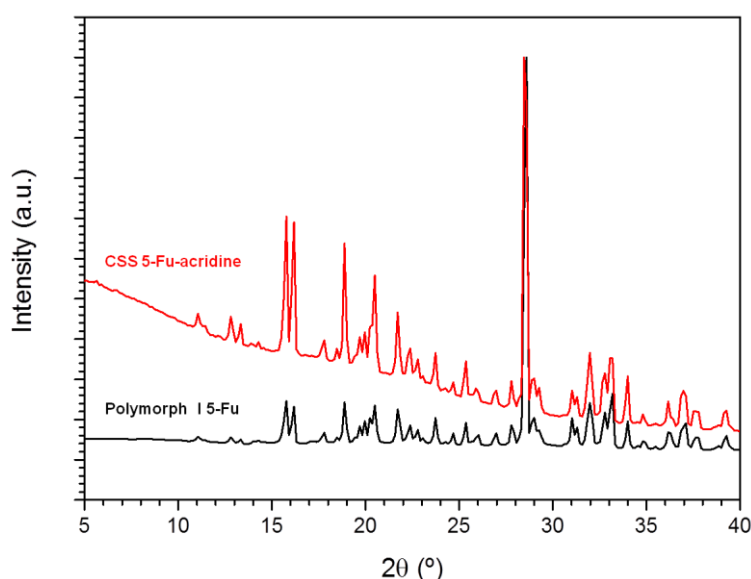


Fig. 5.45 PXRD patterns of: 5-Fu-acridine powder obtained through CSS without methanol (top), and 5-Fu polymorph I calculated from CIF (bottom).

The PXRD pattern of the CSS powders processed without methanol (Fig. 5.45) exhibited only the diffraction peaks of 5-Fu. The behaviour of acridine was therefore similar to the one previously observed in the SAS experiments: acridine seemed to have completely solubilized in supercritical  $\text{CO}_2$  and washed away during depressurization.

The PXRD pattern of the CSS powders processed with methanol (Fig. 5.46) exhibited the diffraction peaks that are present in the co-crystal solved structure



indicating that this phase might be present in the precipitate.<sup>17</sup> The PXRD pattern showed as well diffraction peaks that indicated the presence of 5-Fu homocrystals in the sample.

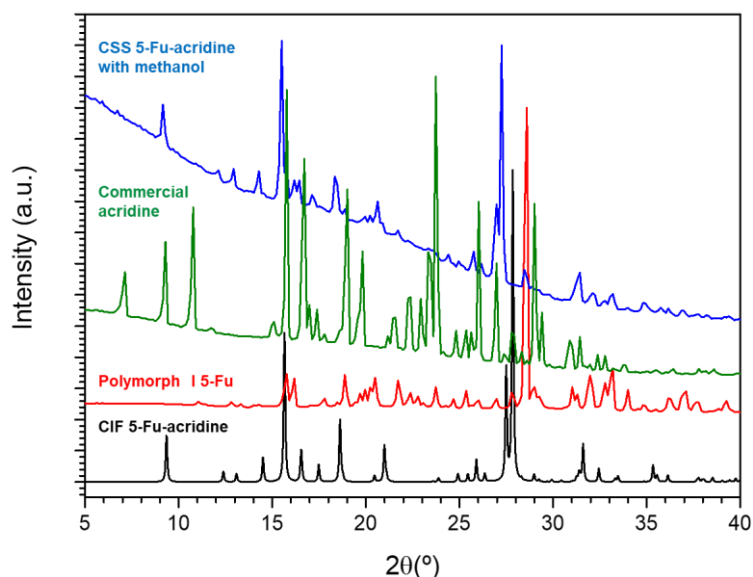


Fig. 5.46 PXRD patterns from top to bottom of: 5-Fu-acridine powder obtained through CSS with methanol, commercial acridine, 5-Fu polymorph I calculated from CIF, and 5-Fu-acridine co-crystal calculated from CIF.

## Thermal characterization

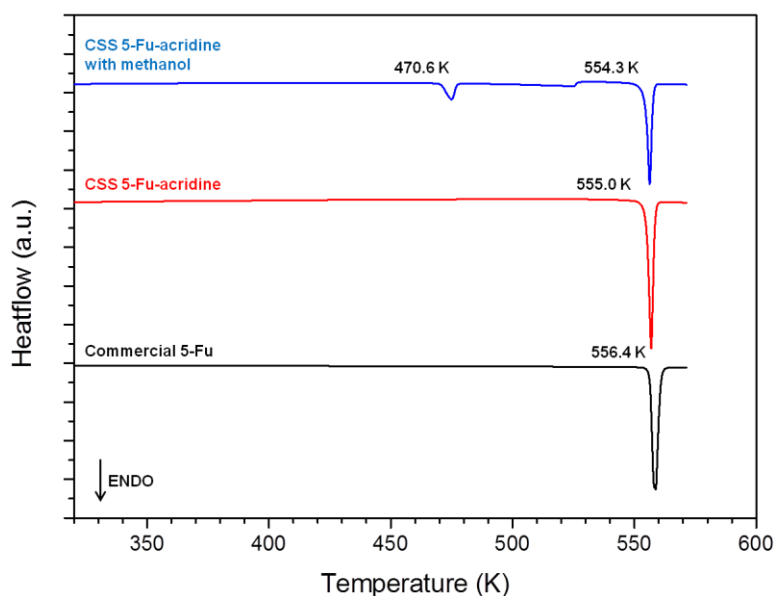


Fig. 5.47 DSC thermograms of: 5-Fu-acridine powder obtained through CSS with methanol (top), 5-Fu-acridine powder obtained through CSS without methanol (middle), and commercial 5-Fu (bottom). Heating rate 5 K/min.

DSC analysis of the CSS samples confirmed the previous PXRD findings. The DSC thermogram of the powder obtained without methanol (Fig. 5.47) presented a

single endothermic peak with a similar onset as that of pure 5-Fu. The fact that no previous thermal event was found for either an eutectic point or the melting and co-crystallization of free acridine indicated that the sample consisted of 5-Fu only.

The DSC analysis of the CSS powder obtained with methanol presented two peaks. Both peaks were above the melting point of acridine (379.8 K). A peak at 554.3 K seemed to correspond to the presence of 5-Fu and a first peak with an onset at 470.6 would probably correspond to the new phase observed in the PXRD pattern of the sample (see Fig. 5.46). These temperature values did not match the two endothermic transitions with onsets at 480.6 and 535.8 K reported by Delori et al.<sup>17</sup> for this co-crystal.

### FTIR characterization

The FTIR spectrum of the powders obtained without cosolvent (Fig. 5.48) showed the same absorption bands as those displayed by commercial 5-Fu confirming the complete solubilisation of acridine in supercritical CO<sub>2</sub>. The experiment carried out with methanol showed a FTIR spectrum similar to the one obtained for the SAS precipitate obtained with an excess of acridine (Fig. 5.49). The major difference was the absorption band at 1313 cm<sup>-1</sup> that did not appear in the CSS powder but was present in the SAS precipitate and found as a weak band in commercial acridine. Another distinctive band appeared at 1040 cm<sup>-1</sup>. This band was present in the CSS powder but not in the SAS precipitate or coformers FTIR spectra.

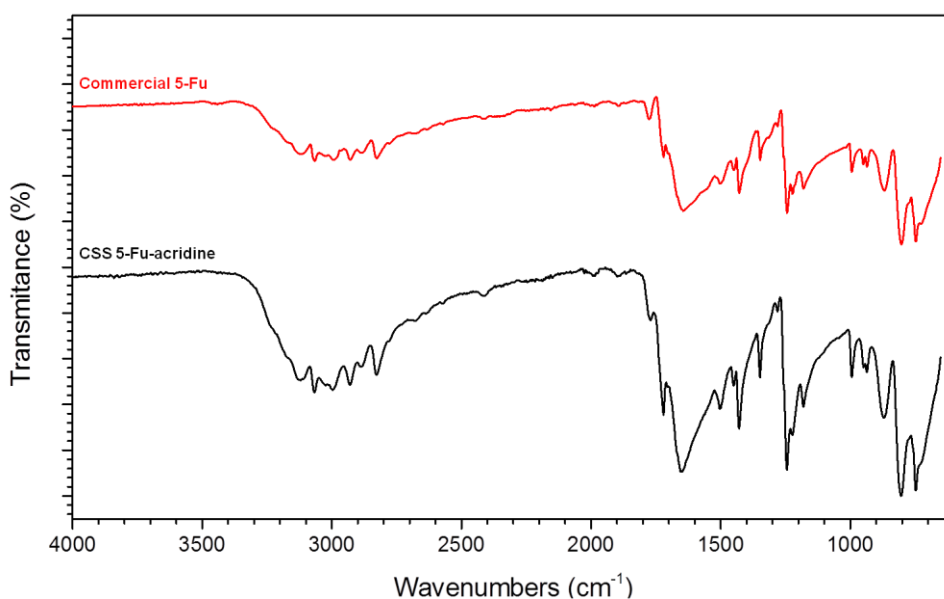


Fig. 5.48 FTIR spectra of: commercial 5-Fu (top) and 5-Fu-acridine powder obtained through CSS without methanol.

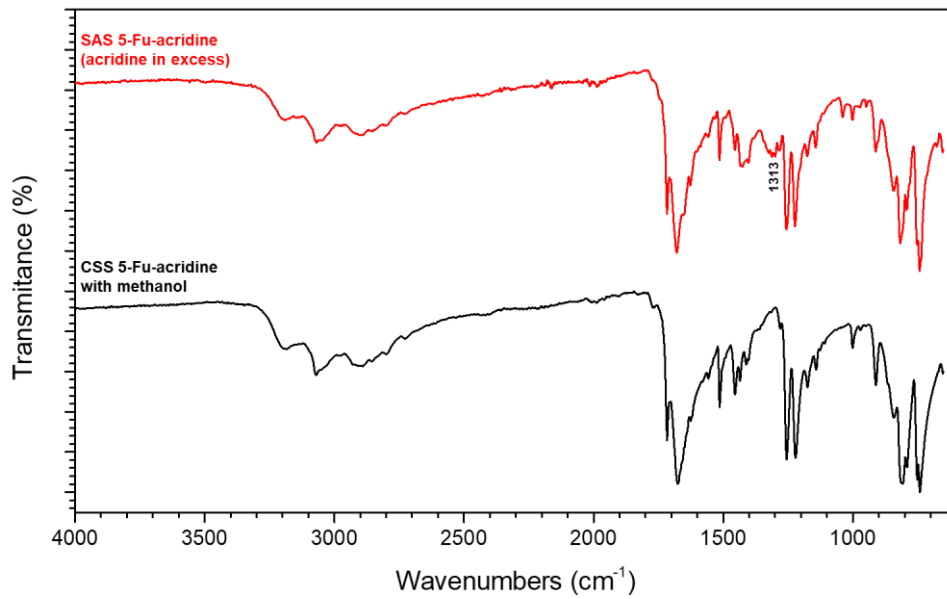


Fig. 5.49 FTIR spectra of 5-Fu-acridine powders: SAS processed with an excess of acridine (top) and CSS processed with methanol (bottom).

### SEM characterization

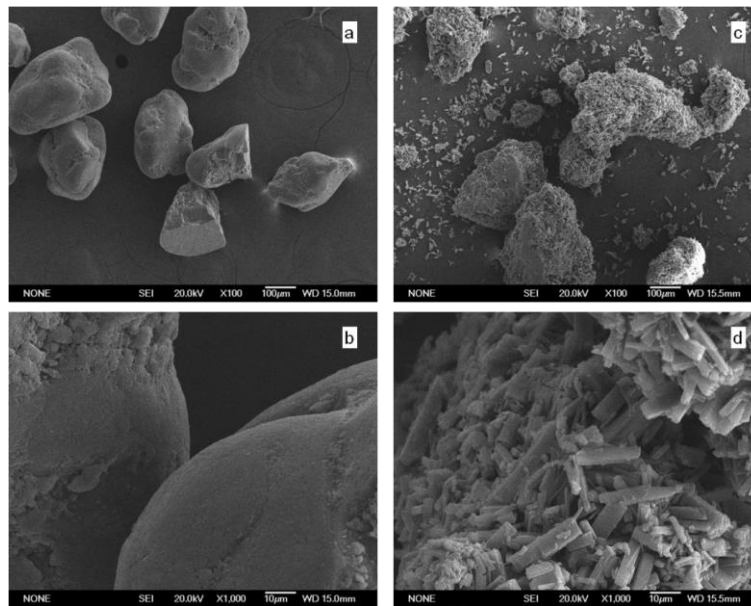


Fig. 5.50 SEM images of CSS 5-Fu-acridine powders processed: without methanol (a,b) and with methanol (c,d).

The SEM images of the CSS samples (Fig. 5.50) showed a similar behaviour as the one observed until now. The experiment conducted without methanol produced particles of smooth surface and heterogeneous sizes ranging from 150 to 350  $\mu\text{m}$ . The particles in the experiments carried out with methanol presented a rough surface. This surface consisted of thin rectangular particles approximately 1  $\mu\text{m}$  thick, 4 to 5  $\mu\text{m}$  wide and 7 to 20  $\mu\text{m}$  long. These rectangular particles were then attached to larger particles

that, as in the experiment conducted without methanol, presented heterogeneous sizes ranging from 150 to 350  $\mu\text{m}$ . The larger particles would probably correspond to 5-Fu.

## 5.6 5-Fu-4HBA CO-CRYSTAL

### 5.6.1 SAS co-crystallization

This co-crystal has been previously produced by Song Li et al.<sup>18</sup> and presents two different polymorphs. Polymorph I (Fig. 5.3 c) was produced using two different methodologies:

- An equimolar mixture of 5-Fu and 4HBA with water was stirred during 24 hours (at room temperature or 323 K). Suspension was filtered and the filtrate was dried under vacuum for 24 hours or left to evaporate slowly.
- An equimolar mixture of 5-Fu and 4HBA was grinded during 30 min with the addition of some drops of water.

The authors also investigated two different methodologies for the production of polymorph II (Fig. 5.3 d):

- An equimolar mixture of 5-Fu and 4HBA was dissolved in water and stirred at 338 K. The solution was filtered immediately, rapid cooled to room temperature and then left 24 hours to dry.
- An equimolar mixture of 5-Fu and 4HBA was grinded during 30 min with the addition of some drops of tetrahydrofuran (THF).

Although water was the solvent used by these authors to obtain the co-crystals of 5-Fu-4HBA, the SAS experiments were carried out in methanol because water is not soluble in supercritical  $\text{CO}_2$  and is therefore non-compatible with the SAS technique. Following the same criteria as in the previous SAS co-crystallization experiments the concentration of 5-Fu in the solution was kept to 5 mg/mL and an equimolar amount of 4HBA was added. Pressure was set to 10.0 MPa, temperature to 313 K, dissolution flow at 1 mL/min and  $\text{CO}_2$  flow at 20 g/min.

The 5-Fu-4HBA co-crystallization showed characteristics similar to those of the 5-Fu-acridine (the amount of 4HBA in the precipitate was smaller than the expected). Values for the solubility of 4HBA in supercritical  $\text{CO}_2$  have been reported by different authors<sup>44, 67, 68</sup> and at similar operational conditions (10.1 MPa and 318 K) the solubility is  $4.52 \times 10^{-7}$  (mol 4HBA/mol  $\text{CO}_2$ ).<sup>44</sup> This value is even smaller than that reported for 5-Fu in supercritical  $\text{CO}_2$  at similar conditions:  $2.81 \times 10^{-6}$  (mol 5-Fu/mol  $\text{CO}_2$ )<sup>41</sup>. There are no data of the solubility enhancement of 4HBA in supercritical  $\text{CO}_2$  modified with

methanol. However, the solubility of their ortho and meta isomers in supercritical CO<sub>2</sub> modified with acetone and methanol has been reported by Gurdial et al,<sup>69</sup> showing a considerable solubility increase.

The solubility of 4HBA at conditions similar to the operational ones was measured using a viewing cell. The resulting solubility value at 313 K, 15.0 MPa and 5% mol fraction of methanol was of  $5.7 \times 10^{-4}$  (mol 4HBA/mol CO<sub>2</sub>). This solubility value is similar to the value of  $3.49 \times 10^{-4}$  (mol 5-Fu/mol CO<sub>2</sub>) reported for 5-Fu at 313 K, 15.0 MPa and 4% mol fraction of ethanol.<sup>41</sup> However, when 5-Fu and 4HBA were precipitated separately the yield of the 5-Fu precipitation was 3 folds higher than that of 4HBA, which indicates that other factors apart from solubility in the CO<sub>2</sub>-solvent mixture need to be considered in SAS precipitation. In order to favour 4HBA precipitation an additional experiment was repeated with a 1:3 5-Fu to 4HBA molar ratio.

### PXRD characterization

The PXRD pattern of commercial 4HBA matched the one of the monoclinic polymorph I.<sup>70</sup> No change to polymorph II<sup>71</sup> was observed after SAS processing at 313 K and 10.0 MPa (Fig. 5.51). The SAS precipitate pattern showed a marked preferred orientation at  $2\theta$  17.6 ° corresponding to the plane (110).

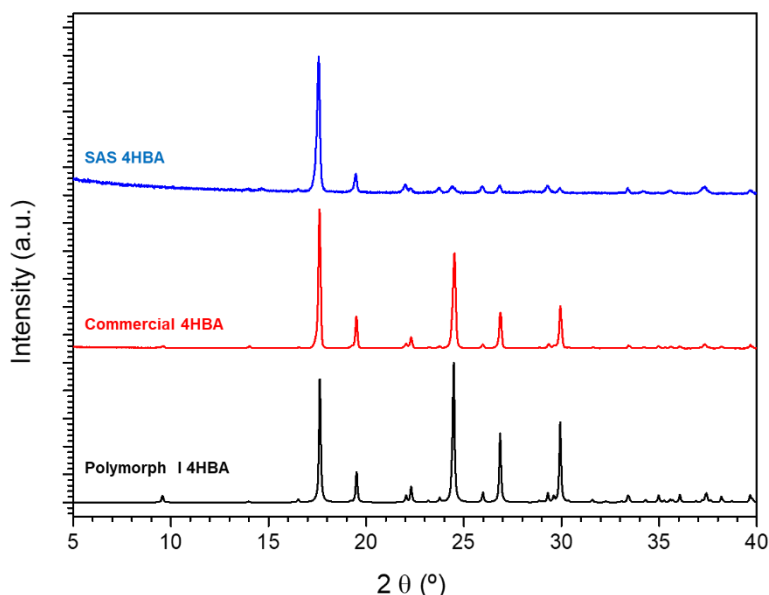


Fig. 5.51 PXRD patterns of: SAS processed 4HBA (top), commercial 4HBA (middle), and 4HBA polymorph I calculated from CIF (bottom).

The precipitate obtained from the SAS experiment with an equimolar ratio displayed a diffraction pattern that did not fully match the patterns of the co-crystal

components (see Fig. 5.52) nor the diffraction patterns of the two reported polymorphs of this co-crystal<sup>18</sup> (see Fig. 5.53). Although the position of most diffraction peaks of the SAS precipitate were coincident with the diffraction patterns of either polymorph I or II of the co-crystal (with different relative intensities) suggesting a possible mixture of both polymorphs in the precipitate, we also found other diffraction peaks at  $2\theta$ : 19.9, 22.3, 30.1, 35.2 and 37.2 ° that were not present. Therefore, the SAS precipitate seemed to be a complex mixture of different phases. Micro-elemental analysis of the powder revealed a nitrogen content of 14.8 % indicating a slight excess of 5-Fu in the sample (theoretical nitrogen content in a 1:1 co-crystal of 5-Fu-4HBA would be of 10.4%).

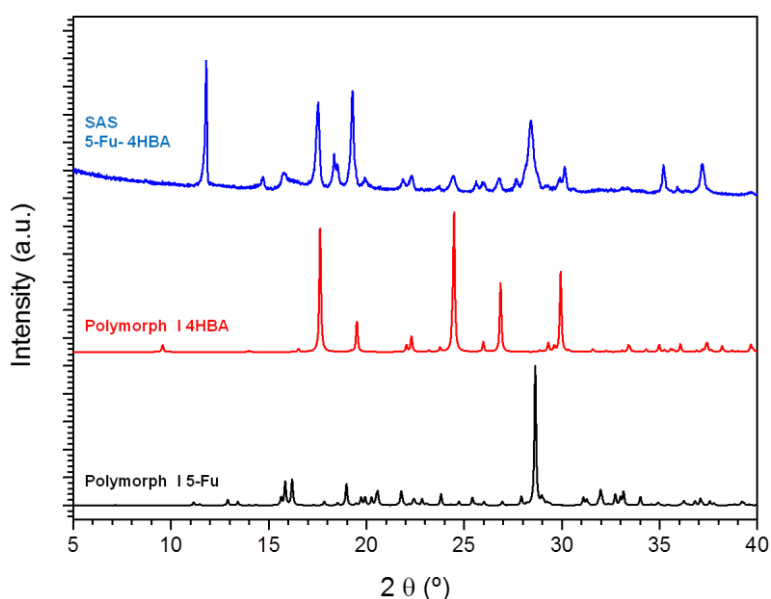


Fig. 5.52 PXRD patterns of: SAS processed 5-Fu-4HBA (top), 4HBA polymorph I calculated from CIF (middle) and 5-Fu polymorph I calculated from CIF (bottom).

PXRD pattern of the SAS precipitate from the experiment carried out with an excess of 4HBA (Fig. 5.54) showed clearly the presence of 4HBA polymorph I, and the most intense diffraction peaks of 4HBA polymorph I at  $2\theta$ : 17.7, 19.5, 24.5, 26.9 and 29.9 ° were present. We could also find diffraction peaks in the sample that were not assignable to any of the expected phases (the most intense at  $2\theta$  11.8 °) indicating again that the sample was a complex mixture of phases. Micro-elemental analysis of the sample confirmed an excess of 4HBA (85.6 % content in 4HBA instead of the theoretical 51.5 % for an equimolar co-crystal of 5-Fu-4HBA).

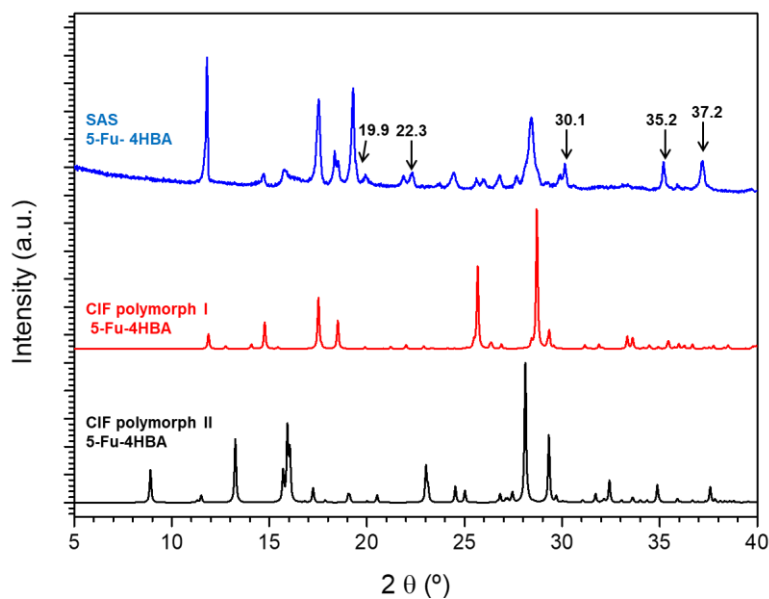


Fig. 5.53 PXRD patterns of: SAS processed 5-Fu-4HBA (top), 5-Fu-4HBA co-crystal polymorph I calculated from CIF (middle), and 5-Fu-4HBA co-crystal polymorph II calculated from CIF (bottom).

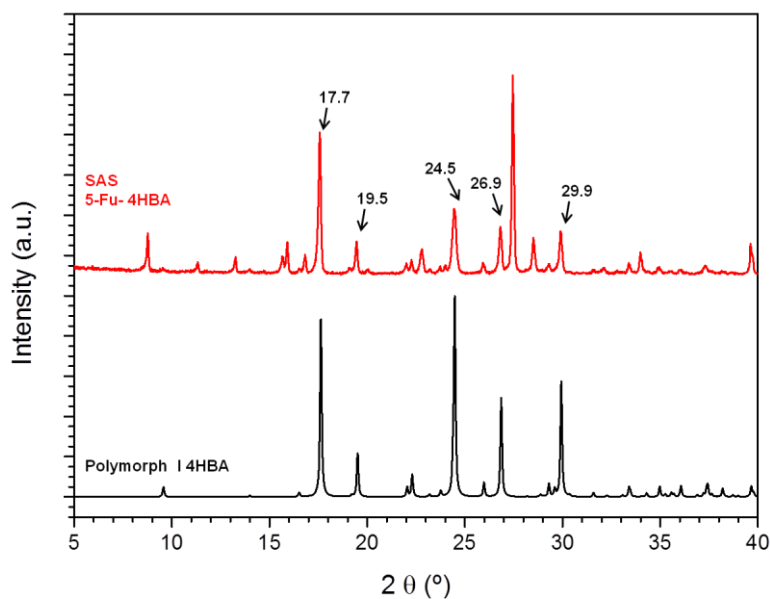


Fig. 5.54 PXRD patterns of: SAS processed 5-Fu-4HBA with an excess of 4HBA (top), and 4HBA polymorph I calculated from CIF (bottom).

## Thermal characterization

DSC thermograms of the SAS powders, commercial 5-Fu and 4HBA are presented in Fig. 5.55. The first endothermic event took place at 488.3 K in the 1:1 5-Fu-4HBA SAS precipitate and has a similar onset as the melting of commercial 4HBA (488.4 K). In the SAS experiment performed with an excess of 4HBA the first endothermic transition had an onset at ca. 475.0 K, lower than the melting point of 4HBA (488.4 K). The values for the fusion onset of both 5-Fu-4HBA co-crystal

polymorphs have not been reported, instead an approximate temperature at which mass loss started (around 452 K) was given<sup>18</sup> which corresponds to the 5-Fu-4HBA co-crystal decomposition.

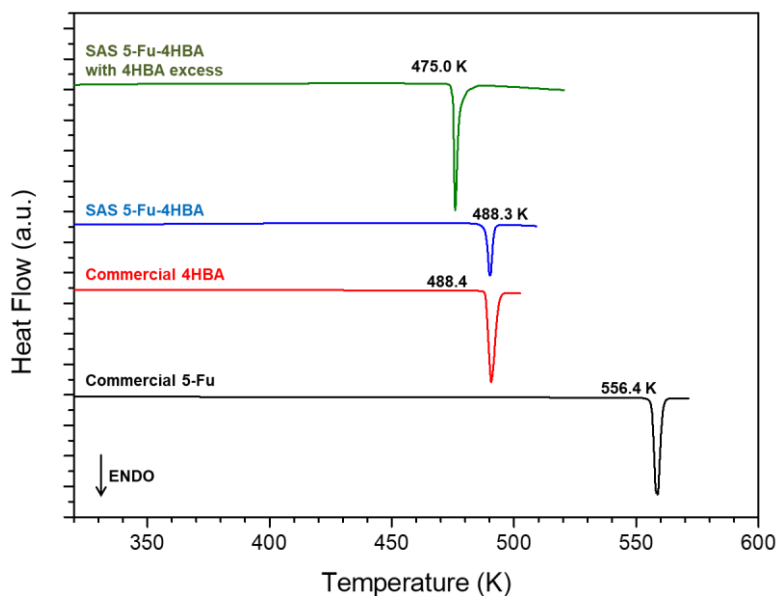


Fig. 5.55 DSC thermograms from top to bottom of: SAS 5-Fu-4HBA processed with an excess of 4HBA, SAS 5-Fu-4HBA processed with an equimolar ratio, commercial 4HBA, and commercial 5-Fu. Heating rate 5 K/min.

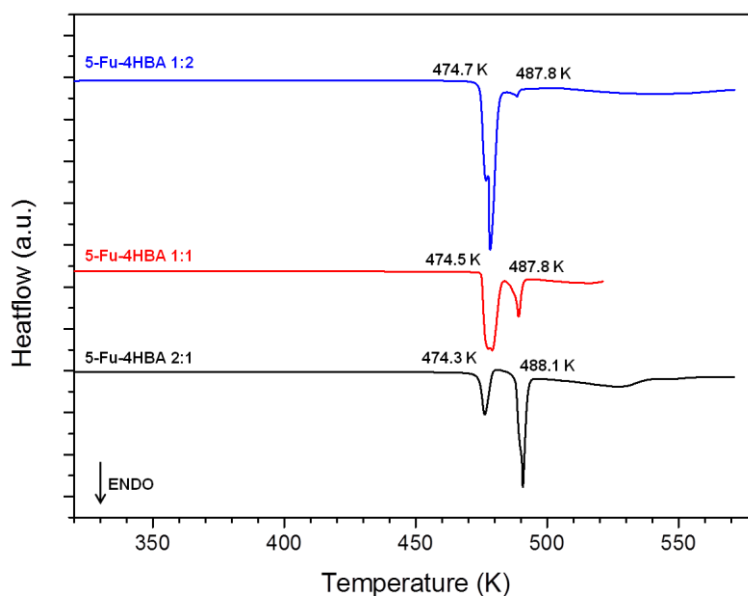


Fig. 5.56 DSC thermograms of 5-Fu-4HBA physical mixtures with molar ratios: 1:2 (top), 1:1 (middle), and 2:1 (bottom). Heating rate 5 K/min.

DSC thermograms of several physical mixtures of 5-Fu-4HBA (in a 1:1; 1:2 and 2:1 molar ratio) were also analysed (Fig. 5.56). In the three mixtures the onset of the first endothermic event (around 474 K in all cases) took place at a temperature lower



than the fusion of 4HBA, and afterwards peaks overlapped indicating several phase transitions (information beyond this point is not reliable due to decomposition of the sample). Most probably the first peak corresponded to the formation of an eutectic mixture followed by a fusion-decomposition event.

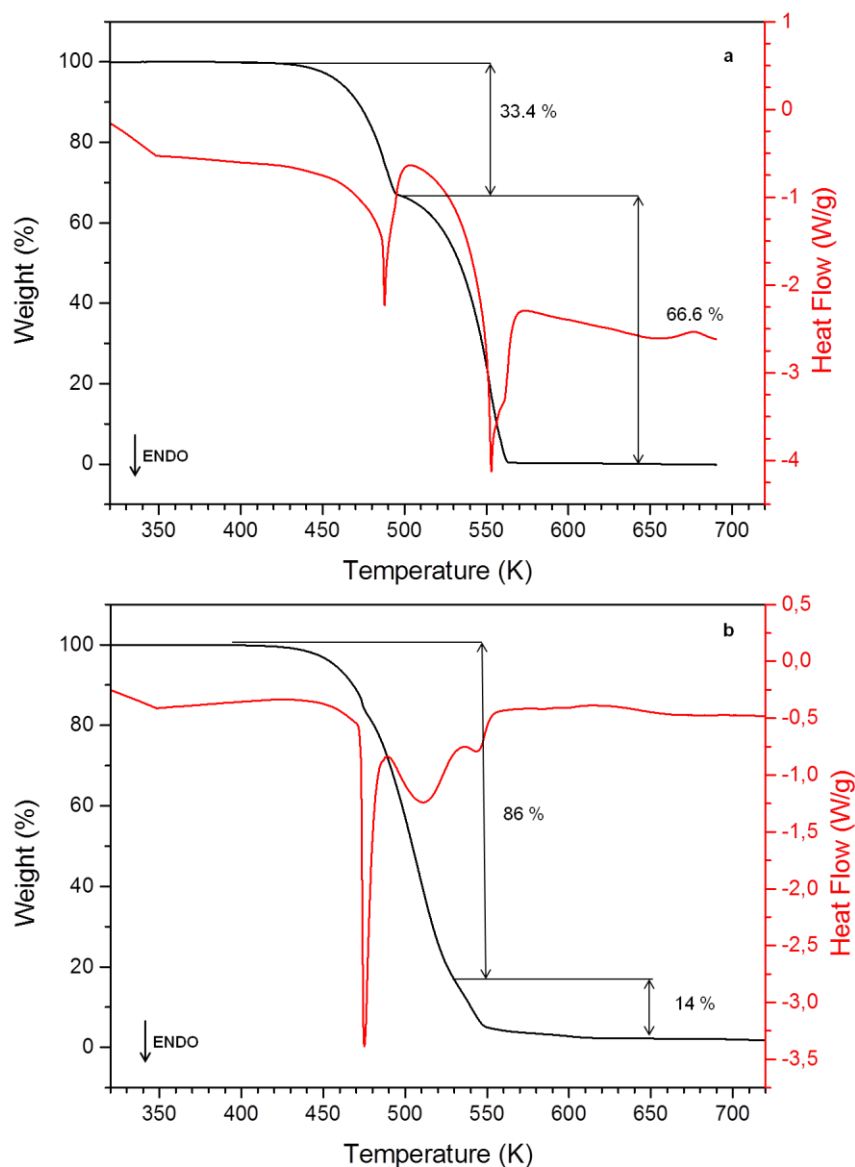


Fig. 5.57 TGA and DSC thermograms of SAS 5-Fu-4HBA processed: with an equimolar ratio (a), and with an excess of 4HBA (b). Heating rate 5 K/min.

TGA of the 1:1 5-Fu-4HBA SAS precipitate showed decomposition in two steps. A first step with onset at ca. 468.6 K representing a 33.4 % mass loss probably associated to the decomposition of 4HBA and a second step until complete decomposition which probably corresponded to the decomposition of 5-Fu (Fig. 5.57 a). These values do not match the theoretical content of 4HBA in a 5-Fu-4HBA 1:1 co-crystal that would be of 51.5 %. On the contrary, this percentage is

close to the 4HBA percentage obtained with micro-elemental analysis equal to 31.1 %, thus confirming an excess of 5-Fu. The endothermic transitions visible in Fig. 5.57 a and b that accompany the decomposition process took place close to the fusion temperatures of both coformers (488.4 and 556.4 K for 4HBA and 5-Fu, respectively). The TGA thermogram of the SAS powders obtained with an excess of 4HBA (Fig. 5.57 b) also showed decomposition in two steps. The first step had associated a 86% mass loss (in agreement with the 85.6% content of 4HBA in the sample obtained by micro-elemental analysis).

### FTIR characterization

The Infrared spectrum of 4HBA is shown in Fig. 5.58. Highlighted are the absorption bands of the functional groups that are more likely to shift in the formation of the co-crystal due to new synthon interaction. These bands would be the stretching vibration of the hydroxyl group at  $3357\text{ cm}^{-1}$  and the stretching vibration of the carboxyl group at  $1670\text{ cm}^{-1}$ .

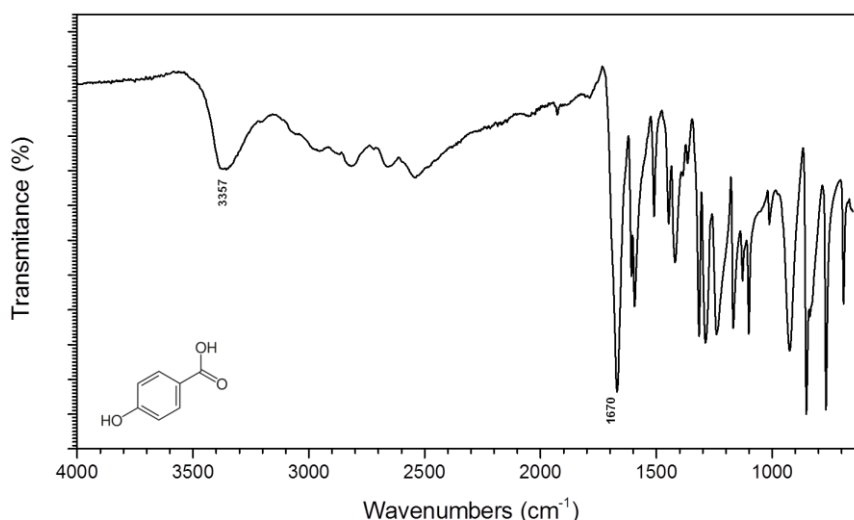


Fig. 5.58 FTIR spectrum of 4HBA.

FTIR spectra of the SAS samples (Fig. 5.59) showed a blue shift in the absorption band of the hydroxyl group of 4HBA from  $3357$  to  $3335\text{ cm}^{-1}$  in both samples. The carboxyl group absorption band at  $1670\text{ cm}^{-1}$  of 4HBA shifted to  $1655\text{ cm}^{-1}$  only in the experiment carried out with an equimolar ratio of coformers. The C=O absorption band of 5-Fu at  $1720\text{ cm}^{-1}$  showed a light shift to  $1713\text{ cm}^{-1}$  in both samples.

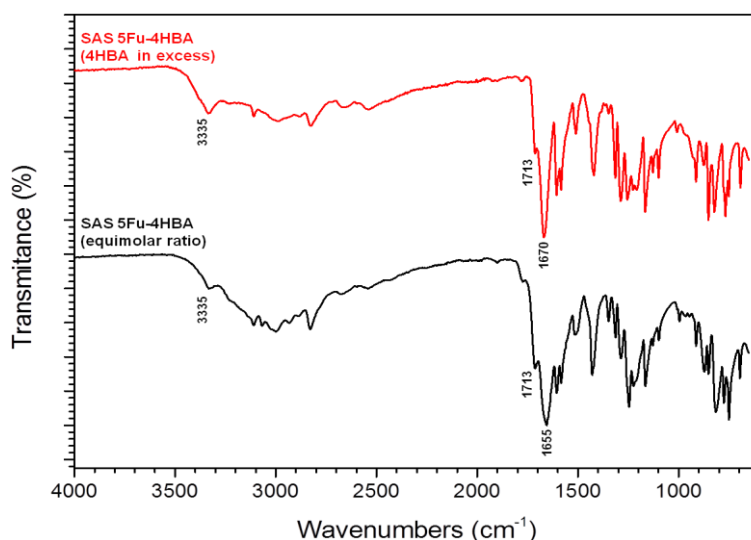


Fig. 5.59 FTIR spectra of : SAS 5-Fu-4HBA processed with an excess of 4HBA (top), and SAS 5-Fu-4HBA processed with an equimolar ratio (bottom).

### SEM characterization

SEM images of commercial and SAS processed 4HBA are shown in Fig. 5.60. Commercial 4HBA presented particles of rough surface with sizes ranging from 30 to 180  $\mu\text{m}$ . On the other hand, SAS processed 4HBA particles showed smooth surfaces and heterogeneous sizes (larger flat crystals of around 200  $\mu\text{m}$  surrounded by smaller fragmented parts ranging 15 to 30  $\mu\text{m}$ ).

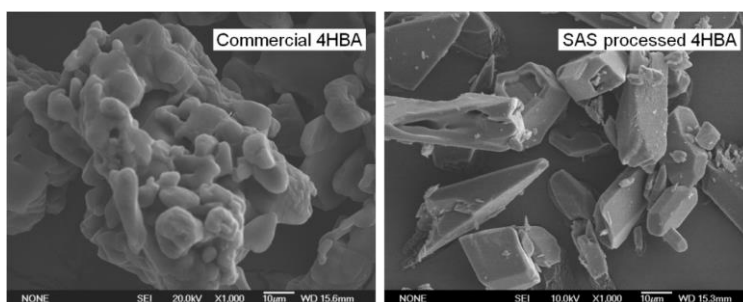


Fig. 5.60 SEM images of commercial and SAS processed 4HBA.

The SAS precipitates (Fig. 5.61) presented similar morphologies. In both precipitates (with an equimolar and with an excess of 4HBA, respectively) two different morphologies could be observed. A rectangular shape morphology with lengths from 10 to 40  $\mu\text{m}$  and widths from 2 to 6  $\mu\text{m}$ , and a second morphology of small agglomerates with a rough surface. This latter morphology was significantly less present in the SAS experiment carried out with an excess of 4HBA.

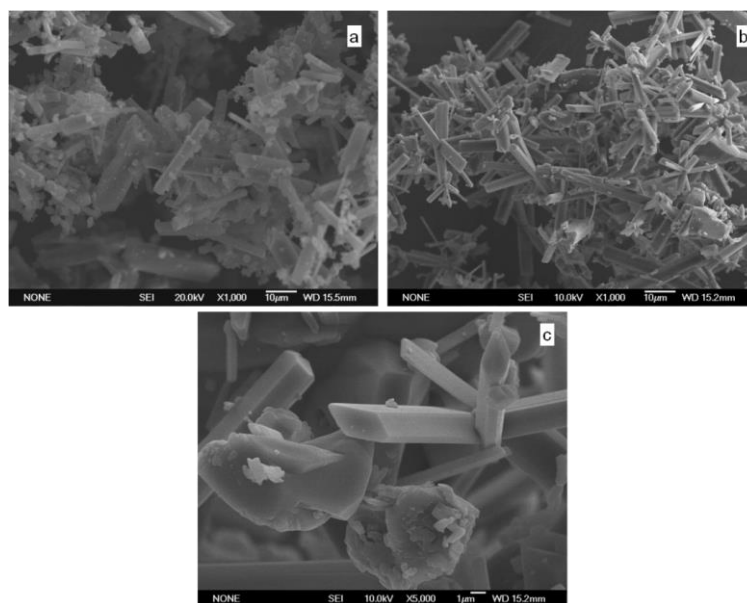


Fig. 5.61 SEM images of 5-Fu-4HBA SAS precipitates: processed with an equimolar ratio (a), processed with an excess of 4HBA (b), and an amplification of the latter to clearly identify both morphologies present (c).

## 5.6.2 CSS co-crystallization

### PXRD Characterization

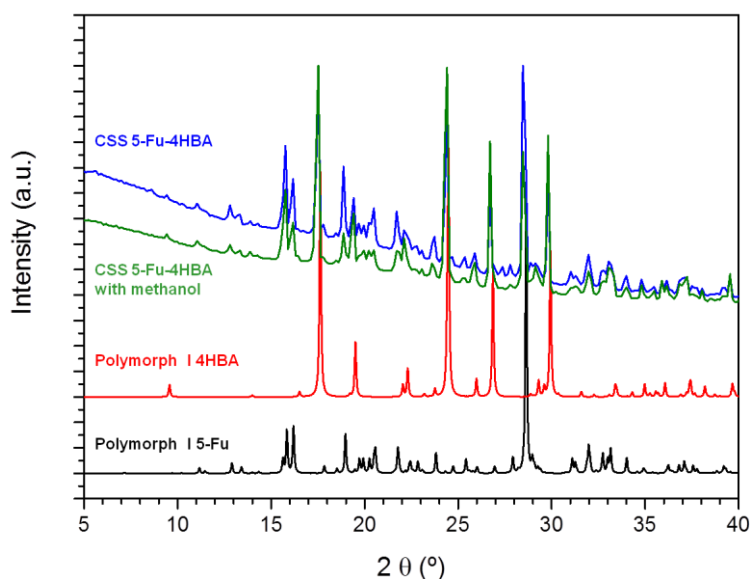


Fig. 5.62 PXRD patterns from top to bottom of: 5-Fu-4HBA powder obtained through CSS without methanol, 5-Fu-4HBA powder obtained through CSS with methanol, 4HBA (polymorph I) calculated from CIF, and 5-Fu (polymorph I) calculated from CIF.

PXRD patterns of the powders obtained through CSS with and without methanol were very similar (Fig. 5.62). Co-crystallization failed in both cases (clear sign was the lack of the diffraction peak at  $2\theta$  11.8°) and the diffraction pattern revealed a mixture of 5-Fu and 4HBA. In contrast to the PXRD patterns of the SAS precipitates, there were not unidentified peaks which suggested the presence of additional phases.

The very low solubility of both co-crystal components in supercritical CO<sub>2</sub> and CO<sub>2</sub> modified with methanol was the most probable reason for this outcome.

### Thermal characterization

The DSC thermograms of both CSS powders shown in Fig. 5.63 exhibited similar onsets for the endothermic transitions that could also be observed in the physical mixtures of 5-Fu-4HBA (see Fig. 5.56) thus confirming the PXRD findings.

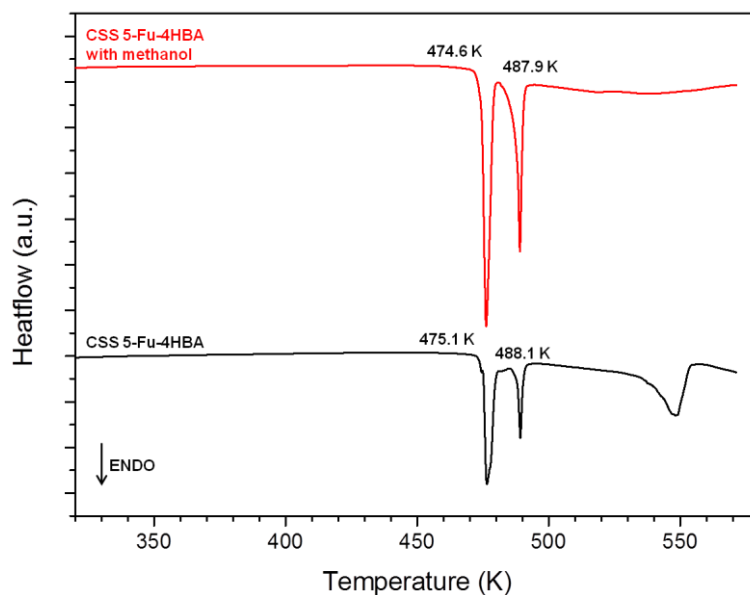


Fig. 5.63 DSC thermograms of 5-Fu-4HBA powders obtained through CSS: with methanol (top), and without methanol (bottom). Heating rate 5 K/min.

### FTIR Characterization

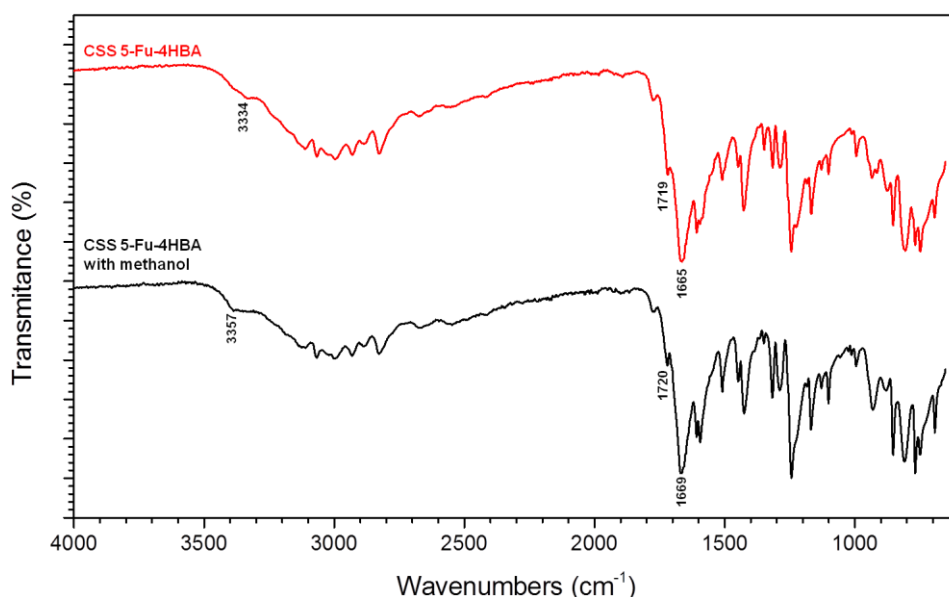


Fig. 5.64 FTIR spectra of: 5-Fu-4HBA powder obtained through CSS without methanol (top), and 5-Fu-4HBA powder obtained through CSS with methanol (bottom).

The FTIR spectra of the CSS powders (Fig. 5.64) showed that the 4HBA intense broad absorption band at  $3357\text{ cm}^{-1}$  for the stretching vibration of the hydroxyl group shifted to a shoulder at  $3387\text{ cm}^{-1}$  for the experiment carried out with methanol and to a shoulder at  $3334\text{ cm}^{-1}$  for the experiment without methanol. The absorption band of the C=O group in 5-Fu at  $1720\text{ cm}^{-1}$  did not show any significant displacement nor did the one at  $1670\text{ cm}^{-1}$  from the 4HBA. The interaction between both molecules was not shown in FTIR spectra.

### SEM characterization

SEM images of the CSS powders (Fig. 5.65) showed big particles of heterogeneous sizes ranging from  $340$  to  $750\text{ }\mu\text{m}$ . Surfaces in the CSS powders obtained without methanol were mostly smooth while in those powders obtained with methanol they were rough, thus indicating again a higher interaction between both cofomers when the cosolvent is used. However, in this sample co-crystal formation was not observed in the PXRD patterns.

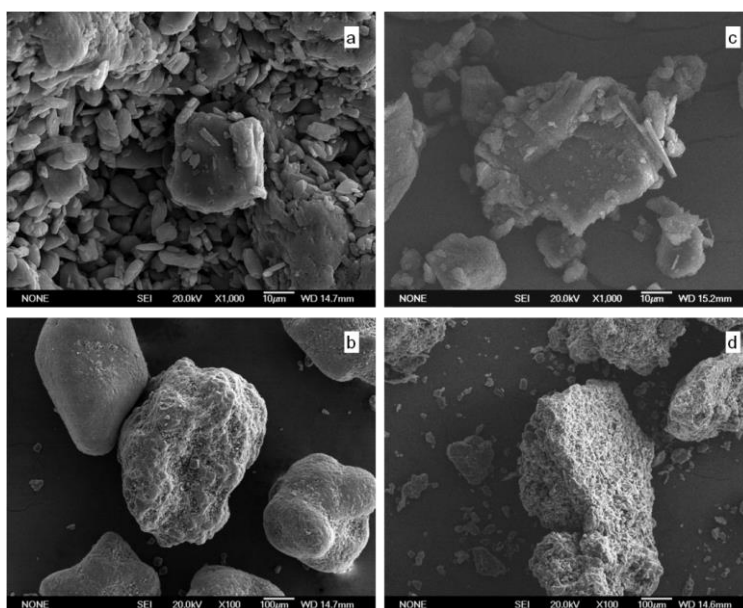


Fig. 5.65 SEM images of: 5-Fu-4HBA CSS powders processed: without methanol (a,b), and with methanol (c,d).

## 5.7 5-Fu-PZA CO-CRYSTAL

### 5.7.1 SAS co-crystallization

Attempts to produce a 2:1 5-Fu-PZA co-crystal via SAS failed: the precipitate collected after the experiments consisted only of 5-Fu. Experiments carried out only

with pyrazinamide also failed to produce any precipitate (precipitation was attempted in: methanol, ethanol, ethyl acetate, DCM and acetone). Due to the lack of solubility data of PZA in supercritical CO<sub>2</sub> observations in a view cell were made. No apparent solubilisation took place when a 9 mg/mL solution of PZA in methanol was introduced in the cell (molar fraction of CO<sub>2</sub> of 0.97). In fact as it can be observed in Fig. 5.66 precipitation of PZA immediately followed the introduction of CO<sub>2</sub> in the view cell. The lack of precipitate does not seem to be due to the solubilisation of PZA in the methanol-CO<sub>2</sub> system. In our laboratory we attempted to measure the solubility of PZA in supercritical CO<sub>2</sub> with no cosolvent at several temperatures (303 to 343 K) and pressures up to 25.0 MPa. Solubility was inferior to the measurement possibilities of our equipment and we could only state that it was less than to  $1.369 \times 10^{-4}$  (mol PZA/mol CO<sub>2</sub>). The lack of precipitate in the SAS precipitation chamber could be due to the precipitation of considerably small particles that will not be retained by the 2 µm frit. Further experimentation is still necessary to fully clarify this issue.

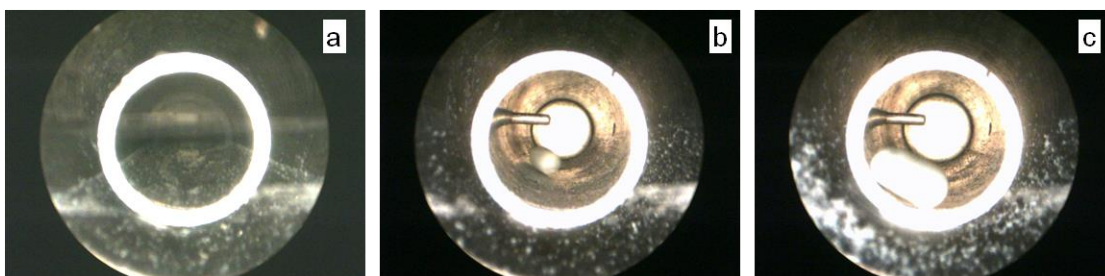


Fig. 5.66 Images of a 9 mg/mL PZA solution in methanol introduced in a view cell with a CO<sub>2</sub> molar fraction of 0.97 at: 5.0 MPa and 303 K (a); 7.7 MPa and 310 K (b); 10.0 MPa and 313 K (c).

## 5.7.2 CSS co-crystallization

### PXRD characterization

In Fig. 5.67 we can see that the PXRD pattern of commercial PZA is coincident with the diffraction pattern of the polymorph  $\alpha^{72}$ .

PXRD analysis revealed that co-crystallization failed in the CSS experiment carried out without methanol as the pattern presented the diffraction peaks of 5-Fu and  $\alpha$  PZA (Fig. 5.68). The PXRD pattern of the material prepared by CSS with methanol showed again the diffraction peaks of 5-Fu and  $\alpha$  PZA (revealing the presence of homocrystals of both components), and new diffraction peaks at  $2\theta$  14.8, 16.4 and 29.8 ° indicating the presence of a new phase (most probably the 5-Fu-PZA co-crystal). For this co-crystal there is no available CIF in the Cambridge Crystallographic Data Centre (CCDC).

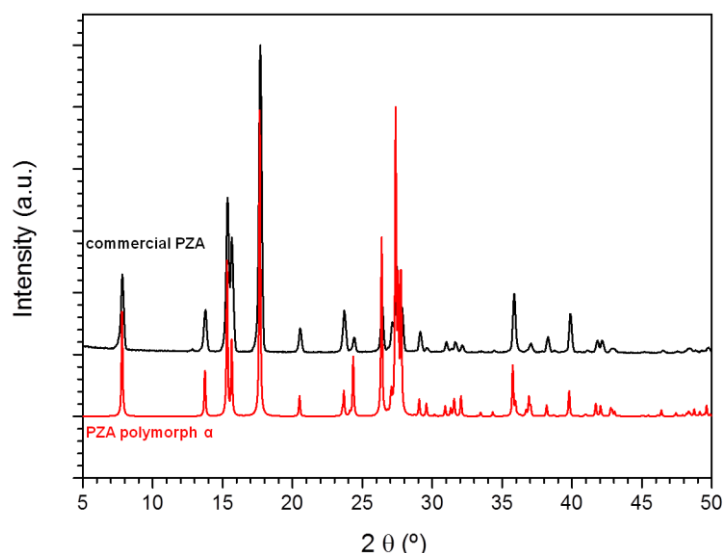


Fig. 5.67 PXRD patterns of: commercial PZA (top), and PZA polymorph  $\alpha$  calculated from CIF (bottom).

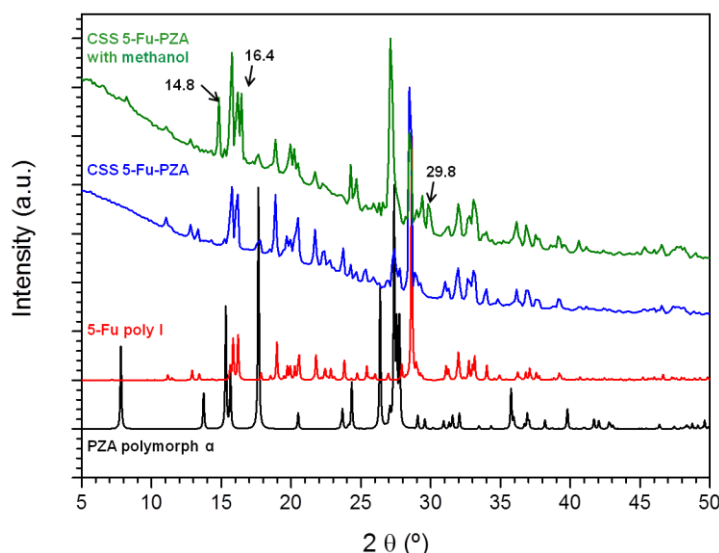


Fig. 5.68 PXRD patterns from top to bottom of: 5-Fu-PZA powder obtained through CSS with methanol, 5-Fu-PZA powder obtained through CSS without methanol, 5-Fu polymorph I calculated from CIF, and PZA polymorph  $\alpha$  calculated from CIF.

## Thermal characterization

Thermal analysis of PZA was not simple due to inherent kinetic processes that the sample underwent during heating. If we observe the curve measured with a heating rate of 5 K/min in Fig. 5.69 we can see that there was a first endothermic event with onset at 420.8 K which is reported to correspond to a polymorphic change of PZA from  $\alpha$  to  $\gamma$ ,<sup>73</sup> followed by what seemed a melting transition at 461.7 K. The onset of these processes changed with the heating rate indicating that they were kinetic processes. The solid-solid transition from the enantiotropic polymorphs  $\alpha$  to  $\gamma$  was described as kinetically non-reversible.<sup>73, 74</sup> This explained the shift in the onset with the heating rate.



In fact, in the cooling experiments (cooling at 20 K/min to 223 K and second heating at 5 K/min) transition to the original form  $\alpha$  was not observed. This means that the stable form at higher temperatures  $\gamma$  can be present at lower temperatures as a metastable form. Fig. 5.70 shows a schematic representation of the Gibbs energy of both polymorphs as a function of temperature. Below  $T_{\alpha \rightarrow \gamma}$  the stable phase is  $\alpha$  and over this temperature the  $\gamma$  form is the stable one.

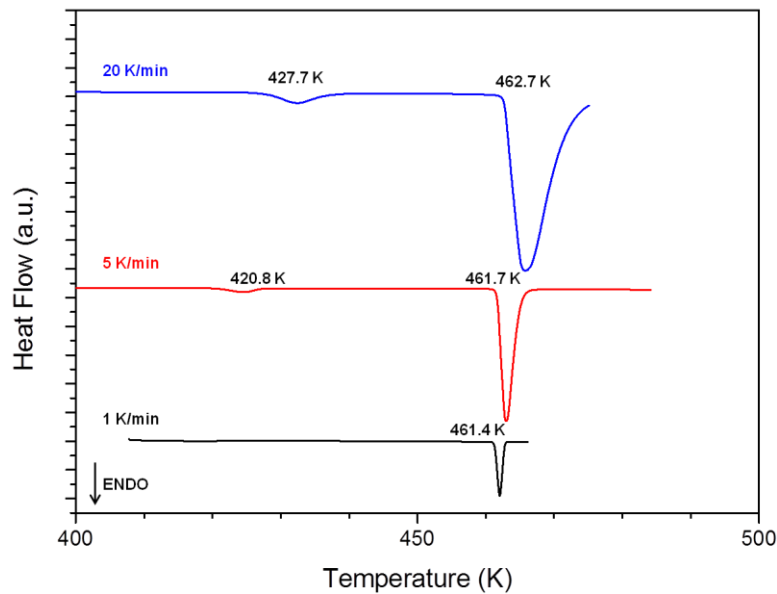


Fig. 5.69 DSC thermograms of commercial PZA with heating rates: 20 K/min (top), 5 K/min (middle) and 1 K/min (bottom).

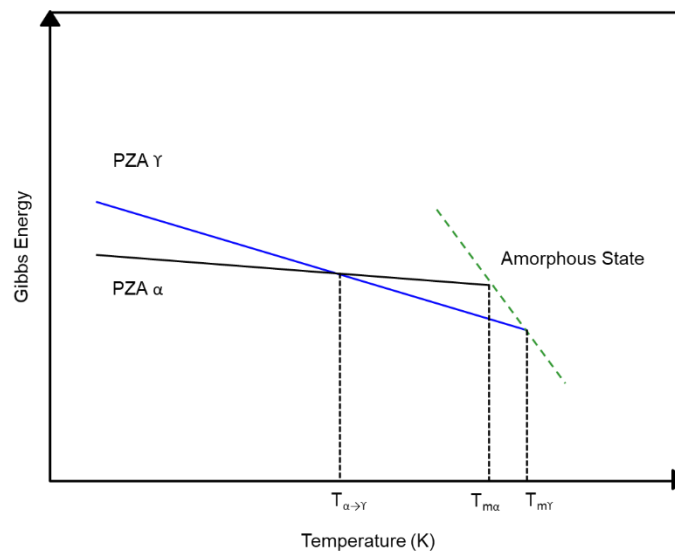


Fig. 5.70 Schematic representation of the solid-solid transition of enantiopric polymorphs  $\alpha$  to  $\gamma$  at temperature  $T_{\alpha \rightarrow \gamma}$ . And melting temperature representation of both polymorphs.

The second transition that we observed in Fig. 5.69 was an apparent melting. In the definition of thermodynamic melting given by Bernhard Wunderlich,<sup>75</sup> melting occurs at a specific temperature where the Gibbs energy difference ( $\Delta G$ ) between the crystal form and the amorphous form is equal to zero and there is no chemical change (decomposition).

$$\Delta G = 0 = \Delta H - T_m \Delta S \quad \text{eq. 4.1}$$

Therefore, the temperature  $T_m$  at which melting occurs is thermodynamic dependent only (see eq. 4.1) and should not be influenced by the heating rate. In the case of PZA this temperature changed with the heating rate, thus indicating that there is another process involved. In the pharmaceutical industry as explained earlier in this chapter this is usually called melt with decomposition. This term seems to imply that the sample firstly melts and then decomposes but as we have seen melting is a pure thermodynamic process and therefore the onset should not be dependent on the heating rate. What we are actually observing is the decomposition as another phenomenon of loss of crystalline structure. Thermal analysis using DSC beyond this point is therefore not recommended.

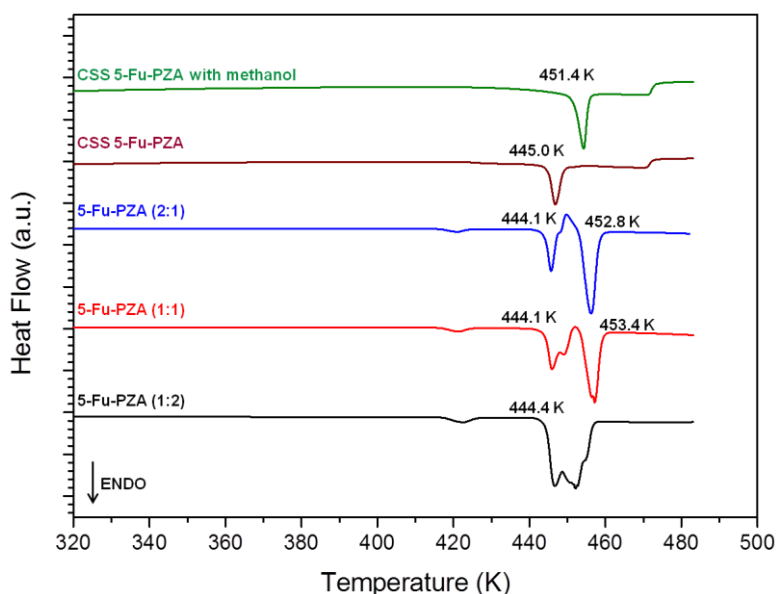


Fig. 5.71 DSC thermograms from top to bottom of: 5-Fu-PZA powder obtained through CSS with methanol, 5-Fu-PZA powder obtained through CSS without methanol, and 5-Fu-PZA physical mixtures with molar ratios: 2:1, 1:1, and 1:2. Heating rate 5 K/min.

The DSC thermograms of the CSS powders together with the thermograms of the physical mixtures are plotted in Fig. 5.71. The solid-solid transition of PZA shifted to a lower temperature (416.7 K) when heated with 5-Fu. As the 5-Fu content in the sample increased, the area associated to this endothermic transition reduced its size

as it could be expected (the heat flow in the ordinate axis is given as a ratio of heat flow and mass of the sample). In the samples collected from the CSS experiments this transition was not observable. PXRD pattern though confirmed the presence of  $\alpha$  PZA in the samples and did not show any evidence of the presence of  $\gamma$  PZA. All physical mixtures had first an endothermic peak with onset at around 444 K which probably corresponded to the eutectic point of the mixture (see Fig 1.6 and 1.7). As the proportion of 5-Fu in the sample increased the exothermic peak that followed this endothermic event also increased. This exothermic peak could be related to the formation of the co-crystal but mass loss in the sample at this stage makes interpretation risky. The CSS sample of the experiment carried out without methanol showed a displacement in the onset of the endothermic peak to 445.0 K and the one obtained with methanol as a cosolvent showed an even further displacement to 451.4 K.

TGA analyses of 5-Fu:PZA physical mixtures with molar ratios of 2:1; 1:1 and 1:2 were carried out in order to examine if PZA was stabilized over its decomposition temperature (461.7 K at a heating rate of 5 K/min) when heated together with 5-Fu during thermogravimetical analysis (Fig. 5.72). The percentage of mass loss associated to the first step in the TGA was coincident with the content in PZA of the sample indicating that no stabilization of PZA (and therefore no co-crystallization) took place during the heating of the samples.

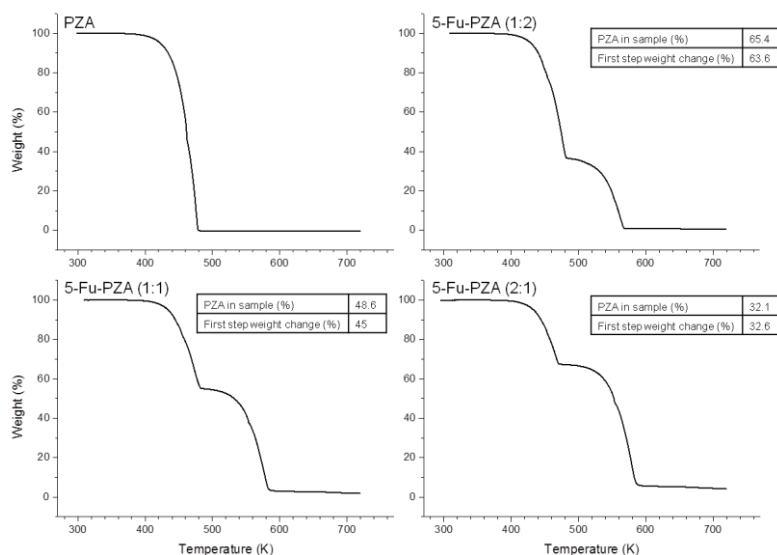


Fig. 5.72 TGA thermograms of commercial PZA (top left), and physical mixtures of 5-Fu-PZA with molar ratios: 1:2 (top right), 1:1 ratio (bottom left), and 2:1 ratio (bottom right). Heating rate of 5 K/min.

## FTIR characterization

The FTIR spectrum of PZA and the assignment of the main absorption bands<sup>76</sup> are detailed in Fig. 5.73 and Table 5.8. The main absorption bands prone to shift after co-crystallization will be those corresponding to the amide group, like the strong absorption C=O stretching band at  $1702\text{ cm}^{-1}$  and the N-H stretching bands at  $3408\text{ cm}^{-1}$  and  $3147\text{ cm}^{-1}$ .

**Table 5.8** Infrared peaks ( $\text{cm}^{-1}$ ) of commercial PZA and their assignments:  $\nu$  stretching;  $\delta$  bending;  $\gamma$  torsion;  $\omega$  wagging;  $\tau$  twisting;  $\rho$  rocking.

Experimental IR wavenumbers ( $\text{cm}^{-1}$ )	Band assignment	Experimental IR wavenumbers ( $\text{cm}^{-1}$ )	Band assignment
3408	$\nu$ (NH)	1376	$\nu$ (C-N)
3287	$\nu$ (NH)	1182	$\delta$ (C-H);
3147	$\nu$ (NH)	1162	$\nu$ (ring)
2750	$\nu$ (CH)	1086	$\omega$ (NH <sub>2</sub> )
1702	$\nu$ (C=O)	1054	$\nu$ (ring)
1608	$\delta$ (NH <sub>2</sub> )	1021	$\delta$ (ring)
1580	$\nu$ (ring)	869	$\gamma$ (C-H); $\gamma$ (NH <sub>2</sub> )
1525	$\nu$ (ring)	785	$\delta$ (ring)
1479	$\delta$ (C-H)	701	$\gamma$ (C=O)
1436	$\delta$ (C-H)	670	$\delta$ (ring)

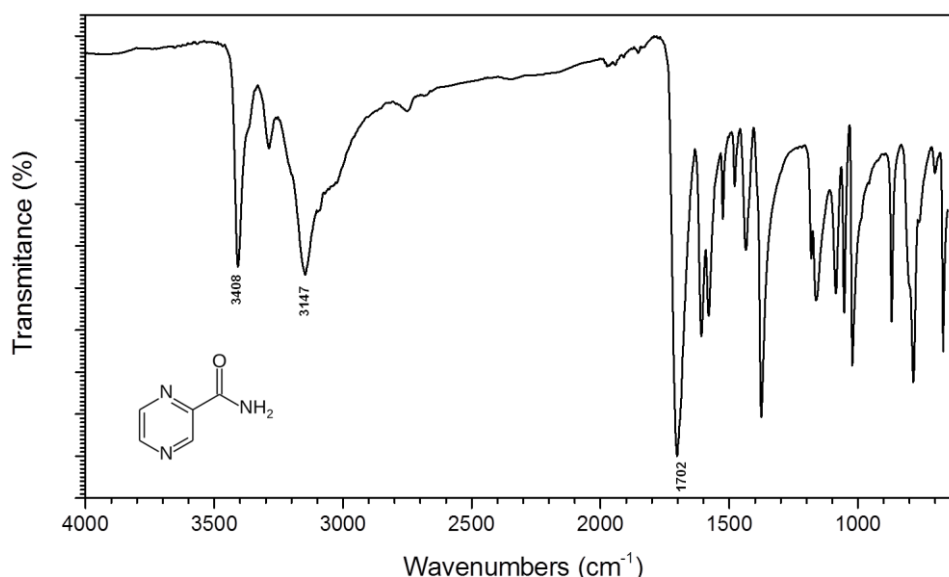


**Fig. 5.73** FTIR spectrum of PZA.

In both CSS samples we found the C=O stretching band at  $1720\text{ cm}^{-1}$ . This frequency is coincident with the stretching of the carbonyl group in pure 5-Fu. The N-H

absorption band at  $3147\text{ cm}^{-1}$  from pure PZA was not visible in the CSS samples where the broader N-H absorption band of pure 5-Fu appeared at  $3115\text{ cm}^{-1}$ . The most distinctive shift observable in the CSS samples affected the absorption band of the N-H stretching at  $3408\text{ cm}^{-1}$  (see Fig. 5.74). There was a light shift to  $3415\text{ cm}^{-1}$  in the CSS experiment carried out without methanol and a bigger shift to  $3435\text{ cm}^{-1}$  in the experiment carried out with methanol. This shift suggests a different intermolecular interaction of the PZA amide group in the latter CSS sample.

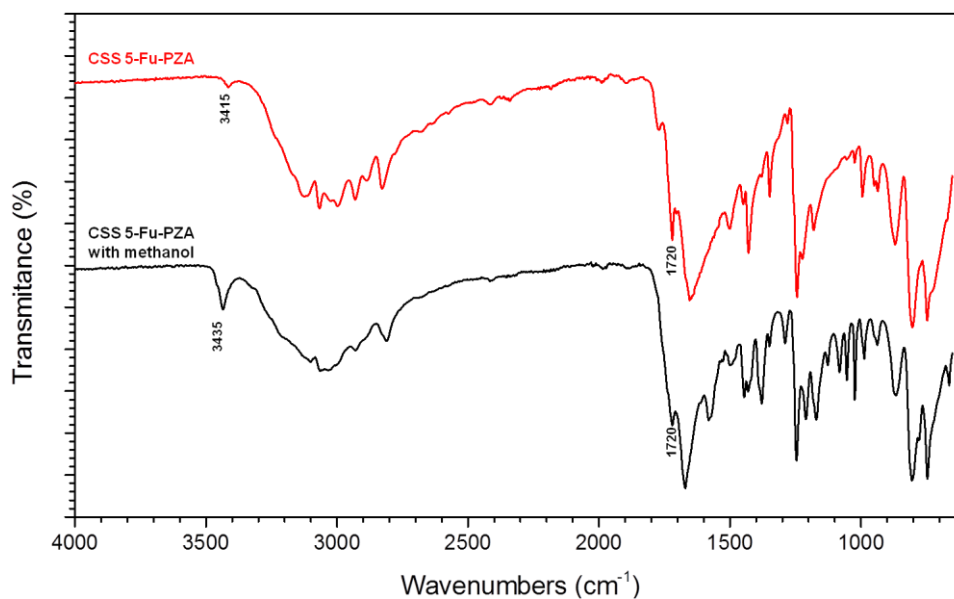


Fig. 5.74 FTIR spectra of 5-FU-PZA powders obtained through CSS: without methanol (top), and with methanol (bottom).

## SEM characterization

SEM images of the different samples are shown in Fig. 5.75. Commercial PZA presented a heterogeneous agglomerated morphology with agglomerate size ranging from  $50$  to  $300\ \mu\text{m}$ . The images of the CSS powders processed without methanol showed as in previous systems studied particles with a morphology akin to the one of commercial 5-Fu (see Fig. 5.15) but again with bigger particle size. In this case measured particle size ranges from  $150$  to  $500\ \mu\text{m}$ .

The CSS sample obtained from the experiment performed with methanol showed two different morphologies. Particles are present either as thin fibres  $1$  to  $2\ \mu\text{m}$  wide and  $50$  to  $100\ \mu\text{m}$  long, or as irregular pieces of  $50$  to  $200\ \mu\text{m}$  with a rough surface.

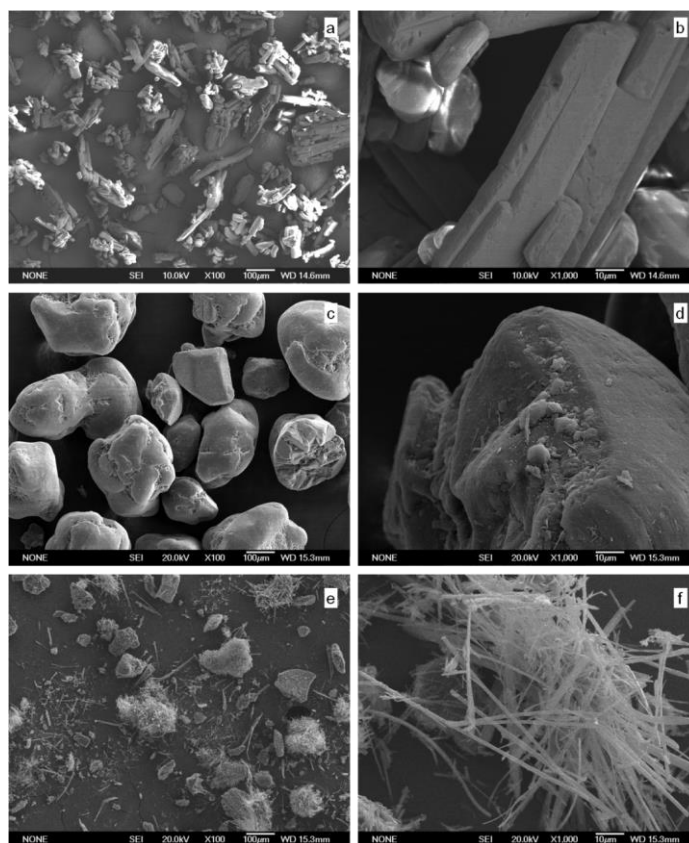


Fig. 5.75 SEM images of: PZA (a,b), 5-Fu-PZA CSS powders processed: without methanol (c,d) and with methanol (e,f).

## 5.8 5-Fu-SAC CO-CRYSTAL

### 5.8.1 SAS co-crystallization

There is no previous report of a 5-Fu-SAC co-crystal. SAC was selected as cofomer on basis of the synthon approach<sup>77</sup>. This approach suggests that for successful co-crystallization cofomers with functional groups complementary to those of the drug should be used. SAC and 5-Fu have an aromatic nitrogen with an adjacent carbonyl group that could originate a homosynthon. Moreover, SAC is a compound frequently used in the pharmaceutical industry as an excipient or as a cofomer in the preparation of pharmaceutical salts and co-crystals, thus it seemed a good candidate to explore possible co-crystallization. Solubility of SAC in CO<sub>2</sub> at 8.0 MPa and 313 K (conditions close to the SAS experiments) is  $2.45 \times 10^{-5}$  mol SAC/mol CO<sub>2</sub>,<sup>45</sup> a value larger than that of 5-Fu at similar conditions ( $2.81 \times 10^{-6}$  mol 5-Fu/mol CO<sub>2</sub> at 10.0 MPa and 313 K<sup>41</sup>).

## PXRD characterization

There is only one known crystal form of SAC<sup>78</sup>. Commercial and processed SAC were coincident with this form (see Fig. 5.76). The PXRD pattern of the SAS processed SAC displayed as usual a preferred orientation with very intense peaks at  $2\theta$ : 9.5 (100), 19.0 (200) and 28.8 ° (300). The 1:1 mixture of 5-Fu and SAC processed by SAS displayed a PXRD pattern (see Fig. 5.77) with low crystallinity and presented only diffraction peaks corresponding to 5-Fu polymorph I. A strong background at very low  $2\theta$  values could indicate the presence of an amorphous phase.

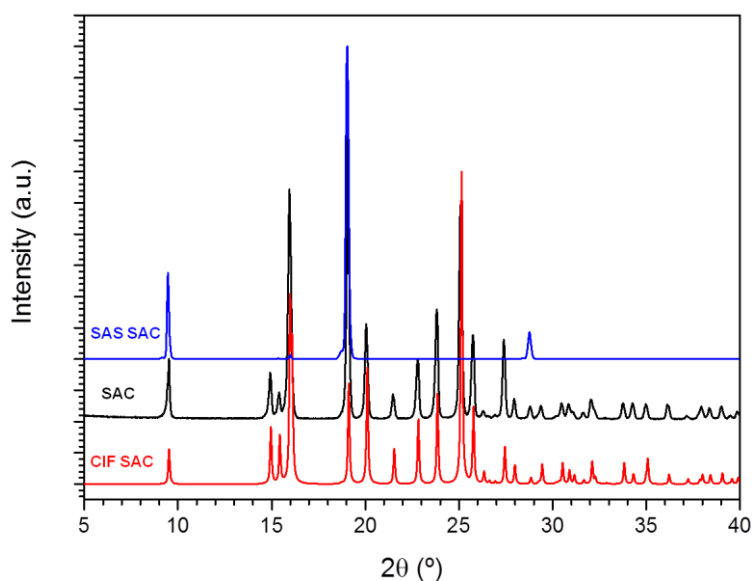


Fig. 5.76 PXRD patterns of: SAS processed SAC (top), comercial SAC (middle), and SAC calculated from CIF (bottom).

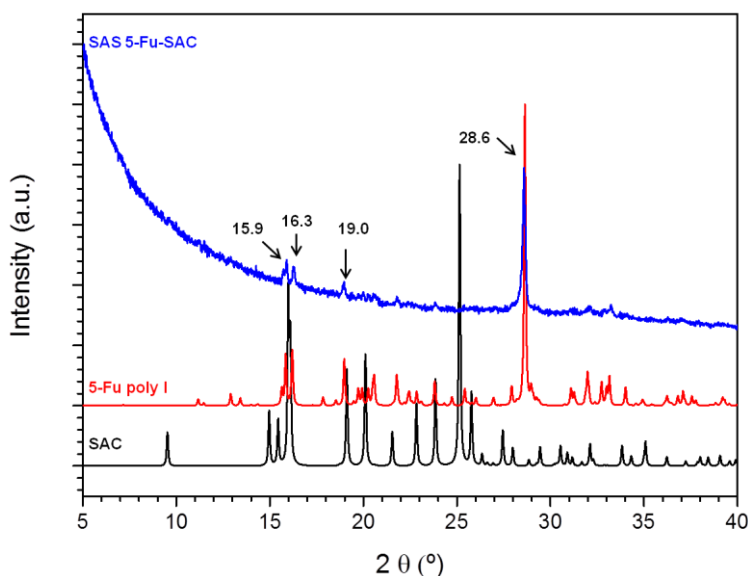


Fig. 5.77 PXRD patterns of: SAS processed 5-Fu-SAC (top), 5-Fu polymorph I calculated from CIF (middle), and SAC calculated from CIF (bottom).

### 5.8.1.1 Thermal characterization

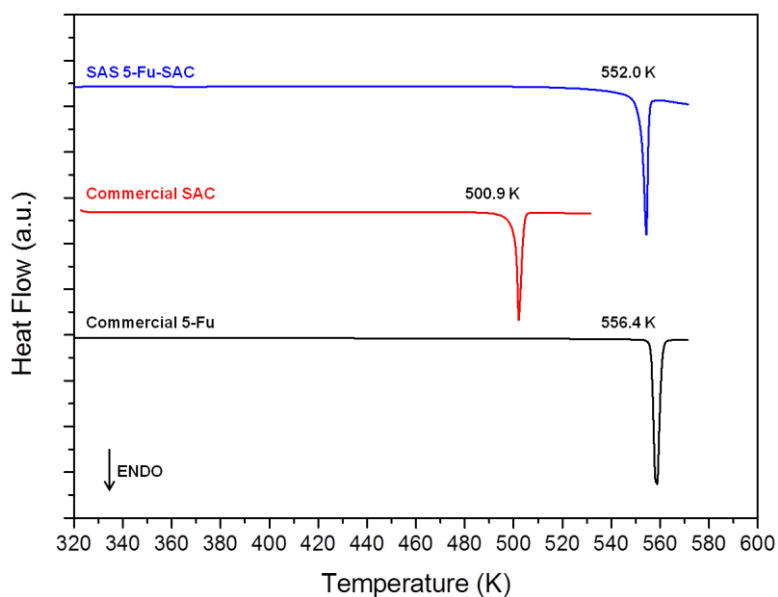


Fig. 5.78 DSC thermograms of: SAS processed 5-Fu-SAC (top), commercial SAC (middle), and commercial 5-Fu (bottom). Heating rate 5 K/min.

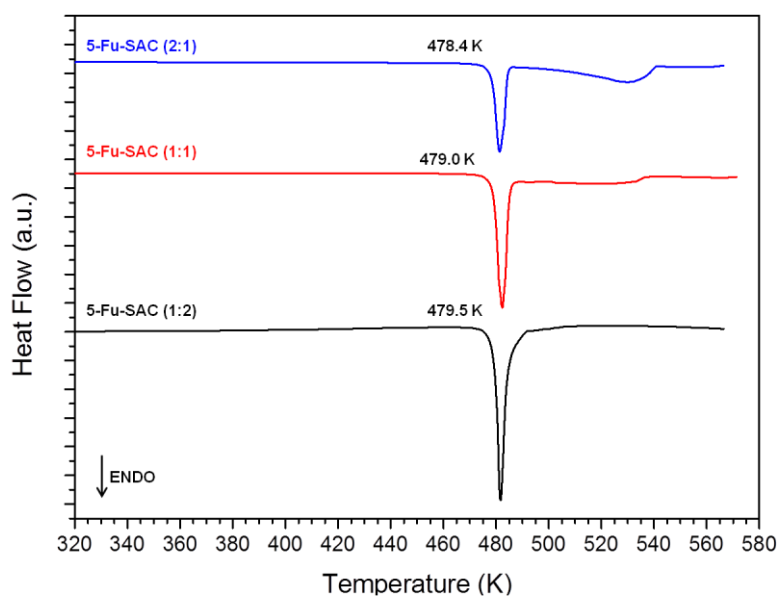


Fig. 5.79 DSC thermograms of 5-Fu-SAC physical mixtures with molar ratios: 2:1 (top), 1:1 (middle) and 1:2 (bottom). Heating rate 5 K/min.

The DSC of the SAS sample (Fig. 5.78) showed only one endothermic peak with an onset at 552.0 K, a temperature close to the apparent melting of 5-Fu (556.4 K) and above the melting temperature of SAC (500.9 K) and the decomposition temperature of SAC (529.0 K onset of mass loss measured with TGA). The shift to lower temperatures and a broader shoulder in the SAS sample in comparison to that of



pure 5-Fu suggests that the sample could be mainly 5-Fu with the presence of impurities. The DSC thermograms of 5-Fu-SAC physical mixtures (molar ratios of 1:1, 1:2 and 2:1) are shown in Fig. 5.79. All mixtures presented an endothermic peak with an onset around 479 K, below the melting temperature of the pure components (probably an eutectic point of the mixture). This peak was not found in the DSC thermogram of the SAS sample. TGA of the samples showed decomposition in one step.

### FTIR characterization

The FTIR spectrum of commercial SAC and the assignments of the absorption bands likely to shift in the co-crystal<sup>79</sup> can be found in Fig. 5.80 and Table 5.9. The FTIR spectrum of the SAS sample showed the same absorption bands as commercial 5-Fu (see Fig. 5.81), thus indicating that the precipitate consisted mainly of 5-Fu.

**Table 5.9** Infrared peaks ( $\text{cm}^{-1}$ ) of commercial SAC and their assignments:  $\nu$  stretching;  $\delta$  bending;  $\gamma$  torsion;  $\omega$  wagging;  $\text{tw}$  twisting;  $\rho$  rocking.

Experimental IR wavenumbers ( $\text{cm}^{-1}$ )	Band assignment	Experimental IR wavenumbers ( $\text{cm}^{-1}$ )	Band assignment
3092	$\nu$ (NH)	1259	$\nu$ ( $\text{SO}_2$ )
2920	$\nu$ (CH)	1159	$\nu$ ( $\text{SO}_2$ )
1715	$\nu$ (C=O)	897	$\nu$ (CNS)
1702	$\nu$ (C=O)		

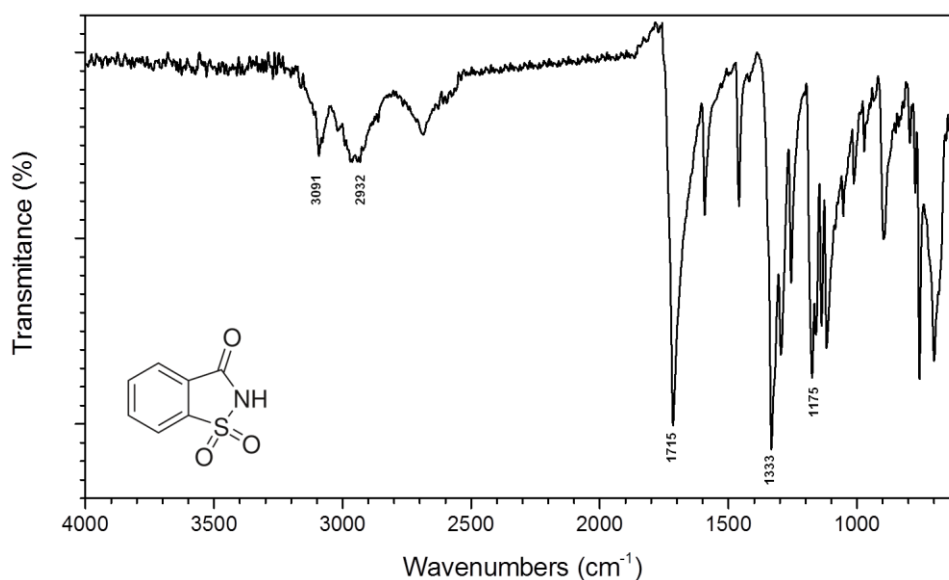


**Fig. 5.80** FTIR spectrum of SAC.

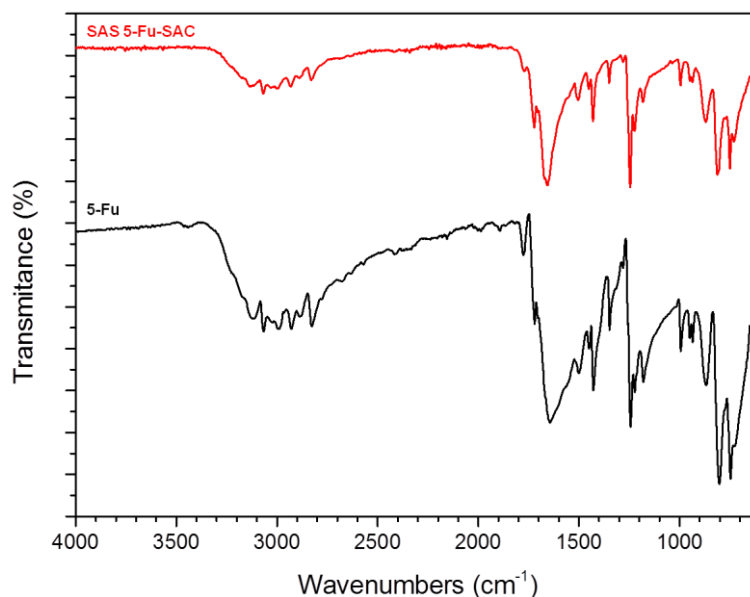


Fig. 5.81 FTIR spectra of: SAS processed 5-Fu-SAC (top) and commercial 5-Fu (bottom).

### SEM characterization

SEM images of the SAS sample showed particles with a morphology similar to that of 5-Fu processed by SAS (see Fig. 5.15). In this case the prismatic particles were smaller with sizes less than 1  $\mu\text{m}$  (Fig. 5.82). SAC precipitated in similar conditions<sup>50</sup> displayed a plate-like morphology.

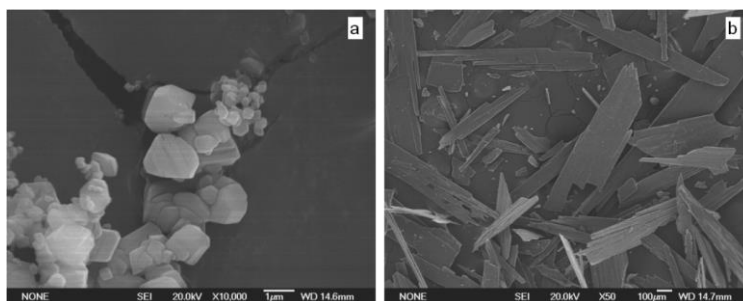


Fig. 5.82 SEM images of: SAS processed 5-Fu-SAC (a), and SAS processed SAC<sup>50</sup>(b).

### 5.8.2 CSS co-crystallization

Due to time constrictions the co-crystallization experiments of 5-Fu and SAC using the CSS technique were only performed in pure CO<sub>2</sub> without the addition of any co-solvent.

### PXRD characterization

The diffraction pattern obtained for the CSS sample (Fig. 5.83) clearly showed a mixture of both co-crystal components indicating unsuccessful co-crystallization.

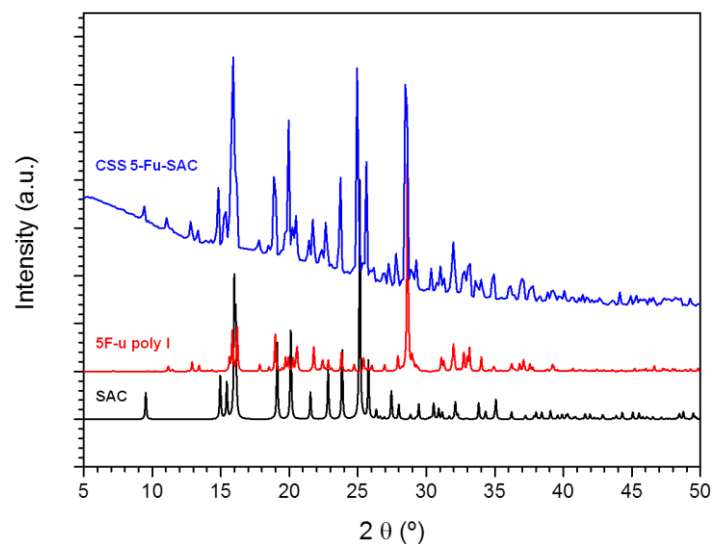


Fig. 5.83 PXRD patterns of: SAC (bottom), 5-Fu polymorph I (middle), CSS 5-Fu-SAC (top).

### Thermal characterization

DSC thermogram of the CSS sample displayed an endothermic peak with onset at 479.1 K (Fig. 5.84). This endothermic transition took place at a temperature lower than the melting point of SAC (500.9 K) and similar to those displayed by the physical mixtures (onsets around 479 K). These results also suggest that the sample was a mixture of 5-Fu and SAC and that co-crystallization did not take place.

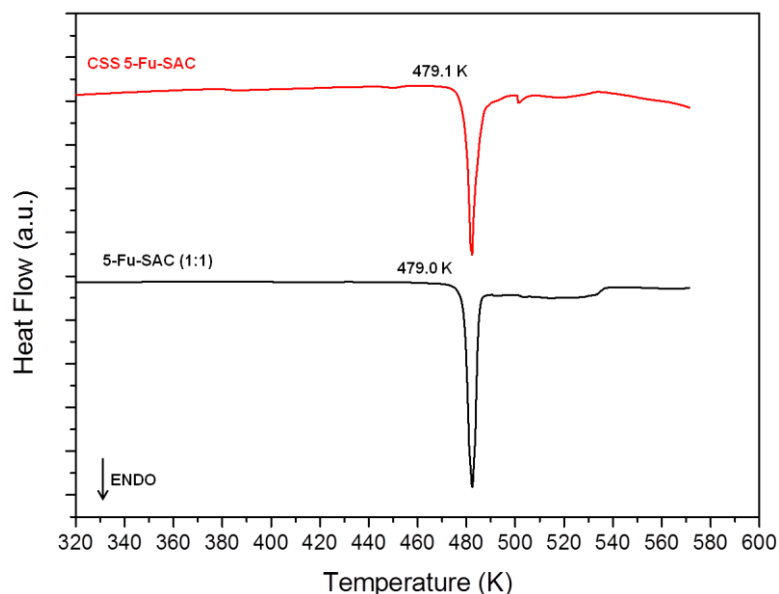


Fig. 5.84 DSC thermograms of: 5-Fu-SAC powder obtained through CSS (top), and 5-Fu-SAC equimolar physical mixture (bottom). Heating rate 5 K/min.

## 5.9 CONCLUSIONS

Co-crystallization of the antitumoral drug 5-Fu with six different coformers has been attempted using two different supercritical CO<sub>2</sub> technologies, SAS and CSS, in which CO<sub>2</sub> acts as antisolvent or solvent, respectively.

The SAS technology was able to produce co-crystals of 5-Fu with urea and thiourea. TGA and micro-elemental analysis showed that the SAS precipitates had the stoichiometric amount of the co-crystal components. PXRD analysis indicated the presence of 5-Fu homocrystals in the SAS precipitates. Neither urea nor thiourea homocrystals were detectable via PXRD or DSC analysis, thus suggesting that impurities in the SAS precipitate consist of 5-Fu homocrystal and amorphous urea and thiourea. Solubilities of urea and thiourea in methanol at 298 K (166 and 94.25 mg/mL, respectively<sup>80</sup>) are much higher than that of 5-Fu (5 mg/mL<sup>49</sup>). This could lead to an incongruent saturating system and the production of homocrystals. Further characterization of the ternary phase diagram is required to define the optimal operating conditions that would lead to a pure co-crystal precipitate.

The co-crystal of 5-Fu with acridine showed the difficulties that major solubility differences of the co-crystal components in supercritical CO<sub>2</sub> may cause when producing co-crystals via SAS. Increasing the amount of acridine to overcome this problem allowed us to produce the co-crystal. However, PXRD analysis revealed the additional presence of a different unknown crystalline phase. A thermal transition different from those present in the thermograms of the physical mixtures was also observed.

Co-crystallization of 5-Fu with 4HBA via SAS produced a complex mixture of phases whose exact composition was difficult to characterize using PXRD analysis. The solubility of 4HBA in methanol at 298 K is very high (389.9 mg/mL<sup>81</sup>) in comparison to that of 5-Fu, this could result in an incongruent saturating system. Nevertheless, other crystalline phases different from those of homocrystals were obtained.

Co-crystallization of 5-Fu with PZA was unsuccessful via SAS. Moreover, despite the low solubility of PZA in supercritical CO<sub>2</sub> the precipitation of this drug alone via SAS was not achieved. Solubility of PZA in methanol (13.8 mg/mL<sup>80</sup>) is not very different from that of 5-Fu (5 mg/mL<sup>49</sup>) so a congruent saturating system could be expected.

Results from SAS co-crystallizations are summarized in Table 5.2.

CSS co-crystallization of all 5-Fu systems investigated was only successful in those experiments carried out with the addition of cosolvent. This fact points out the importance of the solubilization of the co-crystal components in the supercritical phase to achieve a successful co-crystallization. Results from CSS co-crystallizations are summarized in Table 5.3.

Co-crystallization of 5-Fu-SAC was unsuccessful using both techniques. Attempts to produce a co-crystal from solvent evaporation also failed.

While the SAS technique was not able to produce a co-crystal of 5-Fu and PZA, CSS (using CO<sub>2</sub> as a solvent) was able to produce a new phase (probably the co-crystal). Nevertheless, CSS is a technique whose scaling-up is difficult and does not present the micronization advantages of SAS. Moreover, if cosolvents are used further drying steps may be required in the process. As an alternative RESS micronization technology, in which CO<sub>2</sub> acts as a solvent, could be used to produce these co-crystals.

## References

1. Fallon, L., Crystal and molecular structure of 5-Fluorouracil. *Acta Crystallographica Section B-Structural Science* **1973**, 29 (NOV15), 2549-2556.
2. Hulme, A. T.; Price, S. L.; Tocher, D. A., A new polymorph of 5-fluorouracil found following computational crystal structure predictions. *Journal of the American Chemical Society* **2005**, 127 (4), 1116-1117.
3. Heidelberger, C.; Chaudhuri, N. K.; Danneberg, P.; Mooren, D.; Griesbach, L.; Duschinsky, R.; Schnitzer, R. J.; Plevin, E.; Scheiner, J., Fluorinated pyrimidines, a new class of tumor-inhibitory compounds. *Nature* **1957**, 179 (4561), 663-666.
4. Rutman, R. J.; Cantarow, A.; Paschkis, K. E., Studies on 2-acetylaminofluorene carcinogenesis: III. The utilization of uracil-2-C 14 by pre-neoplastic rat liver. *Cancer Res* **1954**, 14, 119-126.
5. Longley, D. B.; Harkin, D. P.; Johnston, P. G., 5-Fluorouracil: Mechanisms of action and clinical strategies. *Nature Reviews Cancer* **2003**, 3 (5), 330-338.
6. Vermorken, J. B.; Remenar, E.; van Herpen, C.; Gorlia, T.; Mesia, R.; Degardin, M.; Stewart, J. S.; Jelic, S.; Betka, J.; Preiss, J. H.; van den Weyngaert, D.; Awada, A.; Cupissol, D.; Kienzer, H. R.; Rey, A.; Desauois, I.; Bernier, J.; Lefebvre, J. L.; Stu, E. T., Cisplatin, fluorouracil, and docetaxel in unresectable head and neck cancer. *New England Journal of Medicine* **2007**, 357 (17), 1695-1704.
7. Sadek, H.; Azli, N.; Wendling, J. L.; Cvitkovic, E.; Rahal, M.; Mamelle, G.; Guillaume, J. C.; Armand, J. P.; Avril, M. F., Treatment of advanced squamous cell carcinoma of the skin with cisplatin, 5-fluorouracil, and bleomycin. *Cancer* **1990**, 66 (8), 1692-1696.
8. Bonadonna, G.; Valagussa, P.; Moliterni, A.; Zambetti, M.; Brambilla, C., Adjuvant Cyclophosphamide, Methotrexate, and Fluorouracil in Node-Positive Breast Cancer. The Results of 20 Years of Follow-up. *New England Journal of Medicine* **1995**, 332 (14), 901-906.
9. Labianca, R.; Marsoni, S.; Pancera, G., Efficacy of adjuvant fluorouracil and folinic acid in colon cancer. *Lancet* **1995**, 345 (8955), 939-944.
10. Douillard, J. Y.; Cunningham, D.; Roth, A. D.; Navarro, M.; James, R. D.; Karasek, P.; Jandik, P.; Iveson, T.; Carmichael, J.; Alakl, M.; Gruia, G.; Awad, L.; Rougier, P., Irinotecan combined with fluorouracil compared with fluorouracil alone as first-line treatment for metastatic colorectal cancer: a multicentre randomised trial. *Lancet* **2000**, 355 (9209), 1041-1047.
11. Fioravanti, A.; Canu, B.; Ali, G.; Orlandi, P.; Allegrini, G.; Di Desidero, T.; Emrilenegger, U.; Fontanini, G.; Danesi, R.; Del Tacca, M.; Falcone, A.; Bocci, G., Metronomic 5-fluorouracil, oxaliplatin and irinotecan in colorectal cancer. *European Journal of Pharmacology* **2009**, 619 (1-3), 8-14.
12. Vincent, J.; Mignot, G.; Chalmin, F.; Ladoire, S.; Bruchard, M.; Chevriaux, A.; Martin, F.; Apetoh, L.; Rebe, C.; Ghiringhelli, F., 5-Fluorouracil Selectively Kills Tumor-Associated Myeloid-Derived Suppressor Cells Resulting in Enhanced T Cell-Dependent Antitumor Immunity. *Cancer Research* **2010**, 70 (8), 3052-3061.
13. Carrillo, E.; Navarro, S. A.; Ramirez, A.; Garcia, M. A.; Grinan-Lison, C.; Peran, M.; Marchal, J. A., 5-Fluorouracil derivatives: a patent review (2012-2014). *Expert Opinion on Therapeutic Patents* **2015**, 25 (10), 1131-1144.
14. Miwa, M.; Ura, M.; Nishida, M.; Sawada, N.; Ishikawa, T.; Mori, K.; Shimma, N.; Umeda, I.; Ishitsuka, H., Design of a novel oral fluoropyrimidine carbamate, capecitabine, which generates 5-fluorouracil selectively in tumours by enzymes concentrated in human liver and cancer tissue. *European Journal of Cancer* **1998**, 34 (8), 1274-1281.
15. Singh, U. P.; Kashyap, S.; Singh, H. J.; Mishra, B. K.; Roy, P.; Chakraborty, A., Effect of adenosine on the supramolecular architecture and activity of 5-fluorouracil. *Journal of Molecular Structure* **2012**, 1014, 47-56.

16. Veverka, M.; Simon, P.; Gallovic, J.; Jorik, V.; Veverkova, E.; Dubaj, T., Imatinib mesylate cocrystals: synthesis, screening, and preliminary characterization. *Monatshefte Fur Chemie* **2012**, *143* (10), 1405-1415.
17. Delori, A.; Eddleston, M. D.; Jones, W., Cocrystals of 5-fluorouracil. *Crystengcomm* **2013**, *15* (1), 73-77.
18. Li, S.; Chen, J.-M.; Lu, T.-B., Synthron polymorphs of 1: 1 co-crystal of 5-fluorouracil and 4-hydroxybenzoic acid: their relative stability and solvent polarity dependence of grinding outcomes. *Crystengcomm* **2014**, *16* (28), 6450-6458.
19. da Silva, C. C. P.; Pepino, R. d. O.; de Melo, C. C.; Tenorio, J. C.; Ellena, J., Controlled Synthesis of New 5-Fluorocytosine Cocrystals Based on the pK(a) Rule. *Crystal Growth & Design* **2014**, *14* (9), 4383-4393.
20. Nadzri, N. I.; Sabri, N. H.; Lee, V. S.; Halim, S. N. A., 5-Fluorouracil Co-crystals and Their Potential Anti-cancer Activities Calculated by Molecular Docking Studies. *Journal of Chemical Crystallography* **2016**, *46* (3), 144-154.
21. Dai, X. L.; Li, S.; Chen, J. M.; Lu, T. B., Improving the Membrane Permeability of 5-Fluorouracil via Cocrystallization. *Crystal Growth & Design* **2016**, *16* (8), 4430-4438.
22. Mohana, M.; Muthiah, P. T.; McMillen, C. D., Supramolecular hydrogen-bonding patterns in 1:1 cocrystals of 5-fluorouracil with 4-methylbenzoic acid and 3-nitrobenzoic acid. *Acta Crystallographica Section C-Structural Chemistry* **2017**, *73*, 259-+.
23. Mohana, M.; Muthiah, P. T.; McMillen, C. D., Supramolecular architectures in two 1:1 cocrystals of 5-fluorouracil with 5-bromothiophene-2-carboxylic acid and thiophene-2-carboxylic acid. *Acta Crystallographica Section C-Structural Chemistry* **2017**, *73*, 481-485.
24. Liu, Z. F.; Rimmer, S., Synthesis and release of 5-fluorouracil from poly (N-vinylpyrrolidinone) bearing 5-fluorouracil derivatives. *Journal of Controlled Release* **2002**, *81* (1-2), 91-99.
25. Gu, C. H.; Le, V. M.; Lang, M. D.; Liu, J. W., Preparation of polysaccharide derivates chitosan-graft-poly(epsilon-caprolactone) amphiphilic copolymer micelles for 5-fluorouracil drug delivery. *Colloids and Surfaces B-Biointerfaces* **2014**, *116*, 745-750.
26. Cuadra, I. A.; Zahran, F.; Martín, D.; Cabañas, A.; Pando, C., Preparation of 5-fluorouracil microparticles and 5-fluorouracil/poly(L-lactide) composites by a supercritical CO<sub>2</sub> antisolvent process. *The Journal of Supercritical Fluids* **2019**, *143*, 64-71.
27. Guney, O.; Akgerman, A., Synthesis of controlled-release products in supercritical medium. *Aiche Journal* **2002**, *48* (4), 856-866.
28. Chen, A. Z.; Pu, X. M.; Kang, Y. Q.; Liao, L.; Yao, Y. D.; Yin, G. F., Preparation of 5-fluorouracil-poly(L-lactide) microparticles using solution-enhanced dispersion by supercritical CO<sub>2</sub>. *Macromolecular Rapid Communications* **2006**, *27* (15), 1254-1259.
29. Chen, A. Z.; Li, Y.; Chen, D.; Hu, J. Y., Development of core-shell microcapsules by a novel supercritical CO<sub>2</sub> process. *Journal of Materials Science-Materials in Medicine* **2009**, *20* (3), 751-758.
30. Kalantarian, P.; Najafabadi, A. R.; Haririan, I.; Vatanara, A.; Yamini, Y.; Darabi, M.; Gilani, K., Preparation of 5-fluorouracil nanoparticles by supercritical antisolvents for pulmonary delivery. *International Journal of Nanomedicine* **2010**, *5*, 763-770.
31. Kalantarian, P.; Haririan, I.; Najafabadi, A. R.; Shokrgozar, M. A.; Vatanara, A., Entrapment of 5-fluorouracil into PLGA matrices using supercritical antisolvent processes. *Journal of Pharmacy and Pharmacology* **2011**, *63* (4), 500-506.
32. Zhang, C.; Li, G. D.; Wang, Y. H.; Cui, F. Y.; Zhang, J.; Huang, Q. S., Preparation and characterization of 5-fluorouracil-loaded PLLA-PEG/PEG nanoparticles by a novel supercritical CO<sub>2</sub> technique vol 436, pg 272, 2012. *International Journal of Pharmaceutics* **2012**, *439* (1-2), 360-360.

33. Zhan, S. P.; Chen, C.; Zhao, Q. C.; Wang, W. J.; Liu, Z. J., Preparation of 5-Fu-Loaded PLLA Microparticles by Supercritical Fluid Technology. *Industrial & Engineering Chemistry Research* **2013**, *52* (8), 2852-2857.
34. Cabezas, L. I.; Gracia, I.; Garcia, M. T.; de Lucas, A.; Rodriguez, J. F., Production of biodegradable porous scaffolds impregnated with 5-fluorouracil in supercritical CO<sub>2</sub>. *Journal of Supercritical Fluids* **2013**, *80*, 1-8.
35. Cabezas, L. I.; Gracia, I.; de Lucas, A.; Rodriguez, J. F., Novel Model for the Description of the Controlled Release of 5-Fluorouracil from PLGA and PLA Foamed Scaffolds Impregnated in Supercritical CO<sub>2</sub>. *Industrial & Engineering Chemistry Research* **2014**, *53* (40), 15374-15382.
36. Salerno, A.; Saurina, J.; Domingo, C., Supercritical CO<sub>2</sub> foamed polycaprolactone scaffolds for controlled delivery of 5-fluorouracil, nicotinamide and triflusal. *International Journal of Pharmaceutics* **2015**, *496* (2), 654-663.
37. Salerno, A.; Domingo, C.; Saurina, J., PCL foamed scaffolds loaded with 5-fluorouracil anti-cancer drug prepared by an eco-friendly route. *Materials Science & Engineering C-Materials for Biological Applications* **2017**, *75*, 1191-1197.
38. Esfandiari, N.; Ghoreishi, S. M., Synthesis of 5-Fluorouracil nanoparticles via supercritical gas antisolvent process. *Journal of Supercritical Fluids* **2013**, *84*, 205-210.
39. Esfandiari, N.; Ghoreishi, S. M., Kinetic Modeling of the Gas Antisolvent Process for Synthesis of 5-Fluorouracil Nanoparticles. *Chemical Engineering & Technology* **2014**, *37* (1), 73-80.
40. Hao, Y. W.; Zhao, J.; Wang, G.; Cao, L. Q.; Wang, J. D.; Yue, F., Grafting of thermo- and pH-responsive polymer inside mesoporous silica foam in supercritical carbon dioxide for controlled release of 5-fluorouracil. *Fibers and Polymers* **2017**, *18* (12), 2476-2480.
41. Zhan, S. P.; Zhao, Q. C.; Chen, S. H.; Wang, J. C.; Liu, Z. J.; Chen, C., Solubility and Partition Coefficients of 5-Fluorouracil in ScCO<sub>2</sub> and ScCO<sub>2</sub>/Poly(L-lactic acid). *Journal of Chemical and Engineering Data* **2014**, *59* (4), 1158-1164.
42. Schmitt, W. J.; Reid, R. C., Solubility of monofunctional organic solids in chemically diverse supercritical fluids. *Journal of Chemical and Engineering Data* **1986**, *31* (2), 204-212.
43. Catchpole, O. J.; Tallon, S. J.; Dyer, P. J.; Lan, J. S.; Jensen, B.; Rasmussen, O. K.; Grey, J. B., Measurement and modelling of urea solubility in supercritical CO<sub>2</sub> and CO<sub>2</sub>+ethanol mixtures. *Fluid Phase Equilibria* **2005**, *237* (1-2), 212-218.
44. Lucien, F. P.; Foster, N. R., Influence of matrix composition on the solubility of hydroxybenzoic acid isomers in supercritical carbon dioxide. *Industrial & Engineering Chemistry Research* **1996**, *35* (12), 4686-4699.
45. Padrela, L.; Rodrigues, M. A.; Tiago, J.; Velaga, S. P.; Matos, H. A.; de Azevedo, E. G., Insight into the Mechanisms of Cocrystallization of Pharmaceuticals in Supercritical Solvents. *Crystal Growth & Design* **2015**, *15* (7), 3175-3181.
46. Bettini, R.; Bonassi, L.; Castoro, V.; Rossi, A.; Zema, L.; Gazzaniga, A.; Giordano, F., Solubility and conversion of carbamazepine polymorphs in supercritical carbon dioxide. *European Journal of Pharmaceutical Sciences* **2001**, *13* (3), 281-286.
47. Reighard, T. S.; Lee, S. T.; Olesik, S. V., Determination of methanol/CO<sub>2</sub> and acetonitrile/CO<sub>2</sub> vapor-liquid phase equilibria using a variable-volume view cell. *Fluid Phase Equilibria* **1996**, *123* (1-2), 215-230.
48. Suzuki, K.; Sue, H., Isothermal vapor-liquid equilibrium data for binary systems at high pressures: carbon dioxide-methanol, carbon dioxide-ethanol, carbon dioxide-1-propanol, methane-ethanol, methane-1-propanol, ethane-ethanol and ethane-1-propanol systems. *Journal of Chemical and Engineering Data* **1990**, *35* (1), 63-66.
49. Lawrence, H. K.; Douglas, B. W., *National toxicology program's chemical solubility compendium*. **1991**; p 448.



50. Cuadra, I. A.; Cabanas, A.; Cheda, J. A. R.; Pando, C., Polymorphism in the co-crystallization of the anticonvulsant drug carbamazepine and saccharin using supercritical CO<sub>2</sub> as an anti-solvent. *Journal of Supercritical Fluids* **2018**, *136*, 60-69.
51. Suleiman, D.; Estevez, L. A.; Pulido, J. C.; Garcia, J. E.; Mojica, C., Solubility of anti-inflammatory, anti-cancer, and anti-HIV drugs in supercritical carbon dioxide. *Journal of Chemical and Engineering Data* **2005**, *50* (4), 1234-1241.
52. Guney, O.; Akgerman, A., Solubilities of 5-fluorouracil and ss-estradiol in supercritical carbon dioxide. *Journal of Chemical and Engineering Data* **2000**, *45* (6), 1049-1052.
53. Leonard C. Thomas; Shelly J. Schmidt, "Apparent Melting": A New Approach to Characterizing Crystalline Structure in Pharmaceutical Materials. *TA instruments TA401 which can be accessed electronically through: (<http://www.tainstruments.com/pdf/literature/TA401.pdf>)*.
54. Dobrowolski, J. C.; Rode, J. E.; Kolos, R.; Jamroz, M. H.; Bajdor, K.; Mazurek, A. P., Ar-matrix IR spectra of 5-halouracils interpreted by means of DFT calculations. *Journal of Physical Chemistry A* **2005**, *109* (10), 2167-2182.
55. Akalin, E.; Akyuz, S.; Akyuz, T., Adsorption and interaction of 5-fluorouracil with montmorillonite and saponite by FT-IR spectroscopy. *Journal of Molecular Structure* **2007**, *834*, 477-481.
56. Rastogi, V. K.; Palafox, M. A., Vibrational spectra, tautomerism and thermodynamics of anticarcinogenic drug: 5-Fluorouracil. *Spectrochimica Acta Part a-Molecular and Biomolecular Spectroscopy* **2011**, *79* (5), 970-977.
57. Keuleers, A.; Desseyn, H. O.; Rousseau, B.; Van Alsenoy, C., Vibrational analysis of urea. *Journal of Physical Chemistry A* **1999**, *103* (24), 4621-4630.
58. Grdadolnik, J.; Marechal, Y., Urea and urea-water solutions-an infrared study. *Journal of Molecular Structure* **2002**, *615* (1-3), 177-189.
59. Wang, S.; Gao, Q. Y.; Wang, J. C., Thermodynamic analysis of decomposition of thiourea and thiourea oxides. *Journal of Physical Chemistry B* **2005**, *109* (36), 17281-17289.
60. Stewart, J. E., Infrared absorption spectra of urea, thiourea, and some thiourea-alkali halide complexes. *Journal of Chemical Physics* **1957**, *26* (2), 248-254.
61. Van Alsten, J. G., *Preprints of papers-Am. Chem. Soc., Div. Fuel Chem.* **1985**, *30* (3), 13-15.
62. Van Alsten, J. G.; Eckert, C. A., Effect of entrainers and of solute size and polarity in supercritical fluid solutions. *Journal of Chemical and Engineering Data* **1993**, *38* (4), 605-610.
63. Lowde, R. D.; Phillips, D. C.; Wood, R. G., The crystallography of acridine I. *Acta Crystallographica* **1953**, *6* (6), 553-556.
64. Clarke, B. P.; Thomas, J. M.; Williams, J. O., The relationship between crystallographic structure and luminescence in single crystals of acridine. *Chemical Physics Letters* **1975**, *35* (2), 251-254.
65. Maryvonne Brigodiot, J. M. L., Étude vibrationnelle de l'acridine et de l'ion acridinium par spectroscopie infrarouge et Raman. Comparaison avec l'antracène. *Journal de Chimie Physique* **1972**, *69*, 964-971.
66. Mattioda, A. L.; Bauschlicher, C. W.; Ricca, A.; Bregman, J.; Hudgins, D. M.; Allamandola, L. J., Infrared spectroscopy of matrix-isolated neutral polycyclic aromatic nitrogen heterocycles: The acridine series. *Spectrochimica Acta Part a-Molecular and Biomolecular Spectroscopy* **2017**, *181*, 286-308.
67. Stahl, E.; Schilz, W.; Schutz, E.; Willing, E., A quick method for microanalytical evaluation of dissolving power of supercritical gases. *Angewandte Chemie-International Edition in English* **1978**, *17* (10), 731-738.
68. Krukonis, V. J.; Kurnik, R. T., Solubility of solid aromatic isomers in carbon dioxide. *Journal of Chemical and Engineering Data* **1985**, *30* (3), 247-249.
69. Gurdial, G. S.; Macnaughton, S. J.; Tomasko, D. L.; Foster, N. R., Influence of chemical modifiers on the solubility of o-hydroxybenzoic acid and m-hydroxybenzoic

- acid in supercritical CO<sub>2</sub>. *Industrial & Engineering Chemistry Research* **1993**, 32 (7), 1488-1497.
70. Heath, E. A.; Singh, P.; Ebisuzaki, Y., Structure of p-hydroxybenzoic acid and p-hydroxybenzoic acid acetone complex (2/1). *Acta Crystallographica Section C-Crystal Structure Communications* **1992**, 48, 1960-1965.
71. Kariuki, B. M.; Bauer, G. L.; Harris, K. D. M.; Teat, S. J., Polymorphism in p-hydroxybenzoic acid: The effect of intermolecular hydrogen bonding in controlling proton order versus disorder in the carboxylic acid dimer motif. *Angewandte Chemie-International Edition* **2000**, 39 (24), 4485-4488.
72. Takaki, Y.; Sasada, Y.; Watanabe, T., The crystal structure of alpha-pyrazinamide. *Acta Crystallographica* **1960**, 13 (9), 693-702.
73. Castro, R. A. E.; Maria, T. M. R.; Evora, A. O. L.; Feiteira, J. C.; Silva, M. R.; Beja, A. M.; Canotilho, J.; Eusebio, M. E. S., A New Insight into Pyrazinamide Polymorphic Forms and their Thermodynamic Relationships. *Crystal Growth & Design* **2010**, 10 (1), 274-282.
74. Kawakami, K.; Ida, Y., Application of modulated-temperature DSC to the analysis of enantiotropically related polymorphic transitions. *Thermochimica Acta* **2005**, 427 (1-2), 93-99.
75. Wunderlich, B., *Thermal Analysis*. Academic Press: San Diego, California, **1990**.
76. Borba, A.; Albrecht, M.; Gomez-Zavaglia, A.; Suhm, M. A.; Fausto, R., Low Temperature Infrared Spectroscopy Study of Pyrazinamide: From the Isolated Monomer to the Stable Low Temperature Crystalline Phase. *Journal of Physical Chemistry A* **2010**, 114 (1), 151-161.
77. Desiraju, G. R., Supramolecular Synthons in Crystal Engineering - A New Organic Synthesis. *Angewandte Chemie-International Edition in English* **1995**, 34 (21), 2311-2327.
78. Bart, J. C. J., Crystal and molecular structure of saccharin (o-sulphobenzoicimide). *Journal of the Chemical Society B-Physical Organic* **1968**, (4), 376-382.
79. Basavoju, S.; Bostrom, D.; Velaga, S. P., Indomethacin-saccharin cocrystal: Design, synthesis and preliminary pharmaceutical characterization. *Pharmaceutical Research* **2008**, 25 (3), 530-541.
80. NCBI National center for biotechnological information, which can be accessed electronically through Web (<https://pubchem.ncbi.nlm.nih.gov>).
81. A. Martin; P. L. Wu; Beerbower, A., Expanded Solubility Parameter Approach II: P-Hydroxybenzoic Acid and Methyl P-Hydroxybenzoate in Individual Solvents. *Journal of Pharmaceutical Sciences* **1984**, 73 (2), 188-194.



# **Chapter 6**

# **Publications**





Contents lists available at ScienceDirect

The Journal of Supercritical Fluids

journal homepage: [www.elsevier.com/locate/supflu](http://www.elsevier.com/locate/supflu)

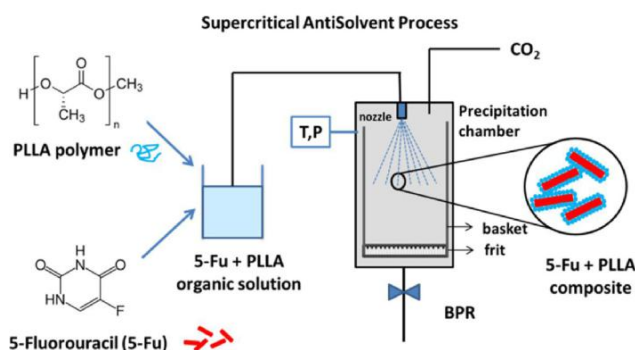
## Preparation of 5-fluorouracil microparticles and 5-fluorouracil/poly(L- lactide) composites by a supercritical CO<sub>2</sub> antisolvent process

Isaac A. Cuadra, Fouad Zahran<sup>1</sup>, Daniel Martín, Albertina Cabañas, Concepción Pando\*

Departamento de Química Física, Universidad Complutense, E-28040 Madrid, Spain



### GRAPHICAL ABSTRACT



### ARTICLE INFO

#### Keywords:

5-Fluorouracil  
Supercritical CO<sub>2</sub>  
Poly(L-lactide)  
Supercritical antisolvent  
Controlled delivery

### ABSTRACT

Microparticles of the anticancer drug 5-fluorouracil (5-Fu) were successfully prepared by supercritical anti-solvent (SAS) precipitation using dimethylsulfoxide as solvent. The effect on particle size (PS) of the experiment parameters was studied. The conditions of temperature and pressure were the most important factors. Mean PS values ranged from 220 to 670 nm. Using as solvent a dimethylsulfoxide + dichloromethane mixture, the SAS process was also used to obtain composite particles in which 5-Fu crystals are coated by a layer of poly(L-lactide) spheres. The particle morphology was studied by SEM. Other characterization included powder X-ray diffraction, DSC, TGA, and the measurement of the dissolution profiles. The composite particles were shown to provide a controlled delivery system.

### 1. Introduction

Particle technology is a key factor in the production of pharmaceuticals. Thus, the micronization of pharmaceuticals facilitates the use of a more appropriate or more convenient administration route, the reduction of the dosage and/or the increase of the drug bioavailability. On the other hand, the pharmaceutical properties may be also improved if microspheres or microcapsules containing the active pharmaceutical

ingredient (API) and a carrier are prepared. The carrier may ease the dissolution of poorly water-soluble drugs or may enable a controlled delivery of the API in the targeted media. Conventional micronization techniques such as spray drying, freeze drying or milling very often require operation at temperatures that can denature heat sensitive compounds, lead to broad size distributions or require additional processing to remove the solvents. In the last years, the application of supercritical fluids has resulted in several technologies that overcome

\*Corresponding author at: Departamento de Química Física, Facultad CC. Químicas, Universidad Complutense, E-28040 Madrid, Spain.

E-mail address: [pando@quim.ucm.es](mailto:pando@quim.ucm.es) (C. Pando).

<sup>1</sup> Permanent address: Chemistry Department, Faculty of Science, Helwan University, El Cairo, Egypt.

<https://doi.org/10.1016/j.supflu.2018.07.027>

Received 13 July 2018; Received in revised form 26 July 2018; Accepted 27 July 2018

Available online 02 August 2018

0896-8446/© 2018 Elsevier B.V. All rights reserved.

the limitations of the micronization techniques based on liquid solvents [1–3]. Recently, Esfandiari [4] has reviewed those used to obtain pure APIs while Pando et al. [5] have revised those employed to prepare pharmaceutical co-crystals. Carbon dioxide is the most commonly used supercritical fluid because it is nontoxic, non-flammable and has moderate critical temperature and pressure (31 °C and 7.4 MPa). Supercritical fluids densities and solvation power are intermediate between those of gases and liquids and can be easily modified with small changes in temperature and pressure; meanwhile the fluid maintains good transport properties. Thanks to these unique properties, supercritical carbon dioxide (scCO<sub>2</sub>) may act as a solvent, as an antisolvent or as a molecular mobility enhancer allowing the development of different processes and applications. A pressure reduction after scCO<sub>2</sub> treatment allows the preparation of solvent-free pharmaceuticals. Other advantages are operation at moderate temperature in a fairly inert atmosphere thus avoiding the product degradation and the reduction of steps in the production process thus enabling a better control. Micro and nanoparticles with narrow size distributions have been obtained for pure materials and composites [2–5]. Many examples can be found about substantially improving the pharmacological properties of existing compounds using these techniques [6–11]. Nevertheless, the great attention paid to the use of scCO<sub>2</sub> is based on its sustainable and environmentally friendly characteristics. Besides being nontoxic, non-flammable and fairly inert, scCO<sub>2</sub> is also cheap and readily available either as a byproduct in ammonia synthesis or from atmosphere. This is very appealing for pharmaceutical companies that are urged to develop production processes with low environmental impact, fewer steps and a reduced use of organic solvents.

The aim of this paper is the preparation of two types of pharmaceutical microparticles, those formed by the pure drug 5-fluorouracil (5-fluoro-1H-pyrimidine-2,4-dione, 5-Fu, a pyrimidine analog drug widely used in the treatment of several types of cancer) [12], and the composite particles formed by 5-Fu and poly(L-lactide) (PLLA). In both cases a supercritical antisolvent (SAS) process is used [11]. The molecular structures of 5-Fu and PLLA are shown in Fig. 1 together with a scheme of the SAS method. This approach is based on the relatively low solvent power of CO<sub>2</sub> for solutes such as pharmaceuticals and its good miscibility with many organic solvents. Either the drug alone or both the drug and the carrier material are dissolved in the organic solvent. When the solution is mixed with scCO<sub>2</sub> in a precipitation chamber, CO<sub>2</sub>

acts as an antisolvent and the solute precipitates as solvent-free micro and nanoparticles. The CO<sub>2</sub> + organic solvent mixtures thus formed are led to a separation chamber where the solvent is recovered. Prior to particle collection, the precipitation chamber is washed with pure CO<sub>2</sub> to assure that the residual organic solvent is removed from the pre-precipitate. The particle size and/or morphology are controlled by varying the process parameters such as temperature, pressure, solute concentration, etc.

5-Fu acts as an anticancer drug in several ways, mainly as a thymidylate synthase inhibitor. By interrupting the action of this enzyme, 5-Fu blocks the synthesis of the pyrimidine thymidine, which is a nucleotide required by the cancerous cells for DNA replication [12]. The drug is usually given orally or intravenously (due to its poor water solubility), but can also be applied as an ointment, especially in the case of skin cancer [13] or in dose inhalers or nebulizers and dry powder formulations in the case of lung cancer [14]. The direct delivery of 5-Fu in an aerosol therapy or an ointment is benefited by the drug micronization. On the other hand, intravenous administration of 5-Fu is improved if the drug is embedded or encapsulated in a biodegradable polymeric matrix that provides a controlled delivery system. This allows a better control of dosage and the reduction of side effects [15,16]. To this end, PLLA is an appropriate choice because of its biocompatibility and biodegradability.

5-Fu is a good candidate for SAS micronization because it is soluble in a variety of solvents highly soluble in scCO<sub>2</sub> such as methanol, acetone, dichloromethane (DCM) and dimethylsulfoxide (DMSO) while it is scarcely soluble in the supercritical fluid. Several authors [17–19] have measured the solubilities of 5-Fu in scCO<sub>2</sub> at pressures ranging from 10 to 30 MPa and temperatures ranging from 35 to 55 °C and found them to vary from 10<sup>-6</sup> to 10<sup>-5</sup> in mole fraction. Kalantarian et al. [20] prepared by SAS 5-Fu microparticles using as solvents methanol or binary mixtures formed by methanol and DCM, acetone or ethanol and studied the influence of the solvent in the SAS micronization. As to the polymer, PLLA microparticles can be also successfully obtained by this method [21,22]. Although SAS processed PLLA microparticles have been later impregnated with 5-Fu [22], the SAS co-precipitation of 5-Fu and PLLA has not been attempted so far. In this paper the SAS method is used in the first place to obtain 5-Fu microparticles using dimethylsulfoxide and examining the influence of the SAS process parameters such as temperature and pressure. Next, 5-Fu-

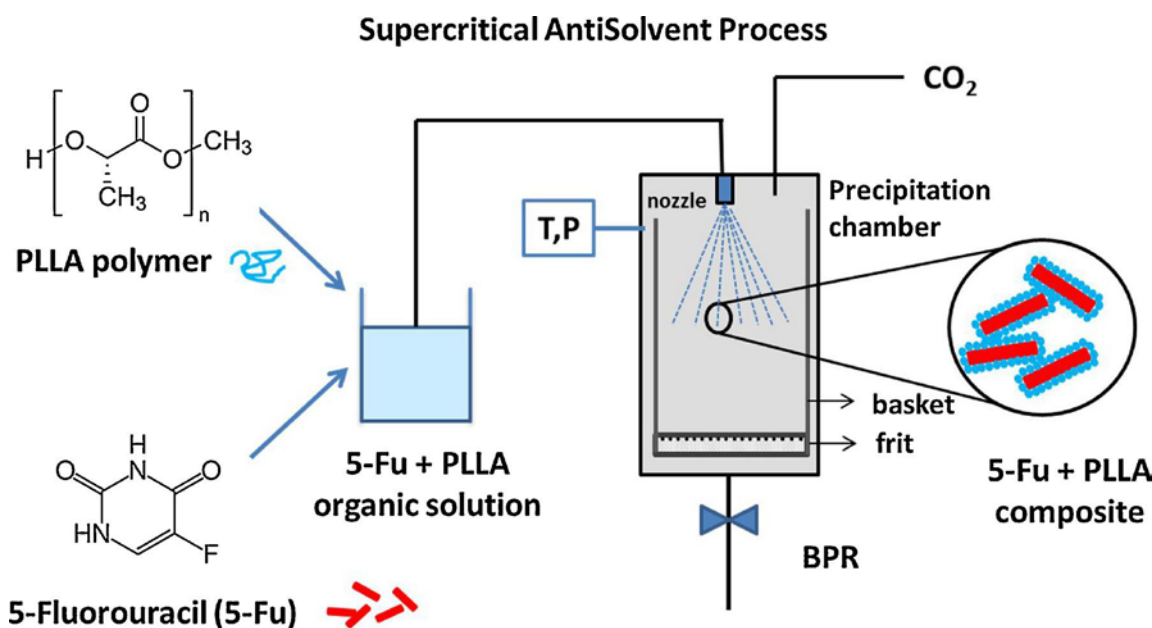


Fig. 1. Molecular structures of 5-Fu and PLLA and schematic representation of the supercritical fluid antisolvent (SAS) micronization technique used to obtain 5-Fu-PLLA composites.

PLLA composites are prepared. In this case, due to the low solubility of PLLA in DMSO a mixture of the organic solvents DCM and DMSO is required.

## 2. Materials and methods

### 2.1. Materials

The materials employed were CO<sub>2</sub> (Air Liquide 99.98 mol% pure), 5-Fu (Sigma-Aldrich ≥ 99 mol % pure), poly(L-lactide) (Sigma-Aldrich, T<sub>g</sub> 60–65 °C), dimethylsulfoxide, DMSO, (Fluka ≥ 99.9 mol % pure), and dichloromethane, DCM, (Scharlau, ≥ 99.8 mol % pure). All water used was pretreated using the Milli-Q Elix water purification system (Millipore Ibérica, Madrid, Spain).

### 2.2. Supercritical fluid antisolvent (SAS) micronization and design of experiments (DOE)

The schematic diagram for the laboratory scale SAS apparatus, its validation, and details about this apparatus and the experimental procedure may be found elsewhere [10]. Supercritical carbon dioxide is introduced in the precipitation chamber using a high-pressure pump at constant flow rate. Then the solvent or directly the organic solution containing the drug is sprayed in the precipitation chamber through a small stainless steel nozzle also at a constant flow rate reaching steady state operating conditions and a given supercritical fluid/solvent ratio. The chamber is heated and both temperature and pressure are controlled. When the fluid dissolves in the solution, the mixture becomes supersaturated and precipitation starts. The solute is collected at the bottom and the walls of the precipitation chamber. At the end of the precipitation process, the chamber is washed with the antisolvent to eliminate the liquid solvent. The CO<sub>2</sub> + organic solvent mixture is introduced into a chamber provided with a cyclone separator where solvent is recovered. The factors to be considered in the SAS process are: the concentration of the solution (C), the temperature (T), the pressure (P), the solution flow rate (Q<sub>L</sub>), the supercritical CO<sub>2</sub> flow rate (Q<sub>CO2</sub>), the drying time (t), and the nozzle diameter (Ø<sub>n</sub>). In this study, the drying time and the nozzle diameter were kept constant at 3 times the time required to fill the precipitation chamber and 100 µm, respectively. SAS experiments described in this paper were carried out at flow rates of 1.0–1.4 mL/min and 15–20 g/min for solution and CO<sub>2</sub>, respectively. These values were chosen to obtain CO<sub>2</sub> mole fractions ≥ 0.96 by combining values for the flow rates of the two pumps. In most cases the concentration of solutes in the organic solutions was 1 or 2 g per 100 mL. The temperature and pressure conditions are usually chosen to make sure that precipitation takes place in the supercritical region or near above the mixture critical point where nanoparticles and microparticles are produced, respectively [23]. In the case of the pure 5-Fu SAS micronization this would require the knowledge of the ternary phase equilibria for the CO<sub>2</sub> + DMSO + 5-Fu system. Although DMSO is a solvent frequently used in SAS, ternary data are available only for a few systems. Usually, it is assumed that the solute presence does not modify the phase behaviour and temperature and pressure conditions are chosen taken into account data for the binary CO<sub>2</sub> + organic solvent system [24]. Choosing cefonicid as a model solute, Campardelli et al. [25] have shown that this assumption is valid at low temperatures (40 °C) and low concentrations (up to 9 g per 100 mL) for the ternary system CO<sub>2</sub> + DMSO + cefonicid. However, large modifications are observed at 60 °C. The phase behaviour becomes more complex in the case of the composite materials because of the PLLA interaction with CO<sub>2</sub> and the use of a mixture of solvents. In this case, temperature and pressure conditions are chosen taking into account the critical loci of the two binary systems CO<sub>2</sub> + DMSO and CO<sub>2</sub> + DCM.

In order to minimize the number of experiments in the micronization of 5-Fu, the Design of Experiments (DOE) approach was used. A detailed description of the factorial fractional design of experiments can

be found in Refs. [26,27]. The factors that could have effects on particle size were C, T, P, Q<sub>L</sub>, and Q<sub>CO2</sub>. Two levels were used for each factor based on process limits and previous work. From among all the possible designs for five factors at two levels, the factorial fractional design 2<sup>5-2</sup> was applied to separate the important effects from the unimportant ones. As a result, eight different combinations of signs for the five factors were created. Particle size of the micronized material was chosen as a response to evaluate the process performance.

The main effect (contrast, *l<sub>i</sub>*) of each factor on particle size was calculated as follows:

$$l_i = \frac{1}{N_+} \sum y_+ - \frac{1}{N_-} \sum y_-$$

where *N<sub>+</sub>* and *N<sub>-</sub>* are the number of runs at high level and low level, respectively, and *y<sub>+</sub>* and *y<sub>-</sub>* are the response value at high level and low level, respectively.

### 2.3. Materials characterization

A JEOL-6400 scanning electron microscope (SEM) working at 10 kV was used to characterize the 5-Fu microparticles and the 5-Fu-PLLA composites obtained in the SAS experiments. Prior to analysis, samples were gold coated. The primary particle size distributions were obtained by counting the particles of different sizes in an electron microscope image using the SEMAFORCE program [28]. Values for the standard deviation (SD) were obtained from these distributions. Particle size (PS) was estimated as the equivalent spherical diameter. The mean particle size was obtained considering all the particles that have a definite surface present in the high-resolution SEM image (an average of 100 particles or even more). Energy-dispersive Detection X-ray analysis (EDX) was conducted on the composite samples using the SEM microscope.

Powder X-ray diffraction (XRD) was used to establish the degree of crystallinity and the polymorphic form of the materials. XRD patterns of the solids prior and after micronization were obtained using a Philips X'pert, model MPD powder diffraction system. The X-ray source was nickel-filtered Kα emission of copper (1.541837 Å). Samples were scanned over the range of 10–50 2θ degrees using the Bragg-Brentano geometry.

Differential Scanning Calorimetry (DSC) and Thermogravimetric Analysis (TGA) studies were carried out using a simultaneous DSC and TGA device, a Delta Series TA-SDT Model Q-600 apparatus, in nitrogen atmosphere using open aluminum crucibles.

### 2.4. Dissolution profiles

The dissolution profile of the 5-Fu samples was followed using a UV/VIS Perkin-Elmer spectrophotometer model Lambda 35 at 265 nm. Approximately, 20 mg of the sample was suspended in 5 mL of a pH 7.4 phosphate buffer medium (0.01 M phosphate buffer) supplied by Sigma-Aldrich and placed into a pretreated dialysis bag (molecular weight cut-off is 12,000). Then the bag was introduced into a flask containing 250 mL of the buffer solution and incubated at 37 °C and 50 rpm speed. Aliquots of 1 mL were taken at time intervals and were analyzed for the drug content by UV/VIS. The volume of the solution was kept constant by adding 1 mL of the phosphate buffer solution each time that samples were withdrawn.

## 3. Results and discussion

### 3.1. Micronization and characterization of 5-Fu

Dimethylsulfoxide was chosen as a solvent for the micronization of 5-Fu. Table 1 shows the low and high level values for the five factors used in the DOE: solution concentration, temperature, pressure, solution flow rate and CO<sub>2</sub> flow rate. As explained in the Experimental



**Table 1**  
Level identification of the DOE factors.

Factor	Unit	Symbol	Low level (-)	High level (+)
Concentration	g/100 mL	C	1.0	2.0
Temperature	°C	T	40	50
Pressure	MPa	P	15.0	18.0
Solution flow rate	mL/min	QL	1.0	1.4
CO <sub>2</sub> flow rate (x ≥0.96)	g/min	Q <sub>CO2</sub>	15	20

**Table 2**  
The fractional factorial 2<sup>5-2</sup> design of experiments with response and con-trast.<sup>a</sup>

Experiment	C (1)	T (2)	P(3)	QL	Q <sub>CO2</sub>	Response <sup>b</sup>	
						Mean PS (nm)	SD (nm)
1	-	-	-	+	+	510	170
2	+	-	-	-	-	670	220
3	-	+	-	-	+	-	-
4	+	+	-	+	-	-	-
5	-	-	+	+	-	580	180
6	+	-	+	-	+	580	170
7	-	+	+	-	-	220	65
8	+	+	+	+	+	440	130
Main effect, contrast, I <sub>i</sub>							
PS, nm	94.5	-420.5	157	15	13.5		

<sup>a</sup> The values for the low level and high level of solution concentration (C), temperature (T), pressure (P), solution flow rate (QL) and supercritical CO<sub>2</sub> flow rate (Q<sub>CO2</sub>) are given in Table 1.

<sup>b</sup> PS: particle size; SD: standard deviation.

Section, the two levels of temperature and pressure were chosen mainly on the basis of isothermal vapor–liquid equilibrium and critical data for CO<sub>2</sub> + DMSO [24]. Flow rate limits were chosen to obtain CO<sub>2</sub> mole fractions ≥ 0.96, in the carbon dioxide- rich region. The low level of concentration was set to obtain a sufficient amount of precipitate for subsequent analysis; the high level was limited by the saturation of the solutions at room temperature.

The mean particle size and particle morphology obtained from SEM images were used as a response to evaluate the process performance. Table 2 shows the eight combinations of signs resulted from the application of the fractional factorial design 2<sup>5-2</sup> (experiments 1–8) together with the mean particle size and standard deviation (SD). The main effect (contrast, I<sub>i</sub>) is also shown in Table 2. The main effect may adopt positive or negative values. A positive value means it has a positive effect on the process performance while a negative value means it has a negative effect. The alias structure that determines which effects are confounded with each other was generated using the MINITAB 15 SOFTWARE [29] and was simplified by neglecting three order and higher interactions. For screening purposes, the interactions between two factors were also considered negligible [27], so the effect value I<sub>i</sub> is caused only by the main factor, by other words, concentration for column 1, temperature for column 2, and so on.

Fig. 2 shows the SEM images of 5-Fu commercial powder. Particles of untreated 5-Fu are greater than 10 μm and exhibit a wide distribution of sizes. As to the SAS micronized 5-Fu, the precipitation was successful in all the experiments and fluffy powders were obtained. Fig. 3 shows SEM images of SAS micronized 5-Fu. Good morphologies (small and nonaggregated particles of similar shape and size) are obtained in experiments 1, 2, 6 and 8. However, at the higher pressure and lower 5-Fu concentration both at 40 and 50 °C (experiments 5 and 7) the elongated particles were somewhat aggregated. On the other hand, much larger particles were obtained in experiments 3 and 4; these particles were not further characterized and for the sake of brevity their SEM images are not shown in Fig. 3. Table 3 lists values for the mean PS and SD. Elongated particles with a mean particle size in the range of

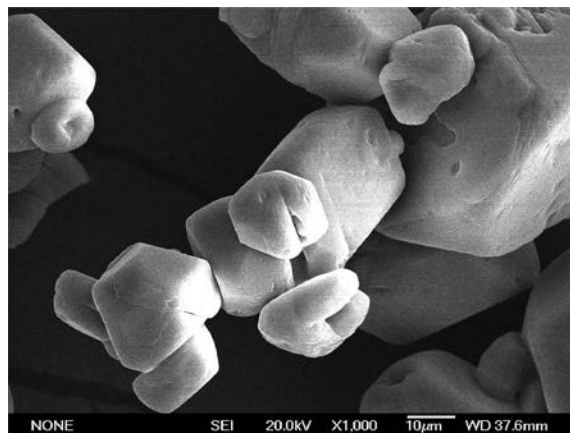


Fig. 2. SEM image of untreated 5-Fu.

220–670 nm and standard deviation within the range of 65–220 nm, respectively, were obtained in experiments 1, 2, 5, 6, 7 and 8.

Fig. 4 shows the effect of the different factors on the particle size. Three key factors with major effect on the particle size and morphology were identified. In order of decreasing importance, these are temperature, pressure and concentration. Taking into account the main effect of the five factors considered their order of importance can be summarized as follows

$$T > P > C >> QL > Q_{CO2}$$

If the influence of QL and Q<sub>CO2</sub> is neglected, the effect on particles size of the 5-Fu concentration in the liquid solution may be established by directly comparing the experiments in the pairs 1–2, 5–6, and 7–8. Particle size increases when the 5-Fu concentration is increased at a given temperature and pressure. In a similar way the temperature and pressure effects may be discussed by comparing the experiments in the pairs 1–3, 2–4, 5–7 and 6–8 (temperature) and the pairs 1–5, 2–6, 3–7 and 4–8 (pressure). However, these effects cannot be established through the direct comparison of pairs of experiments pointing out a binary P–T interaction. Therefore, we chose to compare simultaneously the eight experiments in terms of particle morphology and the response factor or mean PS: The smallest mean particle size (220 nm) was obtained in experiment 7. However, particles in this case appear aggregated in clusters almost 1 μm long. Therefore, best conditions for the 5-Fu micronization could be those of experiment 8: solution concentration, C = 1%, temperature, T = 50 °C, pressure P = 18 MPa, solution flow rate, QL = 1.4 mL/min, supercritical CO<sub>2</sub> flow rate, Q<sub>CO2</sub> = 20 g/min. In this experiment particles were 440 nm in average.

The crystallinity and polymorphic form of the microparticles obtained by SAS in this paper have been evaluated using X-ray diffraction powder. The XRD patterns of the untreated 5-Fu and 5-Fu obtained by SAS at 50 °C and 18.0 MPa using DMSO as solvent (experiment 8) and using a 1:1 v/v % DMSO + DCM mixture are shown in Fig. 5. This mixture of solvents was used to obtain the 5-Fu-PLLA composite as explained in Section 3.2. The XRD pattern of the untreated 5-Fu exhibits a very intense peak at 28.7 °. The high intensity of this peak suggests a preferred orientation of the untreated drug at this position. On the other hand, the preferred orientation is attenuated in the XRD pattern of the 5-Fu precipitated by SAS using the DMSO + DCM mixture and disappears when DMSO is used as solvent. This could be attributed to the decrease in crystal size due to SAS precipitation with respect to that of the untreated drug. On the other hand, 5-Fu is known to present two well characterized polymorphic forms [30]. The three XRD patterns shown in Fig. 5 correspond to form I; there is no change of the polymorphic form due to SAS treatment. This has been confirmed through differential scanning calorimetry performed using the TA-SDT apparatus model Q-600. The investigation was carried out over the

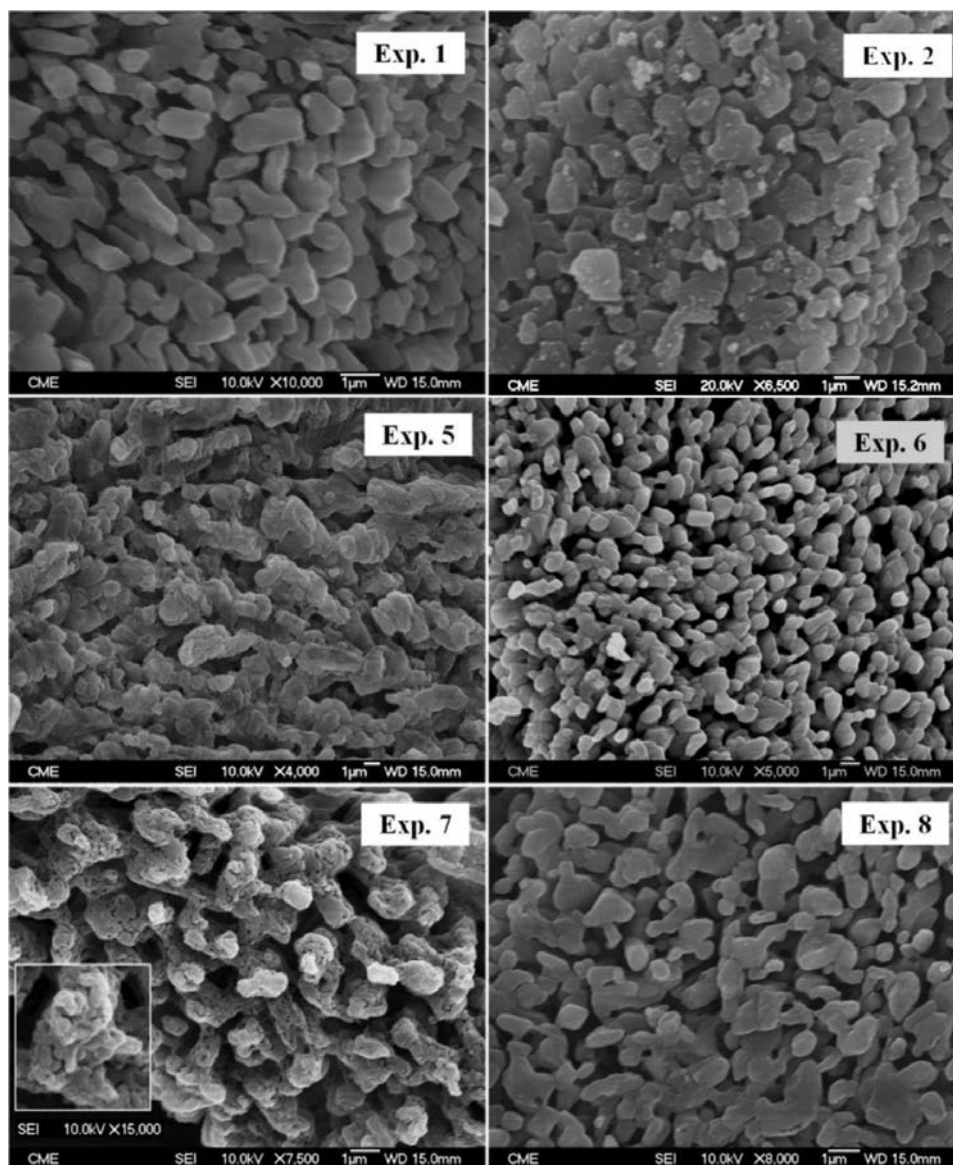


Fig. 3. SEM images of SAS processed 5-Fu. Conditions for SAS experiments are given in Tables 2 and 3.

Table 3

Temperature and pressure conditions for composite preparation using SAS and drug loading obtained.

Experiment	Temperature (°C)	Pressure (MPa)	Drug loading (% w)
9	35	12.0	35
10		18.0	32
11	50	12.0	42
12		18.0	36
13		25.0	18

temperature range 240–360 °C. The melting point was measured reading the onset temperature of the peak and a value of 283 °C corresponding to form I was observed.

Kalantarian et al. [20] micronized 5-Fu by SAS from methanol, methanol + dichloromethane, methanol + acetone, and methanol + ethanol mixtures. The other conditions of the experiments were fixed: a pressure of 10 MPa, a temperature of 40 °C, a solution flow rate of 1 mL/min, and CO<sub>2</sub> flow rate of 20 mL/min. Additionally a pressure of 15 MPa was used for methanol experiments. The particle morphology

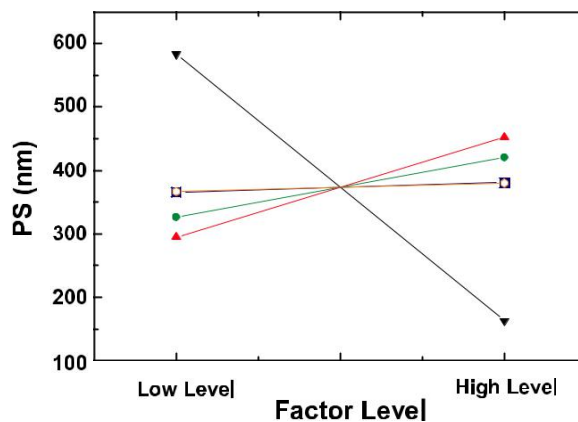


Fig. 4. Effect of temperature (▼, 40 and 50 °C), pressure (▲, 15.0 and 18.0 MPa), solution concentration (●, 1.0 and 2.0 g/100 mL), solution flow rate (■, 1.0 and 1.4 mL/min) and supercritical CO<sub>2</sub> flow rate (○, 15 and 20 g/min) on particle size for 5-Fu SAS micronization.

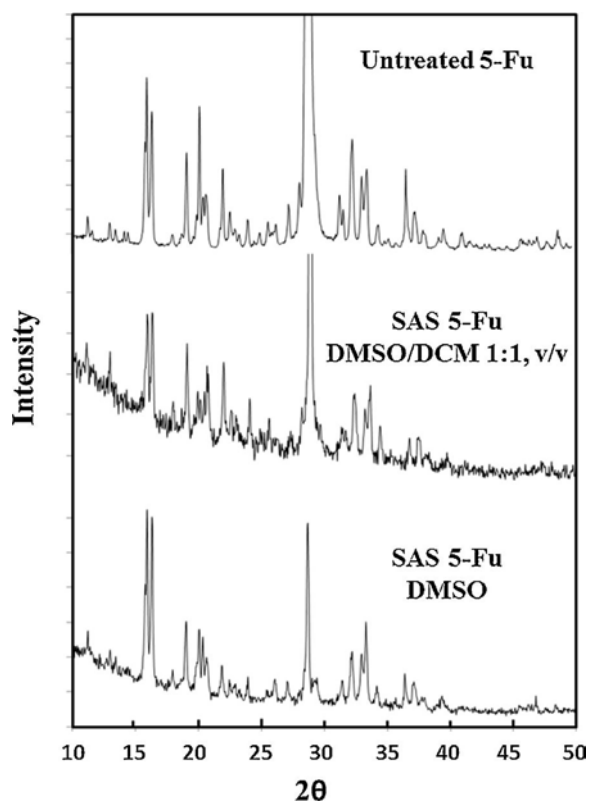


Fig. 5. XRD patterns of untreated 5-Fu and 5-Fu obtained by SAS at 50 °C and 18.0 MPa using DMSO as solvent (experiment 8) and using a 1:1 v/v % DMSO + DCM mixture.

was similar to that found in this study. Mean particle sizes changed significantly with the solvent used. The particles produced from methanol alone and methanol + ethanol mixtures had the biggest sizes (2000–5000 nm) while the particles produced from methanol + acetone had sizes of 730–980 nm and those produced from methanol + dichloromethane mixtures had the smallest sizes (250 to 440 nm). Our study shows that for a given solvent this range of particle sizes may be also attained if temperature, pressure and concentration are adequately chosen. A similar conclusion was reached for the gas antisolvent (GAS) process by Esfandiari and Ghoreishi [31]. On the other hand, 5-Fu microparticles with sizes lower than 500 nm were obtained by Chen et al. [32] through a solution enhanced dispersion by supercritical CO<sub>2</sub> (SEDS method) using a mixture of ethanol and DCM as solvent.

### 3.2. Micronization and characterization of 5-Fu-PLLA composites

The DOE approach was not used in the SAS micronization of the 5-Fu-PLLA composites because of the high number of parameters involved. On the other hand, due to the very low solubility of PLLA in DMSO, a mixture of a poor PLLA solvent (DMSO) and a good PLLA solvent (DCM), both miscible with supercritical CO<sub>2</sub>, was chosen. Gokhale et al. [33] have proposed to use such a mixture in the SAS micronization of pure polymers. The segments of the polymer molecule prefer to be surrounded by the good-solvent molecules (DCM) and the PLLA chain adopts a swollen conformation to maximize contacts between the PLLA segments and DCM. However, the polymer molecule segments avoid contacts with the molecules of the poor solvent (DMSO) and the PLLA chain adopts a compact conformation to minimize contacts between the PLLA segments and acetone. The variation in the solvent ratio provides an effective method to control and manipulate the polymer solubility and the conformation of the polymer molecules in the particles precipitating from the solution injected in the pre-precipitation chamber. Consequently, particle size and morphology may be controlled. At our laboratory we have shown that this is also an

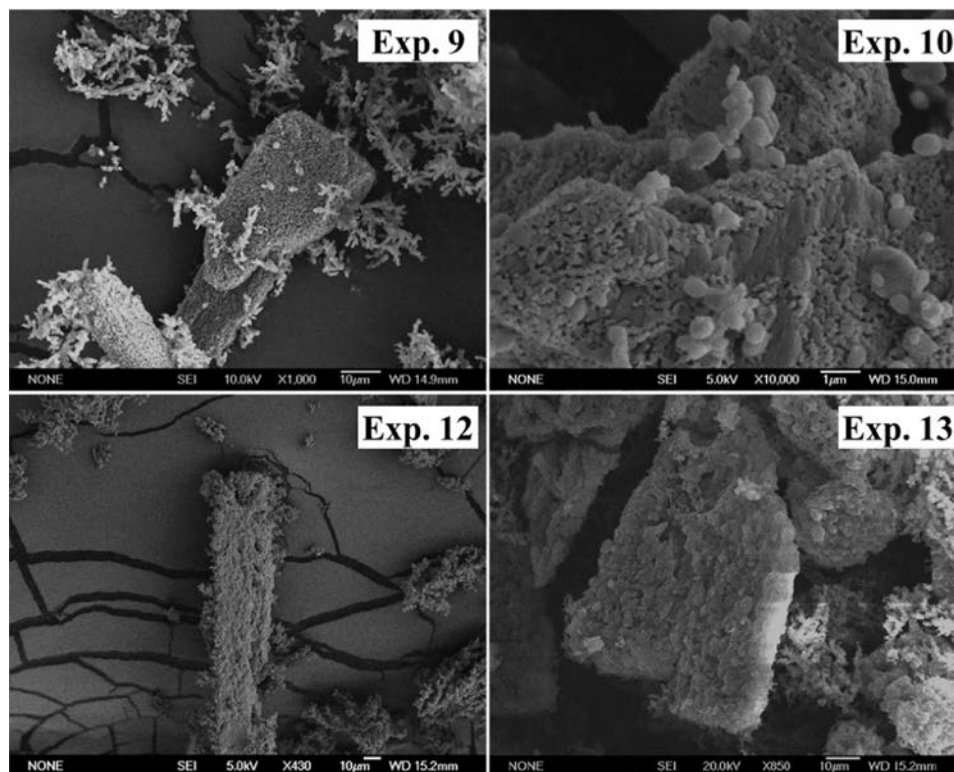


Fig. 6. SEM images of the 5-Fu-PLLA composites.

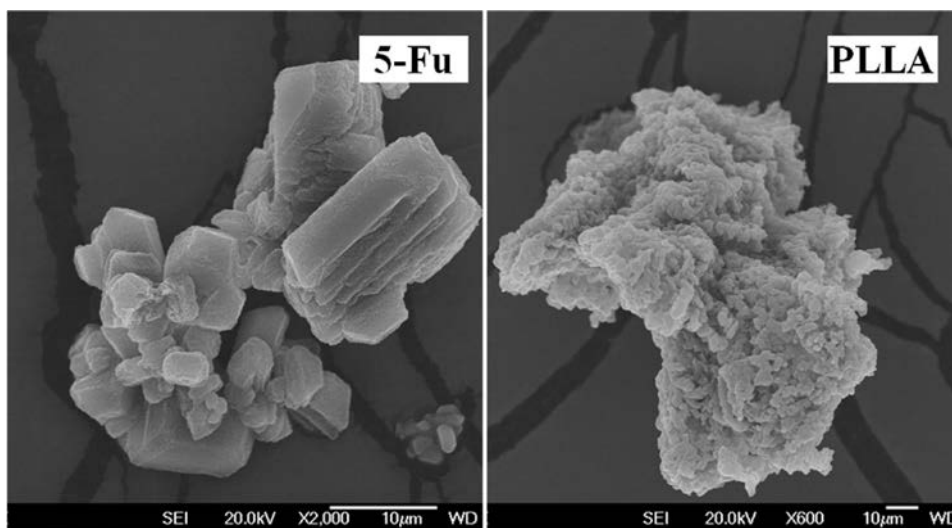


Fig. 7. SEM images of pure 5-Fu and PLLA processed by SAS at 50 °C and 18.0 MPa using as solvent a 1:1 v/v % DMSO + DCM mixture.

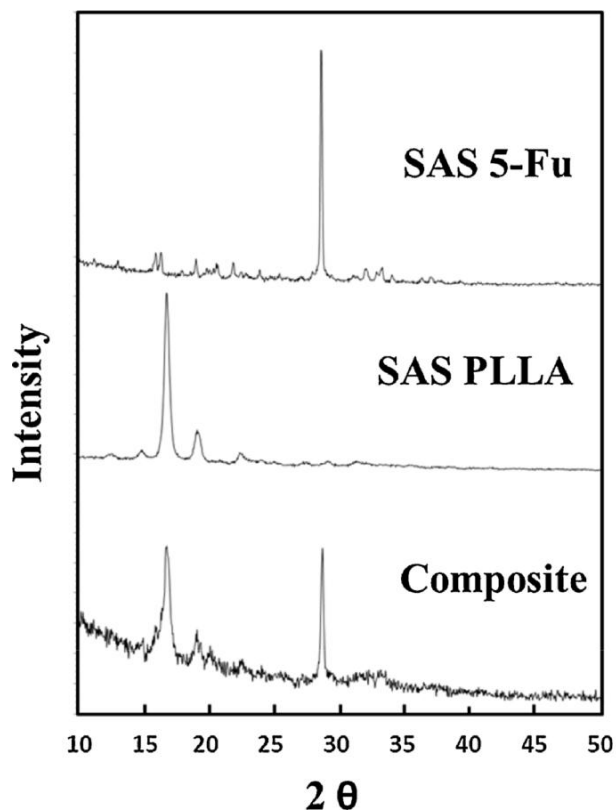


Fig. 8. XRD patterns of 5-Fu, PLLA, and the composite obtained by SAS at 50 °C and 18.0 MPa using as solvent a 1:1 v/v % DMSO + DCM mixture.

effective method when the polymer polyvinylpyrrolidone is coprecipitated by SAS together the anti-inflammatory drug diflunisal [10]. After several trials using different DMSO to DCM ratios a 1:1 v/v % DMSO + DCM mixture was chosen to carry out SAS experiments in this study.

As explained in the Experimental Section, conditions of temperature (35 and 50 °C) and pressure (120, 180 and 150 MPa) were chosen taking into account the critical loci of the two binary systems CO<sub>2</sub> + DMSO and CO<sub>2</sub> + DCM [24,34–36]. The other experimental conditions were solution concentrations of 5 mg/mL for both 5-Fu and PLLA, 1 mL/min solution flow rate, and 20 g/min CO<sub>2</sub> flow rate. The liquid and CO<sub>2</sub> flow rates lead to a value of 0.97 for the CO<sub>2</sub> mole fraction in

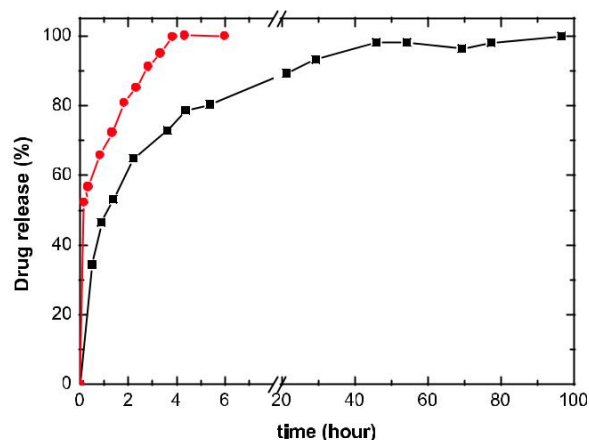


Fig. 9. Dissolution profiles of the pure drug (●) and the 5-Fu-PLLA composite obtained at 50 °C and 18.0 MPa (■).

the mixtures formed in the precipitation chamber. Temperature and pressure conditions and drug loadings determined through thermo-gravimetric analysis are shown in Table 3. 5-Fu loadings were estimated from the mass loss between 100 and 285 °C. Decomposition of PLLA took place from 285 to 370 °C and did not overlap with 5-Fu decomposition. Drug loading for composites obtained at 35 or 50 °C and 12.0 and 18.0 MPa varied from 32 to 42% in mass. The composite obtained at 50 °C and a higher pressure (25.0 MPa) exhibited a much lower loading (18%) Thermogravimetric analysis of our samples was repeated after five months. The samples were kept at ambient conditions and no significant differences were observed in the TGA curves thus showing the composite material stability. SEM images of the composite materials are shown in Fig. 6. Large crystals of 5-Fu (lengths range from 10 to over 100 μm) are coated by a layer of smaller PLLA spheres whose diameters range from 600 nm at 35 °C to 1200 nm at 50 °C (values for the standard deviation are 200 and 300 nm, respectively). EDX analysis confirmed the different chemical composition of the two morphologies and the complete removal of DMSO and DCM. Large crystals of 5-Fu coated by polymer were also obtained by Kalantarian et al. [37] using the GAS and SAS processes, poly(lactide-co-glycolide) (PLGA) as polymer, acetone or methanol + DCM mixtures as solvents, and temperatures and pressures similar to those of this study.

Since the best pressure and temperature conditions for SAS precipitation of 5-Fu using DMSO were 50 °C and 18.0 MPa, for comparison purposes the composite obtained in experiment 12 was chosen for

further characterization and the pure PLLA and the pure 5-Fu were processed by SAS at the conditions of this experiment (50 °C and 18.0 MPa, a 1:1 v/v % DMSO + DCM mixture as solvent, 1 mL/min solution flow rate, and 20 g/min CO<sub>2</sub> flow rate). A solution con-centration of 10 mg/mL was used. SEM images of the SAS processed pure PLLA and 5-Fu are shown in Fig. 7. 5-Fu particles are bigger than those obtained in experiments 1, 2, and 5–8 using DMSO. It is con-firmed that the solvent plays a key role in the particle size. The polymer particles are much smaller and show aggregation. Fig. 8 shows the XRD patterns for pure 5-Fu, pure PLLA and the composite material obtained at the conditions of experiment 12. As could be expected the composite material pattern is a combination of those of 5-Fu and PLLA.

The dissolution profiles of 5-Fu and the composite material obtained at 50 °C and 18.0 MPa are shown in Fig. 9. Thanks to the PLLA coating, the cumulative release rates of the composite are much slower than those of the pure drug. A burst release is observed for the controlled delivery system in the first hour (37%) followed by a moderate release in the next four hours. A sustained release is reached so that the 100% release requires more than four days. The burst release could decrease if the drug loadings were reduced; nevertheless the dissolution profile is similar to those reported for other 5-Fu controlled delivery systems. The release process is controlled by both polymer erosion and drug diffusion [38,39]. The relationship between drug release and time is linear for systems controlled by polymer erosion whereas a parabolic curve is obtained for systems controlled by drug diffusion. Polymers having erosion controlled properties provide a short release time (less than 8 h) and are not adequate for controlled delivery purposes. Since PLLA degrades very slowly, a parabolic curve is obtained for our composites and for most of the 5-Fu delivery systems previously prepared thus in-dicating that the goal of controlled delivery is reached.

#### 4. Conclusions

5-Fu microparticles were successfully prepared by SAS microniza-tion using DMSO as solvent. The mean particle size ranged from 220 to 670 nm and could be varied by modifying the experiment parameters. The conditions of temperature and pressure were the most important factors. Using a DMSO + DCM mixture as organic solvent, the SAS process was also used to obtain composite particles in which 5-Fu crystals were coated by a layer of PLLA spheres. These composite par-ticles were shown to provide a controlled delivery system: the release rate was substantially reduced with respect to that of the pure drug.

#### Acknowledgements

We gratefully acknowledge the financial support of the Spanish Ministry of Science and Innovation (MICINN), research project CTQ2013-41781-P. F. Z. thanks the E. U. for its support through an Erasmus Mundus University II predoctoral grant. We appreciate the help of Prof. J.A.R. Cheda and Dr. M. Ramos in the materials char-acterization.

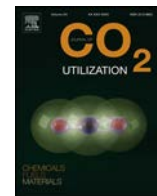
#### References

- [1] A. Martín, M.J. Cocero, Micronization processes with supercritical fluids: fundamentals and mechanisms, *Adv. Drug Deliv. Rev.* 60 (2008) 339–350.
- [2] I. Pasquali, Bettini R, F. Giordano, Supercritical fluid technologies: an innovative approach for manipulating the solid-state of pharmaceuticals, *Adv. Drug Deliv. Rev.* 60 (2008) 399–410.
- [3] R. Campardelli, L. Baldino, E. Reverchon, Supercritical fluids applications in nanomedicine, *J. Supercrit. Fluids* 101 (2015) 193–214.
- [4] N. Esfandiari, Production of micro and nano particles of pharmaceutical by supercritical carbon dioxide, *J. Supercrit. Fluids* 100 (2015) 129–141.
- [5] C. Pando, A. Cabañas, I.A. Cuadra, Preparation of pharmaceutical co-crystals through sustainable processes using supercritical carbon dioxide: a review, *RSC Adv.* 6 (2016) 71134–71150.
- [6] M.J. Cocero, A. Martín, F. Mattea, S. Varona, Encapsulation and co-precipitation processes with supercritical fluids: fundamentals and applications, *J. Supercrit. Fluids* 47 (2009) 546–555.

- [7] B.S. Sekhon, Supercritical fluid technology: an overview of pharmaceutical applications, *Int. J. Pharmtech Res.* 2 (2010) 810–826.
- [8] E. Elizondo, J. Veciana, N. Ventosa, Nanostructuring molecular materials as particles and vesicles for drug delivery using compressed and supercritical fluids, *Nanomedicine* 7 (2012) 1391–1408.
- [9] R. Adami, S. Liparoti, G. Della Porta, P. Del Gaudio, E. Reverchon, Lincomycin hydrochloride loaded albumin microspheres for controlled drug release, produced by supercritical assisted atomization, *J. Supercrit. Fluids* 119 (2017) 203–210.
- [10] F. Zahran, A. Cabañas, J.A.R. Cheda, J.A.R. Renuncio, C. Pando, Dissolution rate enhancement of the anti-inflammatory drug diflunisal by coprecipitation with a biocompatible polymer using carbon dioxide as a supercritical fluid antisolvent, *J. Supercrit. Fluids* 88 (2014) 56–65.
- [11] V. Prosapio, I. De Marco, E. Reverchon, Supercritical antisolvent coprecipitation mechanisms, *J. Supercrit. Fluids* 138 (2018) 247–258.
- [12] D.B. Longley, D.P. Harkin, P.G. Johnston, 5-Fluorouracil: mechanisms of action and clinical strategies, *Nat. Rev. Cancer* 3 (2003) 330–338.
- [13] C.M. Perrett, J.M. McGregor, J. Warwick, P. Karran, I.M. Leigh, C.M. Proby, C.A. Harwood, Treatment of post-transplant premalignant skin disease: a randomised intrapatent comparative study of 5-fluorouracil cream and topical photo-dynamic therapy, *Br. J. Dermatol.* 156 (2007) 320–328.
- [14] M.M. Bailey, C.J. Berkland, Nanoparticle formulations in pulmonary drug delivery, *Med. Res. Rev.* 29 (2009) 196–212.
- [15] A.S. Hasan, M. Socha, A. Lamprecht, F. El Ghazouani, A. Sapin, A. Hoffman, P. Malignant, N. Ubrich, Effect of microencapsulation of nanoparticles on the reduction of burst release, *Int. J. Pharm.* 344 (2007) 53–61.
- [16] H. Zhang, J. Bei, S. Wang, Preparation and drug release behaviors of 5-fluorouracil loaded poly(glycolide-co-lactide-co-caprolactone) nanoparticles, *J. Appl. Poly. Sci.* 106 (2007) 3757–3767.
- [17] O. Guney, A. Akgerman, Solubilities of 5-fluorouracil and  $\beta$ -estradiol in supercritical carbon dioxide, *J. Chem. Eng. Data* 45 (2000) 1049–1052.
- [18] D. Suleiman, L.A. Estévez, J.C. Pulido, J.E. García, C. Mojica, Solubility of anti-inflammatory, anti-cancer, and anti-HIV drugs in supercritical carbon dioxide, *J. Chem. Eng. Data* 50 (2005) 1234–1241.
- [19] S. Zhan, Q. Zhao, S. Chen, J. Wang, Z. Liu, C. Chen, Solubility and partition coefficients of 5-fluorouracil in ScCO<sub>2</sub> and ScCO<sub>2</sub>/poly(L-lactic acid), *J. Chem. Eng. Data* 59 (2014) 1158–1164.
- [20] P. Kalantarian, A.R. Najafabadi, I. Haririan, A. Vatanara, Y. Yamini, M. Darabi, K. Gilani, Preparation of 5-fluorouracil nanoparticles by supercritical antisolvents for pulmonary delivery, *Int. J. Nanomed.* 5 (2010) 763–770.
- [21] C. Chen, S. Zhan, M. Zhang, Z. Liu, Z. Li, Preparation of poly(L-lactide) micro-particles by a supercritical antisolvent process with a mixed solvent, *J. Appl. Polym. Sci.* 124 (2012) 3744–3750.
- [22] S. Zhan, C. Chen, Q. Zhao, W. Wang, Z. Liu, Preparation of 5-Fu-loaded PLLA microparticles by supercritical fluid technology, *Ind. Eng. Chem. Res.* 52 (2013) 2852–2857.
- [23] E. Reverchon, I. De Marco, Mechanisms controlling supercritical antisolvent precipitate morphology, *Chem. Eng. J.* 169 (2011) 358–370.
- [24] F. Zahran, J. Morère, A. Cabañas, J.A.R. Renuncio, C. Pando, Role of excess molar enthalpies in supercritical antisolvent micronizations using dimethylsulfoxide as the polar solvent, *J. Supercrit. Fluids* 60 (2011) 45–50.
- [25] R. Campardelli, E. Reverchon, I. De Marco, Dependence of SAS particles morphologies on the ternary phase equilibria, *J. Supercrit. Fluids* 130 (2017) 271–273.
- [26] G.E.P. Box, W.G. Hunter, J.S. Hunter, Statistics for Experimenters. An Introduction to Design, Data Analysis and Model Building, second ed., Wiley, New York, 1993.
- [27] J. Antony, Design of Experiments for Engineers and Scientists, Elsevier Science & Technology Books, Butterworth-Heinemann, Amsterdam, 2003.
- [28] SEMAFORCE. Available from: <http://www.jeol.se/?page=sema4down>.
- [29] MINITAB 15 SOFTWARE. Available from: <http://www.minitab.com/en-US/products/minitab/free-trial.aspx?langType=1033>.
- [30] A.T. Hulme, S.L. Price, D.A. Tocher, A new polymorph of 5-fluorouracil found following computational crystal structure predictions, *J. Am. Chem. Soc.* 127 (2005) 1116–1117.
- [31] N. Esfandiari, S. Ghoreishi, Synthesis of 5-fluorouracil nanoparticles via supercritical gas antisolvent process, *J. Supercrit. Fluids* 84 (2013) 205–210.
- [32] A.-Z. Chen, X.-M. Pu, Y.-Q. Kang, L. Liao, Y.-D. Yao, G.-F. Yin, Preparation of 5-fluorouracil-poly(L-lactide) microparticles using solution-enhanced dispersion by supercritical CO<sub>2</sub>, *Macromol. Rapid Commun.* 27 (2006) 1254–1259.
- [33] A. Gokhale, B. Khusid, R.N. Dave, R. Pfeffer, Effect of solvent strength and operating pressure on the formation of submicrometer polymer particles in supercritical microfluids, *J. Supercrit. Fluids* 43 (2007) 341–356.
- [34] F.H. Vonderheiden, J.W. Eldridge, The system carbon dioxide-methylene chloride. Solubility, vapor pressure, liquid density, and activity coefficients, *J. Chem. Eng. Data* 8 (1963) 20–21.
- [35] J.T. Reaves, T.G. Aron, C.B. Roberts, Critical properties of dilute carbon dioxide + entrainer and ethane + entrainer mixtures, *J. Chem. Eng. Data* 43 (1998) 683–686.
- [36] A.V. González, R. Tufeu, P. Subra, High-pressure vapor–liquid equilibrium for the binary systems carbon dioxide + dimethyl sulfoxide and carbon dioxide + di-chloromethane, *J. Chem. Eng. Data* 47 (2002) 492–495.
- [37] P. Kalantarian, I. Haririan, A.R. Najafabadi, M.A. Shokrgozar, A. Vatanara, Entrapment of 5-fluorouracil into PLGA matrices using supercritical antisolvent processes, *J. Pharm. Pharmacol.* 63 (2011) 500–506.
- [38] C. Kim, Release kinetics of coated, donut-shaped tablets for water soluble drugs, *Eur. J. Pharm. Sci.* 7 (1999) 237–242.
- [39] S.B. Wang, A.Z. Chen, L.J. Weng, M.Y. Chen, X.L. Xie, Effect of drug-loading methods on drug load, encapsulation efficiency and release properties of alginate/ Poly-L-arginine/chitosan ternary complex microcapsules, *Macromol. Biosci.* 4 (2004) 27–30.



Contents lists available at ScienceDirect

Journal of CO<sub>2</sub> Utilizationjournal homepage: [www.elsevier.com/locate/jcou](http://www.elsevier.com/locate/jcou)

# Pharmaceutical co-crystals of the anti-inflammatory drug diflunisal and nicotinamide obtained using supercritical CO<sub>2</sub> as an antisolvent



Isaac A. Cuadra<sup>a</sup>, Albertina Cabañas<sup>a</sup>, José A.R. Cheda<sup>a</sup>, Francisco J. Martínez-Casado<sup>b</sup>,  
Concepción Pando<sup>a,\*</sup>

<sup>a</sup>Dpto. de Química Física I, Universidad Complutense, E-28040 Madrid, Spain

<sup>b</sup>MAX IV Laboratory, Lund University, Ole Römers väg 1, 223 63 Lund, Sweden

## ARTICLE INFO

### Article history:

Received 23 July 2015

Received in revised form 2 October 2015

Accepted 22 November 2015

Available online 1 December 2015

### Keywords:

Carbon dioxide

Pharmaceutical co-crystals

Supercritical antisolvent diflunisal

Nicotinamide

## ABSTRACT

A method based on using supercritical CO<sub>2</sub> as an antisolvent (SAS method) is explored as a co-crystallization technique. Co-crystallization is an emerging and powerful technique to improve the physicochemical properties of an active pharmaceutical ingredient. The solid-state and solution co-crystallization methods usually employed present several disadvantages. The one-step SAS method has a low environmental impact and overcomes some of the difficulties associated to conventional methods. The 2:1 co-crystals of the anti-inflammatory drug diflunisal (DIF) and nicotinamide (NIC) are prepared for the first time by SAS. Drug concentrations corresponding to the co-crystal stoichiometric composition are used. The influence of the SAS parameters temperature (35 and 40 °C), pressure (10.0 and 12.0 MPa), drug concentration (two levels) and solvent (acetone and ethanol) in the co-crystal formation is studied. A crystalline material in the form of needles of uniform width and more variable length is obtained. For comparison purposes, pure DIF and NIC are also processed by SAS. Co-crystals are characterized in terms of crystallinity, thermal behavior, coformer interactions and drug release; their dissolution rate improves with respect to that of pure DIF. SAS co-crystals exhibit the same crystal structure, melting point and FTIR spectrum as those previously obtained by liquid assisted ball mill grinding and solution crystallization.

© 2015 Elsevier Ltd. All rights reserved.

## 1. Introduction

A key issue in the field of pharmaceuticals is the improvement of the active pharmaceutical ingredient (API) physicochemical properties. To this end, co-crystallization is an emerging and powerful technique that enables to modify properties such as the solubility and chemical stability by establishing a new solid form through the interaction with a coformer [1]. Coformers are usually molecules included on the Generally Recognized as Safe (GRAS) list [2]. Nevertheless, in some cases pharmaceutical co-crystals consist

of two different APIs, thus providing new dual-drugs [3]. A co-crystal may be defined as a multiple component crystal that consists of two or more solid components in a definite stoichiometric ratio held together via noncovalent interactions. The co-crystal structure is the result of weak but directional molecular recognition events. Based on these interactions, crystal engineering provides strategies to search for new co-crystals of a given API. However, the discovery and preparation of a new co-crystal is still to a great extent a matter of trial and error [4,5]. As to the experimental methods, co-crystals can be prepared by solution methods, evaporative or cooling crystallization or solid-state grinding and mixing [5]. Solution co-crystallization is the method preferred if single crystals are desired for crystal structure elucidation although sometimes this method fails in the preparation of a co-crystal already obtained by a mechanochemical method. Phase solubility diagrams are required in order to understand the mechanism of a solution co-crystallization [5,6]. The solution initial composition plays a key role in the process. The different solubilities of the co-crystal components in the chosen solvent may pose a problem. Using a solvent mixture has been suggested to overcome this difficulty [7]. If the desired co-crystal is

*Abbreviations:* API, active pharmaceutical ingredient; BPR, back pressure regulator; C, solution concentration; DIF, diflunisal; DSC, differential scanning calorimetry; FTIR, Fourier transform infrared; GAS, gas antisolvent; GRAS, generally recognized as safe; NIC, nicotinamide; NSAID, non-steroidal anti-inflammatory drug; P, pressure; T, temperature; T<sub>m</sub>, melting point; SAS, supercritical antisolvent; SEM, scanning electron microscopy; XRD, X-ray diffraction.

\* Corresponding author at: Departamento de Química Física I, Facultad C. Químicas, Universidad Complutense, E-28040 Madrid, Spain. Fax: +34 91394 4135.

E-mail addresses: [a.cabanas@quim.ucm.es](mailto:a.cabanas@quim.ucm.es) (A. Cabañas), [cheda@quim.ucm.es](mailto:cheda@quim.ucm.es) (J.A.R. Cheda), [Francisco.Martinez@maxlab.lu.se](mailto:Francisco.Martinez@maxlab.lu.se) (F.J. Martínez-Casado), [pando@quim.ucm.es](mailto:pando@quim.ucm.es) (C. Pando).

<http://dx.doi.org/10.1016/j.jcou.2015.11.006>

2212-9820/© 2015 Elsevier Ltd. All rights reserved.

metastable, kinetics must be taken into account and supersaturation has to be achieved by rapid cooling, fast solvent removal or anti-solvent addition. To overcome some of the difficulties presented by solution and solid state methods, we propose to use a co-crystallization method based on the utilization of supercritical CO<sub>2</sub> as an antisolvent, the supercritical antisolvent (SAS) technique [8–10]. To test this method, the 2:1 co-crystal involving diflunisal (DIF) and nicotinamide (NIC) will be prepared.

Carbon dioxide is the most commonly used supercritical fluid because it is nontoxic, non-flammable, has moderate critical temperature and pressure (31 °C and 7.4 MPa) and is considered a green solvent [10]. Supercritical CO<sub>2</sub> densities and solvation power are intermediate between those of gases and liquids and can be easily modified with small changes in temperature and pressure; meanwhile the fluid maintains good transport properties. The utilization of CO<sub>2</sub> in the SAS method is also based on its relatively low solvent power for solutes such as polymers or pharmaceuticals and its good miscibility with many organic solvents. The solvent-free particles exhibit narrow size distributions. Other advantages are operation at moderate temperatures in an inert atmosphere thus avoiding the drug degradation and the possibility of tuning the fluid properties through changes in temperature and pressure that enable control of particle size and/or morphology.

Pharmaceutical companies are urged to develop production processes with very low environmental impact, processes with fewer steps and a reduced used of organic solvents. Therefore, the SAS method has been frequently used to precipitate drugs alone or to coprecipitate them in combination with a carrier [8–12]. For instance, at our laboratory the non-steroidal anti-inflammatory drug (NSAID) diflunisal was micronized alone and later composite particles formed by the drug and the biocompatible polymer polyvinylpyrrolidone were also obtained [13]. The coprecipitates showed a dissolution rate enhancement. However, the SAS method or the closely related gas antisolvent (GAS) methods have been seldom used to obtain co-crystals [14–20]. Diflunisal, Fig. 1, belongs to class II of the Biopharmaceutical Classification System (low aqueous solubility, high membrane permeability as most NSAIDs) [21], has been approved worldwide and is frequently used [22]. Nicotinamide, a water soluble component of the vitamin B family whose structure is also shown in Fig. 1, is generally regarded as a safe substance and has been used to obtain several co-crystals [23–25] because the nitrogen atom at the pyridine group can interact with APIs through carboxylic acid–pyridine or amide–pyridine interactions, and the amide can also participate in amide–amide or carboxylic acid–amide interactions. In this case, carboxylic acid–amide and carboxylic acid–pyridine nitrogen bonds are established

(see Fig. 1) and the co-crystal solubility is expected to improve with respect to that of pure DIF. On the other hand, nicotinamide has shown an ability to restore cognition in Alzheimer's disease transgenic mice [26]. Therefore, this co-crystal may offer additional or synergistic therapeutic benefits.

Our aim in this paper is to explore the possibilities of SAS as a co-crystallization method and to examine the possible differences among the SAS co-crystals and those prepared by traditional methods. Recently, the 2:1 co-crystal involving diflunisal and nicotinamide has been prepared by liquid assisted ball mill grinding and by solution crystallization from ethanol by two different groups [24,25]. These co-crystals were characterized by powder X-ray diffraction, differential scanning calorimetry, and Fourier transform infrared spectroscopy, and dissolution rates were also reported. Evora et al. [24] also obtained the solid + liquid DIF + NIC binary phase diagram that pointed out the formation of the 2:1 DIF-NIC co-crystal.

## 2. Materials and methods

### 2.1. Materials

The materials employed were CO<sub>2</sub> (Air Liquide 99.98 mol% pure), diflunisal (Fluka, analytical standard), nicotinamide (Fluka, 2:99.5 mol% pure), acetone (Sigma–Aldrich, 2:99.8 mol% pure) and ethanol (PanReac 99.5 v/v % pure). All water used was pretreated using the Milli-Q Elix water purification system (Millipore Ibérica, Madrid, Spain).

### 2.2. Supercritical Fluid Antisolvent (SAS) precipitation and design of experiments

The application of the method to prepare the DIF-NIC co-crystal is illustrated in Fig. 2. The API and the cofomer are simultaneously dissolved in a polar organic solvent such as ethanol or acetone. Supercritical carbon dioxide is introduced in a precipitation chamber using a high-pressure pump at constant flow rate. Then the organic solution containing the drugs is fed through a second pump also at a constant flow rate reaching steady state operating conditions and an adequate supercritical fluid/solvent ratio. A given amount (30 mL) is sprayed in the precipitation chamber through a thin stainless steel nozzle. This single nozzle is drilled in a sapphire plate. The height of the cylindrical basket shown in Fig. 2 is 39.14 cm and the values for its internal and external diameter are 6.65 and 7.59 cm, respectively. The chamber is heated and both temperature and pressure are controlled. When the fluid

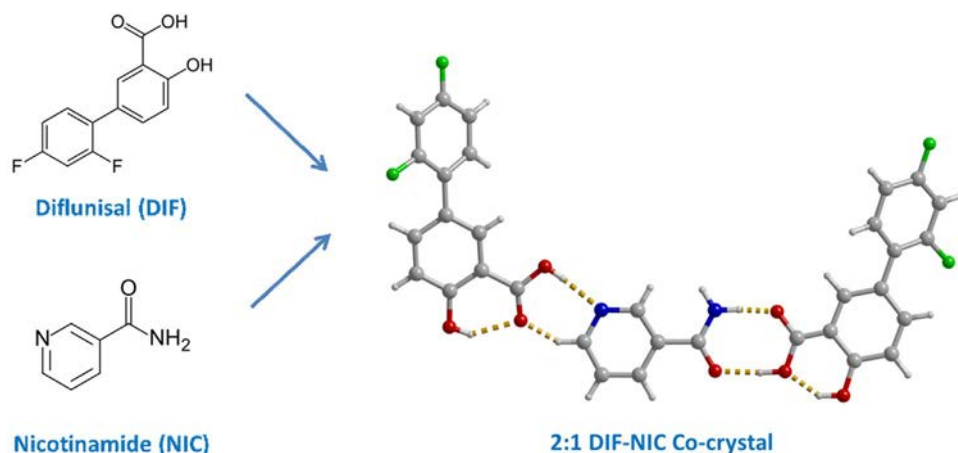


Fig. 1. Molecular structures of diflunisal, nicotinamide, and the 2:1 diflunisal-nicotinamide co-crystal showing the supramolecular heterosynths involved.

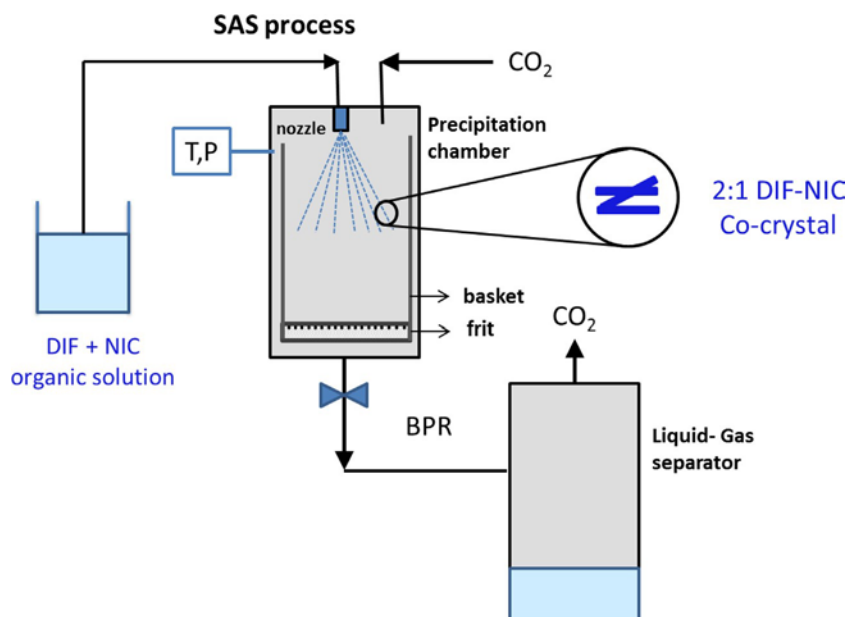


Fig. 2. Schematic representation of the supercritical fluid antisolvent (SAS) technique used to obtain the 2:1 diflunisal-nicotinamide co-crystal. T: temperature; P: pressure; BPR: back pressure regulator.

dissolves in the solution, the mixture becomes supersaturated and precipitation starts. The co-crystals are collected at the bottom and walls of the precipitation chamber. At the end of the precipitation process, the chamber is washed with excess CO<sub>2</sub> to remove the residual content of the liquid solvent. The CO<sub>2</sub> + organic solvent mixture passes to a separation chamber where the solvent is recovered. The schematic diagram for the laboratory scale SAS apparatus, its validation, and details about this apparatus and the experimental procedure may be found elsewhere [13].

The factors to be considered in the SAS process are: the concentration of the solution (C), the temperature (T), the pressure (P), the solution flow rate, the supercritical CO<sub>2</sub> flow rate, the drying time, and the nozzle diameter. In order to minimize the number of experiments a two-level factorial experimental design was applied. Therefore, two levels were used for three SAS factors that were shown to be the most influential in previous studies: temperature, pressure and solute concentration. Flow rates were kept constant at 1 mL/min and 20 g/min for solution and CO<sub>2</sub>, respectively. These values were chosen to obtain CO<sub>2</sub> mole fractions 2:0.97 by combining adequate values for the flow rates of the two pumps. The drying time and the nozzle diameter were also kept constant at 3 times the time required to fill the precipitation chamber and 100 mm, respectively. Acetone was chosen as the polar solvent for most experiments. The phase behavior of the quaternary mixtures formed by CO<sub>2</sub>, the solvent, and the two cofomers is not known. Therefore, we have taken into account the critical locus for the binary CO<sub>2</sub> + acetone system to establish the temperature and pressure conditions [27–29]. A temperature value slightly above the mixture critical temperature (35.0) and a higher value (40.0 °C) were chosen. As to the pressure conditions a value above the mixture critical pressure (10.0 MPa) and a value far above the mixture critical pressure (12.0 MPa) were chosen. The mole ratio of DIF and NIC in these solutions was 2:1, the ratio corresponding to the co-crystal stoichiometric composition. The values used for DIF concentration were 15.00 and 30.00 mg/mL for the low and high level concentration, respectively. This resulted in the experiments 1–8 that are described in Section 3. To check the solvent effect experiment 9 was conducted

using ethanol instead of acetone. At these solute concentrations nozzle plugging was not observed.

### 2.3. Pharmaceuticals characterization

A LECO CHNS-932 microanalyser was used to perform elemental analysis and a JEOL-6400 electron microscope was used to characterize the microparticles obtained in the SAS experiments. Prior to analysis, samples were gold coated.

X-ray diffraction (XRD) on powder or microcrystalline samples was used to study diflunisal and nicotinamide prior and after SAS treatment, and to identify the cocrystal. XRD patterns of the solids were obtained using a Philips X'pert, model MPD powder diffraction system. The X-ray source was nickel-filtered K $\alpha$  emission of copper (1.541837 Å). Samples were scanned over the range of 5–50 2 $\theta$  degrees using the Bragg-Brentano geometry.

Differential scanning calorimetry (DSC) curves of diflunisal, nicotinamide and the co-crystal were obtained using a TA Instruments DSC model Q-20, connected to a RCS cooling unit. Tightly sealed volatile aluminum pans were used, in dry nitrogen, flowing at 50.0 mL min<sup>-1</sup>. A MT5 Mettler microbalance was used to weigh the samples, ranging between 3 and 10 mg (with an error of  $\pm 0.001$  mg). The calorimeter was calibrated in temperature using standard samples of In and Sn, supplied by TA Instruments (purity >99.999% and >99.9%, respectively), and of benzoic acid (purity >99.97%), supplied by the former NBS (lot 39i), and in enthalpy with the In and Sn standards already described.

In order to study co-crystal interactions, Fourier transform infrared (FTIR) spectroscopy was used. Diflunisal, nicotinamide and co-crystal spectra were collected as KBr pellets in the 4000–400 cm<sup>-1</sup> frequency range using a PerkinElmer model Spectrum 100 FTIR spectrophotometer provided with a LiTaO<sub>3</sub> detector and using 16 scans.

### 2.4. Dissolution profiles

The dissolution profile of the diflunisal samples precipitated by SAS was followed by UV-vis spectroscopy using a UV/vis



Table 1  
Values for factors involved in SAS crystallization.<sup>a</sup>

Factor	Unit	Symbol	Low level (-)	High level (+)
Temperature	°C	T	35.0	40.0
Pressure	MPa	P	10.0	12.0
DIF concentration	mg/mL	C	15.00	30.00
NIC concentration	mg/mL	C	3.64	7.28

<sup>a</sup> Values for SAS factors kept constant are: solution flow rate = 1 mL/min; CO<sub>2</sub> flow rate = 20 g/min; drying time = time required to fill three times the precipitation chamber; nozzle diameter = 100 mm.

Perkin-Elmer spectrophotometer model Lambda 35. The absorption spectrum of diflunisal shows two broad bands at 275 and 306 nm [28]; the latter was used to establish the dissolution profile using the appropriate calibration curve. A pH 7.4 phosphate buffer medium (0.01 M phosphate buffer) supplied by Sigma-Aldrich was used to obtain the calibration curve in the concentration range 0.29–148 mg/mL and to carry out the dissolution tests in a Sotax USP apparatus 2 [31]. The pK<sub>a</sub> value for DIF is 2.94 [25]. A hydraulic press at 5000 kg/cm<sup>2</sup> was used to prepare compressed disks in similar fashion to those used for IR spectroscopy by the conventional procedure; approximately 100 mg of powder were used in each case. Then the compressed tablet was added to 0.900 L of the buffer solution thermostated at 37 °C and a vertical stirrer with 50 rpm speed was used. Aliquots of 5 mL were taken after selected periods of time and they were analyzed for the drug content by UV/vis. The volume of the solution was kept constant by adding 5 mL of the phosphate buffer solution each time those samples were withdrawn.

### 3. Results and discussion

The low solubility of the target substance in supercritical carbon dioxide is essential for the supercritical antisolvent precipitation. Coimbra et al. [32] measured the solubility of diflunisal in supercritical CO<sub>2</sub> at 35.0 and 45.0 °C from 9.3 to 25.0 MPa and found solubility values expressed as diflunisal mole fraction ranging from  $0.57 \times 10^{-6}$  to  $5.47 \times 10^{-6}$ . Kotnik et al. [33] found values ranging from  $2.6 \times 10^{-4}$  to  $1.9 \times 10^{-3}$  for nicotinamide solubility at 40.0 °C in the 5.4–29.3 MPa interval. Therefore, in principle diflunisal and nicotinamide could be precipitated by SAS at the conditions of temperature and pressure chosen in this study: 35.0 and 40.0 °C, and 10.0 and 12.0 MPa. Acetone was chosen as a good solvent for DIF and NIC. Table 1 shows the low and high level values for the three factors used in the design of experiments and the values of the SAS factors that were kept constant. The eight combinations of signs resulting from the application of the factorial design are shown in Table 2. An additional experiment carried out using ethanol as solvent is also given in this table. For acetone at 25 °C and atmospheric pressure, a solubility value of 200 mg/mL was measured at our laboratory for DIF and a value of 36.0 mg/mL was estimated from data reported at 10 MPa by Revelli et al. for NIC [34]. For ethanol at 25 °C and atmospheric pressure, solubility values of 83.4 and 97.7 mg/mL were reported for DIF and NIC, respectively [35,36]. Therefore, concentrations of DIF and NIC in ethanol and acetone given in Table 1 are much lower than solubility values at 25 °C. Low concentrations were chosen to minimize the possibility of nozzle plugging.

The nine experiments were successful. Elemental analysis indicated that the purities of co-crystals are 2:99%. To confirm that the co-crystals are solvent-free thermogravimetric analysis (TGA) and differential thermal analysis (DTA) were carried out. TGA curves obtained for two of the samples (experiments 1 and 9) are shown in the supplementary material: no weight loss associated to ethanol or acetone evaporation is observed. For comparison purposes DIF and NIC were also processed by SAS at the conditions

Table 2  
The factorial design of SAS factors and solvents used in experiments.

Experiment	T (1)	P (2)	C (3)	Solvent
1	–	–	–	Acetone
2	–	+	–	Acetone
3	+	–	–	Acetone
4	+	+	–	Acetone
5	–	–	+	Acetone
6	–	+	+	Acetone Acetone
7	+	–	+	Acetone
8	+	+	+	Acetone
9	–	–	–	Ethanol

of temperature and pressure of experiment 1. The recovery ratios (yield) of DIF and NIC were 46 and 36%, respectively. A larger value of 70% was obtained for the co-crystal obtained in experiment 1. A similar effect was reported by Neurohr et al. [19] for the yield of naproxen-nicotinamide co-crystals using the GAS technique.

Images of commercial and SAS processed DIF and NIC are shown in Fig. 3. After SAS treatment uniform crystals are obtained in both cases. As to the crystal morphology, thin needles of uniform width and length were observed for SAS NIC and flat and long crystalline particles for SAS DIF. DIF has been previously processed by SAS using acetone at 40 °C, 9, 12, and 15 MPa, and solute concentrations of 20 and 40 mg/mL, 1 mL/min solution flow rate, and 15 g/min CO<sub>2</sub> flow rate. The different conditions of pressure and concentration did not lead to significant changes in DIF crystal morphology. Also a mixture of acetone and dichloromethane was used as solvent and no change was observed [13,37]. Bladed and lamellar crystals similar to those shown in Fig. 3 were obtained. NIC has been also processed by GAS by Neurohr et al. [19] at 35 °C, 10 MPa and solution concentration of 25 mg/mL and long needles are shown in an optical microscope image.

SEM images of the co-crystals obtained in experiments 1–3, 5, 7 and 9 are shown in Fig. 4 with the same magnification. The co-crystal morphology resembles that of SAS NIC but the crystal width and length are less uniform. Similar morphologies were observed for co-crystals obtained in experiments 1–9. The effect of temperature, pressure, concentration and solvent on the morphology of the precipitate was very weak for the co-crystal. The formation of the 2:1 DIF co-crystal with NIC is demonstrated by examination of the X-ray powder diffractograms and DSC thermograms described next.

The similar sizes of the SAS co-crystals obtained in this paper are in agreement with Reverchon and De Marco previous findings [29]. These authors reviewed morphologies and sizes of crystals obtained by SAS. Although control of crystal habit has been frequently obtained, a very limited control of crystal size was attained. As to the morphology, Reverchon and De Marco proposed two crystal formation mechanisms in a SAS process: (1) droplets drying followed by a fast crystallization kinetics that can lead to mostly spherical crystals and (2) precipitation from an expanded liquid phase that can lead to different morphologies depending on the interactions with the liquid solvent. It seems that at the studied conditions the latter mechanism is followed for the experiments performed both in acetone and ethanol. The solute is not soluble in supercritical CO<sub>2</sub> but it may dissolve in the mixture formed by CO<sub>2</sub> and the organic solvent in the precipitation chamber. After solute solubilization, nucleation and crystal growth would proceed following a liquid-like mechanism and the solute would diffuse on the surface of the growing crystals. The presence of the solute may modify the binary phase diagram shifting the mixture critical point towards higher pressures and precipitation takes place in a two-phase region instead of the supercritical region originally planned when pressure and temperature conditions were established in Section 2.2. Knowledge of the phase behavior of these

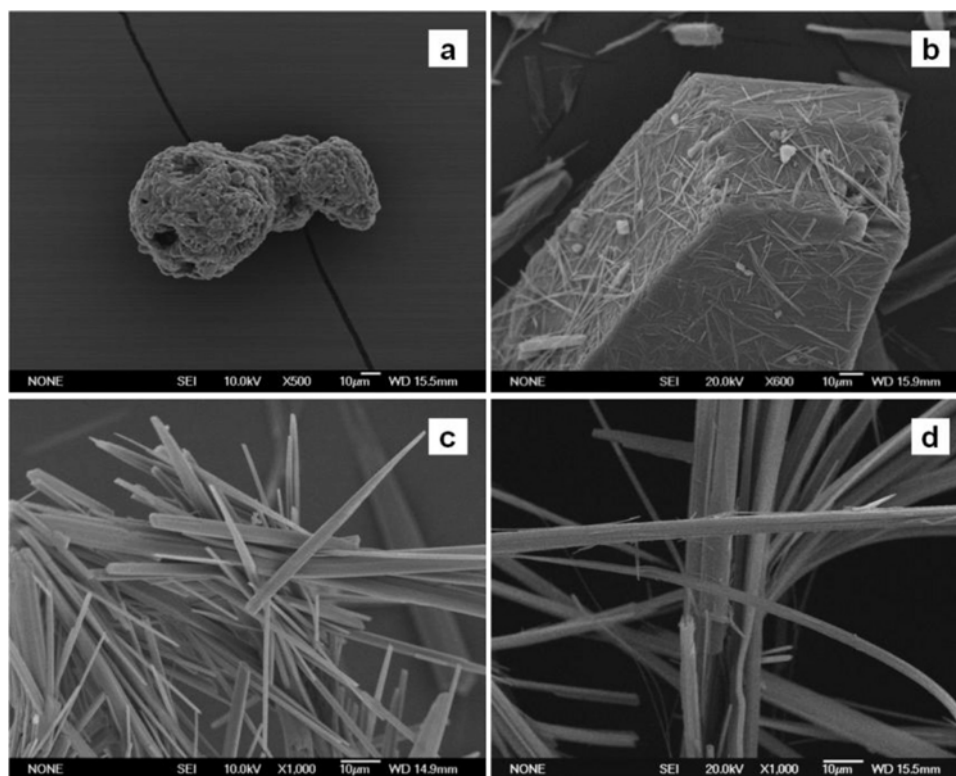


Fig. 3. SEM images of commercial NIC (a), DIF (b) and SAS processed NIC (c) and DIF (d).

ternary or quaternary mixtures would be required to further clarify this mechanism and to choose precipitation conditions where mechanism (1) would be followed thus leading to a particle morphology different from that observed in this study. Another possibility would be exploring in the context of co-crystal formation the technique described by Chen et al. [11,12] in the micronization of methotrexate and puerarin. These authors found that smaller API particles could be obtained by adding a bad solvent to the solution formed by the API and a good solvent. Increasing the bad solvent/good solvent ratio increased the degree

of saturation, and led to a fast precipitation that decreased significantly the particle size and shifted the physical form from crystalline to amorphous.

The X-ray powder diffractogram of the commercial and the SAS processed DIF at the conditions of experiment 1 are shown in Fig. 5. These patterns were compared to those of the five polymorphic forms presented by DIF [30,38–41]. The polymorphism of diflunisal is changed through the SAS process. Commercial XRD pattern is essentially that of polymorph I (the most stable DIF polymorph) but not actually the same suggesting that commercial DIF is

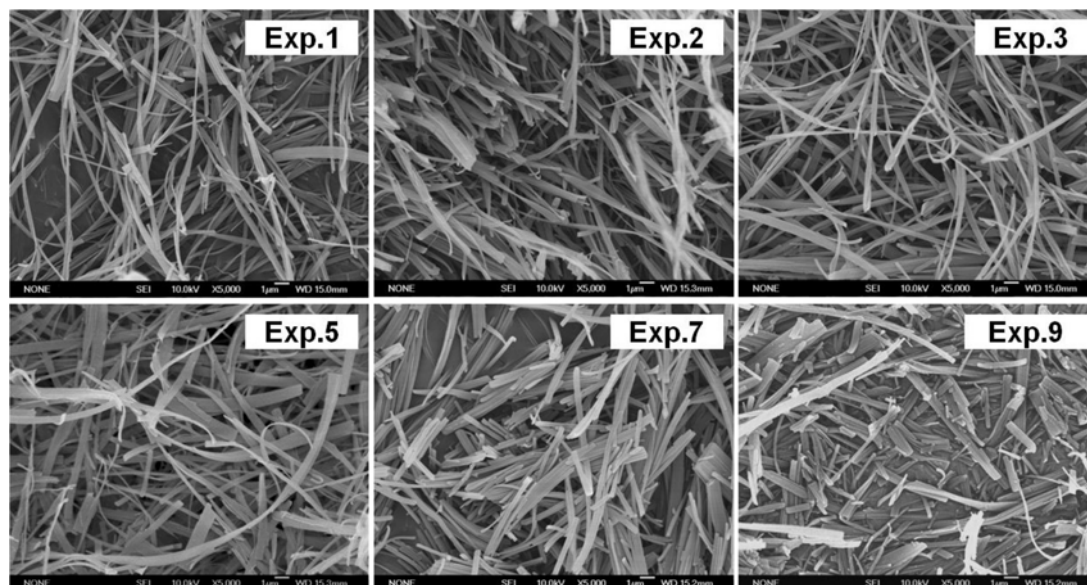


Fig. 4. SEM images of the co-crystals obtained in experiments 1-3, 5, 7 and 9.

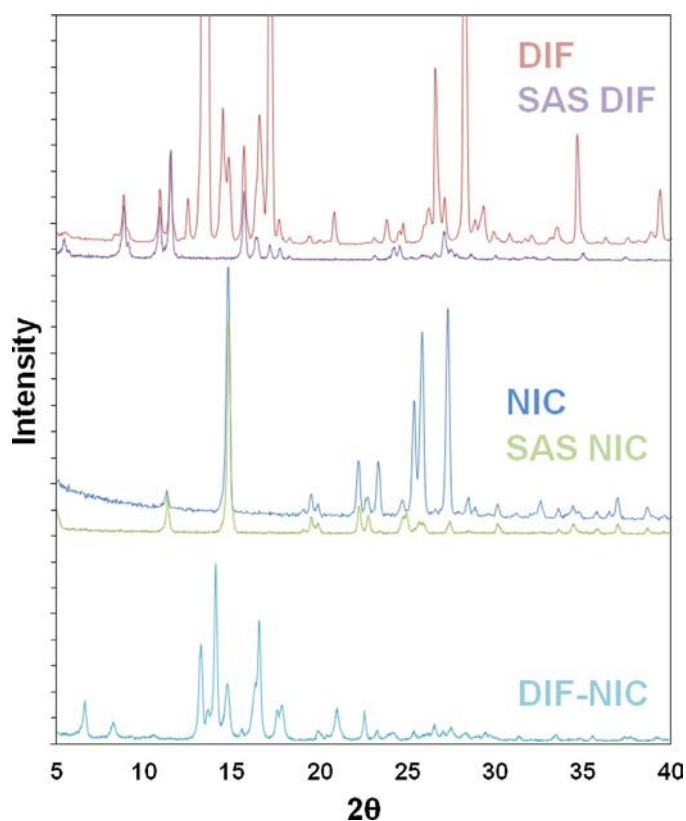


Fig. 5. XRD patterns of untreated and SAS processed DIF and NIC, and the co-crystal obtained in experiment 1.

composed of a mixture of polymorphs. The SAS processed DIF exhibits form V. The change of a crystal polymorphic form through treatment with supercritical CO<sub>2</sub> has been already reported and the possibilities of using CO<sub>2</sub> to control polymorphism have been explored [42,43]. Fig. 5 also shows the coincident XRD patterns for the commercial and the SAS processed NIC at the conditions of experiment 1 that correspond to polymorph I. Two NIC polymorphs are structurally described and two more have been established by differential scanning calorimetry [44–46]. The XRD pattern of the DIF-NIC co-crystal obtained at the conditions of experiment 1 is also shown in Fig. 5. This pattern was compared to those of all the DIF and NIC polymorphs and no coincidence was observed, reflections present in DIF and NIC are absent. On the other hand, new reflections appear in the co-crystal pattern that did not exist in the cofomers:  $2\theta = 6.6, 8.2, 14.0, 16.5$ . This indicates the formation of a new solid phase. Also, the co-crystal pattern shown in Fig. 5 is coincident to those reported by Wang et al. and Évora et al. [24,25]. Co-crystal XRD patterns for the other SAS experiments do not differ from those of experiment 1. Therefore, the SAS method leads to the same structure obtained by conventional methods and co-crystal polymorphism is not observed.

For further characterization of the samples, differential scanning calorimetry was performed. The thermogram curves of DIF, NIC and the co-crystal obtained at conditions of experiment 1 are shown in Fig. 6. The thermal behavior was studied by heating 5 mg of the sample at a scan rate of 5 °C/min in a volatile aluminum pan under nitrogen gas flow. The investigation was carried out over the temperature range -20–250 °C. The melting point was measured reading the onset temperature of the peak. A melting point of 212.3 °C was obtained for commercial DIF (no differences are observed in the melting points of the different DIF polymorphs [39]). Commercial nicotinamide melting point was 129.4 °C as it is expected for polymorph I [45,46]. The co-crystal

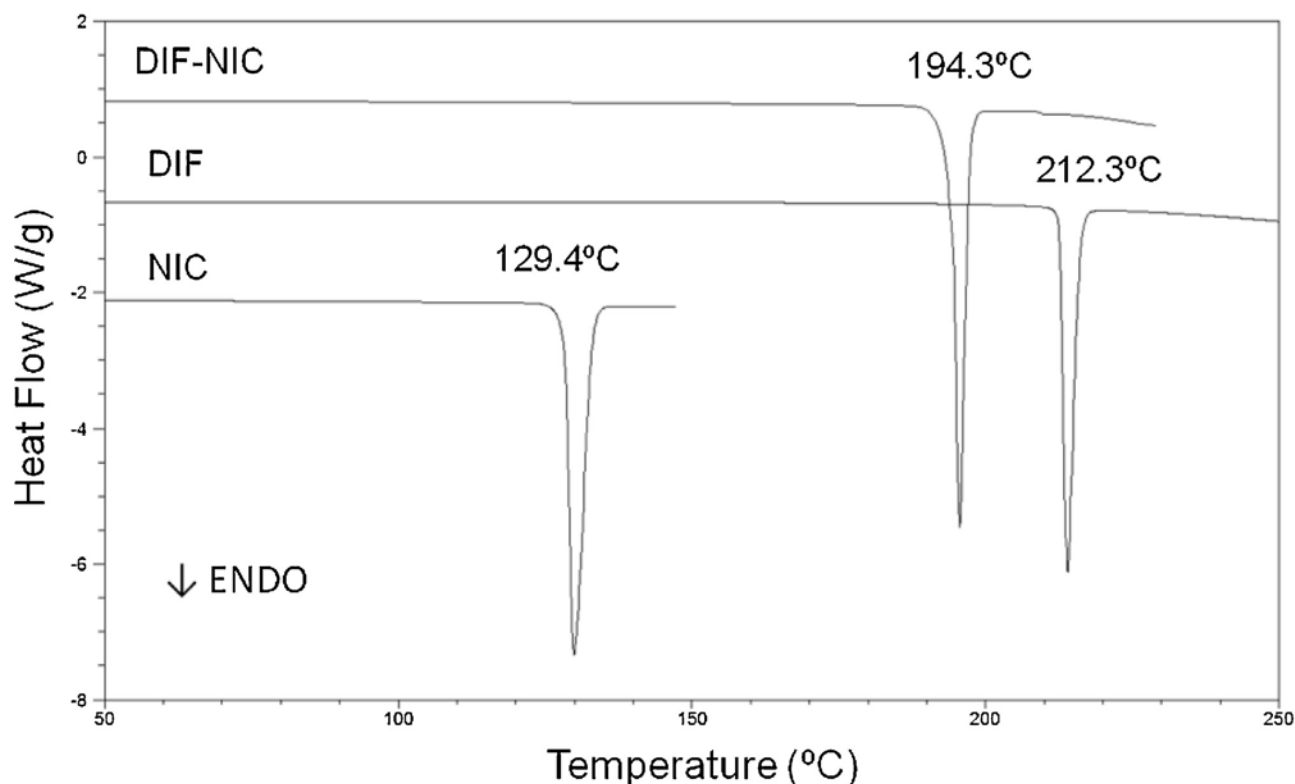


Fig. 6. DSC thermograms of untreated DIF and NIC, and the co-crystal obtained in experiment 1.

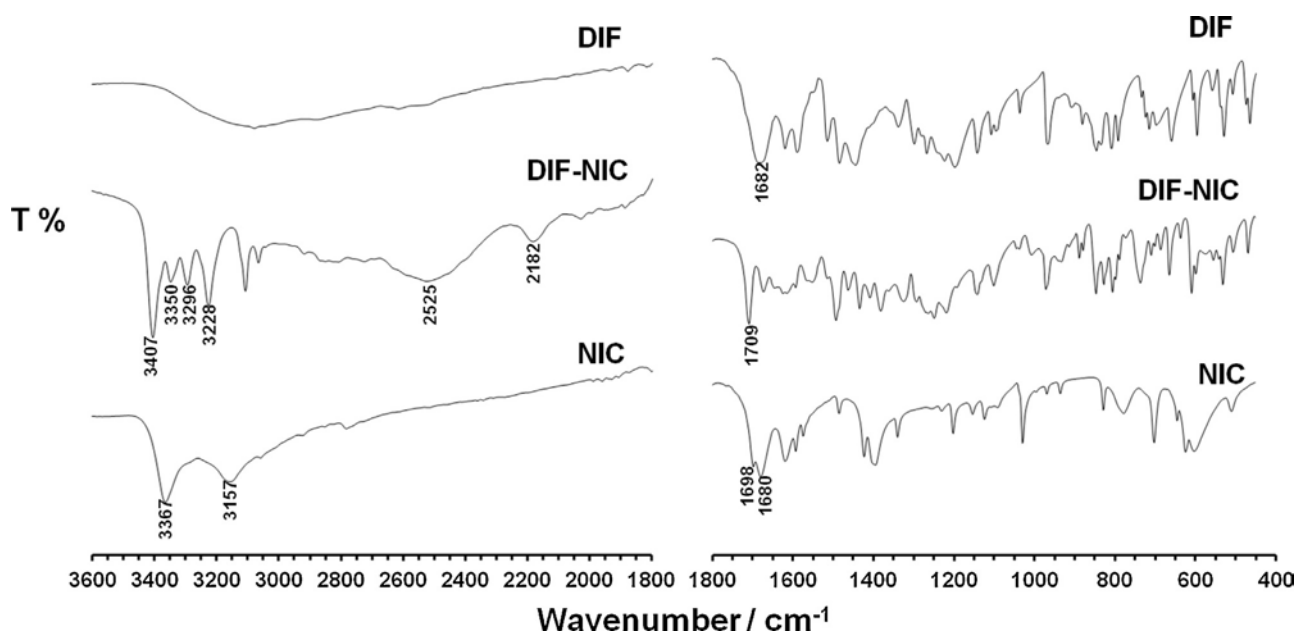


Fig. 7. FTIR-spectra of untreated DIF and NIC, and the co-crystal obtained in experiment 1.

melt at a temperature (194.3 °C) intermediate between those of DIF and NIC with  $D_{fus}H = 104 \text{ kJ mol}^{-1}$ ; no low-temperature endothermic peaks were observed that could indicate the formation of a solvate or hydrate. The  $T_m$  values obtained in this paper for DIF, NIC and their co-crystal are in agreement with those reported by Évora et al. and Wang et al. [24,25]. The value of  $D_{fus}H$  is slightly higher than that of  $95 \text{ kJ mol}^{-1}$  reported by Évora et al. [24]. A DSC study of a physical mixture was performed and an endothermic peak corresponding to the NIC melting followed by an exothermic peak associated to the co-crystal formation by melt fusion phenomenon were obtained (see Supplementary material). The nicotinamide peak was not observed in the DSC curves of the SAS co-crystals obtained at the different conditions which confirms the purity of the materials produced.

Infrared spectroscopy was used to examine the interactions between diflunisal and nicotinamide. Fig. 7 shows the FTIR spectra for diflunisal, nicotinamide, and the 2:1 co-crystal obtained in experiment 1 over the range of 3600–400  $\text{cm}^{-1}$ . As could be expected, the functional groups in the co-crystal FTIR-spectrum showed differences in the wavenumbers and intensity in comparison to those of the DIF and NIC spectra. The two NIC

main bands observed at 3367 and 3157  $\text{cm}^{-1}$  in the  $\text{NH}_2$  stretching vibration region seem to be displaced to 3407 and 3228  $\text{cm}^{-1}$ , respectively, in the co-crystal FTIR-spectrum. Two additional bands are observed for the co-crystal in this region at 3350 and 3296  $\text{cm}^{-1}$ . The  $\text{C}=\text{O}$  stretching vibration of the carboxylic acid group at 1682  $\text{cm}^{-1}$  in DIF, and 1698 and 1680  $\text{cm}^{-1}$  in NIC is shifted to 1709  $\text{cm}^{-1}$  in the co-crystal. On the other hand, the bands characteristic of the acid-pyridine nitrogen synthon at approximately 2500, and 2150  $\text{cm}^{-1}$  are observed in the co-crystal centered at 2525 and 2182  $\text{cm}^{-1}$  [24,25,47]. Furthermore, the two additional bands already mentioned for the co-crystal at 3350 and 3296  $\text{cm}^{-1}$  can be assigned to the carboxylic acid–amide hydrogen bonding interaction [23–25]. Absorption bands of excess NIC or DIF are not observed thus confirming the 2:1 stoichiometry. The co-crystal FTIR-spectrum shown in Fig. 7 is coincident with spectra for samples obtained in experiments 2–9 and is also coincident with spectra shown by Évora et al. and Wang et al. [24,25].

Dissolution profiles for the co-crystal obtained in experiment 1 and commercial diflunisal are presented in Fig. 8 in terms of the co-crystal release percentage vs time. The co-crystal release improves slightly with respect to that of diflunisal. Larger improvements have been observed in similar comparisons carried out by Wang et al. and Évora et al. [24,25] using experimental procedures that differ in some aspects to that used in this study (the main differences are that our tablets were bigger and uncoated). On the other hand, the pharmaceutical activity of NIC in combination to that of DIF may offer additional or synergistic therapeutic benefits. Therefore, the co-crystal may be considered a better diflunisal formulation. In the next section the advantages of using SAS as a co-crystallization method will be summarized.

#### 4. Conclusions

The 2:1 co-crystal of diflunisal with nicotinamide can be successfully prepared through a solution co-crystallization method using supercritical  $\text{CO}_2$  as antisolvent (SAS micronization). This method requires that the two co-crystal components are simultaneously soluble in a polar organic solvent and poorly

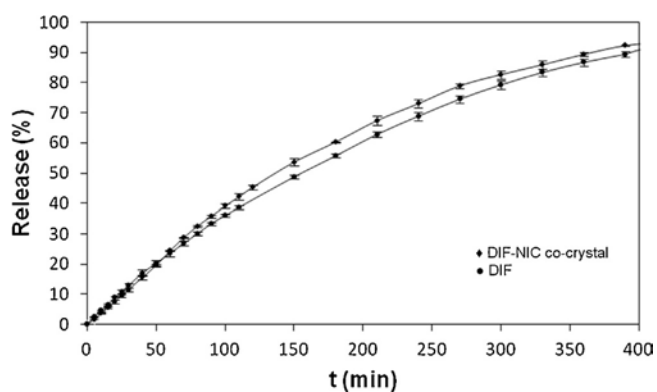


Fig. 8. Dissolution profiles of the untreated diflunisal (\*), and the co-crystal obtained in experiment 1 ( $\Delta$ ) showing error bars for the replicate dissolution rate experiments.

soluble in the supercritical fluid, and allows the use of different cofomer concentrations and, in particular, those corresponding to the co-crystal stoichiometric composition. Upon solution of CO<sub>2</sub> in the droplets formed in the nozzle, the CO<sub>2</sub> + solvent mixture is rapidly established and the new phase is formed according to the 2:1 stoichiometric ratio avoiding the precipitation of pure components.

The influence of the SAS parameters temperature, pressure, drug concentration and solvent in the co-crystal formation within the interval studied is shown to be weak. The application of the SAS technique to pure diflunisal and nicotineamide leads to a change in the diflunisal polymorphic form.

The 2:1 diflunisal-nicotinamide co-crystals were characterized in terms of morphology, crystallinity, thermal behavior, cofomer interactions and drug release. The dissolution rate of the new solid form improved with respect to that of pure diflunisal. The SAS co-crystals properties are very similar to those previously reported by Evora et al. and Wang et al. for co-crystals obtained using liquid assisted ball mill grinding and solution crystallization. The SAS technique is shown to be an alternative and effective co-crystallization method with many advantages with respect to solid-state and solution co-crystallization methods: the process is sustainable since temperatures are moderate and the green solvent supercritical CO<sub>2</sub> is used while the amount of organic solvents is limited, solvent-free co-crystals are obtained in one-step, a solution containing cofomers amounts corresponding to the co-crystal stoichiometric composition may be used and, in principle, the particle size and/or morphology may be controlled through changes in temperature and pressure. The energy consumption required to carry out a SAS experiment, the production rate that can be lower than that of a conventional experiment, and the initial cost associated to the application of SAS technology in the pharmaceutical industry may be mentioned as disadvantages. However, the number of supercritical processes used in the industry is steadily increasing in the last years due to the low environmental impact and the fewer steps associated to these processes [48].

#### Acknowledgements

We gratefully acknowledge the financial support of the Spanish Ministry of Economy and Competitiveness (MINECO), research projects CTQ2010-16940 and CTQ2013-41781-P. I.C. thanks MINECO for its support through a FPI grant. We thank Prof. M.D. Veiga-Ochoa at the Pharmacy Faculty of Universidad Complutense for the use of the dissolution test apparatus. We also acknowledge the use of experimental facilities of Prof. E. Enciso at the Physical Chemistry I Department of Universidad Complutense.

#### Appendix A. Supplementary data

Supplementary data associated with this article can be found, in the online version, at <http://dx.doi.org/10.1016/j.jcou.2015.11.006>.

#### References

- [1] N. Schultheiss, A. Newman, Pharmaceutical cocrystals and their physicochemical properties, *Cryst. Growth Des.* **9** (2009) 2950–2967.
- [2] USGRAS List, <http://www.fda.gov/food/ingredientpackaginglabeling/gras/default.htm>, 2015.
- [3] A.O.L. Evora, R.A.E. Castro, T.M.R. Maria, M.T.S. Rosado, M.R. Silva, A.M. Beja, J. Canotilho, M.E.S. Eusebio, Pyrazinamide-diflunisal: a new dual-drug co-crystal, *Cryst. Growth Des.* **11** (2011) 4780–4788.
- [4] O. Almarsson, M.J. Zaworotko, Crystal engineering of the composition of pharmaceutical phases. Do pharmaceutical co-crystal represent a new path to improved medicines, *Chem. Commun.* (2004) 1889–1896.
- [5] C.C. Sun, Cocrystallization for successful drug delivery, *Expert Opin. Drug Deliv.* **10** (2013) 201–213.
- [6] J.H. ter Horst, M.A. Deij, P.W. Cains, Discovering new cocrystals, *Cryst. Growth Des.* **9** (2009) 1531–1537.
- [7] T. Rager, R. Hilfiker, Cocrystal formation from solvent mixtures, *Cryst. Growth Des.* **10** (2010) 3237–3241.
- [8] A. Martín, M.J. Cocero, Micronization processes with supercritical fluids: fundamentals and mechanisms, *Adv. Drug Deliv. Rev.* **60** (2008) 339–350.
- [9] M.J. Cocero, A. Martín, F. Mattea, S. Varona, Encapsulation and co-precipitation processes with supercritical fluids: fundamentals and applications, *J. Supercrit. Fluids* **47** (2009) 546–555.
- [10] H. Machida, M. Takesue, R.L. Smith, Green chemical processes with supercritical fluids: properties, materials, separation and energy, *J. Supercrit. Fluids* **60** (2011) 2–15.
- [11] A.Z. Chen, Y. Li, F.T. Chau, T.Y. Lau, J.Y. Hu, Application of organic cosolvent in the process of solution-enhanced dispersion by supercritical CO<sub>2</sub> to prepare puerarin fine particles, *J. Supercrit. Fluids* **49** (2009) 394–402.
- [12] A.Z. Chen, L. Li, S.B. Wang, C. Zhao, Y.G. Liu, G.Y. Wang, Nanonization of methotrexate by solution-enhanced dispersion by supercritical CO<sub>2</sub>, *J. Supercrit. Fluids* **67** (2012) 7–13.
- [13] F. Zahran, A. Cabañas, J.A.R. Cheda, J.A.R. Renuncio, C. Pando, Dissolution rate enhancement of the anti-inflammatory drug diflunisal by coprecipitation with a biocompatible polymer using carbon dioxide as a supercritical fluid antisolvent, *J. Supercrit. Fluids* **88** (2014) 56–65.
- [14] L. Padrela, M.A. Rodrigues, S.P. Velaga, H.A. Matos, E.G. de Azevedo, Formation of indomethacin-saccharin cocrystals using supercritical fluid technology, *Eur. J. Pharm. Sci.* **38** (2009) 9–17.
- [15] L. Padrela, M.A. Rodrigues, S.P. Velaga, A.C. Fernandes, H.A. Matos, E.G. de Azevedo, Screening for pharmaceutical cocrystals using the supercritical fluid enhanced atomization process, *J. Supercrit. Fluids* **53** (2010) 156–164.
- [16] A. Shikhar, M.M. Bommana, S.S. Gupt, E. Squillante, Formulation development of carbamazepine-nicotinamide co-crystals complexed with  $\beta$ -cyclodextrin using supercritical fluid process, *J. Supercrit. Fluids* **55** (2011) 1070–1078.
- [17] C.A. Ober, S.E. Montgomery, R.B. Gupta, Formation of itraconazole-*l*-malic acid cocrystals by gas antisolvent cocrystallization, *Powder Technol.* **236** (2013) 122–131.
- [18] C.A. Ober, R.B. Gupta, Formation of itraconazole-succinic acid cocrystals by gas antisolvent cocrystallization, *AAPS PharmSciTech* **13** (2012) 1396–1406.
- [19] C. Neurohr, A.-L. Reveli, P. Billot, M. Marchivie, S. Lecomte, S. Laugier, S. Massip, P. Subra-Paternault, Naproxen-nicotinamide cocrystals produced by CO<sub>2</sub> antisolvent, *J. Supercrit. Fluids* **83** (2013) 78–85.
- [20] L. Padrela, M.A. Rodrigues, J. Tiago, S.P. Velaga, H.A. Matos, E.G. de Azevedo, Tuning physicochemical properties of theophylline by cocrystallization using the supercritical fluid enhanced atomization technique, *J. Supercrit. Fluids* **86** (2014) 129–136.
- [21] T. Takagi, C. Ramachandran, M. Bermejo, S.L. Yamashita, X. Yu, G.L. Amidon, A provisional biopharmaceutical classification of the top 200 oral drug products in the United States, Great Britain, Spain, and Japan, *Mol. Pharm.* **3** (2006) 631–643.
- [22] P. Brooks, Use and benefits of nonsteroidal anti-inflammatory drugs, *Am. J. Med.* **104** (1998) 95–135.
- [23] S.F. Chow, M. Chen, L. Shi, A.H.L. Chow, C.C. Sun, Simultaneously improving the mechanical properties, dissolution performance, and hygroscopicity of ibuprofen and flurbiprofen by cocrystallization with nicotineamide, *Pharm. Res.* **29** (2012) 1854–1865.
- [24] A.O.L. Evora, R.A.E. Castro, T.M.R. Maria, M.R. Silva, J.H. ter Horst, J. Canotilho, M.E.S. Eusebio, A thermodynamic based approach on the investigation of a diflunisal pharmaceutical co-crystal with improved intrinsic dissolution rate, *Int. J. Pharm.* **466** (2014) 68–75.
- [25] L. Wang, B. Tan, H. Zhang, Z. Deng, Pharmaceutical cocrystals of diflunisal with nicotineamide or isonicotinamide, *Org. Process Res. Dev.* **17** (2013) 1413–1418.
- [26] K.N. Green, J.S. Steffan, H. Martínez-Coria, X. Sun, S.S. Schreiber, L.M. Thomson, Nicotinamide restores cognition in Alzheimer's disease transgenic mice via a mechanism involving sirtuin inhibition and selective reduction of Thr231-phosphotau, *J. Neurosci.* **28** (2008) 11500–11510.
- [27] F. Zahran, C. Pando, J.A.R. Renuncio, A. Cabañas, Excess molar enthalpies of CO<sub>2</sub> + acetone at pressures from (9.00 to 18.00) MPa and temperatures from (313.15 to 333.15) K, *J. Chem. Eng. Data* **55** (2010) 3649–3654.
- [28] E. Reverchon, E. Torino, S. Dowy, A. Braeuer, A. Leipertz, Interactions of phase equilibria, jet fluid dynamics and mass transfer during supercritical antisolvent micronization, *Chem. Eng. J.* **156** (2010) 446–458.
- [29] E. Reverchon, I. De Marco, Mechanisms controlling supercritical antisolvent precipitate morphology, *Chem. Eng. J.* **156** (2011) 358–370.
- [30] H.G. Brittain, B.J. Elder, P.K. Isbester, A.H. Salerno, Solid-state fluorescence studies of some polymorphs of diflunisal, *Pharma. Res.* **22** (2005) 999–1006.
- [31] USP, Dissolution. <http://www.usp.org/usp-nf/harmonization/stage-6/dissolution>, 2011.
- [32] P. Coimbra, D. Fernandes, M.H. Gil, H.C. de Sousa, Solubility of diflunisal in supercritical carbon dioxide, *J. Chem. Eng. Data* **53** (2008) 1990–1995.
- [33] P. Kotnik, M. Škerget, Z. Knez, Solubility of nicotinic acid and nicotineamide in carbon dioxide at  $T = (313.15 \text{ to } 373.15) \text{ K}$  and  $p = (5 \text{ to } 30) \text{ MPa}$ : experimental data and correlation, *J. Chem. Eng. Data* **56** (2011) 338–343.
- [34] A.L. Revelli, S. Laugier, A. Errigible, P. Subra-Paternault, High-pressure solubility of naproxen, nicotineamide and their mixture in acetone with supercritical CO<sub>2</sub> as an antisolvent, *Fluid Phase Equilib.* **373** (2014) 29–33.

- [35] G.L. Perlovich, S.V. Kurkov, A. Bauer-Brandl, Thermodynamics of solutions: II. Flurbiprofen and diflunisal as models for studying solvation of drug substances, *Eur. J. Pharm. Sci.* 19 (2003) 423–432.
- [36] A. Shayanfar, S. Velaga, A. Jouyban, Solubility of carbamazepine, nicotinamide and carbamazepine-nicotinamide co-crystal in ethanol-water mixtures, *Fluid Phase Equilib.* 363 (2014) 97–105.
- [37] F. Zahran, Ph. D. Thesis, Universidad Complutense, Madrid, 2012.
- [38] M.L. Cotton, R.A. Hux, Diflunisal, in: K. Florey (Ed.), *Analytical Profiles of Drug Substances*, Academic Press, Orlando, 1985, pp. 491–526 Chapter 14.
- [39] M.C. Martínez-Ohárriz, C. Martín, M.M. Goñi, C. Rodríguez-Espinosa, M.C.T. De Ilarduya-Apaolaza, M. Sánchez, Polymorphism of diflunisal: isolation and solid-state characteristics of a new crystal form, *J. Pharm. Sci.* 83 (1994) 174–177.
- [40] M.C. Martínez-Ohárriz, C. Rodríguez-Espinosa, C. Martín, M.M. Goñi, M.C. Tros-Illarduya, M. Sánchez, Solid dispersions of diflunisal—PVP: polymorphic and amorphous states of the drug, *Drug Dev. Ind. Pharm.* 28 (2002) 717–725.
- [41] W.I. Cross, N. Blagden, R.J. Davey, R.G. Pritchard, M.A. Neumann, R.J. Roberts, R. C. Rowe, A whole output strategy for polymorph screening: combining crystal structure prediction, graph set analysis, and targeted crystallization experiments in the case of diflunisal, *Cryst. Growth Des.* 3 (2003) 152–158.
- [42] A. Kordikowski, T. Shekunov, P. York, Polymorph control of sulfathiazole in supercritical CO<sub>2</sub>, *Pharm. Res.* 18 (2001) 682–688.
- [43] S.P. Velaga, R. Berger, J. Carlfors, Supercritical fluid crystallization of budesonide and flunisolide, *Pharm. Res.* 19 (2002) 1564–1571.
- [44] Y. Miwa, T. Mizuno, K. Tsuchida, T. Taga, Y. Iwata, Experimental charge density and electrostatic potential in nicotinamide, *Acta Crystallogr. B* 55 (1999) 78–84.
- [45] J. Li, S.A. Bourne, M.R. Caira, New polymorphs of isonicotinamide and nicotinamide, *Chem. Commun.* 47 (2011) 1530–1532.
- [46] T. Hino, J.L. Ford, M.W. Powell, Assessment of nicotinamide polymorphs by differential scanning calorimetry, *Thermochim. Acta* 374 (2001) 85–92.
- [47] A. Mukherjee, S. Tothadi, S. Chakraborty, S. Ganguly, Synthons identification in co-crystals and polymorphs with IR spectroscopy. Primary amides as a case study, *CrystEngComm* 15 (2013) 4640–4654.
- [48] I. Pasquali, R. Bettini, Are pharmaceuticals really going supercritical, *Int. J. Pharm.* 364 (2008) 176–187.



Isaac Alfonso Cuadra has completed his B.Sc. Degree in Chemical Engineering and M.Sc. in Industrial Processes Engineering at the University Complutense of Madrid (UCM). As a Ph.D. student at UCM he is working on the micronization of particles using supercritical carbon dioxide as an antisolvent. His previous research focussed on enhanced oil extraction at the Research and Development Centre of the Spanish oil company CEPSA.



Albertina Cabañas is Associate Professor in the Physical Chemistry Department at Universidad Complutense de Madrid (UCM) in Spain since 2007. She received her PhD degree at UCM in 1998 performing thermodynamic studies of mixtures involving supercritical fluids. Afterwards, she investigated the synthesis of metal oxide nanoparticles in supercritical water using continuous reactors (1999–2000, University of Nottingham, U.K.) and the deposition of high-quality metal films from supercritical CO<sub>2</sub> solutions (2001–2003, University of Massachusetts, USA). She was “Ramón y Cajal” Fellow (2003–2007, UCM, Spain). Her current research focuses on the synthesis of nanomaterials using supercritical fluids as green solvents.



José Antonio Rodríguez Cheda is Emeritus Professor of Physical Chemistry at Universidad Complutense de Madrid (UCM). His current research involves the Physical Chemistry of MOFs or Coordination Polymers and DSC–XRD studies of pure metal alkanoates, and pharmaceuticals and their mixtures (cocrystals). At present he is the Director of the UCM Research Group: Ionic Liquid Crystals (<http://www.ucm.es/centros/webs/cristalesliquidosionicos>). His previous positions were: Visiting Scholar, Department of Chemistry, University of Michigan, Ann Arbor, USA, January 1975–February 1976; Visiting Professor, Kent Liquid Crystal Institute, Kent State University USA, May–July 2003.



Francisco Javier Martínez-Casado received his PhD in Applied Physical Chemistry at the Universidad Complutense de Madrid in 2007, studying the thermal behavior and structure of organic salts. Afterwards, he worked at the European Synchrotron Radiation Facility (ESRF, beamline BM16, Grenoble, France) investigating single crystal and powder diffraction with synchrotron radiation, and later at the Laboratory for Crystallographic Studies (Granada, Spain). Since 2013, he works at the I711 Diffraction Beamline at MAX IV Laboratory (Lund University, Sweden), first as Postdoc and now as Beamline Scientist. His current research is focused on organic salts and mixed-ligand MOFs.



Concepción Pando is Professor of Physical Chemistry at Universidad Complutense de Madrid (UCM), Spain. She received her PhD degree at UCM in 1979 and was a Fulbright scholar at Brigham Young University, USA (1981–82), performing calorimetric studies of mixtures involving supercritical fluids. She has studied phase equilibria and thermodynamic properties of fluid and liquid mixtures formed by CO<sub>2</sub>. She has experience in supercritical fluid extraction and is currently involved in the fabrication and micronization of materials in supercritical CO<sub>2</sub> aimed to applications in catalysis and pharmacology.





Contents lists available at ScienceDirect

## The Journal of Supercritical Fluids

journal homepage: [www.elsevier.com/locate/supflu](http://www.elsevier.com/locate/supflu)

## Polymorphism in the co-crystallization of the anticonvulsant drug carbamazepine and saccharin using supercritical CO<sub>2</sub> as an anti-solvent

Isaac A. Cuadra, Albertina Cabañas, José A.R. Cheda, Concepción Pando



Departamento de Química Física I, Universidad Complutense, E-28040 Madrid, Spain

## GRAPHICAL ABSTRACT



## ARTICLE INFO

## Keywords:

Carbon dioxide  
Pharmaceutical co-crystals  
Supercritical anti-solvent  
Carbamazepine  
Saccharin  
Applications

## ABSTRACT

1:1 Co-crystals of carbamazepine (CBZ) and saccharin (SAC) were obtained for the first time through the supercritical anti-solvent (SAS) technique based on using supercritical CO<sub>2</sub> as anti-solvent. The capability of SAS to produce the desired polymorphic form (two polymorphs are known) was assessed. Operational conditions investigated were temperature (40.0 and 60.0 °C), pressure (10.0 and 15.0 MPa), solvent choice and coformer concentration in the organic solution (CBZ: 30 and 15 mg/mL; SAC: stoichiometric ratio). Co-crystals were characterized in terms of crystallinity and coformers interactions. No homocrystals were present. Using methanol, at 40.0 °C polymorph I was obtained with yields up to 65%; whilst at 60.0 °C a mixture of polymorphs was obtained. Mixtures of polymorphs were also obtained in the ethanol and dichloromethane experiments at the studied conditions while the dimethylsulfoxide experiments failed to produce any co-crystal polymorph. For comparison purposes, pure CBZ and SAC were also processed by SAS.

## 1. Introduction

The production of co-crystals is reaching a major importance in the pharmaceutical industry not only to overcome some crucial drawbacks of new produced drugs such as poor solubility, inadequate dissolution profiles or short shelf-life, but also to improve the drug organoleptic and mechanical properties [1]. Moreover, multidrug co-crystallization

is becoming an important field of research in the treatment of some complex disorders [2]. A broad and generally accepted definition of co-crystal would be “a stoichiometric multi-component system connected by non-covalent interactions where all the components present are solid under ambient conditions” [3]. A pharmaceutical co-crystal would therefore involve a bonding through supramolecular synthons of at least an active pharmaceutical ingredient (API) and another API (in

Abbreviations: API, active pharmaceutical ingredient; BCS, Biopharmaceutics Classification System; BPR, back pressure regulator; CBZ, carbamazepine; CSS, co-crystallization with supercritical solvent; DCM, dichloromethane; DSC, differential scanning calorimetry; DMSO, dimethylsulfoxide; EMA, European Medicines Agency; FDA, Food and Drug Administration; FTIR, Fourier transform infrared; GAS, gas anti-solvent; HPLC, high performance liquid chromatography; P, pressure; T, temperature; SAC, saccharin; SAS, supercritical anti-solvent; SEA, supercritical fluid enhanced atomization; SEM, scanning electron microscopy; PXRD, powder X-ray diffraction

Corresponding author at: Departamento de Química Física I, Facultad C. Químicas, Universidad Complutense, E-28040 Madrid, Spain. E-mail address: [pando@quim.ucm.es](mailto:pando@quim.ucm.es) (C. Pando).

<https://doi.org/10.1016/j.supflu.2018.02.004>

Received 18 December 2017; Received in revised form 2 February 2018; Accepted 2 February 2018

Available online 08 February 2018

0896-8446/© 2018 Elsevier B.V. All rights reserved.



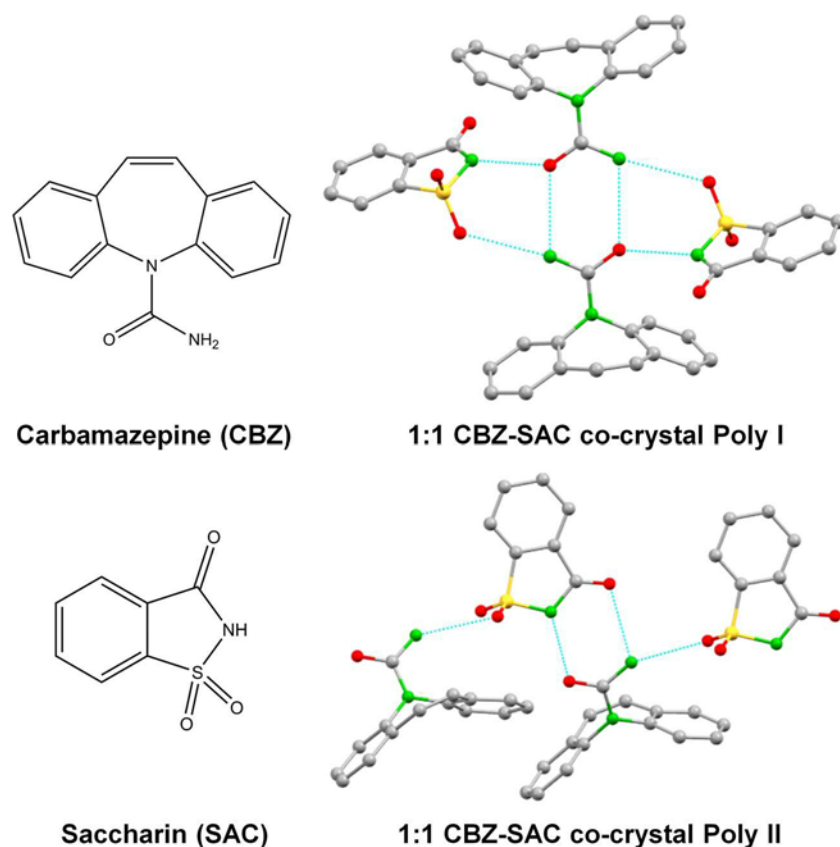


Fig. 1. Molecular structures of carbamazepine, saccharin, and the two polymorphs of the 1:1 carbamazepine-saccharin co-crystal showing the supramolecular synthons involved.

case of multidrug co-crystals), or a suitable coformer. A guidance and regulatory classification for pharmaceutical co-crystals has been recently given by the European Medicines Agency (EMA) [4] and the United States Food and Drug Administration (FDA) [5]. According to the recent rules, co-crystals are considered a drug polymorph rather than a new API and drug development and regulatory submissions are simplified [6].

In this study, we investigate the production of the 1:1 co-crystal of carbamazepine (CBZ) and saccharin (SAC) using the supercritical antisolvent (SAS) technique; this co-crystal consists of CBZ and SAC molecular units in the stoichiometric ratio 1:1 linked through the bonds shown in Fig. 1. CBZ (molar mass = 236.27 g mol<sup>-1</sup>) is a poorly water-soluble drug used primarily in the treatment of epilepsy and trigeminal neuralgia that belongs to BCS class II. CBZ has five known anhydrous polymorphs [7–19] (at room temperature the most stable polymorph is polymorph III, an enantiotropic pair of polymorph I), and several dihydrate and solvate polymorphs. CBZ solubilities in water and simulated gastric fluid may be found in Refs. [20,21]. CBZ major problems are its slow rate of absorption when administered through oral route, and its tendency to adopt the dihydrate form, which reduces its solubility in water to nearly a half of that of its anhydrous form. Therefore, larger doses of the drug are required in order to be effective. Aiming to improve CBZ performance, the co-crystallization of CBZ with coformer SAC has been widely studied during the last decade. Saccharin (molar mass = 183.18 g mol<sup>-1</sup>) is widely used as coformer in the preparation of pharmaceutical salts (acting as a weak acid when combined with a sufficiently basic molecule), or co-crystals (remaining then a neutral molecule). SAC has one known polymorph [22] and good water solubility [21]. The first published structure of the CBZ-SAC co-crystal reported by Fleischman et al. [23] corresponds to the more stable polymorph I [24] and was produced by slow evaporation from an equimolar solution of CBZ and SAC in ethanol. The structures of CBZ and SAC along with the co-crystal polymorphs are shown in Fig. 1. In polymorph

I, the CBZ molecules are bonded to each other through an amide–amide homosynthon and the saccharin molecules bond through a pyridine–carbonyl oxygen H-bond to a CBZ molecule and through a sulfonyl oxygen–amide H-bond to another CBZ molecule. The polymorph II of the co-crystal was discovered later by Porter et al. [25] using evaporation crystallization from an ethanol solution with the aid of functionalized cross-linked polymers. In polymorph II, the amide–amide homosynthon of polymorph I established between the two CBZ molecules disappears and each molecule of CBZ bonds through a pyridine–carbonyl oxygen and an amide–carbonyl oxygen H-bond to one saccharin molecule; and through an amide–sulfonyl oxygen to another saccharin molecule (see Fig. 1). Huskić et al. [26] and Maeshwari et al. [27] reported the formation of other polymorphs, but no crystallographic information file of these polymorphs is available yet and most authors only take into account the co-crystal polymorphs I and II.

A co-crystal can be prepared by several conventional methods with the aid of solvents (evaporative or cooling crystallization and reaction crystallization), directly from the solid state (mechanical grinding or melt crystallization) or using some more novel co-crystallization methods [6]. The use of conventional methods often presents scaling-up difficulties, leads to the presence of crystals of the individual components (homocrystals) in the final product and often involves post purification steps to eliminate solvents [1,28–30]. To overcome these difficulties several processes using supercritical CO<sub>2</sub> have been developed for the preparation of pharmaceutical co-crystals [6,31]. These processes generally involve fewer steps, reduced amounts of organic solvents, and use CO<sub>2</sub> that is considered a green solvent [32] because this fluid is innocuous, non-flammable, may be recycled and has readily accessible critical parameters (31 °C and 7.4 MPa). Thus, the sustainable process requirements of the pharmaceutical industry can be fulfilled using supercritical CO<sub>2</sub> based processes. The CBZ-SAC co-crystal has already been produced using two supercritical techniques: supercritical fluid enhanced atomization (SEA) [33] and co-crystallization

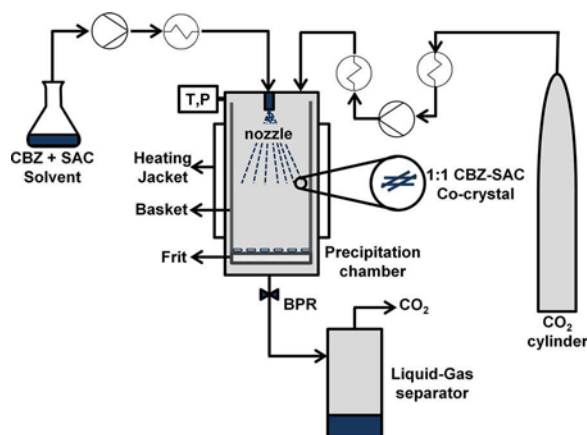


Fig. 2. Schematic representation of the supercritical fluid anti-solvent (SAS) technique used to obtain the 1:1 CBZ-SAC co-crystal. T, P, temperature and pressure measurement; BPR, back pressure regulator.

with supercritical solvent (CSS) [34]. It is not clear though which polymorph was obtained using the SEA technique while the more stable polymorph I was produced using CSS. The SAS technique may be applied to pharmaceuticals with relatively low solubility in supercritical CO<sub>2</sub>. Pharmaceuticals are dissolved in a polar organic solvent miscible with supercritical CO<sub>2</sub>. When the organic solution and the fluid are brought into contact, supersaturation takes place and precipitation starts. Solvent-free particles that exhibit narrow size distributions are obtained. In the case of pure drugs, properties such as particle size, morphology and polymorphism may be easily modified through the SAS technique by selecting different operational variables such as pressure, solution and CO<sub>2</sub> flow rates and temperature [35–38]. At our laboratory, we have already assessed the use of the SAS technique to successfully coprecipitate the biocompatible polymer poly-vinylpyrrolidone and diflunisal [39], and to obtain a co-crystal of di-flunisal and nicotinamide [40]. Also, we have recently reviewed the preparation of pharmaceutical co-crystals using SAS and other super-critical techniques [31]. Each method was described and its application, advantages and disadvantages were discussed. Our aim in this paper is the preparation of the CBZ-SAC co-crystal using the SAS process and the investigation of the SAS co-crystal polymorphism.

Due to the improved properties of the CBZ-SAC co-crystals, other authors have produced them using a wide range of conventional methodologies: grinding co-crystallization [27,41–43]; cooling crystallization [44,45]; membrane based anti-solvent crystallization [46,47]; reaction co-crystallization [48]; ultrasound-induced co-crystallization [49]; continuous hot melt extrusion co-crystallization [50] and anti-solvent co-crystallization [51,52]. We here would like to highlight the studies where polymorphism of the CBZ-SAC co-crystal was observed. Rager and Hilfiker [53] prepared this co-crystal using the reaction co-crystallization method. They were able to obtain pre-cipitates of pure CBZ-SAC co-crystal polymorph I when using pure ethylene glycol, dimethylsulfoxide (DMSO) or dimethylformamide and polymorph II when using pure acetone or dioxane. Wang et al. [54,55] used anti-solvent co-crystallization to prepare the CBZ-SAC co-crystal. As anti-solvent they used water, and as solvent they tried ethanol, acetone, methylacetate, ethylacetate and methanol; the co-crystallization was only successful using the latter. They found that kinetic parameters such as anti-solvent addition rate and agitation speed influenced the polymorphism of the co-crystal obtaining a highly pure polymorph II of the co-crystal when addition rate and agitation speed were lower. Pagire et al. [21] developed a spherical crystallization process using a reverse anti-solvent method in which a solution prepared with a good solvent of the cofomers (DMSO, ethanol or methanol) is added into an anti-solvent solution (water) with bridging liquids (benzene, dichloromethane, DCM, or ethylacetate). They were

able to produce a nearly pure polymorph II CBZ-SAC co-crystal phase and concluded that the formation of a specific polymorph depended on the supersaturation level achieved with respect to both the co-crystal and the reacting components.

## 2. Materials and methods

### 2.1. Materials

The materials employed were CO<sub>2</sub> (Air Liquide 99.98 mol% pure), carbamazepine (Sigma-Aldrich, meeting USP testing specifications), saccharin (Sigma-Aldrich, ≥99 mol% pure), acetone (Sigma-Aldrich ≥99.8 mol% pure), dichloromethane (Sigma-Aldrich ≥99.9 mol% pure), dimethylsulfoxide (Sigma-Aldrich ≥99.9 mol% pure), methanol (Fischer chemical ≥99.9 mol% pure) and ethanol (PanReac 99.5 v/v% pure).

### 2.2. Supercritical fluid anti-solvent (SAS) precipitation and design of experiments

Fig. 2 illustrates the SAS technique used to prepare the CBZ-SAC co-crystal, a complete description of the high-pressure equipment involved can be found elsewhere [40]. Compressed CO<sub>2</sub> was cooled to –1 °C in a chiller and pumped into the system using a high-pressure pump (Thar-SCF high pressure Pump P-50) at a given rate. The CO<sub>2</sub> passed through a heat exchanger, where temperature was raised to the desired experimental value, before entering a 500 mL precipitation chamber. A back pressure regulator (BPR, Thar-SCF ABPR-20) situated at the exit of the chamber kept the pressure constant throughout the experiment. When steady conditions were reached a 1:1 molar ratio solution of CBZ and SAC in one of the studied solvents (methanol, ethanol, DCM or DMSO) was injected using a high performance liquid chromatography (HPLC) pump (lab Alliance series III pump) into the precipitation chamber through a 100 μm nozzle at a given flow rate. The precipitation chamber was equipped with a heating jacket to ensure that the experiment occurred at the desired temperature. After injection the fluid dissolves in the solution, the mixture becomes supersaturated and precipitation starts. Inside the chamber, a basket with a filter (frit, 2 μm) was placed in order to collect the microparticles obtained. The effluent exiting the BPR was directed to a cyclone separator where CO<sub>2</sub> was separated from the waste. After spraying approximately 30 mL of solution the HPLC pump was stopped and CO<sub>2</sub> (three times the volume of the chamber at the same precipitation conditions) was allowed to flow through the chamber at 20 g/min to ensure that the product was dry and free of solvent.

The characteristics of precipitates obtained using the SAS process may be modified by varying the different operational parameters: solution concentration, temperature, pressure, solution flow rate, super-critical CO<sub>2</sub> flow rate, nozzle diameter, drying time and choice of solvent. In this research we will concentrate in the influence of temperature, pressure and concentration which have been shown to be important variables in previous studies [40], and the solvent election which has been shown to be a key factor in obtaining a specific polymorph [56]. The chosen solvents were ethanol and methanol as polar protic solvents (dielectric constants of 24.55 and 33, respectively), and DCM and DMSO as polar aprotic solvents (dielectric constants of 9.2 and 46.7, respectively). CO<sub>2</sub> flow rate was fixed to 20 g/min and solution flow rate to 1 mL/min. As to the pressure and temperature conditions, operating in the supercritical region is usually convenient. However, there is no available phase equilibria data for the quaternary mixtures formed by CO<sub>2</sub>, the solvent, and the two cofomers. Due to the low solubility of CBZ and SAC in supercritical CO<sub>2</sub> [34,57,58] we decided to neglect their possible effect in the system phase diagram, and used the available data for the binary CO<sub>2</sub> + solvent system to establish temperature and pressure conditions above the critical locus [59–61]. The effect of using a different solvent was assessed at 40.0 °C

Table 1

Operational parameters and summary of the results for the 1:1 CBZ-SAC SAS co-crystallization using several solvents at 40.0 °C and 10.0 MPa.<sup>a</sup>

Run	Solvent	CBZ concentration (mg/mL)	Yield (%)	Polymorph	Melting point (°C)	Morphology
1	Methanol	30	65	I	174.7	Plate-like
2	Ethanol	15	55	I + II	163.9; 172.1	Plate-like and needle-like
3	DCM	2.6	40	I + II	172.1	Plate-like and needle-like
4	DMSO	65	–	–	–	–

<sup>a</sup> In all runs: solution flow rate = 1 mL/min; CO<sub>2</sub> flow rate: 20 g/min; nozzle diameter 100 µm; SAC concentration in equimolar ratio.

Table 2

Operational parameters and summary of results for the 1:1 CBZ-SAC SAS co-crystallization using methanol.<sup>a</sup>

Run	T (°C)	P (MPa)	CO <sub>2</sub> density <sup>b</sup> (mg/mL)	CBZ concentration (mg/mL)	Yield (%)	Polymorph	Melting point (°C)	Morphology
1	40.0	10.0	0.63	30	65	I	174.7	Plate-like
5	40.0	15.0	0.78	30	50	I	174.7	Plate-like
6	60.0	15.0	0.60	30	60	I + II	164.9; 170.0	Needle-like
7	60.0	15.0	0.60	15	45	I + II	166.0; 171.5	Needle-like

<sup>a</sup> In all runs: Solution flow rate = 1 mL/min; CO<sub>2</sub> flow rate: 20 g/min; nozzle diameter 100 µm; SAC concentration in equimolar ratio. Each run was repeated three times to assess reproducibility.<sup>b</sup> CO<sub>2</sub> density was taken from Ref. [67].

and 10.0 MPa, a condition slightly above the critical point of the mixture of CO<sub>2</sub> with any of the studied solvents (see Table 1). As to the coformers concentration in the organic solution, solubility data of CBZ, SAC and the co-crystals polymorph I and II in the different solvents previously published [21] were taken into account. The concentration values shown in Table 1 were selected to be relatively close to the saturation values of the less soluble coformer in the solvent and always maintaining the 1:1 stoichiometric ratio. The effects of pressure, temperature and concentration were observed using methanol as solvent, reducing CBZ concentration to 15 mg/mL, and increasing temperature up to 60.0 °C and pressure up to 15.0 MPa (see Table 2).

### 2.3. Solid characterization

A JEOL-6335F JSM electron microscope working with an accelerating voltage of 10 or 20 kV, was used to characterize the size and morphology of the microparticles obtained in the SAS experiments. Prior to analysis, samples were coated with gold in a Q150RS Rotary-Pumped Sputter Coater.

Powder X-ray diffraction (PXRD), was used to study the crystalline form of carbamazepine and saccharin prior and after SAS treatment, to identify the co-crystal form obtained in the SAS experiments and to exclude the presence of homocrystals. PXRD patterns of the solids were obtained using a Philips X'pert, model MPD powder diffractometer with vertical goniometer  $\theta$ -2 $\theta$ . A Cu anode X-ray tube was powered at 40 kV and 40 mA ( $K\alpha_1$  1.54056 Å). Scans were measured between 5° and 60° 2 $\theta$  with a step size of 0.016° 2 $\theta$  and a continuing time of 5 s per step. The detection limit is 2% mass.

Differential scanning calorimetry (DSC) was used to obtain the melting point data of carbamazepine and saccharin prior and after SAS treatment, and the co-crystals obtained in SAS experiments. These data are used together with PXRD patterns to establish the polymorph or polymorphs present in the sample. Also, the broad peak associated to the dehydration of CBZ hydrate is used to detect the presence of this poorly soluble CBZ form. DSC thermograms were measured using a TA Instruments DSC model Q-20 connected to a refrigerating cooling system. Tightly sealed volatile aluminum pans containing the samples were heated at a 5 °C/min rate in dry nitrogen, flowing at 50.0 mL/min. A MT5 Mettler microbalance was used to weigh the samples, ranging between 3 and 10 mg (with an error of  $\pm$  0.001 mg). Temperature and enthalpy of the calorimeter were previously calibrated using standard samples of In (purity > 99.999%), Sn (> 99.9%) and benzoic acid (> 99.97%).

As a complement of DSC, thermogravimetric analysis (TGA) was performed to study the stability of materials with temperature. A TA Instruments Q500 thermobalance was used. Samples were placed in Pt containers and heated at 5 °C/min under a 100 mL/min N<sub>2</sub> flow from room temperature to 400 °C.

Fourier transform infrared (FTIR) spectroscopy was also used to study the intermolecular interactions between the coformers in the co-crystals. The functional groups in the co-crystal spectrum show differences in the wavenumbers and intensity of the vibrational modes in comparison to those of the two coformers individual spectra. Furthermore, bands characteristic of the synthons established are observed. Carbamazepine, saccharin and co-crystal spectra were collected using the spectrum 100 Fourier-transform infrared spectrometer from Perkin Elmer with the universal attenuated total reflection (ATR) sampling accessory at a resolution of 4 cm<sup>-1</sup>. Samples were measured in the 4000–650 cm<sup>-1</sup> range.

## 3. Results and discussion

### 3.1. Influence of solvent

The first experiments were conducted under the same conditions of pressure (10.0 MPa) and temperature (40.0 °C) in order to assess the influence of the solvent. The other conditions used and a summary of the results obtained can be seen in Table 1. Each run was repeated three times to assess reproducibility. The yield shown in Tables 1 and 2 was calculated as an average of values obtained in the three experiments. Each value was estimated using a mass balance. The amounts of co-former injected in the precipitation chamber were calculated taking into account the concentration and flow of solution and the injection time. After precipitation the amount of powder in the precipitation chamber and the waste in the liquid-gas separator were weighed.

The PXRD patterns of polymorphs I and II and those of precipitates obtained in runs 1–3 are shown in Fig. 3. The main diffraction peaks of both co-crystal polymorphs are highlighted, diffractions at 2 $\theta$  = 7.0, 14.1, 23.9 and 28.3° are characteristic of polymorph I, whilst the diffractions at 2 $\theta$  = 5, 11.5, 12.8, 15 and 25.7° correspond to the polymorph II. In run 1 using methanol, only representative diffraction peaks of polymorph I are found. In runs 2 and 3, using ethanol and DCM, respectively, a mix of both polymorphs can be observed. Diffraction peaks associated to homocrystals did not appear in the PXRD patterns shown in Fig. 3 for runs 1–3. In comparison to the single crystals that may be obtained through conventional co-crystallization methods, the

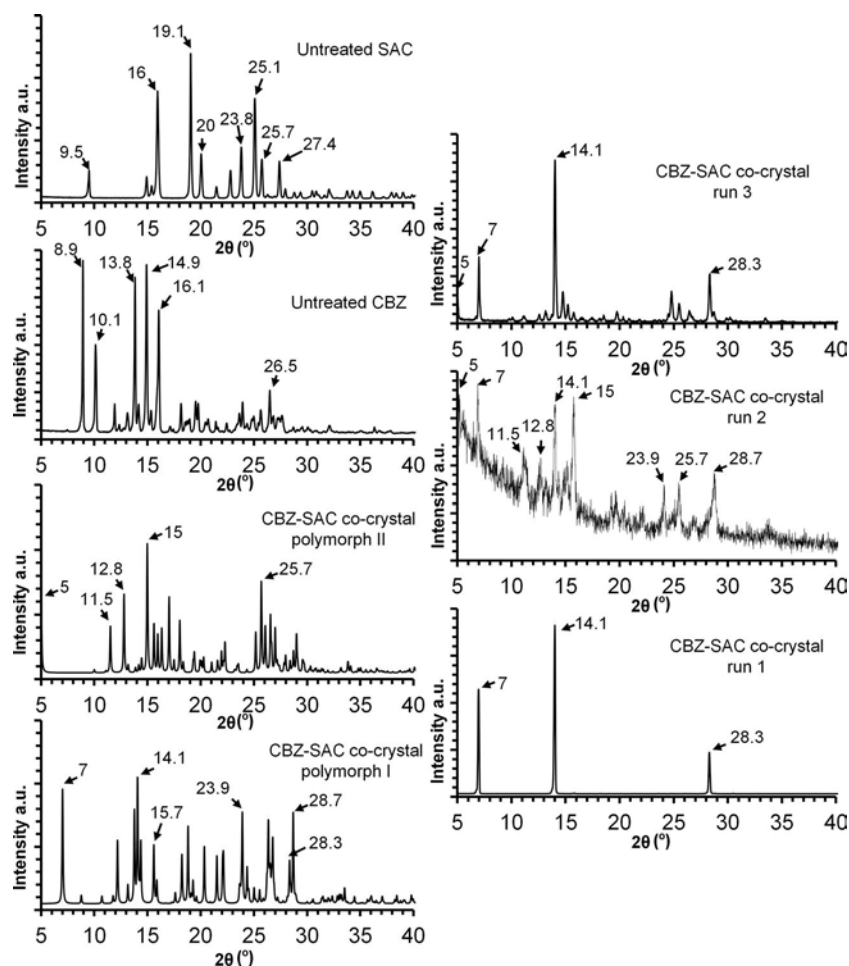


Fig. 3. PXRD patterns of left: CBZ-SAC co-crystals polymorphs I (bottom) and II (top) simulated from crystallographic information file and experimental patterns for untreated CBZ and SAC; right: experimental patterns from CBZ-SAC co-crystals obtained using methanol (bottom), ethanol (middle) and DCM (top).

powder or microcrystalline samples resulting from SAS precipitation exhibit wider diffraction peaks and often show preferential orientation. This is particularly clear in run 2 using ethanol where the precipitate obtained shows less crystallinity. In run 4 where DMSO was the solvent, the experiment failed to produce any precipitate. A probable enhanced solubility of the co-crystal cofomers in the supercritical  $\text{CO}_2$ -DMSO system would explain the lack of precipitate in the precipitation chamber and the clogging formed in the BPR during the experiment. For these reasons, DMSO is not recommended as a solvent in the pre-precipitation of CBZ-SAC co-crystals using the SAS technique.

Further characterization of the samples was carried out using differential scanning calorimetry and thermogravimetric analysis. DSC thermograms of commercial CBZ, SAC and the SAS precipitates are shown in Fig. 4 using the same scale for all thermograms. Melting transitions were measured reading the onset temperature of the peak. Porter et al. [25] carried out a thermogravimetric analysis of both polymorphs of CBZ-SAC co-crystals and found a single nonreversible transition for polymorph I with an onset temperature at 172 °C. For polymorph II a nonreversible transition with an onset at 168 °C was followed by a small non reversible transition with an onset at 172 °C. Threlfall [62] explained the different types of DSC traces which are likely to take place in a dimorphic system. The peak with an onset at 168 °C is characteristic of the less stable polymorph of the CBZ-SAC co-crystal (polymorph II). Precipitates obtained in runs 1–3 show melting temperatures below the melting points of untreated CBZ (189.9 °C) and SAC (227.8 °C). Also, the broad peak associated to the dehydration of CBZ hydrate does not appear in the thermograms [20]. The precipitate obtained using methanol (run 1) melted at 174.7 °C, a value similar to

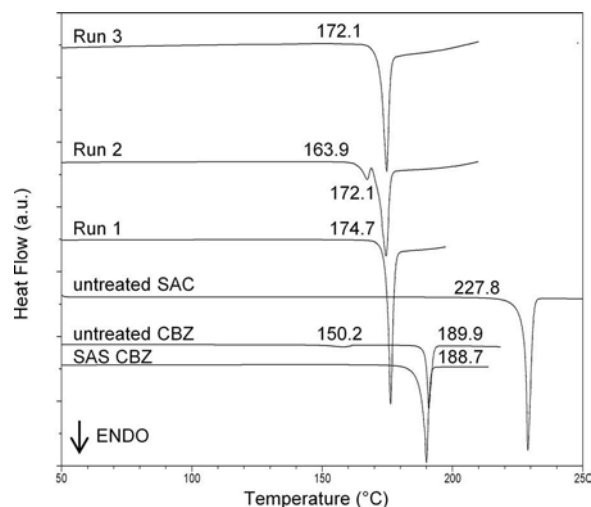


Fig. 4. DSC thermograms measured at a heating rate of 5 °C/min of untreated CBZ and SAC, SAS processed CBZ and the co-crystals obtained in runs 1, 2 and 3.

that reported for polymorph I [23,25]. In the SAS precipitate using ethanol (run 2) the transition appearing at 163.9 °C indicates the presence of polymorph II. Contrary to the published behavior for pure polymorph II, in the ethanol precipitate the smaller transition is the first event suggesting the presence of a mixture of polymorphs I and II. As to the DCM precipitate (run 3), the PXRD pattern evidences the presence

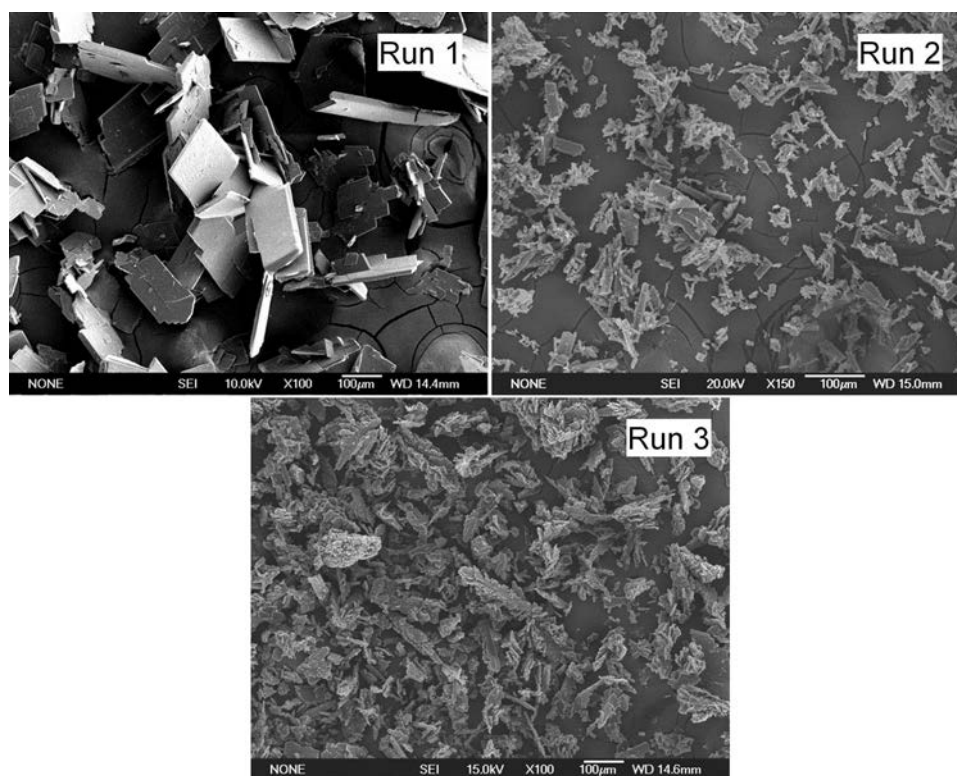


Fig. 5. SEM images of CBZ-SAC co-crystals obtained in runs 1, 2 and 3.

of both polymorphs. However, the thermogram of run 3 only exhibits a melting transition at 172.1 °C. This could be due to a lower content of polymorph II in this sample.

Overlays of DSC/TGA thermograms for runs 1–3 are included as Supplementary material. These thermograms evidence that mass loss in samples started with the melting transition. In the case of run 1 where the precipitate consisted only in polymorph I, an estimate for the heat of fusion can be obtained from peak integration. This value may be corrected taking into account the mass loss. These values are given in the Supplementary material.

The morphology of both polymorphs has already been reported [25]. Polymorph I of the co-crystal presents a plate-like morphology whilst polymorph II exhibits a needle-like one. SEM images of the different SAS precipitates are shown in Fig. 5. Here we can observe that the co-crystals obtained using methanol as a solvent (run 1) present mainly a plate-like morphology accompanied by some plate-like agglomerates. Crystals exhibit heterogeneous sizes with widths varying from 5 to 10 µm. Runs 2 and 3 present a more noticeable mixture of morphologies. In the precipitate obtained using ethanol as a solvent (run 2), a mixture of agglomerated plate-like and agglomerated needle-like morphologies can be observed. In the one obtained using DCM (run

3) plate-like crystals seems to agglomerate in one direction. The presence of plain plate-like and needle-like morphologies in runs 2 and 3 seems to confirm a mixture of both polymorphs of the CBZ-SAC co-crystal. Particles are much smaller in runs 2 and 3 using ethanol and DCM.

Samples obtained were also analyzed using FTIR and results are presented in Fig. 6. As explained in detail in the Introduction, the bonds connecting the cofomers to each other in the CBZ-SAC co-crystals change from polymorph I to polymorph II. As a consequence, the absorption bands corresponding to the amide and carboxylic group present in the carbamazepine in the co-crystal polymorph I will be shifted in the co-crystal polymorph II. The stretching bands of the amide that take place at 3501 cm<sup>-1</sup> (asymmetric) and 3434 cm<sup>-1</sup> (symmetric) in polymorph I red shift to 3430 cm<sup>-1</sup> and 3350 cm<sup>-1</sup> in polymorph II.

The vibration frequency at 1645 cm<sup>-1</sup> in polymorph I, probably due to the asymmetric stretching of the amide carboxylic group, blue shifts to 1668 cm<sup>-1</sup> in polymorph II [25]. In the FTIR spectra of the SAS precipitates, we can see that the precipitate obtained using methanol shows the characteristic absorption bands of polymorph I (3500, 3434 and 1645 cm<sup>-1</sup>). Although the absorption bands obtained using ethanol (3424 cm<sup>-1</sup> with shoulder at 3465, 3344 and 1657 cm<sup>-1</sup>) and DCM (3444, 3336 and 1657 cm<sup>-1</sup>), exhibit frequencies similar to those of polymorph II, PXRD patterns show the presence of both polymorphs in the precipitates.

Only the runs where methanol was the solvent seemed to lead to a pure phase of co-crystal polymorph I. Polymorph I, and mixtures of polymorph I and the CBZ-dihydrate, were the only forms obtained using any of the studied solvents and a 1:1 molar ratio of CBZ and SAC in previous conventional anti-solvent experiments [21]. Polymorph I could also be expected because it has been previously reported that the generation of this polymorph by conventional anti-solvent technique is favoured by higher supersaturation conditions [55], conditions that are characteristic of the SAS technique. An advantage of not using water as an anti-solvent in the SAS process is that none of the precipitates contains the less soluble dihydrate form of CBZ. Experiments were performed using only supercritical CO<sub>2</sub> as anti-solvent. At the studied conditions of temperature, CO<sub>2</sub> molar fraction and pressure, ethanol, methanol, DCM and DMSO are fully miscible with CO<sub>2</sub> forming one supercritical phase [59,61]. We can therefore expect that the different polymorphs obtained in runs 1–4 should also be a result from the solvent-solute interaction. The CBZ-SAC-solvent phase diagram is related to the different solubilities of the co-crystal cofomers in the selected solvent. In the case of methanol, the solubilities of both cofomers are relatively similar [21] and a congruently saturating system can be expected. In the case of ethanol, DMSO and DCM, solubilities differ in one order of magnitude so a ternary phase diagram of an incongruently saturating system could be expected. In a previous investigation of the naproxen-nicotinamide co-crystal formation using the SAS technique [63] it was pointed out that incongruent saturating systems can lead to

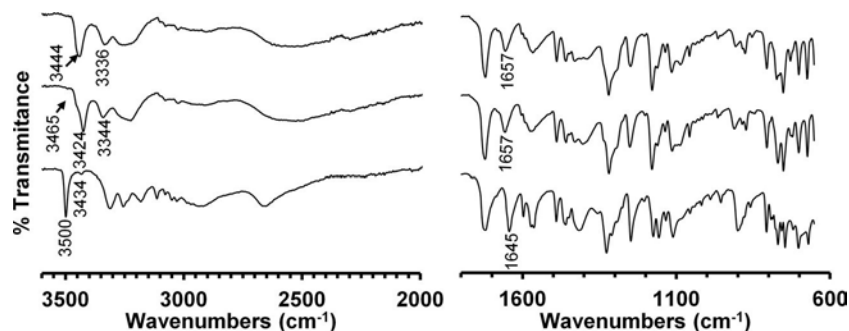


Fig. 6. FTIR spectra of the CBZ-SAC co-crystals: run 1 (bottom), run 2 (middle) and run 3 (top).

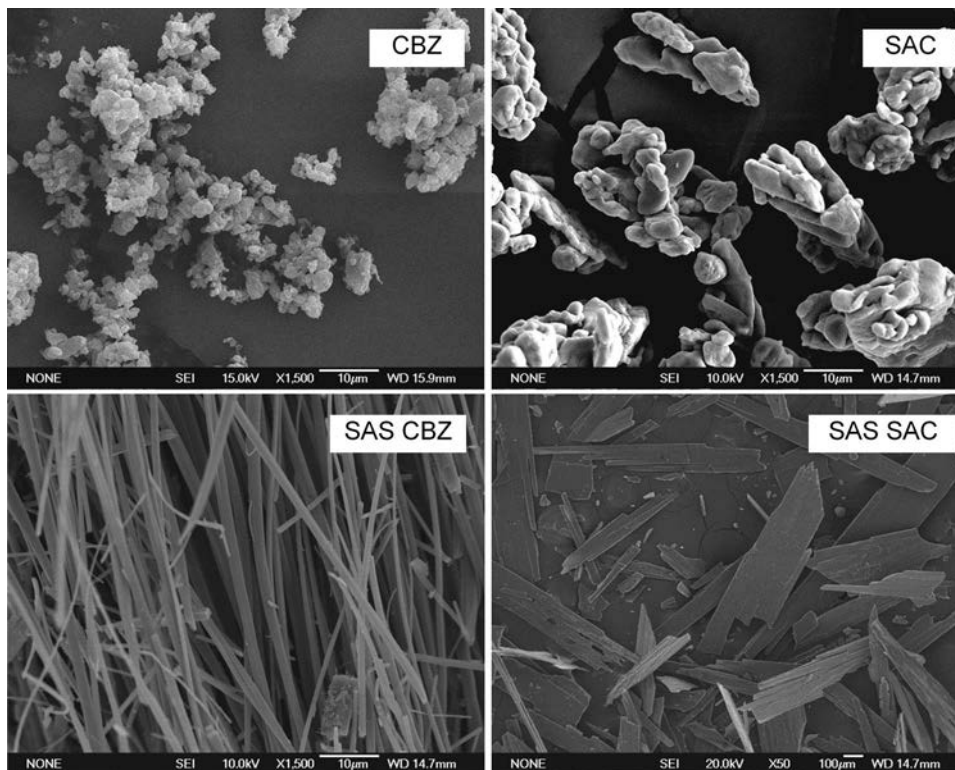


Fig. 7. SEM images of untreated CBZ and SAC, and SAS processed CBZ and SAC using conditions of run 1.

the formation of homocrystals. In our case no homocrystals are formed but a mix of both co-crystal polymorphs is obtained as can be observed in the PXRD pattern shown in Fig. 3.

### 3.2. SAS precipitation of pure CBZ and SAC

Fig. 7 shows SEM images of commercial and SAS processed co-formers at 40.0 °C and 10.0 MPa using methanol as solvent (conditions of run 1). PXRD patterns of commercial CBZ and SAC are shown in Fig. 3. PXRD patterns of SAS processed CBZ and SAC were also obtained and are given as Supplementary material. DSC thermograms for commercial and SAS processed CBZ are shown in Fig. 4. Commercial CBZ consists in a mixture of polymorphs I and III as indicated by the two endothermic peaks at 150.2 and 189.9 °C and the comparison of its PXRD pattern to those of CBZ pure polymorphs. However, the thermogram of SAS processed CBZ exhibits one single endothermic peak at 188.7 °C and the SAS processed CBZ PXRD pattern is coincident with that of CBZ polymorph I. Therefore, commercial CBZ changed its polymorphism as a consequence of SAS treatment. CBZ morphology changed from agglomerate particles to needle-like structures. In previous studies performed for pure CBZ using supercritical CO<sub>2</sub> and the

gas anti-solvent technique (GAS) [64], the starting polymorph III sample changed to mostly polymorph I regardless of the solvent used (acetone, ethylacetate and DCM). Several authors have pointed out the difficulty of producing distinct PXRD pure polymorphic forms of CBZ through SAS or GAS [64–66]. For instance, Padrela et al. [66] obtained a mixture of polymorphs II and III using GAS and starting with polymorph III. On the other hand, saccharin kept its monoclinic form and its morphology changed from agglomerated particles to fragmented thin plates presenting heterogeneous size.

### 3.3. Influence of operational conditions

In order to assess the influence of operational conditions further experiments with methanol as solvent were carried out varying temperature, pressure and coformer concentration. Table 2 shows the conditions studied and a summary of the results obtained. For comparison purposes, results of run 1 and values for the CO<sub>2</sub> density at the temperature and pressure conditions of the experiments are also included in this table.

PXRD and FTIR results for runs 5–7 are shown in Fig. 8. Increasing the pressure in the precipitation chamber did not lead to a polymorphic

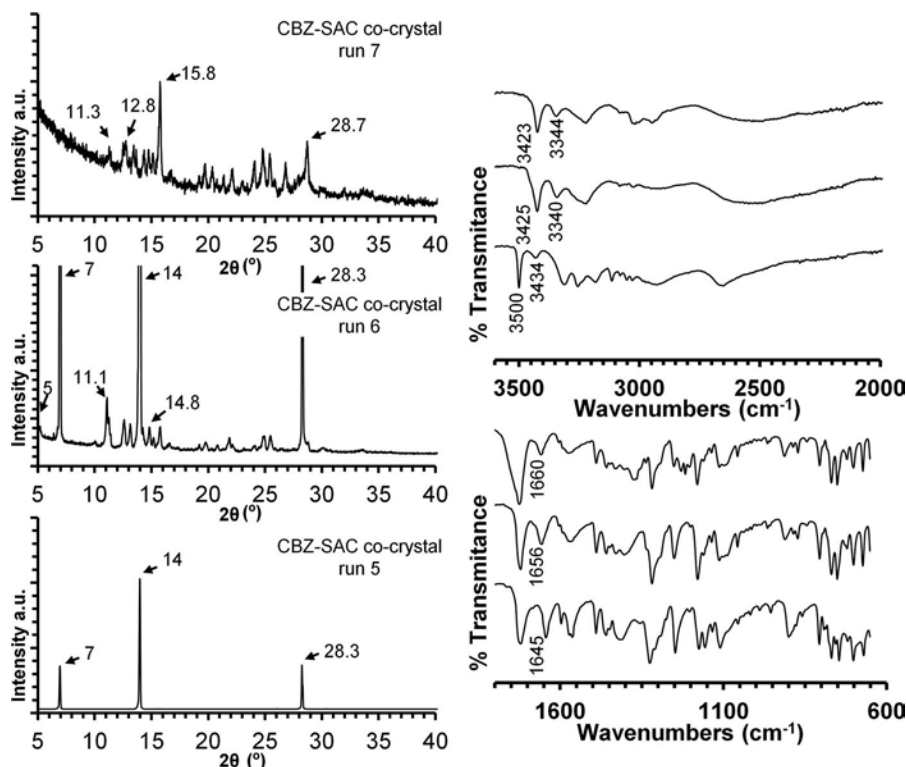


Fig. 8. Left: PXR patterns of run 5 (bottom), run 6 (middle) and run 7 (top); Right: FTIR spectra of run 5 (bottom), run 6 (middle) and run 7 (top).

change and the same reflections peaks and absorption bands of run 1 were found in the powder obtained in run 5. Increasing temperature though resulted in a mixture of polymorphs in the precipitate obtained in run 6. Reducing the concentration of the feeding solution at high temperature (run 7) produced a significant change in the PXR pattern. Intensities of the characteristic reflections for the polymorph I decreased and some reflections of polymorph II increased. The PXR pattern of run 7 shows nevertheless low crystallinity and conclusions about the polymorphs present and their ratio are difficult. Diffraction peaks associated to homocrystals did not appear in the PXR patterns shown in Fig. 8 for runs 5–7. FTIR spectra for runs 6 and 7 show absorption bands with frequencies similar to those of polymorph II.

DSC curves for precipitates obtained in runs 1, 5, 6 and 7 are shown in Fig. 9. Precipitates obtained in runs 5–7 also show melting

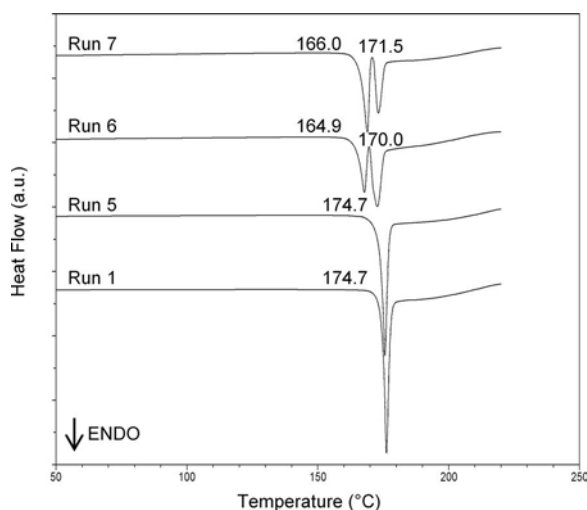


Fig. 9. DSC thermograms measured at a heating rate of  $5^\circ\text{C}/\text{min}$  of the co-crystals obtained in runs 1, 5, 6 and 7.

temperatures below the melting points of untreated CBZ and SAC and the broad peak associated to the dehydration of CBZ hydrate does not appear [20]. The almost identical curves for runs 1 and 5 indicate the presence of only polymorph I in these precipitates. However, DSC shows the presence of the transitions reported for polymorph II [25] when higher temperatures are used (runs 6 and 7). The fact that a pressure increase of 5 MPa (and therefore a supercritical  $\text{CO}_2$  density increase from 0.63 to 0.78  $\text{mg}/\text{mL}$ ) did not change the precipitate polymorphism seems to indicate that the anti-solvent density does not play a significant role in the polymorphic outcome. Nevertheless, a slight decrease in the precipitation yield was observed at the higher pressure. Increasing the temperature however, will influence the solubility of both cofomers in the selected solvent, and will therefore affect the ternary phase diagram leading to different polymorphs and their mixtures, and could also lead to homocrystal formation. As may be seen in Fig. 9, the temperature increase led to a thermogram where the peaks characteristic of polymorph form II are present [25]. In the case of run 6, similar to run 2, the smaller transition is the first one at 164.9  $^\circ\text{C}$ . Reducing the concentration of both crystal cofomers in the initial solution (run 7) resulted in an area increase of the first nonreversible peak (with onset at 166.0  $^\circ\text{C}$ ) with respect to that of the second nonreversible peak (onset at 171.5  $^\circ\text{C}$ ), indicating an increase in the polymorph II to polymorph I ratio. In summary, PXR patterns and DSC thermograms confirm the presence of polymorph I for run 5 and a mixture of poly-morphs for runs 6 and 7.

Overlays of DSC/TGA thermograms for runs 5–7 are included as Supplementary material. These thermograms evidence that mass loss in samples started with the melting transition. In the case of run 5 where the precipitate consisted only in polymorph I, the estimate for the heat of fusion obtained from peak integration and that resulting from taking into account the mass loss are also given in the Supplementary material.

Fig. 10 shows SEM images of CBZ-SAC co-crystals obtained in runs 1, 5, 6 and 7. A change in pressure had an influence on the morphology of the SAS precipitate and a higher amount of agglomerate was obtained when pressure was increased in run 5 with respect to run 1. A temperature increase in runs 6 and 7 with respect to run 5 resulted in a

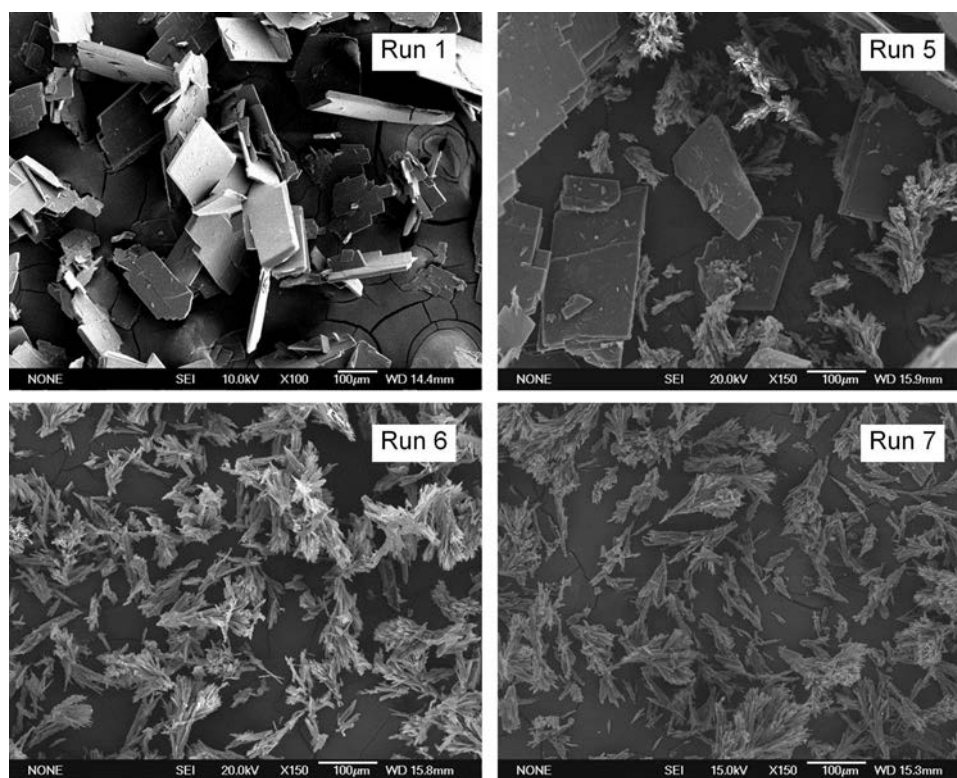


Fig. 10. SEM images of CBZ-SAC co-crystals obtained in runs 1, 5, 6 and 7.

CO<sub>2</sub> density reduction from 0.78 to 0.60 mg/mL and a change of the morphology from plate-like to a needle-like agglomerate, thus con-firming the presence of polymorph II in the precipitate that had also been observed in the PXRD patterns, FTIR spectra and thermal analysis. Reduction of the organic solution concentration did not lead to a sig-nificant change in the morphology and SEM images for runs 6 and 7 are similar. Therefore, it may be concluded that changes in CO<sub>2</sub> density in the range considered in this study influence the co-crystal morphology. However, these changes do not explain the polymorphic outcome. Neither the untreated or SAS processed crystals of CBZ or SAC were found in any of the co-crystal experiments. The SAS crystals and co-crystals images shown in Figs. 5, 7 and 10 demonstrate the reduction of size and the narrow size distribution obtained through this method.

#### 4. Conclusions

Starting from drug concentrations corresponding to the co-crystal stoichiometric composition, the production of 1:1 CBZ-SAC co-crystals using the SAS technique was achieved. SAS co-crystals exhibit the same crystal structure, morphology, FTIR spectra and melting point as those previously obtained by different methodologies. Within the detection limits, precipitates did not show the presence of homocrystals and were solvent free, thus, no further purification steps are required and co-crystals are readily produced in a one-step process with low environ-mental impact. The undesired dihydrate form of CBZ is avoided. Conditions to obtain polymorph I alone are clearly established and yields up to 65% are obtained. Unfortunately, precipitates of pure co-crystal polymorph II could not be obtained at the conditions and solvents used in this study. Variation of pressure and organic solution concentration in the system showed little influence in the polymorphic outcome of the precipitates while temperature and solvent selection were shown to be the key factors. These findings are in accordance with other SAS co-crystal investigations [63]. Changes in temperature or solvent will affect the ternary phase diagram and could lead to an in-congruent saturating system, thus producing different precipitate

outcomes.

The SAS process is therefore a suitable process for production of the pure CBZ-SAC co-crystal polymorph I as it operates at moderate tem-peratures using the green solvent supercritical CO<sub>2</sub> avoiding therefore the degradation of the product and limiting the use of organic solvents.

#### Acknowledgments

We gratefully acknowledge the financial support of the Spanish Ministry of Economy and Competitiveness (MINECO), research project CTQ2013-41781-P. I.A.C. thanks MINECO for its support through a FPI grant.

#### Appendix A. Supplementary data

Supplementary data associated with this article can be found, in the online version, at <https://doi.org/10.1016/j.supflu.2018.02.004>.

#### References

- [1] C.C. Sun, CocrySTALLIZATION for successful drug delivery, *Expert Opin. Drug Deliv.* 10 (2013) 201–213.
- [2] R. Thipparaboina, D. Kumar, R.B. Chavan, N.R. Shastri, Multidrug co-crystals: to-wards the development of effective therapeutic hybrids, *Drug Discov. Today* 21 (2016) 481–490.
- [3] R. Thakuria, A. Delori, W. Jones, M.P. Lipert, L. Roy, N. Rodriguez-Hornedo, Pharmaceutical cocrystals and poorly soluble drugs, *Int. J. Pharm.* 453 (2013) 101–125.
- [4] EMA, Reflection Paper on the Use of Cocrystals and Other Solid State Forms of Active Substances in Medicinal Products, (2015) [http://www.ema.europa.eu/docs/en\\_GB/document\\_library/Scientific\\_guideline/2015/07/WC500189927.pdf](http://www.ema.europa.eu/docs/en_GB/document_library/Scientific_guideline/2015/07/WC500189927.pdf).
- [5] FDA, Guidance for Industry: Regulatory Classification of Pharmaceutical Co-crys-tals, (2011) <https://www.fda.gov/downloads/Drugs/GuidanceComplianceRegulatoryInformation/Guidance/1054s/UCM281764.pdf>.
- [6] D. Douroumis, S.A. Ross, A. Nokhodchi, Advanced methodologies for cocrystal synthesis, *Adv. Drug Deliv. Rev.* (2017), <http://dx.doi.org/10.1016/j.addr.2017.07.008>.
- [7] J.P. Reboul, B. Cristau, J.C. Soyfer, J.P. Astier, 5H-5-dibenz(b, f)azepinecarbox-amide-5 (carbamazepine), *Acta Crystallogr. B: Struct. Sci.* 37 (1981) 1844–1848.
- [8] V.L. Himes, A.D. Mighell, W.H. Decamp, Structure of carbamazepine: 5H-dibenz (b,f)azepine-5-carboxamide, *Acta Crystallogr. B: Struct. Sci.* 37 (1981) 2242–2245.



- [9] J.N. Lisgarten, R.A. Palmer, J.W. Saldanha, Crystal and molecular structure of 5-carbamyl-5H-dibenzo(b,f)azepine, *J. Crystallogr. Spectrosc. Res.* 19 (1989) 641–649.
- [10] M.M.J. Lowes, M.R. Caira, A.P. Lotter, J.G. Vanderwatt, Physicochemical properties and X-ray structural studies of the trigonal polymorph of carbamazepine, *J. Pharm. Sci.* 76 (1987) 744–752.
- [11] M.D. Lang, J.W. Kampf, A.J. Matzger, Form IV of carbamazepine, *J. Pharm. Sci.* 91 (2002) 1186–1190.
- [12] A.L. Grzesiak, M.D. Lang, K. Kim, A.J. Matzger, Comparison of the four anhydrous polymorphs of carbamazepine and the crystal structure of form I, *J. Pharm. Sci.* 92 (2003) 2260–2271.
- [13] P. Fernandes, K. Shankland, A.J. Florence, N. Shankland, A. Johnston, Solving molecular crystal structures from X-ray powder diffraction data: the challenges posed by gamma-carbamazepine and chlorothiazide N,N-dimethylformamide (1/2) solvate, *J. Pharm. Sci.* 96 (2007) 1192–1202.
- [14] K.S. Eccles, S.P. Stokes, C.A. Daly, N.M. Barry, S.P. McSweeney, D.J. O'Neill, D.M. Kelly, W.B. Jennings, O.M.N. Dhubhghaill, H.A. Moynihan, A.R. Maguire, S.E. Lawrence, Evaluation of the Bruker SMART X2S: crystallography for the non-specialist? *J. Appl. Crystallogr.* 44 (2011) 213–215.
- [15] J.B. Arlin, L.S. Price, S.L. Price, A.J. Florence, A strategy for producing predicted polymorphs: catemeric carbamazepine form V, *Chem. Commun.* 47 (2011) 7074–7076.
- [16] N. El Hassan, A. Ikni, J.M. Gillet, A. Spasojevic-de Bire, N.E. Ghermani, Electron properties of carbamazepine drug in form III, *Cryst. Growth Des.* 13 (2013) 2887–2896.
- [17] E.M. Horstman, S. Goyal, A. Pawate, G. Lee, G.G.Z. Zhang, Y.C. Gong, P.J.A. Kenis, Crystallization optimization of pharmaceutical solid forms with X-ray compatible microfluidic platforms, *Cryst. Growth Des.* 15 (2015) 1201–1209.
- [18] I. Sovago, M.J. Gutmann, H.M. Senn, L.H. Thomas, C.C. Wilson, L.J. Farrugia, Electron density, disorder and polymorphism: high-resolution diffraction studies of the highly polymorphic neuronal drug carbamazepine, *Acta Crystallogr. B: Struct. Sci. Cryst. Eng. Mater.* 72 (2016) 39–50.
- [19] E. van Genderen, M.T.B. Clabbers, P.P. Das, A. Stewart, I. Nederlof, K.C. Barentsen, Q. Portillo, N.S. Pannu, S. Nicolopoulos, T. Gruene, J.P. Abrahams, Ab initio structure determination of nanocrystals of organic pharmaceutical compounds by electron diffraction at room temperature using a Timepix quantum area direct electron detector, *Acta Crystallogr. A: Found. Adv.* 72 (2016) 236–242.
- [20] Y. Kobayashi, S. Ito, S. Itai, K. Yamamoto, Physicochemical properties and bioavailability of carbamazepine polymorphs and dihydrate, *Int. J. Pharm.* 193 (2000) 137–146.
- [21] S.K. Pagire, S.A. Korde, B.R. Whiteside, J. Kendrick, A. Paradkar, Spherical crystallization of carbamazepine/saccharin co-crystals: selective agglomeration and purification through surface interactions, *Cryst. Growth Des.* 13 (2013) 4162–4167.
- [22] J.C.J. Bart, Crystal and molecular structure of saccharin (o-sulphobenzoicimide), *J. Chem. Soc. B: Phys. Org.* (1968) 376–382.
- [23] S.G. Fleischman, S.S. Kuduva, J.A. McMahon, B. Moulton, R.D.B. Walsh, N. Rodriguez-Hornedo, M.J. Zavorotko, Crystal engineering of the composition of pharmaceutical phases: multiple-component crystalline solids involving carbamazepine, *Cryst. Growth Des.* 3 (2003) 909–919.
- [24] M.A. Oliveira, M.L. Peterson, R.J. Davey, Relative enthalpy of formation for co-crystals of small organic molecules, *Cryst. Growth Des.* 11 (2011) 449–457.
- [25] W.W. Porter III, S.C. Elie, A.J. Matzger, Polymorphism in carbamazepine co-crystals, *Cryst. Growth Des.* 8 (2008) 14–16.
- [26] I. Huskic, J.C. Christopherson, K. Uzarevic, T. Friscic, In situ monitoring of vapour-induced assembly of pharmaceutical co-crystals using a benchtop powder X-ray diffractometer, *Chem. Commun.* 52 (2016) 5120–5123.
- [27] C. Maheshwari, A. Jayasankar, N.A. Khan, G.E. Amidon, N. Rodriguez-Hornedo, Factors that influence the spontaneous formation of pharmaceutical co-crystals by simply mixing solid reactants, *Cryst. Growth Des.* 11 (2009) 493–500.
- [28] H.G. Brittain, Co-crystal systems of pharmaceutical interest: 2011, *Cryst. Growth Des.* 12 (2012) 5823–5832.
- [29] R.A. Chiarella, R.J. Davey, M.L. Peterson, Making co-crystals – the utility of ternary phase diagrams, *Cryst. Growth Des.* 7 (2007) 1223–1226.
- [30] J.H. ter Horst, M.A. Deij, P.W. Cains, Discovering new co-crystals, *Cryst. Growth Des.* 9 (2009) 1531–1537.
- [31] C. Pando, A. Cabañas, I.A. Cuadra, Preparation of pharmaceutical co-crystals through sustainable processes using supercritical carbon dioxide: a review, *RSC Adv.* 6 (2016) 71134–71150.
- [32] H. Machida, M. Takesue, R.L. Smith, Green chemical processes with supercritical fluids: properties, materials, separations and energy, *J. Supercrit. Fluids* 60 (2011) 2–15.
- [33] L. Padrela, M.A. Rodrigues, S.P. Velaga, A.C. Fernandes, H.A. Matos, E.G. de Azevedo, Screening for pharmaceutical co-crystals using the supercritical fluid enhanced atomization process, *J. Supercrit. Fluids* 53 (2010) 156–164.
- [34] L. Padrela, M.A. Rodrigues, J. Tiago, S.P. Velaga, H.A. Matos, E.G. de Azevedo, Insight into the mechanisms of co-crystallization of pharmaceuticals in supercritical solvents, *Cryst. Growth Des.* 15 (2015) 3175–3181.
- [35] E. Reverchon, I. De Marco, Mechanisms controlling supercritical antisolvent precipitate morphology, *Chem. Eng. J.* 169 (2011) 358–370.
- [36] G.W. Brun, A. Martin, E. Cassel, R.M.F. Vargas, M.J. Cocero, Crystallization of caffeine by supercritical antisolvent (SAS) process: analysis of process parameters and control of polymorphism, *Cryst. Growth Des.* 12 (2012) 1943–1951.
- [37] N. Esfandiari, Production of micro and nano particles of pharmaceutical by supercritical carbon dioxide, *J. Supercrit. Fluids* 100 (2015) 129–141.
- [38] R. Camparelli, E. Reverchon, I. De Marco, Dependence of SAS particle morphologies on the ternary phase equilibria, *J. Supercrit. Fluids* 130 (2017) 273–281.
- [39] F. Zahran, A. Cabañas, J.A.R. Cheda, J.A.R. Renuncio, C. Pando, Dissolution rate enhancement of the anti-inflammatory drug diflunisal by coprecipitation with a biocompatible polymer using carbon dioxide as a supercritical fluid antisolvent, *J. Supercrit. Fluids* 88 (2014) 56–65.
- [40] I.A. Cuadra, A. Cabañas, J.A.R. Cheda, F.J. Martínez-Casado, C. Pando, Pharmaceutical co-crystals of the anti-inflammatory drug diflunisal and nicotina-mide obtained using supercritical CO<sub>2</sub> as an antisolvent, *J. CO<sub>2</sub> Util.* 13 (2016) 29–37.
- [41] A. Jayasankar, A. Somwangthanoj, Z.J. Shao, N. Rodriguez-Hornedo, Co-crystal formation during cogrinding and storage is mediated by amorphous phase, *Pharm. Res.* 23 (2006) 2381–2392.
- [42] A. Jayasankar, D.J. Good, N. Rodriguez-Hornedo, Mechanisms by which moisture generates co-crystals, *Mol. Pharm.* 4 (2007) 360–372.
- [43] S.R. Bysouth, J.A. Bis, D. Igo, Co-crystallization via planetary milling: enhancing throughput of solid-state screening methods, *Int. J. Pharm.* 411 (2011) 169–171.
- [44] M.B. Hickey, M.L. Peterson, L.A. Scoppettuolo, S.L. Morrisette, A. Vetter, H. Guzman, J.F. Remenar, Z. Zhang, M.D. Tawa, S. Haley, M.J. Zavorotko, O. Almarsson, Performance comparison of a co-crystal of carbamazepine with marketed product, *Eur. J. Pharm. Biopharm.* 67 (2007) 112–119.
- [45] Z. Rahman, R. Samy, V.A. Sayeed, M.A. Khan, Physicochemical and mechanical properties of carbamazepine co-crystals with saccharin, *Pharm. Dev. Technol.* 17 (2012) 457–465.
- [46] G. Di Profio, V. Grosso, A. Caridi, R. Caliandro, A. Guagliardi, G. Chita, E. Curcio, E. Drioli, Direct production of carbamazepine-saccharin co-crystals from water/ethanol solvent mixtures by membrane-based crystallization technology, *Cryst. Eng. Comm.* 13 (2011) 5670–5673.
- [47] A. Caridi, G. Di Profio, R. Caliandro, A. Guagliardi, E. Curcio, E. Drioli, Selecting the desired solid form by membrane crystallizers: crystals or co-crystals, *Cryst. Growth Des.* 12 (2012) 4349–4356.
- [48] A. Alhalaweh, L. Roy, N. Rodriguez-Hornedo, S.P. Velaga, pH-dependent solubility of indomethacin-saccharin and carbamazepine-saccharin co-crystals in aqueous media, *Mol. Pharm.* 9 (2012) 2605–2612.
- [49] I. Tomaszewska, S. Karki, J. Shur, R. Price, N. Fotaki, Pharmaceutical characterisation and evaluation of co-crystals: importance of in vitro dissolution conditions and type of coformer, *Int. J. Pharm.* 453 (2013) 380–388.
- [50] H. Moradiya, M.T. Islam, G.R. Woollam, I.J. Slipper, S. Halsey, M.J. Snowden, D. Douroumis, Continuous co-crystallization for dissolution rate optimization of a poorly water-soluble drug, *Cryst. Growth Des.* 14 (2014) 189–198.
- [51] S. Kudo, H. Takiyama, Production method of carbamazepine/saccharin co-crystal particles by using two solution mixing based on the ternary phase diagram, *J. Cryst. Growth* 392 (2014) 87–91.
- [52] M. Nishimaru, S. Kudo, H. Takiyama, Co-crystal production method reducing deposition risk of undesired single component crystals in anti-solvent co-crystallization, *J. Ind. Eng. Chem.* 36 (2016) 40–43.
- [53] T. Rager, R. Hilffker, Co-crystal formation from solvent mixtures, *Cryst. Growth Des.* 10 (2010) 3237–3241.
- [54] I.-C. Wang, M.-J. Lee, S.-J. Sim, W.-S. Kim, N.-H. Chun, G.J. Choi, Anti-solvent co-crystallization of carbamazepine and saccharin, *Int. J. Pharm.* 450 (2013) 311–322.
- [55] M.J. Lee, I.C. Wang, M.J. Kim, P. Kim, K.H. Song, N.H. Chun, H.G. Park, G.J. Choi, Controlling the polymorphism of carbamazepine-saccharin co-crystals formed during antisolvent co-crystallization using kinetic parameters, *Korean J. Chem. Eng.* 32 (2015) 1910–1917.
- [56] P. Subra-Paternault, C. Roy, D. Vrel, A. Vega-Gonzalez, C. Domingo, Solvent effect on tolbutamide crystallization induced by compressed CO<sub>2</sub> as antisolvent, *J. Cryst. Growth* 309 (2007) 76–85.
- [57] R. Bettini, L. Bonassi, V. Castoro, A. Rossi, L. Zema, A. Gazzaniga, F. Giordano, Solubility and conversion of carbamazepine polymorphs in supercritical carbon dioxide, *Eur. J. Pharm. Sci.* 13 (2001) 281–286.
- [58] D. Bolten, M. Türk, Micronisation of carbamazepine through rapid expansion of supercritical solution (RESS), *J. Supercrit. Fluids* 66 (2012) 389–397.
- [59] S.N. Jung, C.W. Yoo, H.Y. Shin, S.Y. Kim, K.P. Yoo, C.S. Lee, W.S. Huh, Measurements and correlation of high-pressure VLE of binary CO<sub>2</sub>-alcohol systems (methanol ethanol, 2-methoxyethanol and 2-ethoxyethanol), *Fluid Phase Equilib.* 185 (2001) 219–230.
- [60] C.J. Chang, C.Y. Day, C.M. Ko, K.L. Chiu, Densities and P-x-y diagrams for carbon dioxide dissolution in methanol, ethanol, and acetone mixtures, *Fluid Phase Equilib.* 131 (1997) 243–258.
- [61] A. Vega-Gonzalez, R. Tufeu, P. Subra, High-pressure vapor-liquid equilibrium for the binary systems carbon dioxide plus dimethyl sulfoxide and carbon dioxide plus dichloromethane, *J. Chem. Eng. Data* 47 (2002) 492–495.
- [62] T.L. Threlfall, Turning DSC charts of polymorphs into phase diagrams: a tutorial paper, *Org. Process Res. Dev.* 13 (2009) 1224–1230.
- [63] C. Neurohr, A. Erriguible, S. Laugier, P. Subra-Paternault, Challenge of the super-critical antisolvent technique SAS to prepare co-crystal-pure powders of naproxen-nicotinamide, *Chem. Eng. J.* 303 (2016) 238–251.
- [64] M. Moneghini, I. Kikic, D. Voinovich, B. Perissutti, P. Alessi, A. Cortesi, F. Princivale, D. Solinas, Study of the solid state of carbamazepine after processing with gas anti-solvent technique, *Eur. J. Pharm. Biopharm.* 56 (2003) 281–289.
- [65] D. Meng, J. Falconer, K. Krauel-Goellner, J. Chen, M. Farid, R.G. Alany, Self-built supercritical CO<sub>2</sub> anti-solvent unit design, construction and operation using carbamazepine, *AAPS PharmSciTech* 9 (2008) 944–952.
- [66] L. Padrela, J. Zeglinski, K.M. Ryan, Insight into the role of additives in controlling polymorphic outcome: a CO<sub>2</sub>-antisolvent crystallization process of carbamazepine, *Cryst. Growth Des.* 17 (2017) 4544–4553.
- [67] NIST Standard Reference Database Number 69, which can be accessed electronically through the NIST Chemistry Web Book (<http://webbook.nist.gov/chemistry/>).

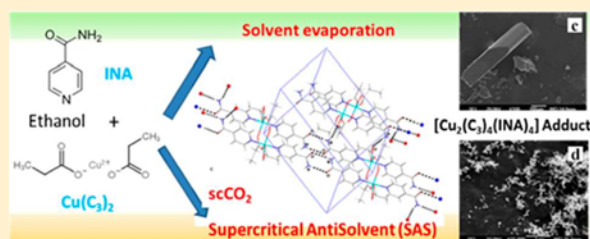
# Production and Characterization of a New Copper(II) Propanoate-Isonicotinamide Adduct Obtained via Slow Evaporation and using Supercritical CO<sub>2</sub> as an Antisolvent

Isaac A. Cuadra, Francisco J. Martínez-Casado,\*<sup>1b</sup> José A. R. Cheda, M. I. Redondo,<sup>1b</sup> Concepción Pando, and Albertina Cabañas\*<sup>1b</sup>

Dpto. Química Física, Universidad Complutense, E-28040 Madrid, Spain

## S Supporting Information

**ABSTRACT:** A new adduct of isonicotinamide (INA) with copper(II) propanoate [Cu(C<sub>3</sub>)<sub>2</sub>] was prepared [Cu<sub>2</sub>(C<sub>3</sub>)<sub>4</sub>(INA)<sub>4</sub>] using two different methods. This type of compound shows high fungicidal activity. Solvent evaporation from ethanol rendered crystals suitable for single-crystal X-ray diffraction. Furthermore, a new semicontinuous method capable of simultaneous crystallization and micronization of the adduct using supercritical CO<sub>2</sub>, the supercritical antisolvent technique (SAS), was also assessed. Crystals were characterized using powder X-ray diffraction, infrared spectroscopy, differential scanning calorimetry, thermogravimetric analysis coupled with mass spectrometry, scanning electron microscopy, and microelemental analysis. In the adduct, two copper(II) ions are coordinated through two bridging and two chelating carboxylates to the propanoate anions forming approximately a plane. Each metal ion is then coordinated with the pyridine nitrogen of two different INA molecules that behave as monodentate ligands. The amide groups of the INA form H-bonds with other amide and carboxylate groups forming a molecular crystal with a three-dimensional H-bond arrangement of the binuclear units. With the SAS technique, crystals 100-fold smaller than those obtained by slow evaporation were obtained, proving SAS as a suitable method for mixed-ligand complexes preparation with reduced particle size and therefore expected bioavailability enhancement.



## 1. INTRODUCTION

The synthesis and behavior of copper(II) alkanooates has been widely studied during the last decades.<sup>1–9</sup> The paddle-wheel configuration in which the carboxylate ligands bond both copper(II) atoms with a bridging ligand confers on these compounds interesting features. They present monotropic polymorphism and mesomorphism, as a hexagonal columnar discotic liquid crystal.<sup>10</sup> Recent research has explored the thermal behavior and structure of the copper(II) alkanooate series in both crystal and liquid crystal phases, where the dimeric complex molecular units are present.<sup>5</sup> Important applications of the copper(II) alkanooates result from their magnetic properties<sup>11,12</sup> and their potential use in the production of nanoreactors.<sup>13–16</sup> Special interest arises from their biological activity, as they have proven pharmaceutical activity in diverse fields such as antiinflammatory, antirheumatic, and antitumoral<sup>17–26</sup> as well as fungicidal activity,<sup>27–31</sup> for which they have been extensively studied as food preservatives. Dimeric complexes involving bridging carboxylate groups, like the copper(II) propanoate (Cu(C<sub>3</sub>)<sub>2</sub>, hereafter), are of special interest for their fungicidal properties.<sup>27</sup> Pyridine-4-carboxamide, or isonicotinamide (INA, hereafter), is a pharmaceutical cofomer of common use in the cocrystal production, as it possesses antitumoral,

antipyretic, thrombolytic, and antibacterial properties.<sup>32</sup> It is also known to behave as a high-yielding supramolecular reagent.<sup>33</sup> The nitrogen atom present in the pyridine readily acts as a hydrogen-bond acceptor when faced with hydrogen-bond donors such as carboxylic acids<sup>34</sup> and can even coordinate directly to the copper.<sup>33</sup> The activity of the metal ions increases with the addition of some already biologically active substances; therefore, a large number of adducts and complexes of copper(II) carboxylates with N donor ligands such as urea, nicotinamide, papaverine, 3-hydroxypyridine, 2-aminopyridine, etc. have already been produced and their crystal structure solved.<sup>28,29,31,35–37</sup>

In this communication we report the preparation of the new adduct formed by Cu(C<sub>3</sub>)<sub>2</sub> and INA. Single crystals were obtained by slow evaporation from an ethanol solution, which allowed the resolution of the crystal structure. However, this method presents several drawbacks for the production of crystals at industrial scale. Cooling crystallizers require temperature to have a considerable effect on solubility. Furthermore, the slow crystal growth rate in slow evaporative

**Received:** July 9, 2018

**Revised:** December 15, 2018

**Published:** January 9, 2019

# **Chapter 7**

## **CONCLUSIONS AND FURTHER WORK**



## 7 CONCLUSIONS AND FURTHER WORK

In this doctoral thesis, the potential of supercritical fluid technologies in the enhancement of the properties of active pharmaceutical ingredients (APIs) is explored. Both co-crystallization and coprecipitation using CO<sub>2</sub> are used

The main supercritical fluid technique used is the supercritical antisolvent technique (SAS). From the experiments performed we can confirm:

- This technique is suitable for the simultaneous processing and micronization of thermolabile drugs and carriers as it operates at relatively low temperatures.
- Thanks to the SAS technique solvent-free drug particles with narrow size distributions are obtained in a semicontinuous single-step process. In principle, polymorphism, particle morphology, and size may be controlled by tuning the operational parameters.
- In comparison to conventional co-crystallization and coprecipitation processes, organic solvents are used in SAS in reduced amounts. Furthermore, CO<sub>2</sub> is innocuous, non-flammable and can be recycled being considered as a green solvent.
- On the other hand, several patents and adaptations of the SAS process to larger scale production taking into account the good manufacturing practice (GMP) requirements of the pharmaceutical industry have already been developed<sup>1</sup>. Therefore, SAS is a promising technique for the industrial processing of pharmaceuticals.

In this thesis different routes of drug formulation enhancement have been studied: micronization of the drug and composite preparation, production of metal adducts, and co-crystal formation. The main conclusions of this study are:

- SAS technique is a suitable method for the production of microparticle composites for controlled drug delivery. A composite of 5-fluorouracil (5-Fu) and the biocompatible and biodegradable polymer poly-L-lactic acid (PLLA) has been prepared using SAS. The precipitate consisted of 5-Fu microparticles coated with nano-spheres of PLLA. Dissolution rate of the SAS 5-Fu-PLLA composite was substantially slower than that of the pure drug (Publication I).

- Production of diflunisal (DIF) and nicotinamide (NIC) co-crystals has been achieved using SAS for the first time. Experiments have been performed using different solvents, concentrations, temperatures and pressures. The system is quite insensitive to the operating conditions studied rendering in all cases a pure solvent-free co-crystal precipitate with a needle like morphology (Publication II).

- Co-crystals of carbamazepine (CBZ) and saccharin (SAC) have been obtained via SAS avoiding the undesirable dihydrate form of CBZ usually present in conventional co-crystallization samples. Co-crystals have been produced using different solvents, concentrations, temperatures and pressures. SAS precipitation allows to control the polymorphism by changing these parameters. The conditions rendering pure polymorph I have been identified. For other conditions, a mixture of polymorphs I and II free of homocrystals is obtained. In this system, the influence of pressure and concentration on the polymorphic outcome is weak. On the other hand, solvent and temperature have a stronger influence. Solute-solvent interaction is a crucial factor affecting polymorphism. Temperature affects the solubilities of the co-crystal components in the solvent and can change therefore, the ternary phase diagram. Thus, the ternary phase diagram has to be taken into consideration when producing co-crystals via SAS (Publication III).

- Two new metallic organic frameworks (MOFs) or adducts of copper propanoate ( $\text{Cu}(\text{C}_3)_2$ ) and isonicotinamide (INA) in a 1:2 molar ratio have been prepared using evaporative crystallization and their crystal structure has been solved.

- In this thesis the production of MOFs using SAS is investigated for the first time. The  $\text{Cu}(\text{C}_3)_2$  and INA adduct has been prepared by SAS using different solvents, molar ratios, temperatures and pressures. Conditions to produce the MOF have been identified. The SAS MOF decomposes at a lower temperature and has a slightly larger nitrogen to carbon ratio than the MOF obtained by evaporative crystallization, indicating the possible partial decomposition of the sample during SAS processing. This study opens up the path to the production of other metal adducts by SAS (Publication IV).

- The preparation of 5-Fu co-crystals with different cofomers has been achieved using two different supercritical fluid techniques: SAS and co-crystallization with supercritical solvent (CSS).

- SAS has been successful in the preparation of 5-Fu co-crystals with urea and thiourea. The very different solubility of the cofomers in the selected solvent suggests an

incongruent saturating system and therefore, 5-Fu homocrystals have been identified in the SAS precipitate.

- The preparation of the 5-Fu and acridine (ACR) co-crystal by SAS has also been achieved. Although the solubility of the cofomers in CO<sub>2</sub> is very different, by adjusting the ACR concentration in the solution co-crystal formation was achieved. The different solubilities of the co-crystal components in the organic solvent or supercritical CO<sub>2</sub> may result in homocrystal precipitation.

- CSS experiments carried out with the addition of cosolvent have been successful. However, homocrystals were present in all samples studied. The solubilization of the co-crystal components in the supercritical phase seems to be a prerequisite for a successful co-crystallization.

- Although CSS has been able to produce co-crystals, its scaling-up is difficult and the method does not present the micronization advantages of SAS. Moreover, if cosolvents are added further drying steps may be required in the process.

As further work, the following lines are under research:

1. A more detailed investigation of the ternary phase diagram influence on the SAS production of the co-crystal formed by theophylline (THP) and DIF is being performed. Preparation of this co-crystal via SAS was initially attempted using a 1:1 THP-DIF molar ratio (for which a known crystal structure has been published<sup>2</sup>) and a 50 % (v/v) mixture of ethanol and dichloromethane (DCM) as this solvent mixture was reported as optimal for THP SAS precipitation.<sup>3</sup> Experiments yielded the co-crystal and THP homocrystals. The difference in solubility of both cofomers in the solvent mixture is large (30 mg/mL for THP and 175 mg/mL for DIF) and therefore, an incongruent saturating system may be expected. Further experiments will involve the measurement of the pseudoternary phase diagram for the THP-DIF-solvent mixture system at different temperatures. Solubility curves will be measured following the procedure described by Chiarella et al.<sup>4</sup> DSC analysis of grinded mixtures will be used to build the binary phase diagram of THP and DIF.

2. Adducts of INA and other copper alkanoates apart from propanoate (pentanoate, hexanoate, octanoate and decanoate) have been studied. Using slow evaporation from ethanol solutions crystals suitable for SCXRD have been obtained and their crystal structures have been elucidated. Adduct formation using SAS was also explored. Preliminary results show that the PXRD pattern of the SAS precipitate and that of the adduct calculated from CIF match. Nevertheless, the SAS precipitate may contain some

impurities associated to its partial decomposition. The fungicidal properties of the MOFs obtained via solvent crystallization and SAS should be evaluated and compared.

**3.** The formation of co-crystals inside aerogel carriers is also being investigated. These innovative formulations could combine the co-crystal improved physicochemical properties and the controlled release provided by an aerogel. Initial experiments have been performed at the Technische Universität Harburg-Hamburg (TUHH). Two different supercritical technologies were assessed (supercritical impregnation and supercritical drying). Naproxen (NPX) and NIC have been simultaneously impregnated in several carriers. Using CO<sub>2</sub> induced gelation and different ratios of calcium carbonate as crosslinker, several biodegradable aerogels with varying pore sizes were produced. In the final solvent exchange step of these aerogels, NPX and NIC were introduced and supercritical CO<sub>2</sub> drying followed. A drug has a higher tendency to adopt its crystalline form (instead of the amorphous one) when the aerogel pores are bigger.<sup>5</sup> Bearing this in mind a sodium alginate aerogel with big pore sizes was produced. Characterization of the samples is undergoing.



## References

1. (a) lao, Z.; Wang, W.; Cheng, J.; Song, J.; Han, S. Improved device for preparing polymer drug-loaded particles by supercritical antisolvent method. CN108905884 (A) — 2018-11-30, **2018**; (b) Jiang, Y.; Liu, X.; Liping., Y.; Yangxiao., L.; Zhixian., L. Multifunctional supercritical CO<sub>2</sub> device for extraction, loading and drying. CN108744579 (A) — 2018-11-06, **2018**; (c) Yanbin., J.; Qing., L.; Zenan., C.; Ziyi., Z. Supercritical antisolvent technique-based gefitinib @PLLA microsphere dry powder inhalant and preparation method thereof. CN107137381 (A) — 2017-09-08, **2017**.
2. Surov, A. O.; Voronin, A. P.; Manin, A. N.; Manin, N. G.; Kuzmina, L. G.; Churakov, A. V.; Perlovich, G. L., Pharmaceutical Cocrystals of Diflunisal and Diclofenac with Theophylline. *Molecular Pharmaceutics* **2014**, *11* (10), 3707-3715.
3. Subra, P.; Laudani, C. G.; Vega-Gonzalez, A.; Reverchon, E., Precipitation and phase behavior of theophylline in solvent-supercritical CO<sub>2</sub> mixtures. *Journal of Supercritical Fluids* **2005**, *35* (2), 95-105.
4. Chiarella, R. A.; Davey, R. J.; Peterson, M. L., Making co-crystals - The utility of ternary phase diagrams. *Crystal Growth & Design* **2007**, *7* (7), 1223-1226.
5. Gurikov, P.; Smirnova, I., Amorphization of drugs by adsorptive precipitation from supercritical solutions: A review. *Journal of Supercritical Fluids* **2018**, *132*, 105-125.



# Curriculum Vitae



Isaac Alfonso Cuadra Mendoza

[icuada@ucm.es](mailto:icuada@ucm.es)

orcid ID: 0000-0002-6615-1907

Scopus Author ID: 56998639200

## Education

---

### Chemical Engineering

Speciality: *Environmental Engineering*

University: *Universidad Complutense de Madrid*

### Master in Industrial Processes Engineering

Speciality: *Industrial Process Technology*

University: *Universidad Complutense de Madrid*

## Research Projects

---

### Preparation of nanomaterials with supercritical CO<sub>2</sub> and their application in catalysis and pharmacology (CTQ2013-41781-P)

Ministry of Economy and Competitiveness

Principal Investigator: Concepción Pando García-Pumarino and Albertina Cabañas Poveda

## Research Grants

---

Ministry of Economy and Competitiveness Predoctoral Grant: BES-2014-067777

Ministry of Economy and Competitiveness Mobility Grant: EEBB-1-17-12090

Ministry of Economy and Competitiveness Mobility Grant: EEBB-1-18-12765

## Research Stays

---

### Karlsruhe Institute of Technology (KIT)

Institute for Technical Thermodynamics and Refrigeration

2017 (3 Months)

Topic: *“Preparation of pharmaceutical co-crystals using supercritical CO<sub>2</sub> as a solvent”*

### Technical University Hamburg (TUHH)

Institute for Thermal Separation Processes

2018 (3 Months)

Topic: *“Preparation of biodegradable aerogels and loading of aerogels with co-crystals via impregnation and precipitation”*

## Publications

---

1. Cuadra, I. A.; Martinez-Casado, F. J.; Cheda, J. A. R.; Redondo, M. I.; Pando, C.; Cabañas, A., *Production and Characterization of a New Copper(II) Propanoate-Isonicotinamide Adduct Obtained via Slow Evaporation and using Supercritical CO<sub>2</sub> as an Antisolvent*. *Crystal Growth & Design* **2019**, 19, 620-629.
2. Cuadra, I. A.; Zahran, F.; Martin, D.; Cabañas, A.; Pando, C., *Preparation of 5-fluorouracil microparticles and 5-fluorouracil/poly(L-lactide) composites by a supercritical CO<sub>2</sub> antisolvent process*. *Journal of Supercritical Fluids* **2019**, 143, 64-71.
3. Cuadra, I. A.; Cabañas, A.; Cheda, J. A. R.; Pando, C., *Polymorphism in the co-crystallization of the anticonvulsant drug carbamazepine and saccharin using supercritical CO<sub>2</sub> as an anti-solvent*. *Journal of Supercritical Fluids* **2018**, 136, 60-69.
4. Pando, C.; Cabañas, A.; Cuadra, I. A., *Preparation of pharmaceutical co-crystals through sustainable processes using supercritical carbon dioxide: a review*. *RSC Adv.*, **2016**, 6, 71134

5. Cuadra, I. A.; Cabañas, A.; Cheda, J. A. R.; Martínez-Casado, F. J.; Pando, C., *Pharmaceutical co-crystals of the anti-inflammatory drug diflunisal and nicotinamide obtained using supercritical CO<sub>2</sub> as an antisolvent*. *Journal of CO<sub>2</sub> Utilization* **2016**, 13, 29-37

## Congresses

---

### **Enhancement of 5-Fluorouracil Pharmaceutical Properties using Supercritical CO<sub>2</sub> Technologies: Micronization, Formation of Composites and Co-crystallization**

Isaac A. Cuadra; Fouad Zahran; Michael Türk; Albertina Cabañas; Concepción Pando

EMSF 2019 17<sup>th</sup> European Meeting on Supercritical Fluids. Ciudad Real (Spain), 2019

Oral communication

### **Preparation of Co-crystals using Supercritical CO<sub>2</sub> as an Antisolvent**

Isaac A. Cuadra; Albertina Cabañas; Lourdes Calvo; M. I. Redondo; José A. R. Cheda; Concepción Pando.

IX Reunión de Expertos en Fluidos Comprimidos (FLUCOMP 2018). Madrid (Spain), 2018

Oral communication

### **Evaluation of the Supercritical Anti-solvent CO<sub>2</sub> Technique in the Preparation of Novel Copper(II)propanoate-Isonicotinamide Adduct**

Isaac A. Cuadra; Francisco J. Martínez-Casado; José A. R. Cheda; M. Isabel Redondo; Albertina Cabañas; Concepción Pando.

VIII. Symposium in produktgestaltung in der partikeltechnologie. Karlsruhe (Germany)

Poster

### **A Comparative Study of Copper(II) Alkanoates-Isonicotinamide Adducts Obtained Via Slow Evaporation and Using Supercritical CO<sub>2</sub> as an Antisolvent**

Isaac A. Cuadra; Francisco J. Martínez-Casado; José A. R. Cheda; M. Isabel Redondo; Albertina Cabañas; Concepción Pando.

EMSF 2017 16<sup>th</sup> European Meeting on Supercritical Fluids. Lisbon (Portugal), 2017

Poster

### **Particle micronization using supercritical CO<sub>2</sub> as Antisolvent**

Isaac A. Cuadra; Albertina Cabañas; Concepción Pando.

I Simposio Anual de Química Avanzada. Madrid (Spain) 2016.

Oral communication

### **Pharmaceutical Co-crystals obtained using Supercritical CO<sub>2</sub> as an Antisolvent**

Isaac A. Cuadra; Albertina Cabañas; José A.R. Cheda; Francisco J. Martínez-Casado; Concepción Pando.

VIII Reunión de Expertos en Fluidos Comprimidos (FLUCOMP2015). Cádiz (Spain), 2015

Poster

### **A Solution Co-crystallization Method Based on using Supercritical CO<sub>2</sub> as an Antisolvent**

Concepción Pando; Isaac A. Cuadra; A. Cabañas; J.A.R. Cheda; J.A.R. Renuncio.

XLI Conference on Phase Equilibria (JEEP2015). Coimbra (Portugal), 2015

Oral Communication

### **Preparation of Nanomaterials en CO<sub>2</sub> supercrítico con aplicaciones en catálisis, captura de carbono y farmacología**

A. Cabañas; C. Pando; Y. Sánchez-Vicente; J. Morere; Isaac A. Cuadra.

Jornadas Aportando Valor al CO<sub>2</sub>. Madrid (Spain)

Oral Communication

### **Preparation of 5-Fluorouracil - Poly(L-lactide) Microparticles using Supercritical CO<sub>2</sub> as Antisolvent**

Isaac A. Cuadra; Albertina Cabañas; Concepción Pando.

VII Reunión de Expertos en Fluidos Comprimidos (FLUCOMP 2014). Barcelona (Spain)

Poster

## **Courses, seminars and workshops**

---

**Methodological aspects to be considered in experimental sciences and engineering doctoral thesis.**

Universidad Complutense de Madrid (Spain)

December 11-14, 2017

**Safety in the handling of cryogenic fluids, gas bottles, and their installation plants.**

Praxair (Spain)

November 10, 2016

**Practical and theoretical aspects in the thermal characterization of materials**

TA Instruments (Spain)

June 22-23, 2016

**Eudragit & Eudraguard Advanced Workshop**

Evonik Industries

May 18-19, 2016

**Winesense Spring School**

High Pressure Processes Group, University of Valladolid

April 18-21, 2016

**Introduction to the structural resolution using X-ray diffraction**

Universidad Internacional de Andalucía

June 8-10, 2015

**Instrumentation, automation and measurement software development**

Universidad Complutense de Madrid

February-April, 2014

## **Teaching activity**

---

**Collaboration in the following teaching activities:**

**General Chemistry**

BSc in Physics, Universidad Complutense de Madrid

Academic year: 2018-2019

2016-2017

**Chemical thermodynamic and kinetics**

BSc in Chemical Engineering, Universidad Complutense de Madrid

Academic year: 2018-2019

2017-2018





